Cloning and expression of lipoxygenase, hydroperoxide lyase and transaminase targeting the synthesis of polymer intermediates

Inaugural-Dissertation

zur Erlangung des Doktorgrades
der Mathematisch-Naturwissenschaftlichen Fakultät
der Heinrich-Heine-Universität Düsseldorf

vorgelegt von

Anna Coenen

aus Viernheim

Frankfurt am Main, Februar 2023

Aus dem Institut für Molekulare Enzymtechnologie (IMET)
der Heinrich-Heine-Universität Düsseldorf
in Kooperation mit der Fakultät für Angewandte Naturwissenschaften der TH Köln

Gedruckt mit der Genehmigung der
Mathematisch-Naturwissenschaftlichen Fakultät der
Heinrich-Heine-Universität Düsseldorf

Berichterstatter:
1. Prof. Dr. Karl-Erich Jaeger
2. Prof. Dr. Ulrich Schörken
Tag der mündlichen Prüfung: 22.06.2023

Table of contents

List of figures IV

List of tables VIII

Abbreviations IX

Summary 1

Zusammenfassung 2

1. Introduction 4

1.1. Scope of the thesis 4

1.2. The lipoxygenase pathway 6

1.3. Enzyme sources, properties, structure and function 7

1.3.1. Lipoxygenases 7

1.3.2. Hydroperoxide lyases 10

1.3.3. Transaminases 13

1.4. Biotechnological application of LOXs, HPLs and ω-TAs 17

2. Materials & Methods 20

2.1. Reagents, enzymes and antibodies 20

2.2. Vectors 21

2.3. Cell strains and cultivation of bacteria 24

2.4. Bioinformatic analyses 25

2.5. Molecular biology methods 26

2.5.1. Polymerase chain reaction (PCR) 26

2.5.2. Fusion PCR 27

2.5.3. Isolation of plasmid DNA from *E. coli* 29

2.5.4. Restriction of DNA and ligation of restriction products 29

2.5.5. Generation and transformation of competent *E. coli* cells 30

2.5.6. Agarose gel electrophoresis and DNA extraction 31

2.5.7. DNA sequencing 31

2.6. Protein biochemistry methods 32
2.6.1. Protein expression in shaking flasks and fermenter cultures 32
2.6.2. Extraction and purification of soluble enzyme fractions 33
2.6.3. Size exclusion chromatography 34
2.6.4. Protein quantification with Bradford reagent 34
2.6.5. SDS-PAGE 35
2.6.6. Western Blot 36
2.7. Enzyme assays and biocatalytic methods 37
2.7.1. Activity analysis of LOX and HPL 37
2.7.2. Enzyme activity analysis of ω-TAs 38
2.7.3. Photometrical analysis of enzyme cascades with ω-TA 38
2.7.4. Enzyme reactions with HPL and one-pot reactions with lipase, LOX and HPL 39
2.7.5. Enzymatic preparation of 12-oxo-9(*Z*)-dodecenoic acid 40
2.7.6. Enzyme catalysis with ω-TA and one-pot reactions with LOX, HPL and ω-TA 40
2.8. Analytic methods 41
2.8.1. Sample hydrogenation for GC analysis 41
2.8.2. Product analysis by gas chromatography coupled to MS and FID detection 41
2.8.3. Product analysis with HPLC coupled with MS and ELSD detection 42
3. Results 43
3.1. Lipoxygenase 43
3.1.1. Cloning and expression of soybean lipoxygenase LOX-1 43
3.1.2. Purification of LOX-1 45
3.2. Hydroperoxide lyases 46
3.2.1. Selection and cloning of HPLs 46
3.2.2. Expression of HPLs 49
3.2.3. Optimization of expression and solubilization of $HPL_{CP\text{-}N}$ 51
3.2.4. Fermentation, purification and biochemical characterization of $HPL_{CP\text{-}N}$ 55
3.2.5. Monitoring of the $HPL_{CP\text{-}N}$ reaction 58
3.3. ω-Transaminases 61

3.3.1. Selection and cloning of ω-transaminases 61
3.3.2. Expression, purification and substrate specificity of ω-TAs 63
3.3.3. Monitoring of the TR_{AD} reaction 65
3.4. Development of enzyme cascades for the synthesis of 12-oxo- and 12-aminododecenoic acid 68
3.4.1. Coupling of lipase, LOX and HPL in one-pot reactions 69
3.4.2. Synthesis of 12-aminododecenoic acid from linoleic acid by coupling LOX, HPL and ω-TA 71
4. Discussion 73
4.1. Expression of recombinant LOX-1 and comparison with soybean flour and commercially LOX-1 preparations 73
4.2. Cloning and expression of plant-derived hydroperoxide lyases 76
4.3. Purification and characterization of papaya $HPL_{CP\text{-}N}$ 80
4.4. Comparison of ω-TAs for the amination of 12-oxododecenoic acid and hexanal 82
4.5. Challenges and opportunities of enzyme cascades targeting 12-oxo- and 12-aminododecenoic acid synthesis 86
5. References 89
6. Appendix 111
Publications 145
Danksagung 147
Eidesstattliche Erklärung 148

List of figures

Fig. 1 Reaction scheme of the enzyme cascade for the synthesis of 12-aminododecenoic acid and hexylamine starting from safflower oil using a lipase, a lipoxygenase (LOX), a hydroperoxide lyase (HPL) and a ω-transaminase (ω-TA).....5
Fig. 2 The lipoxygenase (LOX) pathway in plants. LOX catalyzes the hydroperoxidation of linoleic acid/ α-linolenic acid to the hydroperoxides 9(*S*)- or 13(*S*)-HPODE/ HPOTE.....7
Fig. 3 Crystal structure (**a**) and active site (**b**) of lipoxygenase LOX-1 from *G. max* (PDB: 1YGE) [53].....8
Fig. 4 Reaction mechanism of lipoxygenases consisting of (1) hydrogen abstraction, (2) radical rearrangement, (3) oxygen incorporation and (4) reduction of the hydroperoxy radical. 9
Fig. 5 Reaction mechanism of HPL catalysis on the example of 13(*S*)-HPODE.....11
Fig. 6 Crystal structure of (**a**) allene oxide synthase (AOS) from *A. thaliana* (PDB: 3CLI) [89] and (**b**) Swiss-model [90] of putative papaya hydroperoxide lyase HPL_{CP}, based on *A. thaliana* AOS sequence. 12
Fig. 7 Crystal structures of the two fold type transaminases with (**a**) homodimer from *C. violaceum* transaminase (PDB: 4A6T) [125] as a fold type I (*S*)-ATA and (**b**) homodimer from *A. terreus* transaminase (PDB: 4CE5) [128] as a fold type IV (*R*)-ATA.....15
Fig. 8 Reaction mechanism of ω-TA catalysis.....16
Fig. 9 Two-binding site model of (*S*)- and (*R*)-selective ATAs.....17
Fig. 10 Expression vector pET-21b::His*lox-1* for expression of *G. max* LOX-1 (**a**) and agarose gel of restriction digest of pET-21b::His*lox-1* with *Nde*I and *Bam*HI (**b**). 43
Fig. 11 Dependence of LOX-1 expression on different temperatures (**a + b**) and cultivation media (**c**).....44
Fig. 12 Effect of salt concentration and addition of imidazole on activity of LOX-1.....45
Fig. 13 Purification process of LOX-1.....46
Fig. 14 Expression vectors for HPL expression (**a**) and agarose gels of restriction digest of the vectors with *Nde*I and *Bam*HI (**b**), exemplified for *C. papaya* HPL_{CP}.....48
Fig. 15 Multiple sequence alignment of the N-terminal sequences of HPLs obtained with ClustalΩ [178]. 48
Fig. 16 SDS-PAGEs of enzyme expression of HPLs in full-length, N-terminal truncated constructs and NusA–HPL fusion proteins with HPLs from (**a**) *P. guajava* (PG), (**b**) *S. bicolor* (SB) (**c**) *H. vulgare* (HV) and (**d**) *C. papaya* (CP).....50
Fig. 17 Comparison of specific activities of HPL (grey bars), truncated HPL-N (blue bars) and fusion NusAHPL-N (red bars) proteins from *P. guajava* (PG), *H. vulgare* (HV), *S. bicolor* (SB) and *C. papaya* (CP).....51

Fig. 18 Evaluation of the optimal expression strain for $HPL_{CP\text{-}N}$ production. 52
Fig. 19 Evaluation of optimal cultivation temperature (**a**) and cultivation medium (**b**) for $HPL_{CP\text{-}N}$ expression. 53
Fig. 20 Evaluation of optimal buffer for $HPL_{CP\text{-}N}$ solubilization and activity assay. 54
Fig. 21 Purification process of $HPL_{CP\text{-}N}$, determined by SDS-PAGE (**a**) and Western Blot (**b**). 56
Fig. 22 Determination of molecular weight of native $HPL_{CP\text{-}N}$ by gel filtration (**a**) after calibration with carboanydrase (29 kDa), alcohol dehydrogenase (150 kDa), apoferritin (443 kDa) and thyroglobulin (669 kDa) (**b**). 56
Fig. 23 Determination of pH dependence of purified $HPL_{CP\text{-}N}$ from pH 6 to 9. 57
Fig. 24 Enzyme activity was measured in dependence of substrate concentrations ranging from 0.005 mM to 0.1 mM with (**a**) 13(*S*)-HPODE and (**b**) 13(*S*)-HPOTE. 57
Fig. 25 GC-FID spectra of 13(*S*)-HPODE (**a**) and after incubation with soluble fraction of $HPL_{CP\text{-}N}$ at 22 °C for 10 sec (**b**) and for 120 min (**c**) 59
Fig. 26 Mass spectra of GC-peaks from 2.3 min (hexanal), 11.9 min (12-oxo-9(*Z*)-dodecenoic acid) and 12.2 min (12-oxo-10(*E*)-dodecenoic acid) retention time. 60
Fig. 27 Time-course experiments of $HPL_{CP\text{-}N}$ catalysis. 61
Fig. 28 Expression vector pET-21b::His*tr* (**a**) for expression of *A. denitrificans* (AD), *C. violaceum* (CV), *P. denitrificans* (PD) and *S. delicatus* (SD) ω-TAs and agarose gels of restriction digests of pET-21b::His*tr* (**b**) with *Nde*I and *Bam*HI. 63
Fig. 29 Evaluation of overexpression (**a**) and purification (**b**) of ω-TAs. 64
Fig. 30 Coupled enzymatic activity assay with a ω-TA and LDH. 65
Fig. 31 Analysis of TR_{AD} catalyzed synthesis of 12-aminododecenoic acid, monitored with HPLC-ELSD 66
Fig. 32 Mass spectra analyses of TR_{AD} enzyme reactions. 67
Fig. 33 Analysis of reaction conditions for TR_{AD} catalysis. 68
Fig. 34 Time-course of one-pot enzymatic reactions with LOX-1 and $HPL_{CP\text{-}N}$. 69
Fig. 35 Determination of optimal reaction setup with either simultaneous or consecutive enzyme addition in (**a**) one-pot reactions containing LOX-1 and $HPL_{CP\text{-}N}$ and (**b**) one-pot reactions with Amano lipase from *P. fluorescens*, LOX-1 and $HPL_{CP\text{-}N}$. 70
Fig. 36 Coupled photometric enzyme assay with lipoxygenase (LOX), hydroperoxide lyase (HPL), ω-transaminase (ω-TA) and lactate dehydrogenase (LDH). 71
Fig. 37 Comparison of optimal one-pot reaction setups with coupled $HPL_{CP\text{-}N}$ and TR_{AD} (**a**) and coupled LOX-1, $HPL_{CP\text{-}N}$ and TR_{AD} (**b**) cascade reaction 72
Fig. 38 Phylogenetic tree of HPL sequences with known HPLs from literature and HPLs analyzed in this work. 77
Fig. 39 Formation of 12-oxo-10(*E*)-dodecenoic acid (traumatin). 82
Fig. 40 Phylogenetic neighbor-joining tree of ω-transaminases, tested in this study. 84

Fig. A 1 LOX-1 protein sequence and codon-optimized *lox-1* gene sequence with His6-tag marked in grey and restriction sites underlined. 111
Fig. A 2 Alignment of *A. thaliana* AOS_{AT} (PDB number: 3CLI) as template and *C. papaya* HPL_{CP} model 112
Fig. A 3 Guava HPL_{PG} protein sequence and codon-optimized hpl_{PG} gene sequence with His6-tag marked in grey and restriction sites underlined. 113
Fig. A 4 Papaya HPL_{CP} protein sequence and codon-optimized hpl_{CP} gene sequence with His6-tag marked in grey and restriction sites underlined. 114
Fig. A 5 Barley HPL_{HV} protein sequence and codon-optimized hpl_{HV} gene sequence with His6-tag marked in grey and restriction sites underlined. 115
Fig. A 6 Sorghum HPL_{SB} protein sequence and codon-optimized hpl_{SB} gene sequence with His6-tag marked in grey and restriction sites underlined. 116
Fig. A 7 Expression vector pET-28a::His*hpl* (**a**) for expression of HPL_{PG} = *P. guajava*, HPL_{CP} = *C. papaya,* HPL_{HV} = *H. vulgare* and HPL_{SB} = *S. bicolor* and agarose gels of restriction digests of pET-28a::His*hpl* (**b**) with *Nde*I and *Bam*HI. 117
Fig. A 8 Multiple sequence alignment of HPL sequences obtained with ClustalΩ [178]. 120
Fig. A 9 Scheme for the cloning of N-terminal truncated HPLs. 121
Fig. A 10 Expression vector pET-28a::His*hpl-N* (**a**) for expression of N-terminal truncated $HPL_{PG\text{-}N}$ = *P. guajava*, $HPL_{CP\text{-}N}$ = *C. papaya,* $HPL_{HV\text{-}N}$ = *H. vulgare* and $HPL_{SB\text{-}N}$ = *S. bicolor* and agarose gels of restriction digests of pET-28a::His*hpl-N* (**b**) with *Nde*I and *Bam*HI. 122
Fig. A 11 Scheme for the cloning of NusA – HPL fusion proteins. A PCR was performed to amplify the *nusA* and the *hpl-N* sequences with overlapping fragments. 123
Fig. A 12 NusA protein sequence and *nusA* gene sequence. 124
Fig. A 13 NusA$HPL_{CP\text{-}N}$ fusion protein sequence and $nusAhpl_{CP\text{-}N}$ fusion gene sequence with His6-tag marked in grey and restriction sites underlined. 125
Fig. A 14 NusA$HPL_{PG\text{-}N}$ fusion protein sequence and $nusAhpl_{PG\text{-}N}$ fusion gene sequence with His6-tag marked in grey and restriction sites underlined. 126
Fig. A 15 NusA$HPL_{HV\text{-}N}$ fusion protein sequence and $nusAhpl_{HV\text{-}N}$ fusion gene sequence with His6-tag marked in grey and restriction sites underlined. 127
Fig. A 16 NusA$HPL_{SB\text{-}N}$ fusion protein sequence and $nusAhpl_{SB\text{-}N}$ fusion gene sequence with His6-tag marked in grey and restriction sites underlined. 129
Fig. A 17 Expression vector pET-28a::*NusAhpl* (**a**) for expression of fusion proteins with NusA and $HPL_{PG\text{-}N}$ = *P. guajava*, $HPL_{CP\text{-}N}$ = *C. papaya,* $HPL_{HV\text{-}N}$ = *H. vulgare* and $HPL_{SB\text{-}N}$ = *S. bicolor* and agarose gels of restriction digests of pET-28a::*nusAhpl-N* (**b**) with *Nde*I and *Bam*HI. 130
Fig. A 18 SDS-PAGE of $HPL_{CP\text{-}N}$ expression in *E. coli* C41(DE3). 131

Fig. A 19 SDS-PAGEs of HPL_{CP-N} expression in *E. coli* Lemo21 and BL21(DE3) in the crude extract (**a**) and the soluble fraction (**b**). 131
Fig. A 20 Initial purification process of HPL_{CP-N}, determined by SDS-PAGE (**a**) and photometrical enzyme assay (**b**). 132
Fig. A 21 Purification process of HPL_{CP-N} purification using a gradient of imidazole for elution, determined by SDS-PAGE (**a**) and photometrical enzyme assay (**b**). 132
Fig. A 22 Mass spectra of reference standards analyzed with GC-MS of (**a**) 12-oxo-9(*Z*)-dodecenoic acid, (**b**) 12-oxo-10(*E*)-dodecenoic acid and (**c**) hexanal. 133
Fig. A 23 Calibration curves of hydrogenated and silylated linoleic acid (**a**), 13(*S*)-HPODE (**b**), 12-hydroxydodecanoic acid (**c**) and hexanal (**d**), measured on GC-FID. 134
Fig. A 24 Protein sequence of ω-transaminase TR_{CV} from *C. violaceum* and codon-optimized tr_{CV} gene sequence with His6-tag marked in grey and restriction sites underlined. 135
Fig. A 25 Protein sequence of ω-transaminase TR_{SD} from *S. delicatus* and codon-optimized tr_{SD} gene sequence with His6-tag marked in grey and restriction sites underlined. 136
Fig. A 26 Protein sequence of ω-transaminase TR_{AD} from *A. denitrificans* and codon-optimized tr_{AD} gene sequence with His6-tag marked in grey and restriction sites underlined. 137
Fig. A 27 Protein sequence of ω-transaminase TR_{PD} from *P. denitrificans* and codon-optimized tr_{PD} gene sequence with His6-tag marked in grey and restriction sites underlined. 138
Fig. A 28 Protein sequence of ω-transaminase TR_2 from *Acidihalobacter* sp. and codon-optimized tr_2 gene sequence with His6-tag marked in grey and restriction sites underlined. 139
Fig. A 29 Protein sequence of ω-transaminase TR_3 from *Rhodobacteraceae* bacteria and codon-optimized tr_3 gene sequence with His6-tag marked in grey and restriction sites underlined. ... 140
Fig. A 30 Protein sequence of ω-transaminase TR_6 from *Rhodobacteraceae* bacteria and codon-optimized tr_6 gene sequence with His6-tag marked in grey and restriction sites underlined. ... 141
Fig. A 31 Calibration curve 12-aminododecanoic acid analyzed with HPLC-ELSD. 142
Fig. A 32 Multiple sequence alignment of ω-TA sequences using ClustalΩ [178]. 144

List of tables

Table 1 Vectors used in this work with description and reference. 21
Table 2 Bacteria used in the experiments for cultivation and expression. 24
Table 3 Compositions of the cultivation media lysogeny broth (LB), terrific broth (TB) and the auto-induction medium ZYM5052. 25
Table 4 Oligonucleotides for PCR with restriction sites underlined and His6-tags highlighted in grey. 26
Table 5 Oligonucleotides used for fusion PCR with restriction sites underlined and His6-tags highlighted in grey. 27
Table 6 Oligonucleotides used for DNA sequencing. 32
Table 7 Solubilization and binding buffers for LOX, HPL and ω-TA solubilization and affinity purification. 33
Table 8 Composition of discontinuous SDS gels consisting of a stacking gel and a resolving gel. 35
Table 9 Purification process of LOX-1 from 50 ml cultivation medium after cultivation at 15 °C in TB medium. 46
Table 10 Fermentation and purification process of $HPL_{CP\text{-}N}$ determined with activity assays. 55
Table 11 Kinetic parameters of $HPL_{CP\text{-}N}$ reaction with 13(*S*)-HPODE and 13(*S*)-HPOTE as substrates. 58
Table 12 Sequence identities of ω-TAs, calculated with BLAST [177]. 62
Table 13 Comparison of specific activities of lipoxygenases (LOX). 75
Table 14 Comparison of enzymatic activities of hydroperoxide lyases (HPL). 78

Abbreviations

α-AAT	α-Amino acid aminotransferase
ADH	Alcohol dehydrogenase
ALA	δ-Aminolevulinic acid
Amp	Ampicillin
Amp^R	Ampicillin resistance
AOS	Allene oxide synthase
APS	Ammonium persulfate
Asn	Asparagine
ATA	Amine transaminase
BLAST	Basic local alignment search tool
bp	Base pairs
BSA	Bovine serum albumin
BSTFA-TMCS	N,O-Bis(trimethylsilyl)-trifluoroacetamide-trimethylchlorosilane
BVMO	Baeyer-Villiger monooxygenase
CYP450	Cytochrome P450 enzymes
Da	Dalton
ddH_2O	Double distilled water
DES	Divinyl ether synthase
DHA	Docosahexaenoic acid
DMSO	Dimethyl sulfoxide
DNA	Deoxyribonucleic acid
dNTP	Deoxyribonucleoside triphosphate
EAS	Epoxyalcohol synthase
EC	Enzyme class
EDTA	Ethylenediaminetetraacetic acid
EI	Electron ionization
EK	Enterokinase cleavage site
ELSD	Evaporative light scattering detector
ESI	Electron spray ionization
et al	*et alii* (and others)
FID	Flame ionization detector
FPLC	Fast protein liquid chromatography
g	Gravity
GC	Gas chromatography

GLV	Green Leaf Volatile
HF	High-Fidelity
His	Histidine
HPL	Hydroperoxide lyase
HPLC	High performance liquid chromatography
HPODE	Hydroperoxyoctadecadienoic acid
HPOTE	Hydroperoxyoctadecatrienoic acid
HRP	Horseradish peroxidase
IEX	Ion exchange chromatography
Ile	Isoleucine
IPTG	Isopropyl β-D-1-thiogalactopyranoside
Kan	Kanamycin
Kan^R	Kanamycin resistance
LB	Lysogeny broth
LDH	Lactate dehydrogenase
LOX	Lipoxygenase
Lys	Lysine
MOPS	3-(N-morpholino)propanesulfonic acid
MS	Mass spectrometry
MTBE	tert-Butyl methyl ether
NADH	Nicotinamide adenine dinucleotide
NADPH	Nicotinamide adenine dinucleotide phosphate
NCBI	National Center for biotechnology information
OD	Optical density
PAGE	Polyacrylamide gel electrophoresis
PCR	Polymerase chain reaction
PDB	Protein data bank
pH	Negative common logarithm of proton concentration
PHA	Polyhydroxyalkanoates
PHB	Polyhydroxybutyrate
PLA	Polylactic acid
PLAT	Polycystin-1, Lipoxygenase, Alpha-Toxin
PLP	Pyridoxal-5-phosphate
PMP	Pyridoxamine 5'-phosphate
PMSF	Phenylmethylsulfonyl fluoride
POX	Peroxygenase

PUFA	Polyunsaturated fatty acid
PVDF	Polyvinylidene difluoride
rpm	Revolutions per minute
SDS	Sodium dodecyl sulfate
SEC	Size exclusion chromatography
TA	Transaminase
TBST	Tris-buffered saline with Tween20
TE	Tris-EDTA
TEMED	Tetramethylethylenediamine
Tris	Tris(hydroxymethyl)aminomethane
U	Unit
UV	Ultraviolet
V	Volt

Summary

In this work, novel enzyme cascades for the synthesis of polymer building blocks 12-oxododecenoic acid and 12-aminododecenoic acid were developed starting from linoleic acid or safflower oil. For this purpose, one soybean lipoxygenase (LOX), four plant hyroperoxide lyases (HPL*s*) and seven bacterial ω-transaminases (ω-TA*s*) were cloned, expressed in *Escherichia coli* and characterized.

13(*S*)-specific lipoxygenase LOX-1 from *Glycine max* (soybean), which catalyzes the hydroperoxidation of linoleic acid to 13(*S*)-hydroperoxyoctadecadienoic acid (13(*S*)-HPODE) was successfully cloned, expressed in *E. coli* and purified. An activity of 4.2 U·mg^{-1} in the soluble fraction and 150.3 U·mg^{-1} after affinity chromatography purification was achieved. Four plant-derived HPLs with 13(*S*)-specificity were selected from literature and databank searches. The synthetic genes were cloned, expressed and the corresponding proteins were analyzed. Since activity of the full-length HPL*s* was low, the hydrophobic, unconserved N-terminus were removed. In addition, NusAHPL fusion proteins were constructed. The specific activities of all HPLs were increased significantly. Truncated $HPL_{CP\text{-}N}$ from *Carica papaya* (papaya) showed highest activity with 0.85 U·mg^{-1} in the soluble fraction and was hence selected for further experiments. A rapid cleavage of linoleic acid hydroperoxide to 12-oxo-9(*Z*)-dodecenoic acid and hexanal was demonstrated for $HPL_{CP\text{-}N}$ by gas chromatography. The isomerization of 12-oxo-9(*Z*)-dodecenoic acid to 12-oxo-10(*E*)-dodecenoic acid (traumatin) could be reduced by utilization of purified HPL instead of the soluble fraction. Furthermore, seven bacterial ω-TAs were actively expressed and affinity-purified. A coupled photometric assay with lactate dehydrogenase and NADH was developed, demonstrating activity of all enzymes towards hexanal, 12-oxo-9(*Z*)-dodecenoic acid and 12-oxo-10(*E*)-dodecenoic acid. ω-TA from *Aquitalea denitrificans* (TR_{AD}) showed the highest activity with 1.17 U·mg^{-1} on hexanal, 0.62 U·mg^{-1} on the 9(*Z*) isomer and 0.52 U·mg^{-1} on the 10(*E*) isomer. In addition, mass spectrometric analysis demonstrated the formation of 12-aminododecenoic acid and hexylamine as transamination products of the oxo acid and hexanal.

One-pot reactions were carried out in small scale for the synthesis of 12-oxo-9(*Z*)-dodecenoic acid with *Pseudomonas fluorescens* lipase, LOX-1 and $HPL_{CP\text{-}N}$ starting from linoleic acid-rich safflower oil. A yield of 43 % 12-oxo-9(*Z*)-dodecenoic acid was achieved. In addition, one-pot reactions were conducted for the synthesis of 12-aminododecenoic acid using LOX-1, $HPL_{CP\text{-}N}$ and TR_{AD} with linoleic acid as substrate. A yield of 12 % of 12-aminododecenoic acid was reached. To our knowledge, in this work, the enzymes of the oxylipin pathway were coupled for the first time with a ω-TA for the synthesis of the nylon-12 monomer 12-aminododecenoic acid. This provides a new route for obtaining nylon-12 from C_{18}-rich plant oils.

Zusammenfassung

In dieser Arbeit wurden neue Enzymkaskaden für die Synthese der Polymervorstufen 12-Oxododecensäure und 12-Aminododecensäure aus Linolsäure bzw. Distelöl entwickelt. Hierfür wurden eine Sojabohnen-Lipoxygenase (LOX), vier pflanzliche Hyroperoxidlyasen (HPLs) und sieben bakterielle ω-Transaminasen (ω-TAs) kloniert, in *Escherichia coli* exprimiert und charakterisiert.

Die 13(*S*)-spezifische Lipoxygenase LOX-1 aus *Glycine max* (Sojabohne), die die Hydroperoxidierung von Linolsäure zu 13(*S*)-Hydroperoxyoctadecadiensäure (13(*S*)-HPODE) katalysiert, wurde erfolgreich kloniert, in *E. coli* exprimiert und aufgereinigt. Es wurde eine Aktivität von 4,2 U·mg^{-1} in der löslichen Fraktion und 150,3 U·mg^{-1} nach Reinigung mit einer Affinitätschromatographie erreicht. Vier pflanzliche 13(*S*)-spezifische HPLs wurden mithilfe einer Literatur- und Datenbanksuche ausgewählt. Die synthetischen Gene wurden kloniert, exprimiert und die entsprechenden Proteine analysiert. Da die Aktivität der Wildtyp-HPLs in voller Länge gering war, wurden die hydrophoben, nicht-konservierten N-terminalen Sequenzen entfernt. Darüber hinaus wurden NusAHPL-Fusionsproteine konstruiert. Dadurch konnte die spezifische Aktivität aller HPLs signifikant erhöht werden. Die N-terminal deletierte $HPL_{CP\text{-}N}$ aus *Carica papaya* (Papaya) zeigte mit 0,85 U·mg^{-1} in der löslichen Fraktion die höchste Aktivität und wurde daher für weitere Versuche ausgewählt. Eine schnelle Spaltung des Linolsäurehydroperoxids zu 12-Oxo-9(*Z*)-Dodecensäure und Hexanal wurde für $HPL_{CP\text{-}N}$ mittels Gaschromatographie nachgewiesen. Die Isomerisierung von 12-Oxo-9(*Z*)-dodecensäure zu 12-Oxo-10(*E*)-dodecensäure (Traumatin) konnte durch die Verwendung von gereinigtem HPL anstelle der löslichen Fraktion deutlich reduziert werden. Darüber hinaus wurden sieben bakterielle ω-TAs aktiv exprimiert und mit Affinitätschromatographie aufgereinigt. Es wurde ein gekoppelter photometrischer Assay mit einer Laktatdehydrogenase und NADH entwickelt, der die Aktivität aller Enzyme gegenüber Hexanal, 12-Oxo-9(*Z*)-Dodecensäure und 12-Oxo-10(*E*)-Dodecensäure nachwies. Die ω-TA aus *Aquitalea denitrificans* (TR_{AD}) zeigte die höchste Aktivität mit 1,17 U·mg^{-1} gegenüber Hexanal, 0,62 U·mg^{-1} gegenüber dem 9(*Z*)-Isomer und 0,52 U·mg^{-1} gegenüber dem 10(*E*)-Isomer. Zusätzlich wurde die Bildung von 12-Aminododecensäure und Hexylamin als Transaminationsprodukte der Oxosäuren und Hexanal durch Massenspektrometrische Analysen nachgewiesen.

Des Weiteren wurden Eintopfreaktionen im kleinen Maßstab für die Synthese von 12-Oxo-9(*Z*)-dodecensäure mit einer *Pseudomonas fluorescens* Lipase, LOX-1 und $HPL_{CP\text{-}N}$ aus linolsäurereichem Distelöl durchgeführt. Hierbei konnte eine Ausbeute von 43 % 12-Oxo-9(*Z*)-Dodecensäure erzielt werden. Außerdem wurden Eintopfreaktionen zur Synthese von 12-Aminododecensäure mit LOX-1, $HPL_{CP\text{-}N}$ und TR_{AD} aus Linolsäure durchgeführt, wobei eine

Ausbeute von 12 % 12-Aminododecensäure erreicht wurde. Unseres Wissens nach wurden in dieser Arbeit die Enzyme des Oxylipinwegs das erste Mal mit einer ω-TA zur Synthese des Nylon-12 Monomers 12-Aminododecensäure gekoppelt. Dies eröffnet einen neuen Weg zur Gewinnung von Nylon-12 aus C_{18}-reichen Pflanzenölen.

1. Introduction

1.1. Scope of the thesis

In 2020, around 367 million tons of plastics were produced worldwide [1], the majority of which were synthesized through energy-intensive chemical routes using petroleum-derived naphtha. In contrast, biopolymers are a more sustainable alternative, as they are mostly produced biotechnologically from renewable raw materials such as vegetable oil, cellulose or starch, and in many cases are more biodegradable [2]. Although the use of microorganisms and enzymes for the synthesis of a wide variety of products such as pharmaceuticals and fine chemicals is gaining importance [3, 4], only 2 % of all polymers were biobased in 2018 [5]. An increase in the proportion of biotechnologically produced polymers is expected, as they are synthesized under mild conditions such as low temperature and without the use of toxic chemicals [6]. Another advantage of using microorganisms and enzymes is the suppression of unwanted by-products, which facilitates product processing. Furthermore, due to the higher chemo- and regioselectivity, fewer reaction steps are often required compared to chemical processing [6, 7]. Important bio-based polymers are polyhydroxyalkanoates (PHA), polylactic acid (PLA), polyhydroxybutyrate (PHB), polyurethanes and polyamides [6, 8].

Polyamides are linear polymers with repeating amide bonds. Medium- to long-chain polyamides such as nylon-11 or nylon-12 are highly resistant to UV, chemicals and temperature. They find application as specialty polymers in the automotive industry or electronic industry [9]. Traditionally, the production of nylon-12 is based on petroleum-derived butadiene and upon trimerization, cyclododecane oxime synthesis and Beckmann rearrangement, ω-laurolactam is formed. Finally, nylon-12 is obtained by ring opening polymerization of the laurolactam [10, 11]. For 2026 the global market for polyamides is expected to reach a value of $38 billion, making biobased polyamide production a rewarding target [12].

To circumvent the use of fossil resources, several processes for the production of biobased nylon precursors have been developed in recent years. For the synthesis of 11-aminoundecanoic acid, an enzyme cascade including alcohol dehydrogenase (ADH), Baeyer-Villiger monooxygenase (BVMO), esterase and ω-transaminase (ω-TA) was developed starting from 12-hydroxystearic acid [13]. In another approach, 12-aminododecanoic acid methyl ester was synthesized from methyl laurate using a whole-cell biocatalyst for expression of an alkane monooxygenase and a ω-TA [14]. This process was further improved by implementation of an alanine regeneration system to supply cosubstrates and thereby increasing 12-aminododecanoic acid methyl ester synthesis [11, 15].

Although this biocatalytic process reveals an interesting route to nylon-12, the use of methyl laurate is problematic. Biobased lauric acid can only be obtained from the oils of coconut palms and oil palms, which are growing in wet tropical climate zones. An increased use of these tropical oils would raise up the issue of deforestation of pristine rainforests to gain additional land for palm cultivation [16, 17]. Thus, the scope of this thesis was the development of a more sustainable process for the synthesis of nylon-12, based on linoleic acid-rich vegetable oils, which grow in temperature to subtropical climate zones (Fig. 1).

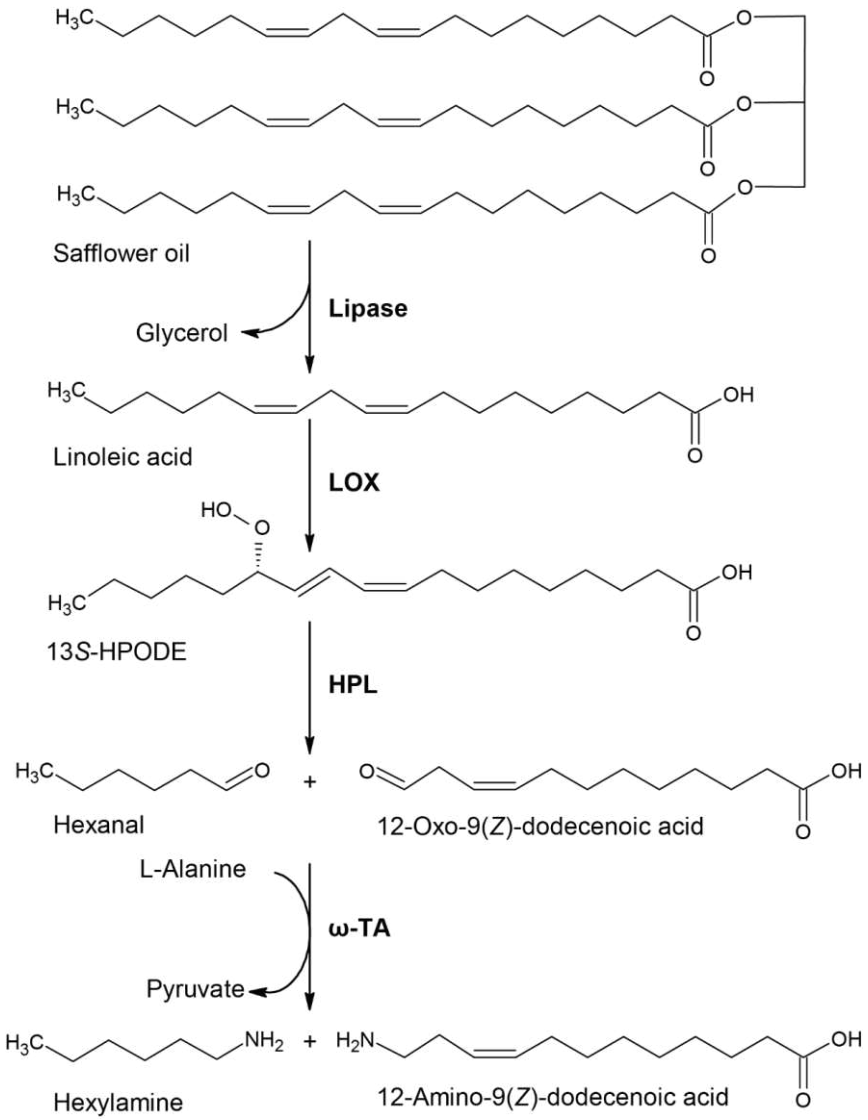

Fig. 1 Reaction scheme of the enzyme cascade for the synthesis of 12-aminododecenoic acid and hexylamine starting from safflower oil using a lipase, a lipoxygenase (LOX), a hydroperoxide lyase (HPL) and a ω-transaminase (ω-TA).

This thesis is part of the BMBF-funded project Linopol, which covered the development of chemical and enzymatic routes to nylon-12 precursors. Starting from safflower oil, an enzymatic cascade was proposed via lipase catalyzed triglyceride hydrolysis, lipoxygenase (LOX) mediated hydroperoxidation, followed by hydroperoxide lyase (HPL) cleavage and finally transamination

of the resulting aldehydes with a ω-transaminase (ω-TA). Valentin Gala Marti, who was also involved in the project, optimized the lipase hydrolysis and LOX hydroperoxidation with commercially available enzymes in his doctoral thesis. The topic of this thesis was the cloning, microbial expression and purification of soybean LOX-1, plant-derived HPLs and microbial ω-TAs. The enzymes were screened for activity, the reaction conditions were optimized and finally, the enzymes were coupled in cascade reactions.

1.2. The lipoxygenase pathway

Plants are exposed to numerous environmental changes and must adapt quickly to survive. In this regard, lipid-derived oxylipins play an important role in plant development, growth and defense [18]. Many of these compounds are metabolized via the lipoxygenase pathway, which comprises the transformation of polyunsaturated fatty acids (PUFAs) by several enzymes. After hydrolysis of a triglyceride containing linoleic or α-linolenic acid, a lipoxygenase (LOX) catalyzes the hydroperoxidation of linoleic and α-linolenic acid to the corresponding 9(*S*)- or 13(*S*)-hydroperoxide (9(*S*)- or 13(*S*)-HPODE/ HPOTE). Subsequently, different enzymes catalyze their further transformation, including allene oxide synthase (AOS), hydroperoxide lyase (HPL), epoxyalcohol synthase (EAS), divinyl ether synthase (DES), peroxygenase (POX), lipoxygenase (LOX) and reductase [19] (Fig. 2).

AOS synthesizes unstable allene oxides, which are further converted into the plant hormone jasmonic acid and its derivatives. These metabolites are important molecules for plant development and response to biotic and abiotic stress [20–22]. HPL catalyzes the lysis of the fatty acid hydroperoxide into an oxoacid and a volatile aldehyde. These aldehydes, also known as green leaf volatiles (GLVs) obtain a “fresh green” scent of plants and act as signaling molecules, which induce cell defense in itself and surrounding plants after herbivore attack. Additionally, they exhibit antimicrobial and antifungal activity [23–25]. The C_{12} oxoacid 12-oxo-9(*Z*)-dodecenoic acid is further isomerized to 12-oxo-10(*E*)-dodecenoic acid, also known as traumatin. Traumatin acts as a plant wound hormone and growth promoter [26]. DES synthesizes divinyl ethers such as colnelenic and colneleic acid, which possess antimicrobial activity [27]. POX and EAS catalyze the synthesis of epoxy hydroxy polyunsaturated fatty acids, which exhibit antifungal properties [28, 29]. The products formed by EAS are regiochemically identical to those of POX, but differ in terms of their stereochemistry [19]. In addition, a reductase can form hydroxy PUFAs and LOX can further convert fatty acid hydroperoxides into keto derivatives [19, 30].

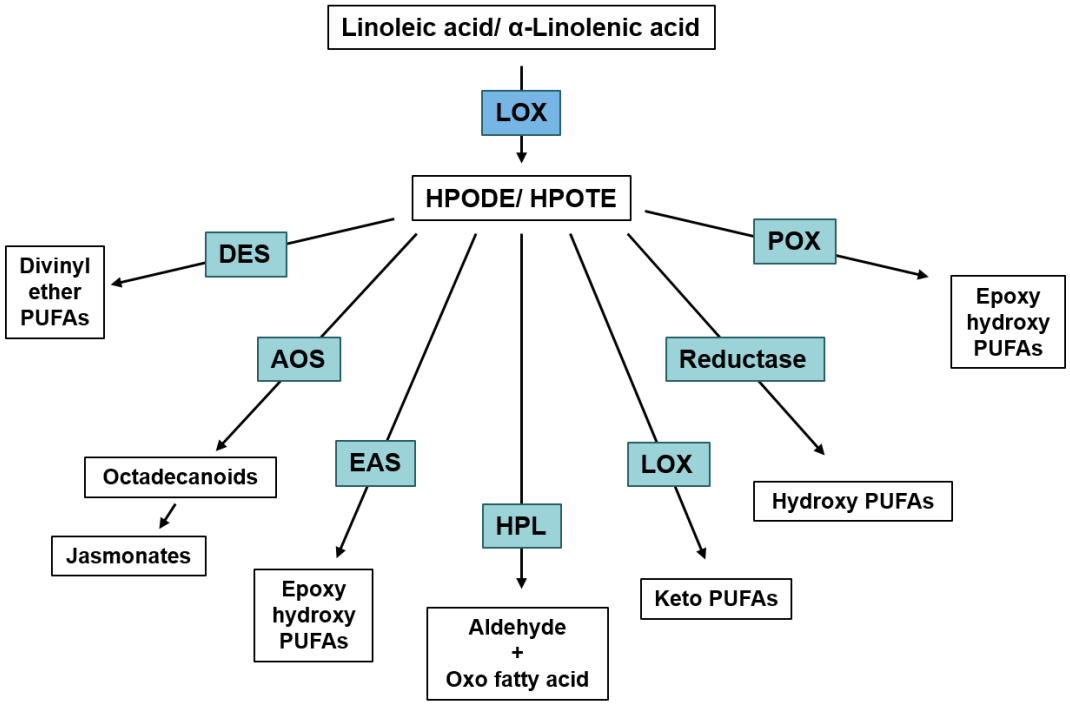

Fig. 2 The lipoxygenase (LOX) pathway in plants. LOX catalyzes the hydroperoxidation of linoleic acid/ α-linolenic acid to the hydroperoxides 9(*S*)- or 13(*S*)-HPODE/ HPOTE. The hydroperoxides can be further metabolized with an allene oxide synthase (AOS), a hydroperoxide lyase (HPL), a divinyl ether synthase (DES), an epoxyalcohol synthase (EAS), a peroxygenase (POX) and a lipoxygenase (LOX) (figure adapted and modified from [19]).

1.3. Enzyme sources, properties, structure and function

1.3.1. Lipoxygenases

Lipoxygenases (EC 1.13.11.X) are non-heme iron- or manganese-containing dioxygenases that catalyze the regio- and stereospecific oxygenation of polyunsaturated fatty acids, yielding conjugated unsaturated fatty acid hydroperoxides [31]. They are widely distributed in plants, as well as in animals, fungi and bacteria [32–34]. Known LOXs accept PUFAs such as arachidonic acid, linoleic acid, α-linolenic acid, eicosapentaenoic acid or docosahexaenoic acid as substrates and are able to catalyze peroxidation at positions 5-15 of the substrate carbon chain [35–38]. Accordingly, they are termed 5-LOX, 8-LOX and so on based on their preferred oxygenation site [39]. Plant LOXs exhibit a limited natural substrate spectrum comprising linoleic acid and α-linolenic acid and catalyze hydroperoxidation at position 9 or 13. Consequently, they are termed 9-LOX and 13-LOX [35].

In addition, LOXs can be classified into type-1 LOX and type-2 LOX based on their sequence similarities. Type-1 LOXs are mainly located outside the plastids and have a high sequence similarity to each other (>75 %), whereas type-2 LOXs have a plastidial transit peptide and are therefore mainly found in chloroplasts. They have a sequence similarity of about 35 % [40].

Besides the common iron-containing LOXs, enzymes binding manganese in the active site have been detected in some fungi and are termed MnLOXs [41–43]. Additionally, fusion LOXs, which have a dual catalytic function as LOX-AOS or LOX-HPL were identified in some corals and cyanobacteria [44, 45]. Mini LOXs have been found in some cyanobacteria and are significantly shorter than normal LOXs, but exhibit full functionality [46–48]. Often, there are multiple LOX isoforms in a species that differ in terms of pH optimum, substrate preference and regiospecificity [49]. *Glycine max* (soybean), for example, has at least eight isozymes, three of which are located in the seeds and five in the vegetative tissues [50].

Plant LOXs are monomeric proteins that contain two domains and have a molar mass of 94-100 kDa [51] (Fig. 3a). The smaller N-terminal β-barrel domain, known as the PLAT (Polycystin-1, Lipoxygenase, Alpha-Toxin) domain of 25–50 kDa has a membrane binding site [52, 53]. The larger C-terminal domain, consisting mainly of α-helices and coils, is around 55-65 kDa in size and contains the active site with a bound iron atom as cofactor inside the substrate binding pocket [53, 54]. In plant LOXs, iron is coordinated in an octahedral form by three histidines, an amino group of e.g. asparagine, a carboxyl group of mostly isoleucine and a water molecule (Fig. 3b) [53, 55]. In mammalian LOXs, the iron cation is coordinated by four histidines, a carboxyl group of isoleucine and a water molecule [40]. When a PUFA binds the LOX in the binding pocket, the water molecule is replaced by the fatty acid [56].

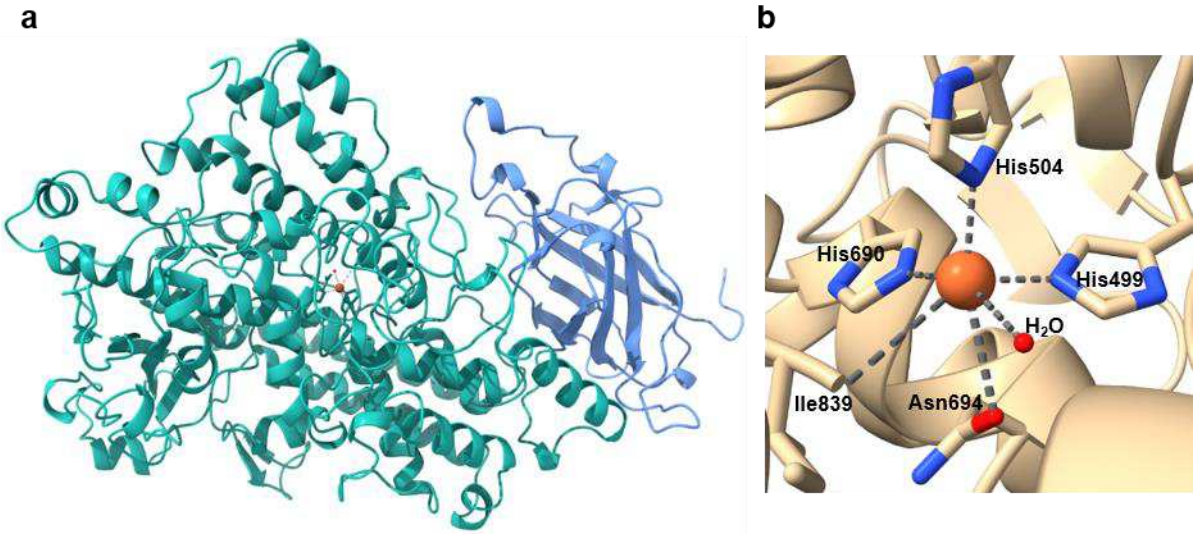

Fig. 3 Crystal structure (**a**) and active site (**b**) of lipoxygenase LOX-1 from *G. max* (PDB: 1YGE) [53]. (**a**) The N-terminal domain is colored turquoise, the bound iron is colored orange and the C-terminal domain is colored blue. (**b**) The active site with the iron (orange ball) is coordinated in an octahedral form by His499, His504, His690, Asn694, Ile839 and a water molecule. The protein images were drawn with UCSF ChimeraX [57].

The reaction mechanism of lipoxygenases consists of four reaction steps as outlined in Fig. 4 [54]. In its inactive form, the LOX-bound iron is present as Fe^{2+} and is activated by oxidation to Fe^{3+},

presumably due to traces of fatty acid hydroperoxides. In its activated form, Fe^{3+} can bind the PUFA substrate. Then, in the first reaction step, the hydrogen is abstracted from the methyl group of the carbon between the cis-cis bond of the PUFA and Fe^{3+} is reduced to Fe^{2+}. Next, the radical electron is shifted either towards the carboxyl or methyl end of the PUFA and a radical rearrangement occurs. In the third step, oxygen is inserted antarafacially and a hydroperoxy radical is formed. Finally, the hydroperoxy radical is reduced by Fe^{2+} to its anion, while the iron is reoxidized to Fe^{3+} and is ready for another catalytic cycle [54, 58]. Starting from linoleic acid as substrate, either 13(*S*)-hydroperoxyoctadecadienoic acid (13(*S*)-HPODE) or 9(*S*)-hydroperoxyoctadecadienoic acid (9(*S*)-HPODE) are formed, whereas 13(*S*)-hydroperoxyoctadecatrienoic acid (13(*S*)-HPOTE) or 9(*S*)-hydroperoxyoctadecatrienoic acid (9(*S*)-HPOTE) are the products from α-linolenic acid transformation.

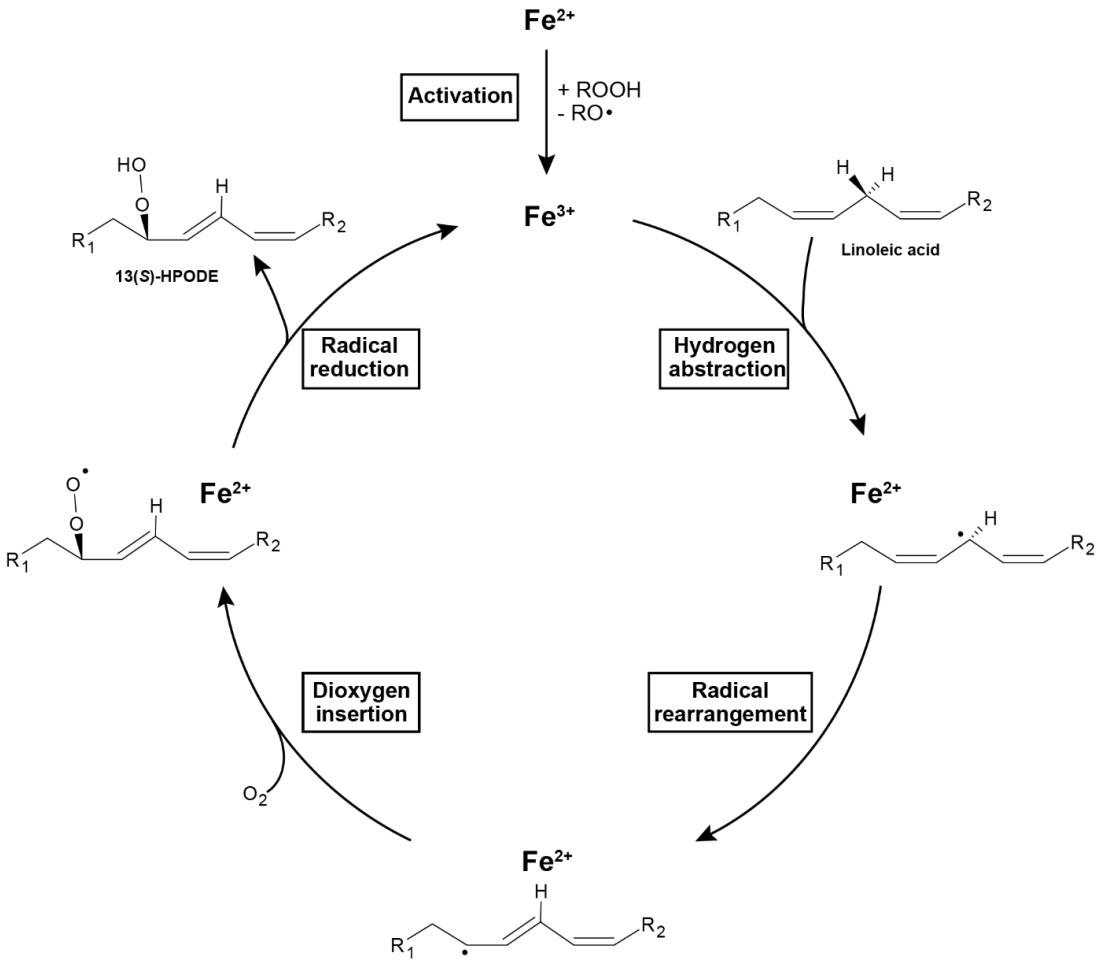

Fig. 4 Reaction mechanism of lipoxygenases consisting of (1) hydrogen abstraction, (2) radical rearrangement, (3) oxygen incorporation and (4) reduction of the hydroperoxy radical (figure adapted and modified from [54]).

LOX enzymes can be obtained either from plant seeds and tissues or by recombinant expression in microbial hosts. Soybean flour has a relatively high lipoxygenase content, which, combined with its easy access and low costs, makes it a suitable source of lipoxygenase [59, 60]. However,

soybeans possess many different isozymes with varying regioselectivity leading to simultaneous formation of the 9(*S*)-HPODE or 13(*S*)-HPODE regioisomers. Hence, separation and purification processes are required to obtain pure isozyme for regiospecific product synthesis [61, 62]. Several purification steps such as ammonium sulfate precipitation, ion-exchange and size-exclusion chromatography can be applied to obtain pure LOX enzyme from plant material [63, 64].

However, since multi-step purification of plant-based LOXs is tedious, heterologous expression of lipoxygenases in a microbial expression system may be advantageous. In recent years, several lipoxygenases have been heterologously expressed in bacteria (e.g. *Escherichia coli*), yeasts (e.g. *Pichia pastoris* or *Saccharomyces cerevisiae*) or other fungi (e.g. *Aspergillus nidulans*) [65–67]. Furthermore, heterologously expressed LOXs were purified with chromatography systems, either by ion-exchange and size-exclusion chromatography or by simple one-step affinity chromatography [46, 65, 68]. Various attempts were made to improve the yield of active enzyme from expression, such as lowering the cultivation temperature to 8-20 °C or by adding low amount of ethanol as an elicitor for heat-shock proteins, which are known to promote proper protein folding [65, 69, 70]. In addition, extracellular enzyme secretion was performed by adding signal peptides for the expression of *Pseudomonas aeruginosa* LOX in *E. coli* or of *Gaeumannomyces graminis* MnLOX in *P. pastoris* [71, 72].

1.3.2. Hydroperoxide lyases

Hydroperoxide lyases (HPLs) are heme- and iron-binding P450 cytochrome enzymes of the CYP74 family of enzymes [73]. Despite their name, hydroperoxide lyases were re-classified as isomerases [74]. They catalyze the isomerization of LOX-derived HPODEs and HPOTEs into a hemiacetal that is spontaneously decomposed into an aldehyde and an oxoacid [74]. HPLs are divided into the subgroups CYP74B comprising 13-HPLs and CYP74C comprising both 9-HPLs and 9/13-HPLs. The enzymes are categorized according to the regiospecificity of substrate recognition, e.g. 13-HPL accept 13-HPODE and 13-HPOTE [75–78]. Other enzymes of the CYP74 family include allene oxide synthases, divinyl ether synthases and epoxy alcohol synthases [79, 80]. Unlike other cytochrome P450 proteins, the members of the CYP74 family do not require molecular oxygen or NADH/NADPH for their catalytic activity [81, 82].

The reaction mechanism of HPLs, proposed by Grechkin et al., is shown exemplarily for a 13-HPL in Fig. 5. In the first reaction step, the hydroperoxide is cleaved and an epoxy radical is formed, while the hydroxyl radical binds the iron and a ferryl-hydroxo complex is formed. The epoxy radical is cleaved at the oxirane C-C-bond and rebinds the hydroxyl radical, forming a hemiacetal and reducing iron back to Fe^{3+}. The unstable, short-lived hemiacetal spontaneously dissociates to a C_6 aldehyde (hexanal or 3(*Z*)-hexenal) and a C_{12} enol. The enol is further converted to

12-oxo-9(*Z*)-dodecenoic acid and the isomer 12-oxo-10(*E*)-dodecenoic acid (traumatin) is formed as a side product by shifting the conjugated double bond system. Some traumatin was also supposed to be formed directly from the enol [74]. Similarly, the hemiacetal spontaneously dissociates into a C_9 aldehyde (nonanal or 3(*Z*)-nonenal) and a C_9 oxoacid (9-oxononanoic acid) when 9(*S*)-HPODE or 9(*S*)-HPOTE was the substrate [83].

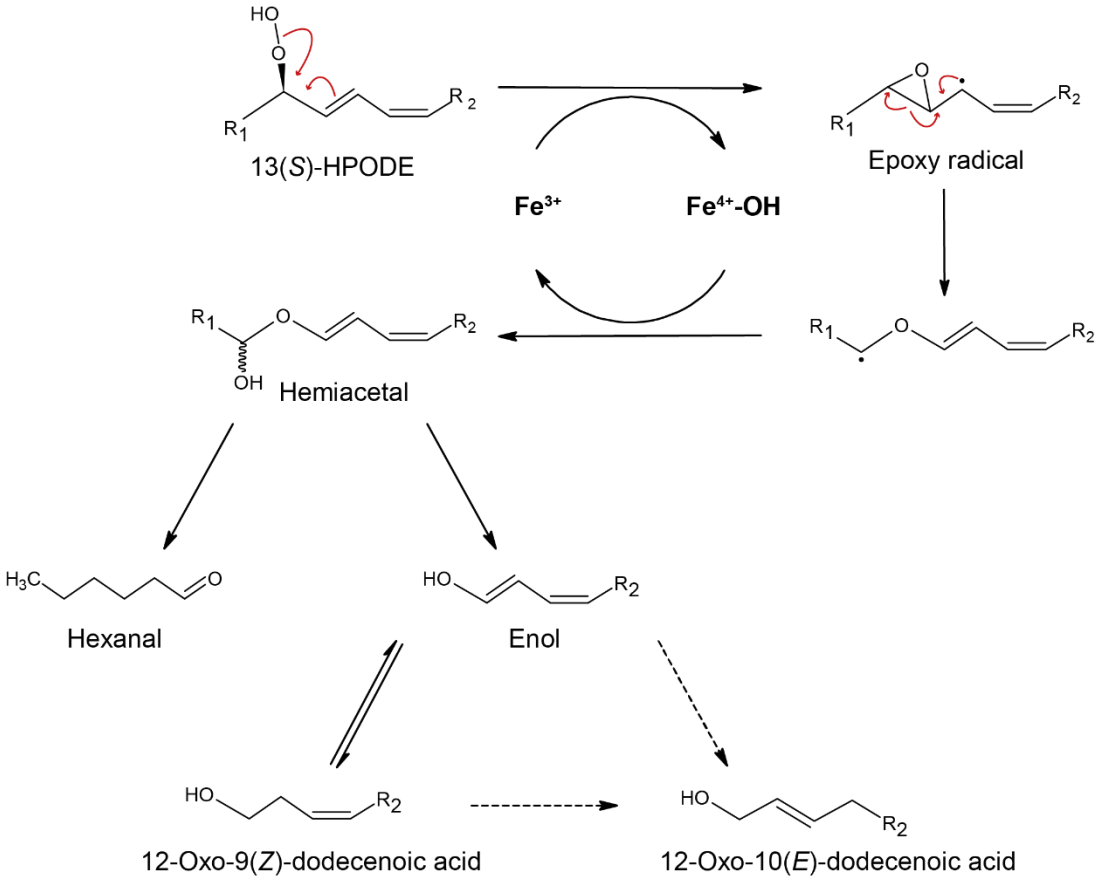

Fig. 5 Reaction mechanism of HPL catalysis on the example of 13(*S*)-HPODE. A hemiacetal is formed after cleavage of 13(*S*)-HPODE at the O-O-bond. The hemiacetal is decomposed to hexanal and a C_{12} enol that is further converted to 12-oxo-9(*Z*)-dodecenoic acid. 12-Oxo-10(*E*)-dodecenoic acid (traumatin) is either formed through isomerization of 12-oxo-9(*Z*)-dodecenoic acid or directly from the C_{12} enol (figure adapted and modified from [74]).

HPLs are hydrophobic enzymes of around 55-72 kDa [39]. Analyses revealed that the enzymes occur either as tetramers, e.g. shown for guava or sunflower HPL [84, 85], or as trimers in the case of green bell pepper HPL [86]. In their active site, HPLs obtain a heme type *b* that binds an iron [87]. To date, no crystal structure of a HPL has been published. However, two crystal structures of the CYP74-member AOS have been solved for *Parthenium argentatum* AOS and *Arabidopsis thaliana* AOS (Fig. 6a) [88, 89]. Since HPL and AOS share high sequence homology, these tertiary structures may serve as structural models for HPL structure. A putative model of papaya HPL was constructed based on the AOS crystal structure of *A. thaliana* (PDB number: 3CLI) using the Swiss-model program [90] (Fig. 6b; template-model alignment in appendix, Fig. A2).

Since the unconserved N-terminal sequences of HPLs and AOSs are highly variable, the HPL model did not forecast the N-terminal region (as shown for AOS in blue). In accordance to other P450 enzymes, the iron-coordinating heme in AOS is located between two helices. It is likely that this is similar for HPLs, although it was not observed in the model enzyme. Interestingly, an amino acid substitution of phenylalanine at position 137 to leucine of *A. thaliana* AOS resulted in a variant with HPL activity [89]. Phenylalanine was found to be highly conserved at this position in AOSs with its aromatic site in proximity to the bound substrate. It was suggested that it is important for the stabilization of the epoxide radical intermediate, leading to the formation of an allene oxide. In contrast, HPLs contain a conserved leucine at this position, which cannot stabilize the radical intermediate, leading to electron rearrangement and formation of an unstable hemiacetal. In addition, replacement of the highly conserved serine (Ser155), which is also located near the substrate pocket, with an alanine increased HPL activity [89]. Similarly, single amino acid substitutions at these positions of AOSs from *Oryza sativa* and *Lycopersicon esculentum* resulted in a change in activity to a HPL [89, 91].

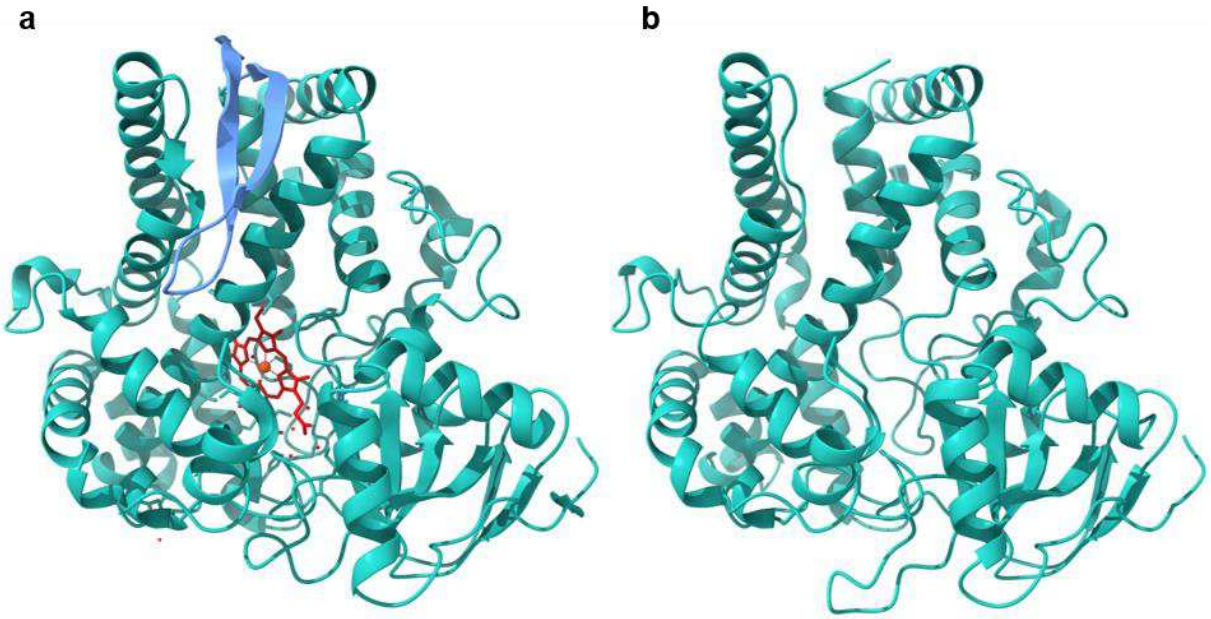

Fig. 6 Crystal structure of (**a**) allene oxide synthase (AOS) from *A. thaliana* (PDB: 3CLI) [89] and (**b**) Swiss-model [90] of putative papaya hydroperoxide lyase HPL_{CP}, based on *A. thaliana* AOS sequence (template-model alignment in Fig. A2). The N-terminal sequence in AOS is colored in blue and due to high unconserved amino acids, cannot be seen in the HPL_{CP} Swiss-model. The heme in the AOS is colored in red and the iron is colored in orange. The protein images were drawn with UCSF ChimeraX [57].

HPLs are widely distributed and are found in both higher and lower plants such as mosses [78, 92, 93]. While 13-HPLs are mainly found in leaves and green tissues, 9/13-HPLs have also been identified in roots [94]. The hydrophobic HPLs are most likely membrane-bound and localized in chloroplasts, microsomes and some were even found in lipid bodies [75, 95, 96]. A

N-terminal chloroplast transit peptide sequence has been identified in HPLs from *A. thaliana* and *Olea europaea* (olive), whereas HPLs from *L. esculentum* (tomato) and *Medicago sativa* (alfalfa) do not exhibit this sequence [97–99].

HPLs can be extracted and purified from plant tissue [100, 101]. However, unlike LOXs, HPLs are not expressed in high quantities in plants, resulting in low yields. In addition, the availability of plant material depends on seasons and changing agricultural conditions [39, 102]. Due to these problems, heterologous expression became the method of choice and several HPLs have been successfully expressed for enzyme characterization and fragrance production [103–106]. Different expression strains were used such as bacteria (e.g. *E. coli*) [107], yeasts (e.g. *P. pastoris* or *Yarrowia lipolytica*) [108, 109] and plant cells (e.g. *Nicotiana tabacum*) [110]. Still it remains difficult to obtain soluble and active enzyme. The addition of salt in high concentration, glycine or glycerol has been shown to improve enzyme stability and activity [107, 111–113]. Since most HPLs are membrane associated, they need to be solubilized. This has often been achieved by the addition of detergents such as Triton X-100, emulphogene or polyvinylpolypyrrolidone [84, 114, 115]. Another approach to improve the solubility of HPLs was sequence modification either by abstraction of the hydrophobic, unconserved N-terminal sequence, by coupling HPL to a fusion protein or by directed evolution [84, 97, 103]. The hydrophobic N-terminal sequence of HPLs is about 20 to 30 amino acids in length and shows no homology between the HPL homologs. In *A. thaliana* HPL, this sequence was considered to be a plastidic transit sequence, whereas in other HPLs, this sequence was designated as part of a pro-enzyme within a post-translational regulation mechanism [97]. After deletion of the unconserved N-terminus in different HPLs, activity increased significantly [84, 97, 103]. Brühlmann et al. (2013) engineered an improved guava HPL by N-terminal deletion, fusion with the fusion protein MBP (maltose binding protein) and directed evolution. The randomly mutated HPL reached a 15-fold higher product yield factor compared to the MBP-HPL fusion protein [103].

1.3.3. Transaminases

Transaminases (EC 2.6.1.X) are pyridoxal-5-phosphate (PLP)-dependent enzymes catalyzing the transfer of an amino group from a primary amine (amine donor) to an aldehyde, ketone or α-keto acid (amine acceptor) [116]. Transaminases are ubiquitous distributed in all organisms where they play key roles in metabolic pathways [117]. They were first described in the 1930s [118, 119] and were, for example, shown to be essential for amino acid and nitrogen metabolism, where they transfer amino groups among amino and keto acids [117].

Transaminases are divided into α-amino acid aminotransferases (α-AATs) and ω-amino acid transferases, hereafter referred to as ω-transaminases (ω-TAs). α-AATs require the presence of a

carboxylic group in the α-position to the amine/ ketone for transamination, whereas the carboxylic group can be more distal to the amine/ ketone for ω-TAs [117, 120]. Some ω-TAs are also capable of transaminating amine/ keto substrates that lack the carboxylate function. They are referred to as amine transaminases (ATAs) and are of great interest for industrial and pharmaceutical applications for the synthesis of chiral amines [121, 122]. ATAs in turn are divided into (*S*)-selective amine transaminases ((*S*)-ATAs) and (*R*)-selective amine transaminases ((*R*)-ATA) [123]. (*S*)-ATAs catalyze the (*S*)-selective transamination and many representatives have been identified and characterized in recent years, including, for example, (*S*)-ATA from *Chromobacterium violaceum*, *Paracoccus denitrificans* and *Vibrio fluvalis* [124–126]. (*R*)-ATAs catalyze the (*R*)-selective transamination and are less common than (*S*)-ATAs [123]. The first (*R*)-ATA was discovered in *Arthrobacter* sp. KNK168 in 2006 [127]. Other examples were identified, for example, in *Aspergillus fumigatus* and *Aspergillus terreus* [128, 129]. Höhne et al. identified key motifs for the enantioselectivity and substrate preferences, allowing *in silico* prediction of (*R*)-ATAs. In this way, 17 (*R*)-ATAs were identified [121].

Besides the division into α-AATs and ω-TAs, transaminases can be classified into six classes based on their amino acid sequences [119, 123]. In addition, transaminases can be categorized based on their structure. PLP-dependent enzymes that not only comprise transaminases but also enzyme classes such as lyases or racemaces can be classified into seven structurally distant fold types [130, 131]. Herein, transaminases are only found in fold types I and IV. Fold type I comprises class I and II TAs (aspartate and aromatic α-AATs), class III TAs (ω-TAs including (*S*)-ATAs) and class V TAs (phosphoserine α-AATs). Fold type IV transaminases covers class IV TAs (branched chain α-AATs, D-amino acid transaminases and ω-TAs including (*R*)-ATAs,) and class VI TAs (sugar α-AATs) [119, 132].

The crystal structures of several transaminases have been solved in recent years [124, 125, 128, 129], highlighting that TAs of both fold types are homodimers. Each monomer has a small and a large domain with the active site in their interface [129]. Fig. 7 shows the crystal structures of the two folding types exemplified by the (*S*)-ATA from *C. violaceum* (fold type I) and (*R*)-ATA from *A. terreus* (fold type IV). The two folding types differ in their active site, with folding type I and folding type IV transaminases being like mirror images of each other, leading to either (*S*)- or (*R*)-enantioselectivity [129].

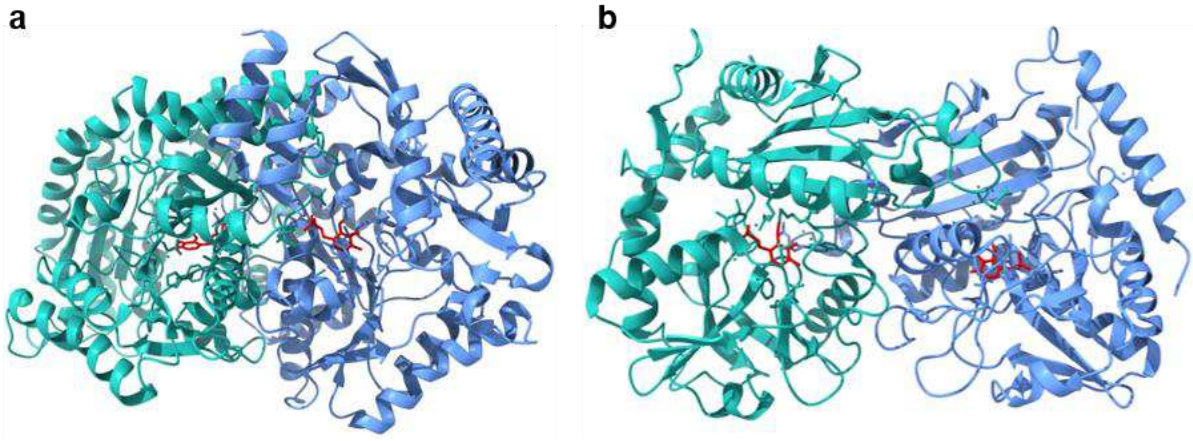

Fig. 7 Crystal structures of the two fold type transaminases with (**a**) homodimer from *C. violaceum* transaminase (PDB: 4A6T) [125] as a fold type I (*S*)-ATA and (**b**) homodimer from *A. terreus* transaminase (PDB: 4CE5) [128] as a fold type IV (*R*)-ATA. The different chains of the homodimers are colored in blue and in turquoise. Pyridoxal-5-phosphate is colored in red. The protein images were drawn with UCSF ChimeraX [57].

ω-Transaminases harbor a PLP cofactor that functions as a molecular shuttle of the amine group [133]. The reaction mechanism is a so called "ping-pong bi-bi reaction mechanism" and can be divided into two part: the transfer of the amino group from an amine donor to pyridoxal 5'-phosphate, forming pyridoxamine 5'-phosphate (PMP) and the transfer of the amino group from PMP to the amine acceptor forming PLP again (Fig. 8) [134]. In the active site of ω-TAs, PLP is bound to the enzyme via the amino group of the catalytic lysine, forming a Schiff' base. When an amine donor (e.g. alanine) is added, a nucleophilic attack of the amino group at the C4' of PLP occurs and the amine donor replaces the catalytic lysine, resulting in an external aldimine. The proton at the Cα atom is abstracted by the catalytic lysine, forming a ketimine. Subsequently, the ketimine is hydrolyzed, resulting in the release of a deaminated carbonyl product (e.g. pyruvate) and PMP. In the second half of the reaction, PMP is regenerated to PLP, while the amine acceptor (e.g. acetophenone) is aminated, resulting in an aminated product (e.g. (*S*)-phenylethylamine) [132, 135, 136].

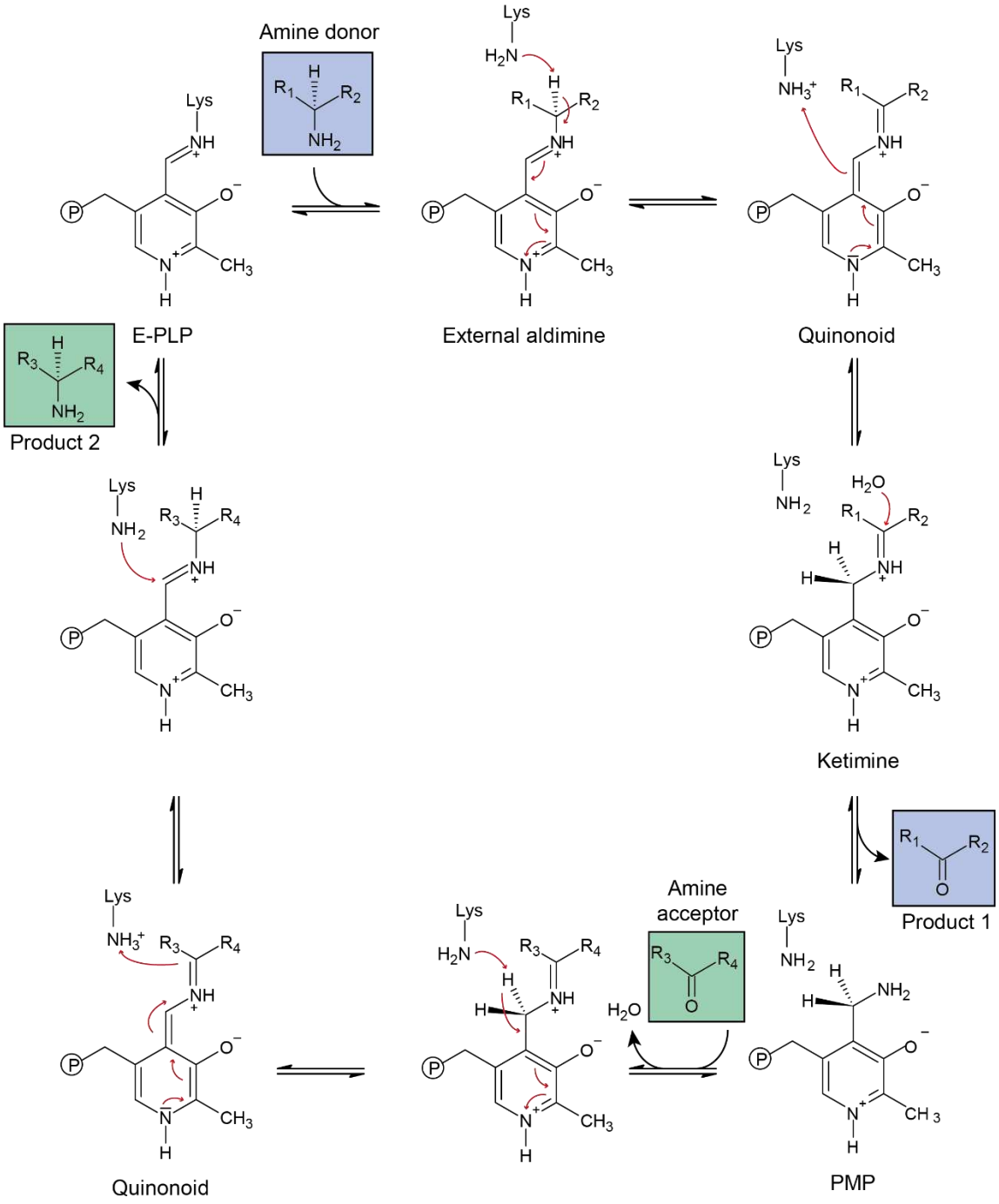

Fig. 8 Reaction mechanism of ω-TA catalysis. First, an amino group displaces the bound catalytic lysine and binds pyridoxal 5'-phosphate (PLP), forming an external aldimine. The lysine abstracts a proton from the Cα atom of PLP and a ketimine is formed. The carbonyl product is released and pyridoxamine 5'-phosphate (PMP) is formed. Subsequently, an amine acceptor binds PMP and the reactions are performed similarly. Blue: amine donor with respective product, green: amine acceptor with respective product. The circled "P" represents a phosphate group (figure adapted and modified from [136]).

Transaminases possess an active site with a large (L) and a small (S) binding pocket and a catalytic lysine in between [126, 128, 129, 137]. Enantiomeric selectivity is governed by the binding pockets and the position of the catalytic lysine relative to the PLP (Fig. 9). In (*R*)-ATAs and other fold type IV transaminases, the catalytic lysine is located on the *re*-face of the PLP, forming an (*R*)-

enantiomer. In (*S*)-ATAs and other fold type I transaminases, the catalytic lysine is located on the *si*-face of the PLP, leading to an (*S*)-enantiomer [128, 138].

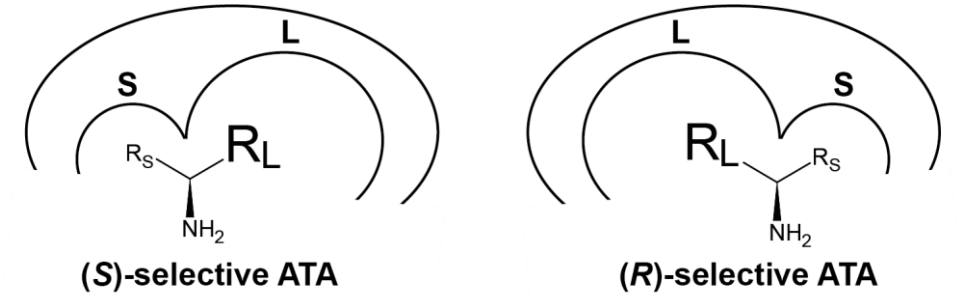

Fig. 9 Two-binding site model of (*S*)- and (*R*)-selective ATAs. The active site of transaminases has a large (L) and a small (S) binding pocket in which the large substituent (R_L) and the small substituent (R_S) can bind. (*S*)-selective ATAs (left) are transaminases of the PLP fold class I, whereas (*R*)-selective ATAs (right) are transaminases of the PLP fold class IV (figure adapted and modified from [121]).

Chiral amines can be synthesized either by kinetic resolution or by asymmetric synthesis [139]. In kinetic resolution, a stereoselective ω-TA catalyzes the conversion of one amine enantiomer from a racemic mixture to its corresponding ketone. The non-transformed amine enantiomer can then be isolated in good enantiomeric excess. This is an efficient method for the synthesis of enantio-pure amines, however, the yield is limited to a maximum of 50 % [140]. In contrast, a theoretical yield of 100 % can be obtained in asymmetric synthesis starting from a non-chiral ketone substrate. In this process, the ketone is aminated enantioselectively by a (*S*)- or (*R*)-selective ω-TA to its corresponding chiral amine [140]. As a drawback, the amination reaction often has an unfavorable reaction equilibrium and, in particular when alanine is used, yields are limited [117]. In order to direct the equilibrium towards the preferred product, different approaches were followed, such as replacement of the amine donor, addition of an amine donor in excess or removal of the carbonyl product [139]. Shin & Kim, for example, synthesized (*S*)-α-methylbenzylamine from acetophenone using L-alanine as amine donor, obtaining a yield of up to 90 % in asymmetric synthesis. For this, pyruvate, the carbonyl by-product, was removed continuously by lactate dehydrogenase reaction to shift the equilibrium [141]. Moreover, reaction systems have been developed using an alanine dehydrogenase for the regeneration of alanine from pyruvate [142].

1.4. Biotechnological application of LOXs, HPLs and ω-TAs

The LOX pathway provides some interesting enzymes and products for industrial application. In particular, lipoxygenases and hydroperoxide lyases have great potential for biotechnological utilization. LOX-preparations like enriched soybean flour are applied as additive for bleaching of textiles, flour for bread or pasta production and dairy products such as milk, cream or whey

products [143–146]. The bleaching is a consequence of the co-oxidation of carotenoid pigments or other colored components by the hydroperoxides formed [147, 148]. Furthermore, co-oxidation of the thiol groups of glutenin protein in wheat flour leads to the formation of disulfide bonds and crosslinking of the proteins, thereby improving dough properties in baking processes [149, 150].

The combined LOX – HPL reaction is of special interest for the biotechnological synthesis of GLVs, which generate a fresh, green scent and are therefore demanded by the flavor, fragrance and food industry [94]. For the production of the C_6 and C_9 volatile aldehydes and their corresponding alcohols and esters, various LOX and HPL enzymes were either extracted from plants or heterologously expressed and combined in one-pot reactions [151–153]. Cleavage of 13(*S*)-HPODE and 13(*S*)-HPOTE yields the C_6 aldehydes hexanal and 3(*Z*)-hexenal, which can be further reduced to the corresponding alcohols. They possess a fresh, green, grassy to banana-like scent. In contrast, cleavage of 9(*S*)-HPODE and 9(*S*)-HPOTE yields the C_9 aldehydes 3(*Z*)-nonenal and 3(*Z*),6(*Z*)-nonadienal as well as corresponding alcohols by further reduction. These compounds have fresh, cucumber- and melon-like odors [154].

In addition, some volatiles such as 2(*E*)-hexenal, 2(*E*)-nonenal and 2(*E*),6(*Z*)-nonadienal are toxic to mites and have therefore been suggested to be used in food storage [155]. Besides the synthesis of C_6 and C_9 volatiles, plants containing LOX and HPL enzymes also synthesize 12-oxo-9(*Z*)-dodecenoic acid, which is further metabolized to the wound hormones traumatin and traumatic acid upon herbivore attack. Interestingly, Jabłońska-Trypuć and co-workers recently postulated a positive effect of traumatic acid on many skin diseases related to oxidative stress and collagen biosynthesis [156]. Moreover, they studied the effect of traumatic acid on human breast cancer MCF-7 cells and observed a decrease in cell proliferation and viability [157]. Thus, for pharmaceutical application it could also be interesting to use lipoxygenases and hydroperoxide lyases for traumatin and traumatic acid biosynthesis.

Many amines are important biologically active compounds for pharmaceutical, chemical and agrochemical application [139]. Approximately 40 % of all pharmaceuticals have a chiral amine in their structure, highlighting the potential of ω-TAs and other enzymes for enantioselective synthesis [158, 159]. The use of enzymes often requires only mild reaction conditions and leads to high enantioselectivity, so ω-TAs can be a good alternative to chemical routes for the synthesis of chiral amines [159]. An example for the synthesis of an enantio-pure pharmaceutical is the amination of prositagliptin to sitagliptin, a therapeutic for type II diabetes, using the engineered (*R*)-ATA117-11Rd from Merck & Co and Codexis [160]. Furthermore, ω-TAs have been applied for the preparation of (*S*)-rivastigmine to treat of Alzheimer's disease [161] and for the synthesis of (*R*)-mexiletine, an antiarrhythmic drug [162]. ω-TAs have also been used for the synthesis of

unnatural α and β amino acids, which are interesting building blocks for the synthesis of peptides and proteins with enhanced stability [117, 164].

Furthermore, ω-TAs have been used for the synthesis of polymer precursors such as ω-amino fatty acids or diamines [13, 164, 165]. A biosynthetic pathway has been developed for the synthesis of poylamide-6 monomer 6-aminohexanoic acid from cyclohexanol. For this, an alcohol dehydrogenase was coupled with a BVMO and an esterase for the synthesis of 6-oxohexanoic acid. 6-Oxohexanoic acid in turn was aminated to 6-aminohexanoic acid by ω-TA from *P. denitrificans* [166]. In addition, long-chain ω-aminocarboxylic acids (e.g. C_{11} or C_{12}) were produced in enzyme cascades or with whole-cell biocatalysts [11, 13–15].

2. Materials & Methods

2.1. Reagents, enzymes and antibodies

The reference standards 13(*S*)-hydroperoxyoctadecadienoic acid (13(*S*)-HPODE), 12-oxo-9(*Z*)-dodecenoic acid and 12-oxo-10(*E*)-dodecenoic acid were purchased from Larodan (Sweden), while the 12-aminododecanoic acid standard was from Alfa Aesar (USA). 12-Hydroxydodecanoic acid, linoleic acid and hexanol were supplied from Thermo Fisher Scientific (USA). Hexanal and hexylamine were obtained from Sigma Aldrich (USA). Pyridoxal-5-phosphate monohydrate was supplied from Acros organics, Thermo Fisher Scientific (USA). Safflower oil composing of 77.2 % linoleic acid, 13.3 % oleic acid, 6.7 % palmitic acid, 2.4 % stearic acid and 0.4 % of other fatty acids [167] was purchased from Gefro (Germany). Triton X-100, β-nicotine amide adenine dinucleotide disodium salt (NADH), L-alanine, δ-aminolevulinic acid (ALA), isopropyl β-d-1-thiogalactopyranoside (IPTG), imidazole, ampicillin sodium salt, kanamycin sulfate, chloramphenicol and N,O-bis(trimethylsilyl)-trifluoroacetamide-trimethylchlorosilane (BSTFA-TMCS) (99:1) were obtained from Carl Roth (Germany). 13(*S*)-HPODE and 13(*S*)-HPOTE were synthesized by Valentin Gala Marti as described in [167]. Other chemicals and solvents not listed here were supplied by Thermo Fisher Scientific (USA), Carl Roth (Germany) or Sigma Aldrich (USA).

Glycine max LOX-1, *Pseudomonas fluorescens* Amano lipase and L-lactate dehydrogenase (LDH) were purchased from Sigma Aldrich (USA). FastDigest restriction enzymes, 10× FastDigest buffer, T4 DNA ligase and 10× T4 DNA ligase buffer were obtained from Thermo Fisher Scientific (USA). Phusion Hot Start DNA polymerase, 5× Phusion High-fidelity buffer and dNTPs were from Thermo Fisher Scientific (USA) as well. Transaminases TR_2, TR_3 and TR_6 were obtained from Prof. Dr. Manuel Ferrer from the CSIC, Madrid, Spain.

For Western Blot detection of LOX-1, the Anti-LOX1 antibody (affinity purified) and the Goat anti-Rabbit IgG, HRP conjugated antibody were purchased from Agrisera (Sweden). For histidine-tagged proteins, the monoclonal AP-conjugated Anti-His (C-term) antibody (AB_2556555) was supplied by Thermo Fisher Scientific (USA). Western Blue® Stabilized Substrate for Alkaline Phosphatase and SuperSignal™ West Pico PLUS Chemiluminescent Substrate for visualization were obtained from Promega (USA) and Thermo Fisher Scientific (USA).

2.2. Vectors

All vectors used for cloning and protein expression are listed in Table 1. Vector maps are shown in the results chapter and in the appendix as outlined in Table 1.

Table 1 Vectors used in this work with description and reference. Amp^R: ampicillin resistance, Kan^R: kanamycin resistance.

Vector	Description	Reference	Figure
pET-21b(+)	Expression vector, Amp^R	Merck (Germany)	
pET-21b::His*lox1*$_{GM}$	Expression vector for His*lox1*$_{GM}$ from *G. max* with sequence for His6-tag, Amp^R	This work	Fig. 10
pET-28a(+)	Expression vector, Kan^R	Merck (Germany)	
pET-28a::His*hpl*$_{CP}$	Expression vector for His*hpl*$_{CP}$ from *Carica papaya* with sequence for His6-tag, Kan^R	This work	Fig. 14 Fig. A7
pET-28a::His*hpl*$_{HV}$	Expression vector for His*hpl*$_{HV}$ from *Hordeum vulgare* with sequence for His6-tag, Kan^R	This work	Fig. A7
pET-28a::His*hpl*$_{SB}$	Expression vector for His*hpl*$_{SB}$ from *Sorghum bicolor* with sequence for His6-tag, Kan^R	This work	Fig. A7
pJET1.2/blunt	Cloning vector, Amp^R	ThermoFisher Scientific (USA)	
pJET1.2::His*hpl*$_{CP-N}$	Cloning vector for truncated His*hpl*$_{CP-N}$ from *C. papaya* with sequence for His6-tag, Amp^R	This work	
pJET1.2::His*hpl*$_{HV-N}$	Cloning vector for truncated His*hpl*$_{HP-N}$ from *H. vulgare* with sequence for His6-tag, Amp^R	This work	
pJET1.2::His*hpl*$_{SB-N}$	Cloning vector for truncated His*hpl*$_{SB-N}$ from *S. bicolor* with sequence for His6-tag, Amp^R	This work	
pET-28a::His*hpl*$_{CP-N}$	Expression vector for truncated His*hpl*$_{CP-N}$ from *C. papaya* with sequence for His6-tag, Kan^R	This work	Fig. 14 Fig. A10

Vector	Description	Reference	Figure
pET-28a::His*hpl*$_{PG-N}$	Expression vector for truncated His*hpl*$_{PG-N}$ from *Psidium guajava* with sequence for His6-tag, Kan^R	This work	Fig. A10
pET-28a::His*hpl*$_{HV-N}$	Expression vector for truncated His*hpl*$_{HV-N}$ from *H. vulgare* with sequence for His6-tag, Kan^R	This work	Fig. A10
pET-28a::His*hpl*$_{SB-N}$	Expression vector for truncated His*hpl*$_{SB-N}$ from *S. bicolor* with sequence for His6-tag, Kan^R	This work	Fig. A10
pET-43.1a(+)	Expression vector for *nusA*, Amp^R	Merck (Germany)	
pJET1.2::*nusAhpl*$_{CP-N}$	Cloning vector for fusion construct with *nusA* and truncated His*hpl*$_{CP-N}$ from *C. papaya* with sequence for His6-tag, Amp^R	This work	
pJET1.2::*nusAhpl*$_{PG-N}$	Cloning vector for fusion construct with *nusA* and truncated His*hpl*$_{PG-N}$ from *P. guajava* with sequence for His6-tag, Amp^R	This work	
pJET1.2::*nusAhpl*$_{HV-N}$	Cloning vector for fusion construct with *nusA* and truncated His*hpl*$_{HV-N}$ from *H. vulgare* with sequence for His6-tag, Amp^R	This work	
pJET1.2::*nusAhpl*$_{SB-N}$	Cloning vector for fusion construct with *nusA* and truncated His*hpl*$_{SB-N}$ from *S. bicolor* with sequence for His6-tag, Amp^R	This work	
pET-28a::*nusAhpl*$_{CP-N}$	Expression vector for fusion construct with *nusA* and truncated His*hpl*$_{CP-N}$ from *C. papaya* with sequence for His6-tag, Kan^R	This work	Fig. 14 Fig. A17
pET-28a::*nusAhpl*$_{PG-N}$	Expression vector for fusion construct with *nusA* and truncated His*hpl*$_{PG-N}$ from *P. guajava* with sequence for His6-tag, Kan^R	This work	Fig. A17

Vector	Description	Reference	Figure
pET-28a::*nusAhpl*$_{HV-N}$	Expression vector for fusion construct with *nusA* and truncated His*hpl*$_{HV-N}$ from *H. vulgare* with sequence for His6-tag, Kan^R	This work	Fig. A17
pET-28a::*nusAhpl*$_{SB-N}$	Expression vector for fusion construct with *nusA* and truncated His*hpl*$_{SB-N}$ from *S. bicolor* with sequence for His6-tag, Kan^R	This work	Fig. A17
pET-21b::His*tr*$_{AD}$	Expression vector for *tr*$_{AD}$ from *Aquitalea denitrificans* with sequence for His6-tag, Amp^R	This work	Fig. 28
pET-21b::His*tr*$_{CV}$	Expression vector for *tr*$_{CV}$ from *Chromobacterium violaceum* with sequence for His6-tag, Amp^R	This work	Fig. 28
pET-21b::His*tr*$_{PD}$	Expression vector for *tr*$_{PD}$ from *Paracoccus denitrificans* with sequence for His6-tag, Amp^R	This work	Fig. 28
pET-21b::His*tr*$_{SD}$	Expression vector for *tr*$_{SD}$ from *Sulfitobacter delicatus* with sequence for His6-tag, Amp^R	This work	Fig. 28
pRhokHi-2::His*tr2*	Expression vector for *tr2* from *Acidihalobacter* sp. with sequence for His6-tag, Kan^R	[168]	
pBXCH::His*tr3*	Expression vector for *tr3* from uncultured *Rhodobacteraceae* bacterium with sequence for His6-tag, Amp^R	[168]	
pBXCH::His*tr6*	Expression vector for *tr6* from uncultured *Rhodobacteraceae* bacterium with sequence for His6-tag, Amp^R	[168]	

2.3. Cell strains and cultivation of bacteria

Escherichia coli XL1-Blue was used for high copy amplification of vector DNA and *E. coli* BL21(DE3) was applied for protein expression (Table 2). *E. coli* C41(DE3) and *E. coli* Lemo21(DE3) are derivatives of BL21(DE3) and were used for HPL expression as well.

Table 2 Bacteria used in the experiments for cultivation and expression. Abbreviations for *E. coli* genotypes according to Berlyn (1998) [169].

Strain	Description	Reference
E. coli XL1-Blue	endA1 gyrA96(nal^R) thi-1 recA1 relA1 lac glnV44 F'[::Tn10 proAB$^+$ lacI^q Δ(lacZ)M15] hsdR17(r_{K^-} m_{K^+})	Agilent Technologies (USA)
E. coli BL21(DE3)	*E. coli* str. B F$^-$ *ompT gal dcm lon hsdS$_B$*($r_B^-m_B^-$) λ(DE3 [*lacI lacUV5-T7p07 ind1 sam7 nin5*]) [*malB*$^+$]$_{K-12}$(λ^S)	[170]
E. coli C41(DE3)	*F$^-$ ompT gal dcm hsdS$_B$ (r_{B^-} m_{B^-}) (DE3)*	[171]
E. coli Lemo21(DE3)	*fhuA2 [lon] ompT gal (λ DE3) [dcm] ΔhsdS/* pLemo(Cam^R) *λ DE3 = λ sBamHIo ΔEcoRI-B int::(lacI::PlacUV5::T7 gene1) i21 Δnin5* pLemo = pACYC184-*PrhaBAD-lysY*	[172]

Lysogeny broth (LB) medium was used for standard cultivation or pre-cultures of *E. coli* [173]. To obtain higher cell densities, the complex medium terrific broth (TB) or the auto-induction medium ZYM5052 [174] was prepared (Table 3). For TB medium, the solution of yeast extract, tryptone and glycerol was autoclaved, while the buffer was sterile filtered and added immediately before cultivation. For ZYM5052 medium, the solution of tryptone, yeast extract and salt was autoclaved, and the solution of glucose, lactose and glycerol, as well as the trace metal mix, magnesium sulfate and the buffer were sterile-filtered and added before cultivation. For the preparation of solid media, 1.8 % (w/v) agar was added. Autoclaving was performed for 20 min at 121 °C and a pressure of 0.2 MPa. If necessary, ampicillin (Amp), kanamycin (Kan) or chloramphenicol were added after autoclaving to a final concentration of 100 µg·ml^{-1}, 50 µg·ml^{-1} or 30 µg·ml^{-1}. If not noted otherwise, *E. coli* was cultivated at 37 °C with continuous shaking at 200 rpm in Erlenmeyer flasks with baffles. Glycerol stocks were prepared for storage of the generated bacterial strains. For this purpose, overnight cell cultures were mixed with sterile glycerol to a final concentration of 20 % (v/v) and stored at -80 °C until further use.

Table 3 Compositions of the cultivation media lysogeny broth (LB), terrific broth (TB) and the auto-induction medium ZYM5052. Table reproduced from [175] with permission from Springer Nature.

Component	Final Concentration
LB	
Yeast extract	5 $g \cdot l^{-1}$
Tryptone	10 $g \cdot l^{-1}$
NaCl	10 $g \cdot l^{-1}$
TB	
Yeast extract	24 $g \cdot l^{-1}$
Tryptone	20 $g \cdot l^{-1}$
Glycerol	4 $ml \cdot l^{-1}$
Phosphate buffer	17 mM KH_2PO_4, 72 mM K_2HPO_4
ZYM5052	
ZY	10 $g \cdot l^{-1}$ Tryptone, 5 $g \cdot l^{-1}$ Yeast extract
$MgSO_4$	2 mM
1000×Trace metal mix	10 mM $FeCl_3$, 4 mM $CaCl_2$, 2 mM $MnCl_2$, 2 mM $ZnSO_4$, 0.4 mM $CoCl_2$, 0.4 mM $CuCl_2$, 0.4 mM $NiCl_2$, 0.4 mM Na_2MoO_4, 0.4 mM Na_2SeO_3, 0.4 mM H_3BO_3
5052	0.5 % Glycerol, 0.05 % Glucose, 0.2 % Lactose
Buffer	25 mM Na_2HPO_4, 25 mM KH_2PO_4, 50 mM NH_4Cl

2.4. Bioinformatic analyses

DNA and protein sequences were downloaded from the "National Center for Biotechnology Information" (NCBI) website [176]. The Basic Local Alignment Search Tool (BLAST) [177] from the NCBI website was used to identify putative novel homologous sequences of hydroperoxide lyases and transaminases. Multiple sequence alignments were conducted with Clustal Omega [178] using the BLOSUM62 matrix. Phylogenetic trees were created with ClustalX [179] and NJPlot [180] with the neighbor-joining algorithm and a bootstrap value of 1000.

Protein structures were obtained from the RCSB Protein Data Bank (RCSB PDB) [181] and the protein images were drawn with UCSF ChimeraX [57]. A putative model of papaya HPL was created with the Swiss-model program [90] based on the crystal structure of *A. thaliana* AOS.

2.5. Molecular biology methods

2.5.1. Polymerase chain reaction (PCR)

Polymerase chain reactions (PCR) were performed to amplify *hpl* genes. The pET-28a::His*hpl* vectors were used as templates. Oligonucleotides, which were synthesized by eurofins genomics (Ebersberg, Germany) are outlined in Table 4 and were used as primers.

Table 4 Oligonucleotides for PCR with restriction sites underlined and His6-tags highlighted in grey.

Designation	Sequence (5' - 3')	Restriction site
hplCP-Nter_fw	aaaCATATGCTGCCGCTGCGTACC	*Nde*I
hplCP_His6_rv	aaaGGATCCTTAATGGTGATGATGATGATGTTTGG	*Bam*HI
hplHV-Nter_fw	aaaCATATGCCGCCGCCTAAACCG	*Nde*I
hplHV_His6_rv	aaaGGATCCTTAATGGTGATGATGATGATGACTGCTCG	*Bam*HI
hplSB-Nter_fw	CATATGCCGCCTCCGCGTCCTATTCC	*Nde*I
hplSB_His6_rv	GGATCCTTAATGGTGATGATGATGATGCTGCTGAGC	*Bam*HI

PCR was performed using Phusion Hot Start II DNA-Polymerase (Thermo Fisher Scientific, USA) with proof-reading function. The protocol was carried out as follows:

PCR using Phusion Hot Start II DNA-Polymerase:

5×Phusion GC buffer	10 µl
Phusion Hot Start II DNA-Polymerase	0.5 µl
dNTPs (each 10 pmol·µl^{-1})	1 µl
Primer fw (10 µM)	1 µl
Primer rv (10 µM)	1 µl
Template DNA	1 µl
DMSO (10 % (v/v))	5 µl
ddH_2O	30.5 µl

Step	Temperature	Time	Cycles
Initial denaturing	98 °C	30 sec	1×
Denaturing	98 °C	10 sec	30×
Annealing	Primer specific	30 sec	
Elongation	72 °C	45 sec	
Final elongation	72 °C	5 min	1×

2.5.2. Fusion PCR

A fusion PCR enables the ligation and amplification of a DNA construct out of two or more DNA fragments without the need of restriction enzymes and a ligase [182]. It was applied to synthesize fusion proteins of HPL and NusA. DNA sequences with overlapping regions were amplified in a PCR cycle with oligonucleotides outlined in Table 5. In addition, a sequence encoding an enterokinase (EK) cleavage site was added in between the *hpl* and the *nusA* genes for post-translational restriction of the fusion proteins. For amplifying the *nusA* sequences, primers P1 and P2 were used and for amplifying the *hpl* sequences, primers P3 and P4 were employed.

Table 5 Oligonucleotides used for fusion PCR with restriction sites underlined and His6-tags highlighted in grey.

Designation	Sequence (5' - 3')	Restriction site
P1_nusA_NdeI_fw	CATATGAACAAAGAAATTTTGGC	*Nde*I
P2_nusA_EK_hplPG_rv	CGAACAGGCAGACTCTTGTCGTCGTCATCACTAGTCGCTTCG TCACC	
P3_hplPG_EK_NusA_fw	CGAAGCGACTAGTGATGACGACGACAAGAGTCTGCCTGTTC GCACCATTC	
P4_hplPG_BamHI_rv	GGATCCTTAATGGTGATGATGATGATGATTGGCTTTTTC	*Bam*HI
P2_nusA_EK_hplCP_rv	GACACTCTTGTCGTCGTCATCACTAGTCGCTTCGTCACCG	
P3_hplCP_EK_NusA_fw	GAAGCGACTAGTGATGACGACGACAAGAGTGTCCTGCCGCT GCGTACC	
P4_hplCP_His6_rv	AAAGGATCCTTAATGGTGATGATGATGATGTTTGG	*Bam*HI
P2_nusA_EK_hplHv_rv	CGGCGGGACACTCTTGTCGTCGTCATCACTAGTCGCTTCGTC ACCGAACc	
P3_hplHV_EK_NusA_fw	GAAGCGACTAGTGATGACGACGACAAGAGTGTCCCGCCGCCT AAACCG	
P4 hplHV_His6_rv	AAAGGATCCTTAATGGTGATGATGATGATGACTGCTCG	*Bam*HI
P2_NusA_EK_hplSB_rv	GGGACGACACTCTTGTCGTCGTCATCACTAGTCGCTTCGTCA CCGAAC	
P3_hplSB_EK_Nus_fw	GAAGCGACTAGTGATGACGACGACAAGAGTGTCGTCCCGCCT CCGCGTC	
P4 hplSB_BamHI_rv	GGATCCTTAATGGTGATGATGATGATGCTGCTGAGC	*Bam*HI

In the following fusion PCR, the overlapping regions of the DNA fragments served as primers and as template DNA. Annealing of the overlapping regions was performed by addition of DNA fragments in equimolar concentrations as described in the protocol below.

PCR using Phusion Hot Start DNA polymerase:

5×Phusion GC buffer	4 µl
Phusion Hot Start DNA polymerase	0.5 µl
dNTPs (each 10 pmol·µl^{-1})	0.4 µl
Fragment 1 (*nusA*)	1 µl
Fragment 2 (*hpl*)	1 µl
DMSO (10 % (v/v))	2 µl
ddH_2O	11.1 µl

Step	**Temperature**	**Time**	**Cycles**
Initial denaturing	98 °C	1 min	1×
Denaturing	98 °C	10 sec	
Annealing	Primer specific	90 sec	20×
Elongation	72 °C	90 sec	
Final elongation	72 °C	5 min	1×
Cooling	8 °C	∞	

In the second part of the fusion PCR, the DNA fragments were ligated and the fusion DNA constructs were amplified. For this, the primers P1_NusA_NdeI_fw and P4_hpl_BamHI_rv (Table 5) were added to the upper reaction mix on ice and the PCR cycle was performed as described below.

PCR using Phusion Hot Start DNA polymerase:

5×Phusion GC buffer	6 µl
Phusion Hot Start DNA polymerase	0.5 µl
dNTPs (each 10 pmol·µl^{-1})	0.6 µl
Primer 1 (10 µM)	1 µl
Primer 2 (10 µM)	1 µl
DMSO (10% (v/v))	3 µl
ddH_2O	17.9 µl

Step	Temperature	Time	Cycles
Initial denaturing	98 °C	1 min	1×
Denaturing	98 °C	10 sec	20×
Annealing	Primer specific	90 sec	
Elongation	72 °C	90 sec	
Final elongation	72 °C	5 min	1×
Cooling	8 °C	∞	

2.5.3. Isolation of plasmid DNA from *E. coli*

Plasmid DNA was isolated from *E. coli* with the GeneJET Plasmid Miniprep Kit (Thermo Fisher Scientific, USA). Cells were cultivated overnight on LB plates with the appropriate antibiotic. Cell material was scraped off the plate and dissolved in 250 µl resolving buffer. Then, the instructions were followed according to the manufacturer's instructions. In brief, 250 µl of lysis solution was added to the samples and the tubes were inverted five times before 350 µl of neutralization solution was added and the tubes were inverted five times again. The tubes were centrifuged for 5 min and the supernatant was transferred to a GeneJET Spin Column. The tubes were centrifuged for 1 min and then washed twice with 500 µl of wash solution. Purified DNA was eluted with 50 µl of elution buffer after 2 min incubation and 2 min centrifugation.

2.5.4. Restriction of DNA and ligation of restriction products

Restriction of plasmid DNA was performed with FastDigest enzymes from Thermo Fisher Scientific (USA). The reaction mixtures were prepared as described below and incubated at 37 °C for 30 min.

Restriction digest:

Plasmid/ DNA fragment	x µl
10×FastDigest buffer	2 µl
Restriction enzyme 1	2 µl
Restriction enzyme 2	2 µl
ddH_2O	*ad* 20 µl

For blunt-end ligation of PCR products into the pJET1.2/blunt cloning vector, the CloneJET PCR Cloning Kit from Thermo Fisher Scientific (USA) was used according to the manufacturer's

instructions. The reaction mixtures were prepared and incubated for 5 min at room temperature. *E. coli* XL1-Blue was then transformed with the ligated vectors for amplification.

Blunt-end ligation:

pJET1.2/blunt (50 ng·µl^{-1})	1 µl (0.05 pmol end concentration)
PCR product	8 µl (0.15 pmol end concentration)
T4 DNA ligase	1 µl
2×reaction buffer	10 µl
ddH_2O	*ad* 20 µl

For sticky-end ligation of the restricted DNA fragments into the pET-28a(+) vector, T4 DNA ligase was used according to the protocol below. The reaction mixtures were incubated for 60 min at room temperature. *E. coli* XL1-Blue was transformed with the respective vectors for amplification.

Sticky-end ligation:

pET-28a(+)	x µl
Insert DNA	x µl
T4 DNA ligase	1 µl
10×T4 ligase buffer	2 µl
ddH_2O	*ad* 20 µl

2.5.5. Generation and transformation of competent *E. coli* cells

Chemically competent *E. coli* cells (XL1-Blue, BL21(DE3), C41(DE3) and Lemo21(DE3)) were generated for plasmid transformation according to Hanahan (1983). A pre-culture of *E. coli* was grown overnight in 50 ml LB medium at 37 °C. The main culture of 50 ml LB was inoculated with 2 % of the pre-culture and grown at 37 °C until reaching an OD_{600nm} of 0.3-0.5. Cells were incubated on ice for 15 min and then centrifuged at 7000 × *g* for 10 min and 4 °C. After discarding the supernatant, the cell pellet was suspended in 18 ml RF1-solution and centrifuged as described above. Again, the supernatant was discarded. Then the cells were suspended in 4 ml RF2-solution and aliquoted in 200 µl portions. The aliquots were stored at -80 °C until further use.

RF1-solution:	**RF2-solution:**
100 mM RbCl	10 mM RbCl
50 mM $MnCl_2$	75 mM $CaCl_2$
30 mM potassium acetate	10 mM MOPS
10 mM $CaCl_2$	15 % (v/v) glycerol
→ adjust to pH 5.8 with glacial acetic acid	→ adjust to pH 5.8 with NaOH

Transformation of plasmid DNA was performed with 200 µl of the competent *E. coli* cell suspension. Either the complete ligation mixture (20 µl) or 1 µl of previously generated plasmids was added to the competent cells and incubated on ice for 30 min. A heat shock was performed at 42 °C for 90 sec. Cells were immediately cooled on ice for 2 min and then 500 µl LB medium was added. Cells were incubated for 1 h at 37 °C before they were streaked out on LB plates with the respective antibiotic and incubated overnight at 37 °C.

2.5.6. Agarose gel electrophoresis and DNA extraction

Agarose gel electrophoresis was performed to separate DNA fragments according to their molecular mass. For this, 1 % agarose (w/v) was dissolved in 1× Rotiphorese TAE buffer (Carl Roth, Germany) and heated. A gel was poured and placed in an electrophoresis chamber filled with 1× Rotiphorese TAE buffer. Samples were mixed with 1× Orange Loading Dye (Thermo Fisher Scientific, USA) and loaded onto the gel. GeneRuler™ 1 kb DNA ladder (Thermo Fisher Scientific, USA) was added as marker. An electric field of 120 V was applied for electrophoresis. The gel was incubated into a 2 $\mu g \cdot ml^{-1}$ ethidium bromide staining solution for 20 min, followed by visualization of the DNA under UV light at 312 nm. DNA fragments were isolated from agarose gels with the "Monarch DNA Gel Extraction Kit" (New England Biolabs, Germany) according to the manufacturer's protocol. In brief, the excised gel fragments were dissolved in four volumes of gel dissolving buffer and incubated at 50 °C until the gel fragments were dissolved. The samples were loaded onto a small purification column delivered with the kit and centrifuged for 1 min. The column was washed twice with 200 µl of DNA wash buffer and centrifuged again. The DNA was eluted with 6-20 µl DNA elution buffer.

2.5.7. DNA sequencing

Correct cloning was verified by DNA sequencing by Eurofins Genomics (Germany). For sample preparation, the Mix2Seq Kit (Eurofins Genomics, Germany) was used according to the manufacturer's protocol. 10 µl of vector solution was mixed with 2 µl primer and sent to Eurofins

Genomics for DNA sequencing. The T7_Promoter_forward and the T7_Terminator_reverse primer (Table 6) were applied. For long DNA constructs of HPL – NusA fusion proteins, additional samples were prepared with the primers nusA_sequencing and hpl_sequencing. Sequences were analyzed using the ApE program (A plasmid Editor, Version v2.0.61) [184].

Table 6 Oligonucleotides used for DNA sequencing.

Designation	Sequence (5' - 3')
T7_Promoter_foward	TAATACGACTCACTATAGGG
T7_Terminator_reverse	GCTAGTTATTGCTCAGCGG
nusA_sequencing	AAGCCGGAGCACTGATTATG
hplPG_sequencing	TCACTAATCGGACCCAGCAGC
hplCP_sequencing	GATCGCTCAGCGGACCCAGC
hplHV_sequencing	ACGCAGCGGGCCCAGAACCG
hplSB_sequencing	ACGCAGCGGACCCAGAACCG

2.6. Protein biochemistry methods

2.6.1. Protein expression in shaking flasks and fermenter cultures

E. coli BL21(DE3) cells expressing LOX, HPL or ω-TA were cultivated in 500 ml Erlenmeyer flasks with baffles containing 50 ml cultivation broth (Chapter 2.3.) and the respective antibiotic. For HPL expression, 2.5 mM δ-aminolevulinic acid and 0.1 mM ammonium ferric citrate were optionally added. Cultivation was started with inoculation of 2 % (v/v) of an overnight cell culture. Cells were grown at 37 °C with continuous shaking at 200 rpm until an OD_{600} of 0.6 (for LB medium) or 1 (for TB and ZYM5052 medium) was reached. Temperature was decreased to 15 °C for LOX expression, 25 °C for HPL expression and 20 °C for ω-TA expression. In case of LB and TB cultivation, protein expression was induced with 1 mM Isopropyl β-d-1-thiogalactopyranoside (IPTG), whereas in case of ZYM5052 cultivation, auto-induction was achieved by lactose (0.2 % (w/v)). Cells were cultivated for 24 h and subsequently harvested by centrifugation at 4500 × *g* for 15 min. Cell pellets were frozen at -20 °C until further use.

Expression optimization of LOX-1 was performed by analyzing cultivation temperatures ranging from 10 to 37 °C and comparing the cultivation media LB, TB and ZYM5052. Expression optimization of $HPL_{CP\text{-}N}$ was conducted by testing the cultivation media LB, TB and ZYM5052, the additives δ-aminolevulinic acid and ammonium ferric citrate and cultivation temperatures between 15 to 37 °C. Moreover, the expression strains C41(DE3) and Lemo21(DE3) were compared to expression in *E. coli* BL21(DE3). For expression with Lemo21(DE3), varying

concentrations of L-rhamnose from 0 to 2000 µM as well as 30 µg·ml^{-1} chloramphenicol were added in the beginning.

For preparative scale production of $HPL_{CP\text{-}N}$, a 3 l BioFlo Fermenter 115 (Eppendorf, Germany) was used. The bioreactor was filled with 1.5 l ZYM5052 medium containing 50 µg·ml^{-1} kanamycin and 2.5 mM δ-aminolevulinic acid. An overnight pre-culture of *E. coli* expressing $HPL_{CP\text{-}N}$ was used to inoculate the bioreactor with a concentration of 2 % (v/v). The temperature was set to 25 °C, the stirrer to 400-800 rpm and the aeration was adjusted to 1.5 vvm (2.25 l·m^{-1}), keeping a minimum dissolved oxygen level (DO) of 30 %. Cells were cultivated for 24 h and subsequently harvested by centrifugation at 4500 × *g* at 4 °C.

2.6.2. Extraction and purification of soluble enzyme fractions

Cell pellets were suspended in the appropriate solubilization buffer (Table 7) containing 300 µg·ml^{-1} lysozyme. 40 mM of imidazole was added to the binding buffer, in case protein purification was intended. Cells were incubated on ice for 1 h and then disrupted by sonication in seven cycles of 15 sec each, with a 15 sec pause on ice between the cycles. The crude extract (CE) was centrifuged at 21,000 × *g* for 10 min and 4 °C to obtain the soluble enzyme fraction (SF). Purification of LOX-1, HPLs and ω-TAs was performed by immobilized metal affinity chromatography (IMAC) using a nickel-bound HisTrap™ FF column (Cytiva, USA). The soluble fraction was dissolved in binding buffer and loaded onto the column. The column was washed with the appropriate buffer containing 40 to 100 mM imidazole and finally eluted with 500 mM imidazole (Table 7). To remove imidazole, the purified fractions were concentrated with Pierce™ Protein Concentrators 10 K MWCO (Thermo Fisher Scientific, USA) and dissolved in elution buffer without imidazole.

Table 7 Solubilization and binding buffers for LOX, HPL and ω-TA solubilization and affinity purification.

Step	Buffer
LOX-1	
Solubilization	0.05 M Tris buffer pH 7.5 with 0.05 M NaCl
Binding	0.05 M Tris buffer pH 7.5 with 0.5 M NaCl and 0.04 M imidazole
Washing	0.05 M Tris buffer pH 7.5 with 0.5 M NaCl and 0.04 M imidazole
Elution	0.05 M Tris buffer pH 7.5 with 0.5 M NaCl and 0.5 M imidazole
$HPL_{CP\text{-}N}$	
Solubilization	0.05 M KPO_4 buffer pH 6 with 1 M NaCl and 0.2 % Triton X-100
Binding	0.05 M KPO_4 buffer pH 6 with 1 M NaCl, 0.04 M imidazole and 0.2 % Triton X-100

Step	Buffer
Washing 1	0.05 M KPO_4 buffer pH 6 with 1 M NaCl and 0.04 M imidazole and 0.1 % Triton X-100
Washing 2	0.05 M KPO_4 buffer pH 6 with 1 M NaCl and 0.1 M imidazole and 0.1 % Triton X-100
Elution	0.05 M KPO_4 buffer pH 6 with 1 M NaCl and 0.5 M imidazole and 0.1 % Triton X-100
ω-TAs	
Solubilization	0.05 M KPO_4 buffer pH 7.5 with 0.05 M NaCl
Binding buffer	0.05 M KPO_4 buffer pH 7.5 with 0.5 M NaCl and 0.04 M imidazole
Washing	0.05 M KPO_4 buffer pH 7.5 with 0.5 M NaCl and 0.04 M imidazole
Elution	0.05 M KPO_4 buffer pH 7.5 with 0.5 M NaCl and 0.5 M imidazole

2.6.3. Size exclusion chromatography

Size exclusion chromatography (SEC) was performed to determine the native molecular weight of $HPL_{CP\text{-}N}$. A Superdex™ 200 Increase 10/300 column (Cytiva, USA) was equilibrated with 50 mM potassium phosphate buffer pH 7 containing 0.5 M NaCl and 0.1 % Triton X-100. The eluate fraction from IMAC purification was loaded onto the column and the retention time was measured. For calibration of the column, the gel filtration markers kit containing proteins from 29,000-700,000 Da (Sigma Aldrich, USA) was used. The distribution coefficient K_{AV} was calculated as follows:

$$K_{AV} = \frac{V_e - V_0}{V_c - V_0}$$

with V_e = elution volume, V_0 = void volume and V_c = volume of the column.

A calibration curve of K_{AV} against the logarithm of the protein molecular weight was drawn ($y = -0.3582x + 1.04$) and used for determination of native molecular mass of $HPL_{CP\text{-}N}$.

2.6.4. Protein quantification with Bradford reagent

Quantitative determination of proteins was performed photometrically using the Bradford reagent, which contains Coomassie Brillant Blue G [185]. During interacting with proteins, Coomassie Brillant Blue G changes its absorption maximum from 465 nm to 595 nm. 1 ml of Bradford reagent was mixed with 20 µl of sample in an appropriate dilution and incubated for 10 min at 22 °C in the dark. The absorbance was measured in a photometer at 595 nm and protein

concentrations were calculated using a calibration curve generated with bovine serum albumin (BSA).

Bradford reagent:

70 mg Coomassie Brilliant Blue G

50 ml ethanol (96 % (v/v))

100 ml phosphoric acid (85 % (v/v))

ad 1000 ml ddH_2O

2.6.5. SDS-PAGE

SDS-PAGE (sodium dodecyl sulfate polyacrylamide gel electrophoresis) is a biochemical method for separating proteins according to their molecular mass in an electric field [186]. Samples of 10 µg protein were mixed with 1× SDS denaturing buffer and the samples were heated at 95 °C for 10 min for protein denaturation. Discontinuous gels were poured with a stacking gel (4.5 % polyacrylamide) to line up the proteins and a resolving gel (11.5 % polyacrylamide) to separate the proteins (Table 8).

Gels were placed in a vertical gel chamber filled with 1× Rotiphorese SDS-PAGE buffer (Carl Roth, Germany) and the samples were loaded onto the gel. As marker, 5 µl of Page Ruler Prestained Protein Ladder (Thermo Fisher Scientific, USA) was added. An electric filed was applied (40 mA) and the proteins were separated according to their molecular mass. For visualization, the gel was stained with a Coomassie staining solution for 1 h under constant shaking and then placed in 10 % acetic acid overnight for discoloration.

Table 8 Composition of discontinuous SDS gels consisting of a stacking gel and a resolving gel.

	Stacking gel (4.5 %)	**Resolving gel (11.5 %)**
ddH_2O	5.625 ml	5.7 ml
Acrylamide/ bis-acrylamide	1.41 ml	6 ml
Stacking gel buffer	2.34 ml	-
Resolving gel buffer	-	3.9 ml
TEMED	6.6 µl	7.5 µl
Ammonium persulfate (40 % (w/v))	33 µl	37.5 µl

Stacking gel buffer:

30.23 g Tris/HCl

2 g SDS

ad 500 ml H_2O

pH = 6.8

Resolving gel buffer:

90.75 g Tris/HCl

2 g SDS

ad 500 ml H_2O

pH = 8.9

3x SDS denaturing buffer:

20 ml glycerol

4 g SDS

10 ml β-mercaptoethanol

18.6 mg EDTA

2.5 mg bromophenol blue

ad 50 ml 100 mM Tris/HCl (pH= 6.8)

Coomassie staining solution:

40 % (v/v) Isopropanol

10 % (v/v) acetic acid

0.1 % Coomassie Brilliant Blue R250

ad 1000 ml H_2O

2.6.6. Western Blot

LOX and HPL expression was verified by Western Blot. Proteins were separated with SDS-PAGE and then transferred to a polyvinylidene difluoride (PVDF) membrane. For this purpose, the membrane was pretreated with methanol and equilibrated in transfer buffer. Then, a blot 'sandwich' was prepared, which consists of two sheets of filter paper that were pre-incubated in transfer buffer, followed by the membrane, the gel and two more sheets of filter paper that were pre-incubated in transfer buffer on top. The blot 'sandwich' was placed in the blotting chamber and blotting was performed at 15 V for 45 min.

For specific immunological detection of the membrane-bound LOX-1 protein, the affinity purified Anti-LOX1 antibody (Agrisera, Sweden) was used. First, the free binding sites on the membrane were blocked with 5 % milk powder in TBST (tris-buffered saline with Tween20) for 1 h under continuous shaking. The membrane was washed three times with TBST and the primary antibody (Anti-LOX1) was added at a dilution of 1:5000 in 20 ml TBST containing 5 % milk powder and incubated for 1 h under continuous shaking at 22 °C. Subsequently, the membrane was washed three times with TBST and incubated with the secondary antibody (Goat anti-Rabbit IgG, HRP-conjugated (Agrisera, Sweden) at a dilution of 1:10,000 in 20 ml TBST containing 5 % milk powder for 1 h under continuous shaking at 22 °C. For chemiluminescence detection, SuperSignal™ West Pico PLUS chemiluminescent substrate (Thermo Fisher Scientific, USA) was used and a mixture of luminol and H_2O_2 was freshly prepared and applied to the membrane. This

led to a catalytic reaction of horseradish peroxidase (HRP) and chemiluminescence was detected at 425 nm using a ChemiDoc (Bio-Rad Laboratories, USA).

For immunological detection of the His-tagged $HPL_{CP\text{-}N}$ protein, the monoclonal AP-conjugated Anti-His (C-term) antibody AB_2556555 (Thermo Fisher Scientific, USA) was used. The membrane was washed as described above and the antibody was added with a 1:2000 dilution in 20 ml TBST containing 5 % milk powder. The membrane was incubated at 22 °C for 1 h under continuous shaking before the membrane was washed as described above. Western Blue® Stabilized Substrate for Alkaline Phosphatase (Promega, USA) was added and the His-tagged proteins became visible.

Transfer buffer:	**1 x TBST:**
25 mM Tris-HCl	20 mM Tris
192 mM glycine	150 mM NaCl
20 % (v/v) methanol	0.1 % (w/v) Tween® 20
→ pH 8.3	

2.7. Enzyme assays and biocatalytic methods

2.7.1. Activity analysis of LOX and HPL

The activity of LOX-1 and HPL was determined photometrically at 234 nm, which correlates to an absorbance peak of the conjugated double bond system of 13(*S*)-HPODE and 13(*S*)-HPOTE. In case of LOX-1, the absorbance increased proportional to the formation of the conjugated peroxide, whereas in case of HPL, it decreased due to the cleavage of the conjugated double bond system. To determine the enzymatic activity of LOX-1, reaction mixtures were prepared with 10 µl of an appropriate LOX-1 dilution with 1 mM linoleic acid in 50 mM borate buffer pH 9 to a final volume of 1 ml. Reactions were measured photometrically at 234 nm for 300 sec at 22 °C. To determine the enzymatic activity of HPL, reaction mixtures were prepared with 10 µl of HPL in an appropriate dilution and 40 µM 13(*S*)-HPODE in 50 mM potassium phosphate buffer pH 7.5 with 1 M NaCl. Buffer optimization was performed for $HPL_{CP\text{-}N}$ catalysis. For this, different buffer components, salt concentrations, pH values and addition of detergents were tested. Each component was tested in turn for solubility and performance in the photometric activity assay. The absorbance was measured in a 1 ml cuvette at 234 nm for 300 sec at 22 °C. Volumetric activity was calculated as follows:

$$\frac{\Delta c}{\Delta t} = \Delta E * \frac{1}{d} * \frac{1}{\varepsilon} * \frac{1}{\Delta t}$$

with an extinction coefficient ε=23,000 $M^{-1} \cdot cm^{-1}$ and d=1cm. One Unit (U) was defined as the amount of enzyme that transforms 1 µmol substrate per minute. Protein concentrations were used for calculating specific activities. Mean values and standard deviations were determined with Microsoft Excel.

The kinetic parameters K_m and v_{max} of $HPL_{CP\text{-}N}$ were determined photometrically in triplicate with substrate concentrations ranging from 0.005 to 0.1 mM 13(*S*)-HPODE and 13(*S*)-HPOTE. Nonlinear regression was performed to determine the kinetic parameters with standard errors using the program GraphPad Prism 6.05.

2.7.2. Enzyme activity analysis of ω-TAs

The enzymatic activity of ω-TAs was measured photometrically in a coupled enzyme assay with lactate dehydrogenase (LDH) and NADH. Unless otherwise indicated, 10 µl of ω-TA solution was mixed with 10 µl of a 50 $U \cdot ml^{-1}$ LDH solution (Sigma Aldrich, USA), 10 mM L-alanine, 0.1 mM NADH, 0.1 mM pyridoxal-5-phosphate and 0.1 mM substrate in 1 ml 50 mM potassium phosphate buffer pH 7.5 containing 50 mM NaCl in a cuvette. 12-Oxo-9(*Z*)-dodecenoic acid, 12-oxo-10(*E*)-dodecenoic acid or hexanal were used as substrates. The decrease in absorbance was measured at 340 nm for 300 sec at 22 °C, which correlates with the conversion of $NADH+H^+$ to NAD^+. The volumetric activity was calculated with the following formula:

$$\frac{\Delta c}{\Delta t} = \Delta E * \frac{1}{d} * \frac{1}{\varepsilon} * \frac{1}{\Delta t}$$

with the extinction coefficient of NADH ε=6220 $M^{-1} \cdot cm^{-1}$ and d=1cm. Activity was measured in Units defined as the amount of enzyme catalyzing 1 µmol substrate per minute. Protein concentrations were used for determination of specific activities. Mean values including standard deviations were calculated with Microsoft Excel.

2.7.3. Photometrical analysis of enzyme cascades with ω-TA

The functionality of a two- and three-enzyme cascade with a ω-TA was determined photometrically in one-pot reaction mixtures coupled with LDH and NADH. The decrease in absorbance was measured at 340 nm and 22 °C for 300 sec. Reaction mixtures for the coupled $HPL_{CP\text{-}N}$ and ω-TA reactions and the LOX-1, $HPL_{CP\text{-}N}$ and ω-TA reactions were mixed in a cuvette to a final volume of 1 ml and were prepared as follows:

HPL_{CP-N} – ω-TA:	**LOX-1 – HPL_{CP-N} – ω-TA:**
10 µl ω-TA solution	10 µl ω-TA solution
10 µl of a 20 U·ml^{-1} solution HPL_{CP-N}	10 µl of a 50 U·ml^{-1} LOX-1
10 µl of a 50 U·ml^{-1} LDH solution	10 µl of a 20 U·ml^{-1} solution HPL_{CP-N}
10 mM L-alanine	10 µl of a 50 U·ml^{-1} LDH solution
0.1 mM NADH	10 mM L-alanine
0.1 mM pyridoxal-5-phosphate	0.1 mM NADH
0.1 mM 13(*S*)-HPODE	0.1 mM pyridoxal-5-phosphate
	0.1 mM linoleic acid
ad 1 ml 50 mM KPO_4 buffer pH 7.5, 50 mM NaCl	*ad* 1 ml 50 mM KPO_4 buffer pH 7.5, 50 mM NaCl

2.7.4. Enzyme reactions with HPL and one-pot reactions with lipase, LOX and HPL

Gas chromatographic (GC) analysis of hexanal and 12-oxododecenoic acid formation during HPL catalyzed 13(*S*)-HPODE cleavage required slightly modified reaction conditions compared to the photometrical analysis of HPL activity described in chapter 2.7.1. For this, reactions were carried out with 10 U·ml^{-1} HPL_{CP-N} and 1 mM 13(*S*)-HPODE in 50 mM potassium phosphate buffer pH 6 containing 1 M NaCl and 0.2 % Triton X-100, typically in a total volume of 3 ml. Samples were incubated for up to 120 min at 22 °C or 0 °C and samples were taken in the course of the reaction for GC-FID analysis. For this, reactions were hydrogenated and derivatized by silylation (chapter 2.8.1.).

Coupled LOX-1 (Sigma-Aldrich, USA) and HPL_{CP-N} reactions were performed as one-pot reactions, with either simultaneous or consecutive enzyme addition. 400 µl of 50 mM potassium phosphate buffer pH 7.5 with 0.5 M NaCl and 0.05 % Triton X-100 containing LOX-1 (100 U·ml^{-1}) was mixed with an initial concentration of 1, 2.5 or 5 mM linoleic acid to start the enzyme reaction. 400 µl of 50 mM potassium phosphate buffer pH 7.5 with 0.5 M NaCl and 0.05 % Triton X-100 containing purified HPL_{CP-N} (20 U·ml^{-1}) was added either simultaneously or consecutively after pre-incubation of LOX-1. Simultaneous reactions were performed for 1 to 5 h before GC analysis, while in consecutive reactions, LOX-1 was pre-incubated with linoleic acid for 1 to 5 h before HPL_{CP-N} was added for further 15 min. The reactions were performed at 22 °C with open cups.

Moreover, one-pot reactions were conducted with *P. fluorescens* lipase, LOX-1 and HPL_{CP-N}. For simultaneous enzyme addition, 300 µl of each enzyme solution dissolved in 50 mM potassium phosphate buffer pH 7.5 containing 0.5 M NaCl and 0.05 % Triton X-100 was mixed with 17.6 U·ml^{-1} lipase, 100 U·ml^{-1} LOX-1 and 20 U·ml^{-1} HPL_{CP-N}. Safflower oil equivalent to a final concentration of 0.67 mM linoleic acid was added as substrate. Reactions were performed for 3 h

before GC analysis. For consecutive enzyme addition, 300 µl of lipase (17.6 U·ml^{-1}) was mixed with safflower oil equivalent to an initial concentration of 2 mM linoleic acid. 300 µl of LOX-1 (100 U·ml^{-1}) was added over a period of 3 h in 12 portions of each 25 µl before 300 µl of HPL_{CP-N} (20 U·ml^{-1}) was applied for 1 or 15 min before analysis. The diluted concentration of safflower oil corresponds to 0.67 mM linoleic acid.

2.7.5. Enzymatic preparation of 12-oxo-9(*Z*)-dodecenoic acid

12-Oxo-9(*Z*)-dodecenoic acid was synthesized by HPL serving as substrate for ω-TA biocatalysis. In a typical reaction set up, 5 mM 13(*S*)-HPODE was mixed with 20 U·ml^{-1} HPL_{CP-N} in 10 ml of 50 mM potassium phosphate buffer pH 6 containing 1 M NaCl. The reaction was carried out at 22 °C for 15 min before solvent extraction with 5 ml methyl tert-butyl ether (MTBE). The volatile co-product hexanal and the solvent were evaporated in a Concentrator plus vacuum concentrator (Eppendorf SE, Germany) at 22 °C until the solvent was totally evaporated. The remaining 12-oxo-9(*Z*)-dodecenoic acid was dissolved in ethanol, analyzed by GC-FID analysis and frozen at -80 °C until further use.

2.7.6. Enzyme catalysis with ω-TA and one-pot reactions with LOX, HPL and ω-TA

ω-TA catalyzed transamination of hexanal and 12-oxododecenoic acid was analyzed with high performance liquid chromatography (HPLC). For this, reaction conditions were slightly modified compared to photometrical analysis. Purified ω-TA was mixed with 50 mM L-alanine, 0.1 mM pyridoxal-5-phosphate and 2.5 mM substrate (12-oxo-9(*Z*)-dodecenoic acid, 12-oxo-10(*E*)-dodecenoic acid or hexanal) in 50 mM potassium phosphate buffer pH 7.5 containing 50 mM NaCl in a total volume of 500 µl. Reactions were conducted at 22 °C for 1 to 5 h. 100 µl of reaction solution was mixed with 900 µl of a 50:50 acetonitrile-water mixture for stopping the enzyme reaction and samples were filled into tight LC vials for HPLC analysis (chapter 2.8.3).

Furthermore, coupled enzymatic reactions with HPL_{CP-N} and TR_{AD} were performed and the formation of the reaction product 12-aminododecenoic was monitored by HPLC. Reaction mixtures were prepared with 250 µl HPL_{CP-N} (20 U·ml^{-1}) in 50 mM potassium phosphate buffer pH 7.5 containing 0.5 M NaCl with 50 mM L-alanine, 0.1 mM pyridoxal-5-phosphate and 250 µl TR_{AD} (5 U·ml^{-1}) in the same buffer. 13(*S*)-HPODE was added as substrate to a final concentration of 1 or 2.5 mM and reactions were carried out at 22 °C. Enzymes were either added simultaneously or consecutively. For simultaneous enzyme addition, both enzymes were added at the beginning and incubated for 1 h, whereas for consecutive enzyme addition, HPL_{CP-N} was incubated for 5 min before TR_{AD} was added for 1 h. In a second reaction setup for consecutive enzyme addition, HPL_{CP-N} was incubated for 5 min before TR_{AD} was added each 10 min (each

41.6 µl, resulting in 250 µl in total) over 1 hour. For analysis, samples were prepared as described above.

One-pot reactions with LOX-1, $HPL_{CP\text{-}N}$ and TR_{AD} were carried out either simultaneously or consecutively at 22 °C. Reactions were conducted with 100 U·ml^{-1} LOX-1, 20 U·ml^{-1} $HPL_{CP\text{-}N}$ and 5 U·ml^{-1} TR_{AD} in 50 mM potassium phosphate buffer pH 7.5 containing 0.5 M NaCl in a total volume of 500 µl. 50 mM L-alanine, 0.1 mM pyridoxal-5-phosphate and linoleic acid with a final concentration of 1 or 2.5 mM were applied. Reactions were performed at 22 °C. Three different reaction setups were prepared. For simultaneous enzyme addition, all enzymes were added at the beginning and reaction was conducted for 1 h. For consecutive enzyme addition, LOX-1 was pre-incubated with linoleic acid for 3 h, before $HPL_{CP\text{-}N}$ was added for 5 min and then TR_{AD} was applied together with L-alanine and pyridoxal-5-phosphate for another hour. In another reaction setup, LOX-1 was pre-incubated with linoleic acid for 3 h before TR_{AD} was added with L-alanine and pyridoxal-5-phosphate, and $HPL_{CP\text{-}N}$ was applied every 10 min for one hour. For HPLC analysis, samples were prepared as described above.

2.8. Analytic methods

2.8.1. Sample hydrogenation for GC analysis

Aldehydes were hydrogenated to alcohols for higher stability in gas chromatography analysis. For this, samples were mixed with an equivalent volume of 4 mg·ml^{-1} sodium borohydride in 20 mM NaOH and incubated for 1 h. Subsequently, the reaction mixtures were stopped by acidification with HCl to pH 2. A solvent extraction was performed with MTBE and the alcohols were then derivatized by silylation with 20 % (v/v) BSTFA-TMCS (99:1) for one hour at 80 °C.

2.8.2. Product analysis by gas chromatography coupled to MS and FID detection

LOX-1 and $HPL_{CP\text{-}N}$ reaction products were analyzed with GC-MS, using the GC-MS-QP2020 gas chromatograph, coupled to a mass spectrometer from Shimdazu (Japan) using electron ionization (EI). An ERAcc-5MS column from Isera (Germany) (length: 15 m, film thickness: 0.1 µm, inner diameter 0.32 mm) was used for chromatographic fractionation. Reduced and silylated samples of 1 µl volume were injected with a split ratio of 10 and a temperature gradient was applied as follows: 40 °C to 200 °C with 15 °C·min^{-1}, 200 °C to 280 °C with 5 °C·min^{-1} and hold at 280 °C for 2 min. Helium was used as carrier gas. Mass spectra were recorded between 40-500 m·z^{-1}. The reference substances 13(*S*)-HPODE, 12-oxo-9(*Z*)-dodecenoic acid, 12-oxo-10(*E*)-dodecenoic acid, hexanal and linoleic acid were used for spectra comparison.

Substances were quantified using a GC-2100 gas chromatograph with flame ionization detector (FID) (Shimadzu, Japan). The instrument was equipped with an MTX-Biodiesel TG column (length: 14 m, film thickness: 0.16 µm, inner diameter: 0.53 mm) from Restek (Germany). 1 µl of the reduced and silylated samples were injected with a split ratio of 10 and a temperature gradient was applied as follows: 40 °C to 175 °C with 12 °C·min^{-1}, 175 °C to 210 °C with 5 °C·min^{-1}, 210 °C to 330 °C with 25 °C·min^{-1} and hold at 330 °C for 2 min. Helium was used as carrier gas. Calibration curves were prepared for product quantification using the reduced and silylated reference substances linoleic acid, 13(*S*)-HPODE, 12-hydroxydodecanoic acid and hexanal.

2.8.3. Product analysis with HPLC coupled with MS and ELSD detection

ω-TA product formation was verified with HPLC coupled with mass spectrometry (MS). A LC-30AD Nexera LC/MS system from Shimadzu (Japan), equipped with a Shimadzu SPD-M20A UV detector and a Shimadzu LCMS-2020 mass spectrometry detector was used. 5 to 10 µl of sample was injected onto an Orbit-100-C18 5 µm column (30 mm × 4.6 mm) from Kromasil (Sweden). Water (A) and acetonitrile (B), each containing 0.1% formic acid, were used as the mobile phase and a linear gradient was applied with 0.1 min 20 % B; 20 % B to 90 % B within 4 min; 1.1 min holding at 90 % B, using a flow rate of 1.0 ml·min^{-1}. Ionization of the samples was performed by electron spray ionization (ESI) in negative and position mode and spectra were recorded from 50 to 700 m·z^{-1}. Reference spectra were obtained with the standards 12-aminododecanoic acid and hexylamine.

12-Aminododecenoic acid was quantified using an LC-20AD XR Nexera Liquid Chromatograph (Japan) equipped with an evaporative light scattering detector (ELSD) 100 (VWR, Germany). Samples of 10 to 20 µl were injected onto a LaChrom II+ C18 RP column (250 mm × 4.6 mm, 5 µm particle size) from Hitachi (Japan). A linear gradient was applied as follows: 20 % B to 60 % B within 14 min; 60 % B to 80 % B within 3 min; 80 % B to 90 % B within 5 min using a flow rate of 1.0 ml·min^{-1} and water (A) and acetonitrile (B) with 0.1 % formic acid as mobile phase. Calibration of the detector was performed with 12-aminododecanoic acid.

3. Results

In this work, a novel enzymatic route towards nylon-12 was developed. Starting from linoleic acid-rich oils, the coupling of lipoxygenase pathway enzymes and ω-transaminase enabled 12-aminododecenoic acid synthesis. For this purpose, one LOX, four HPLs and seven ω-TAs were cloned, expressed and characterized. Subsequently, enzyme cascades were established as one-pot reactions and the efficacy of the new route was demonstrated.

3.1. Lipoxygenase

3.1.1. Cloning and expression of soybean lipoxygenase LOX-1

13(*S*)-Specific lipoxygenase 1 from *G. max* (LOX-1) catalyzes the hydroperoxidation of linoleic acid to 13(*S*)-HPODE. This enzyme was chosen as expression target because good activity has been demonstrated in previous studies [65]. The encoding gene sequence was obtained from NCBI GenBank accession number AAA33986.1 and was codon-optimized for *E. coli* (Fig. A1). A synthetic gene of 2517 bp with a His6-tag sequence was synthesized and cloned into the expression vector pET-21b(+) by BioCat (Germany). Correct vector construction was verified by restriction analysis (Fig. 10) and DNA sequencing.

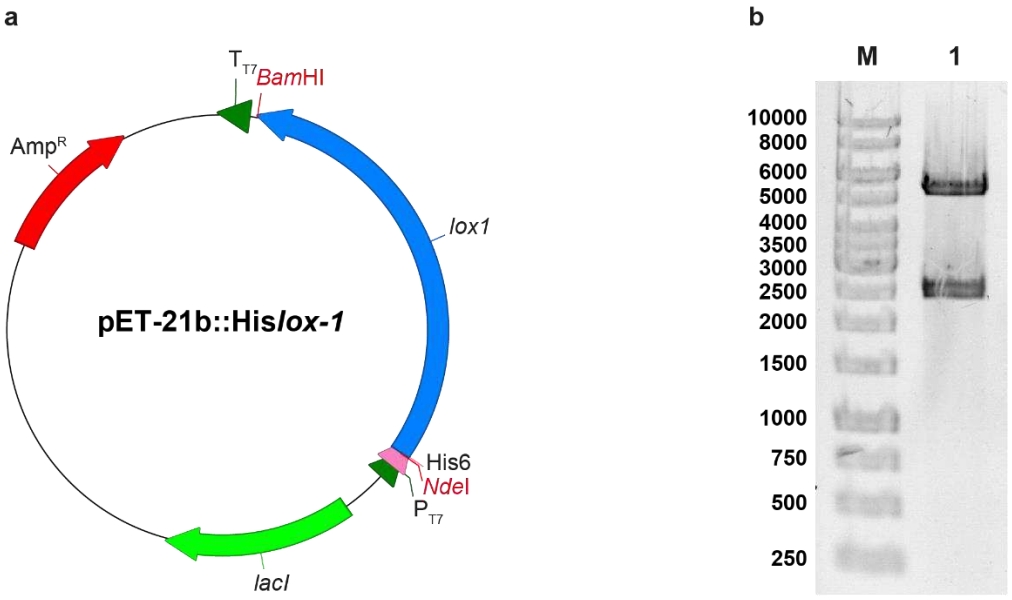

Fig. 10 Expression vector pET-21b::His*lox-1* for expression of *G. max* LOX-1 (**a**) and agarose gel of restriction digest of pET-21b::His*lox-1* with *Nde*I and *Bam*HI (**b**). M: DNA ladder marker with sizes in bp.

For LOX-1 expression, *E. coli* BL21(DE3) was grown for 24 h at 37 °C. Cells were harvested by centrifugation and disrupted by sonication to obtain the crude extract (CE). Insoluble fragments were removed by centrifugation, yielding the soluble fraction (SF). The enzymatic activity was

measured photometrically at 234 nm, detecting the formation of hydroperoxides with conjugated double bond system. Initial expression revealed that an active form of LOX-1 was obtained with a visible protein band in the crude extract on SDS-PAGE of around 95 kDa corresponding to the theoretical molecular weight of LOX-1 (Fig. 11). However, only 16 $U \cdot l^{-1}$ of soluble, active enzyme were obtained. Different cultivation temperatures and cultivation media were tested to determine the optimal expression conditions (Fig. 11). Cultivation was performed at temperatures between 10 to 37 °C (Fig. 11a+b). The highest LOX-1 activity was measured after cultivation at 15 °C reaching 1356 $U \cdot l^{-1}$. To further increase the enzyme expression, different cultivation media were tested and evaluated based on LOX-1 activity and cell density at OD_{600} (Fig. 11c). The OD_{600} increased from ~ 4.3 after cultivation in LB medium to ~16.5 in TB and ~17.3 in ZYM5052. The complex media TB and ZYM5052 provide a multiple of nutrients compared to LB, resulting in higher cell densities. Up to 11,447 $U \cdot l^{-1}$ soluble LOX-1 were obtained in TB medium while up to 1647 $U \cdot l^{-1}$ soluble LOX-1 were produced in ZYM5052. Consequently, in further experiments, expression of LOX-1 was performed in TB medium at 15 °C.

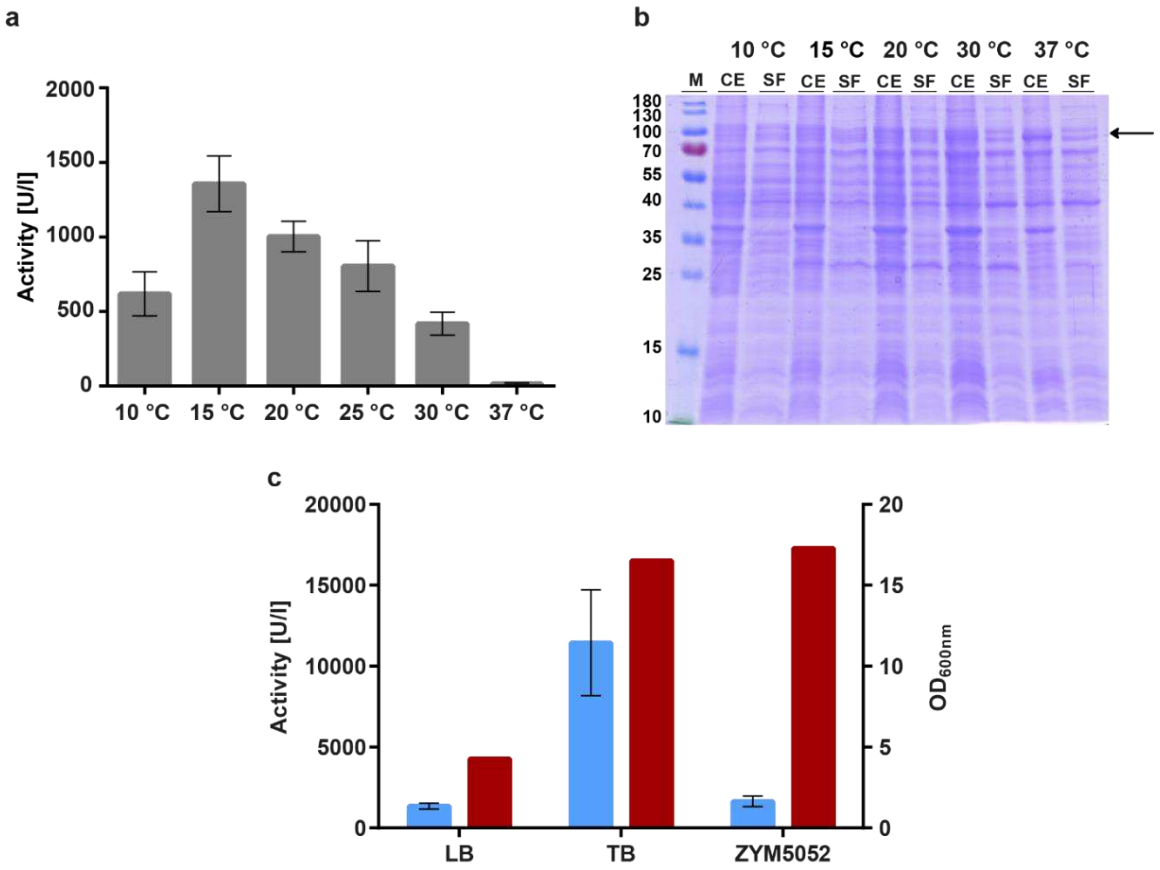

Fig. 11 Dependence of LOX-1 expression on different temperatures (**a + b**) and cultivation media (**c**). (**a**) Volumetric activity of soluble fractions was measured in triplicate after expression at different cultivation temperatures in LB. (**b**) SDS-PAGE with M: protein marker with sizes in kDa, CE: crude extract and SF: soluble fraction. The arrow marks the theoretical size of LOX-1. (**c**) Optical density (OD_{600}; red bars) measured after 24 h of expression in different cultivation media at 15 °C and volumetric activity of soluble fractions (blue bars) measured in triplicate after expression.

The effect of salt and imidazole concentration on LOX-1 activity was determined to analyze effects of buffer components during LOX-1 purification. For metal affinity chromatography of His-tagged proteins, imidazole is regularly used for elution. In addition, high salt concentrations are often added for purification. Cell pellets were suspended in in buffers containing either 50 or 500 mM NaCl or 40 or 500 mM imidazole. Activity was measured photometrically in borate buffer pH 9 (Fig. 12). The addition of salt in concentrations of 50 to 500 mM had a positive effect on the activity of LOX-1, as most of the activity from the crude extract was retained in the soluble fraction. However, the addition of imidazole resulted in a decrease of activity in the crude extract from 100 % to 78 % when 500 mM imidazole was added. Consequently, in further purification experiments, imidazole was removed by filtration after the purification process.

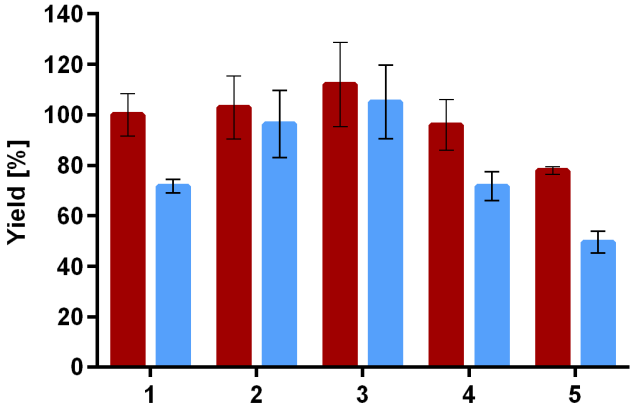

Fig. 12 Effect of salt concentration and addition of imidazole on activity of LOX-1. Photometric enzyme assays were performed with different buffers with the crude extract (red bars) and soluble fraction (blue bars) in triplicate. Buffer compositions: (**1**) 50 mM Tris, (**2**) 50 mM Tris + 50 mM NaCl, (**3**) 50 mM Tris + 500 mM NaCl, (**4**) 50 mM Tris + 40 mM imidazole and (**5**) 50 mM Tris + 500 mM imidazole.

3.1.2. Purification of LOX-1

His6-tagged LOX-1 was purified by metal affinity chromatography using a HisTrap™ FastFlow column from Cytiva, USA (Fig. 13a). In the purification process, the specific activity increased 54-fold from around 3 U·mg^{-1} in the crude extract to around 150 U·mg^{-1} in the eluate fraction after buffer exchange to remove imidazole (Table 9). SDS-PAGE was performed to monitor the purification process (Fig. 13b). While no clearly defined overexpression band was found on the SDS gel in either the crude extract or the soluble fraction, the eluate fraction contained a protein band of around 100 kDa corresponding to the size of LOX-1. A second protein band around 70 kDa and some faint bands were also visible on the SDS gel. A Western Blot was performed using specific antibody staining with an Anti-LOX-1 antibody (Agrisera, Sweden), which confirmed the presence of LOX-1 in all fractions (Fig. 13c). It was also shown that the band around 70 kDa and the other bands must be degradation products of LOX-1, because the specific multiclonal antibody

gave a positive response. To prevent protein degradation, several protease inhibitors were tested. However, neither the addition of phenylmethylsulfonyl fluoride (PMSF), a serine protease inhibitor, nor the addition of cOmplete™ Mini, EDTA-free Protease Inhibitor Cocktail (Roche, Switzerland) could reduce lipoxygenase degradation.

Table 9 Purification process of LOX-1 from 50 ml cultivation medium after cultivation at 15 °C in TB medium.

	Total Activity [U]	Volume [ml]	Volumetric activity [U·ml^{-1}]	Protein concen-tration [mg·ml^{-1}]	Specific activity [U·mg^{-1}]	Purifi-cation (fold)
Crude extract	1038	25	41.5	14.8	2.8	1
Soluble fraction	523	23	22.7	5.4	4.2	1.5
Eluate	271	6	45.1	0.3	150.3	53.7

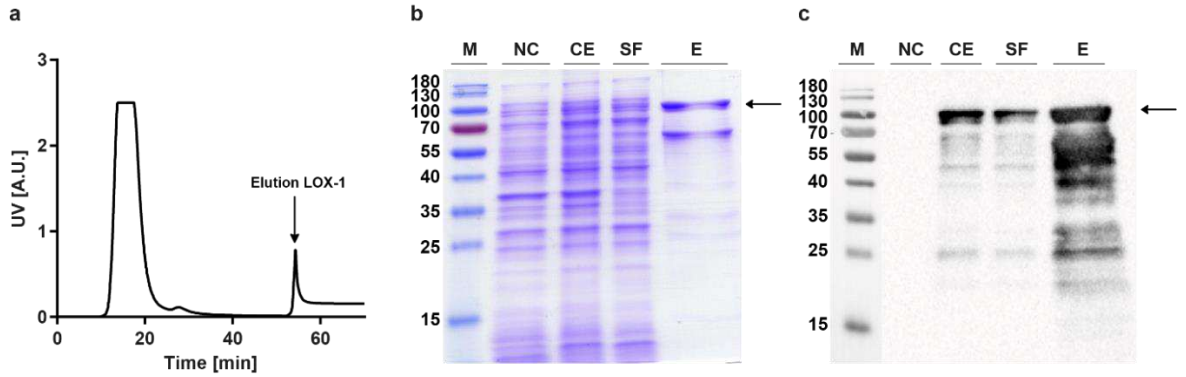

Fig. 13 Purification process of LOX-1. (**a**) Metal affinity chromatography purification was recorded at 280 nm. SDS-PAGE (**b**) and Western blot (**c**) with M: protein marker with sizes in kDa, NC: negative control, CE: crude extract, SF: soluble fraction and E: elution with 500 mM imidazole.

3.2. Hydroperoxide lyases

3.2.1. Selection and cloning of HPLs

Hydroperoxide lyases catalyze the cleavage of linoleic or α-linolenic acid hydroperoxide into a C_{12}-oxoacid and a C_6-aldehyde. HPLs are unstable enzymes and thus not available commercially. Therefore, gene sequences coding for potential HPLs were derived from literature and databank searches and four HPLs were selected for cloning and expression in *E. coli*:

- HPL from *P. guajava* (Acc. no.: AAK15070.1),
- HPL from *H. vulgare* (Acc. no.: AJ318870),
- Putative HPL from *C. papaya* (Acc. no.: XP_021890218.1) and

- Putative HPL from *S. bicolor* (Acc. no.: OQU84187.1).

HPL_{PG} from *P. guajava* is a well-characterized 13-HPL that was used for the synthesis of hexanal and 3(*Z*)-hexenal before [84, 103]. HPL_{HV} from *H. vulgare* was previously characterized as well and showed good activity towards 13(*S*)-HPOTE and 13(*S*)-HPODE [107]. A BLAST search was performed to identify putative novel, yet uncharacterized HPL homologs. HPL sequences from *C. papaya* (HPL_{CP}) and from *S. bicolor* (HPL_{SB}) were selected which exhibited sequence identities of 66.17 % and 48.13 % compared to HPL_{PG} and 50.97 % and 71.46 % compared to HPL_{HV}. The *hpl* genes were codon-optimized for expression in *E. coli* (Fig. A3-Fig. A6). Synthetic genes with a His6-tag were cloned into the pET-28a(+)vector by BioCat (Germany). The expression vectors were verified by DNA sequencing and DNA restriction, confirming correct insertion of the ~1500 bp *hpl* genes (Fig. 14 & Fig. A7).

Since previous studies have shown that guava HPL activity increased significantly after removal of the hydrophobic, unconserved N-terminus [103], this gene was directly synthesized without this region. In HPLs, the N-terminal sequence is not conserved and contains hydrophobic amino acids that may affect enzyme solubility. To identify the unconserved N-terminus of the other HPLs, a multiple sequence alignment was performed using ClustalΩ [178] (Fig. 15 & Fig. A8). Subsequently, the N-terminal sequences were removed by PCR-based subcloning (Fig. A9). The truncated sequences were then cloned into the cloning vector pJET1.2 and *E. coli* XL1-Blue was transformed for amplification. The gene sequences (Fig. A3-A6) were ligated into the expression vector pET-28a(+) and verified by restriction digestion (Fig. 14 & Fig. A10) and DNA sequencing, confirming the correct cloning of the ~1450 bp truncated *hpl-N* genes.

Moreover, fusion proteins were generated with the solubility-enhancing protein NusA. NusA is a transcription elongation factor of RNA polymerase with high solubility. Solubility enhancement has been demonstrated for several NusA fusion proteins [187–189]. In this work, fusion proteins were generated by fusion PCRs using the pET-43.1a(+) vector for amplification of *nusA* (Fig. A12) and pET-28::*hpl-N* for amplification of *hpl-N* (Fig. A11). An enterokinase cleavage site was added in between the two proteins, enabling post-translational cleavage. The fusion PCR constructs (Fig. A13-A16) were ligated into the pET-28a(+) vector and verified by restriction digestion (Fig. 14 & Fig. A17) and DNA sequencing, confirming the correct fusion constructs of ~3000 bp.

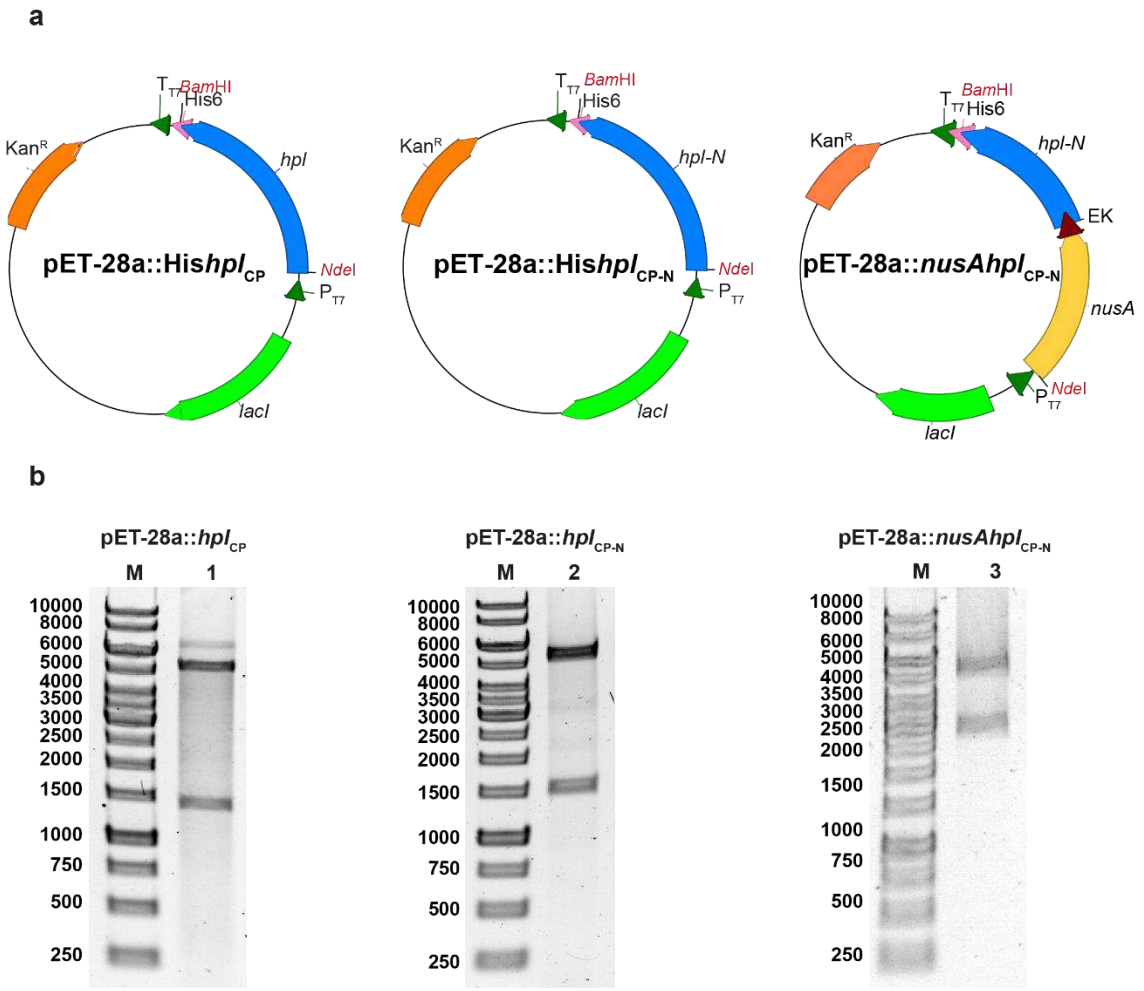

Fig. 14 Expression vectors for HPL expression (**a**) and agarose gels of restriction digest of the vectors with *Nde*I and *Bam*HI (**b**), exemplified for *C. papaya* HPL$_{CP}$. Restriction digests of the other HPLs are found in the appendix (Fig. A7, Fig. A10, Fig. A17). M: DNA ladder marker with sizes in bp. Figure modified and reproduced from [175] with permission from Springer Nature.

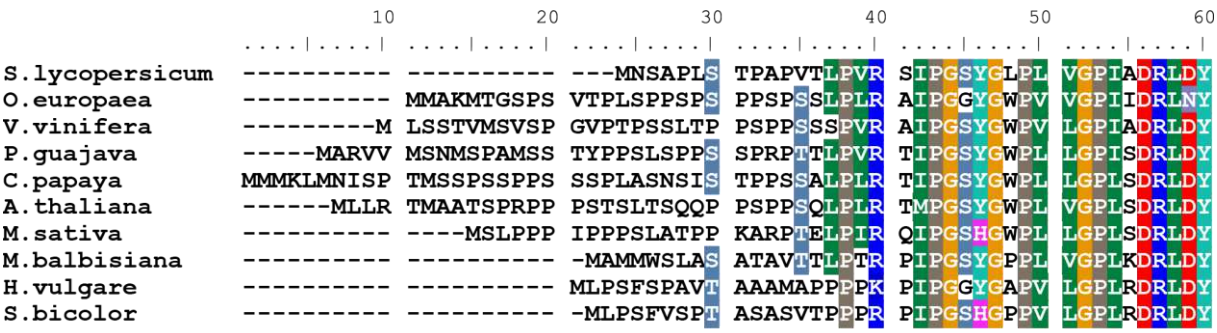

Fig. 15 Multiple sequence alignment of the N-terminal sequences of HPLs obtained with ClustalΩ [178]. The first 60 amino acids are shown. The full-length sequence alignment is presented in appendix Fig. A8. Figure reproduced from [175] with permission from Springer Nature.

3.2.2. Expression of HPLs

E. coli BL21(DE3) was transformed with the appropriate vectors and protein expression was performed in TB medium for 24 h at 25 °C. For N-terminally truncated guava HPL_{PG-N} a protein band was detected in the crude extract around 50 kDa on SDS-PAGE, which corresponds to the calculated molecular weight of the enzyme (Fig. 16a). However, in the soluble fraction no protein band was visible at the corresponding position, so a large amount of HPL_{PG-N} was probably expressed as insoluble protein. Overexpression of the fusion protein $NusAHPL_{PG-N}$ was observed in the crude extract with a protein band around 95 kDa, which again was not preserved in the soluble fraction. Full-length and N-terminally truncated sorghum HPL_{SB} and HPL_{SB-N} showed weak protein bands in the crude extract around 50 kDa and no band in the soluble fraction on SDS-PAGE, suggesting again insoluble enzyme expression (Fig. 16b). No protein band was visible for the fusion protein $NusAHPL_{SB-N}$ at the corresponding position of 95 kDa. Full-length as well as N-terminally truncated barley HPL_{HV} and HPL_{HV-N} showed strong protein bands in the crude extract around 50 kDa, but again no protein band in the soluble fraction (Fig. 16c). Thus, most of the enzyme seems to be expressed insolubly. In contrast, no protein bands were visible for the fusion protein $NusAHPL_{HV-N}$ at 95 kDa. For papaya HPL_{CP} and fusion $NusAHPL_{CP-N}$ no protein bands were detected at the corresponding positions. However, a protein band was visible in the crude extract of N-terminally truncated HPL_{CP-N} at 50 kDa, but not in the soluble fraction, suggesting expression of mainly unsoluble enzyme (Fig. 16d).

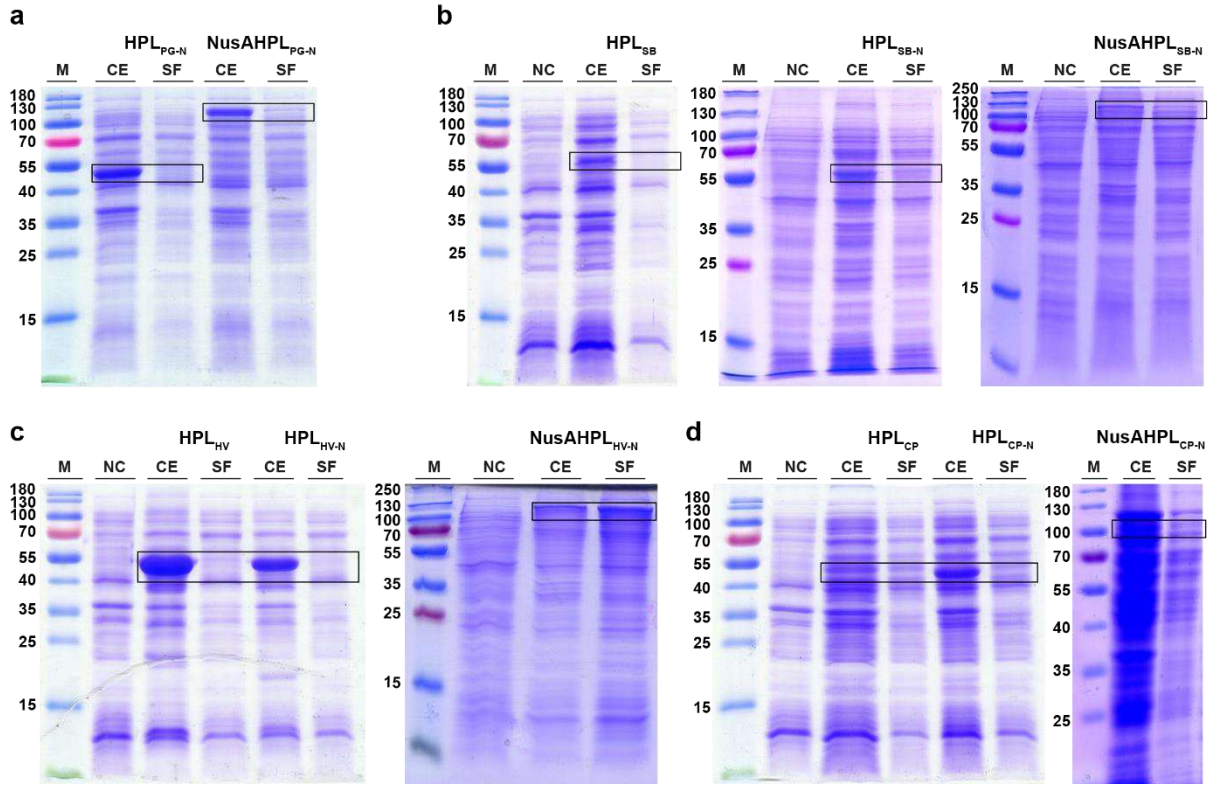

Fig. 16 SDS-PAGEs of enzyme expression of HPLs in full-length, N-terminal truncated constructs and NusA–HPL fusion proteins with HPLs from (**a**) *P. guajava* (PG), (**b**) *S. bicolor* (SB) (**c**) *H. vulgare* (HV) and (**d**) *C. papaya* (CP). M: protein marker with sizes in kDa, NC: negative control, CE: crude extract and SF: soluble fraction. Figure modified and reproduced from [175] with permission from Springer Nature.

Only low activity was measured for full-length HPLs from papaya and barley (0.03 and 0.04 U·mg^{-1}), whereas no activity was measured for sorghum HPL (Fig. 17). Increased activity was detected for all N-terminal truncated enzymes and NusA fusion proteins. For guava, sorghum and papaya HPL, activities of the N-terminal truncated enzymes were approximately equal to the activities of the NusA fusion proteins, whereas for barley HPL, the activity of the NusA fusion protein was significantly higher. HPL from *S. bicolor* showed only low activity in the N-terminal truncated form and the NusA fusion construct with 0.02 and 0.03 U·mg^{-1}. The highest specific activities were measured with HPL$_{CP-N}$ and NusAHPL$_{CP-N}$ with 0.85 and 0.84 U·mg^{-1} in the soluble fraction. Since the activity of the N-terminal truncated construct and the fusion construct were in the same range, further experiments were performed with the truncated construct to avoid possible interfering of the NusA protein during characterization of papaya HPL.

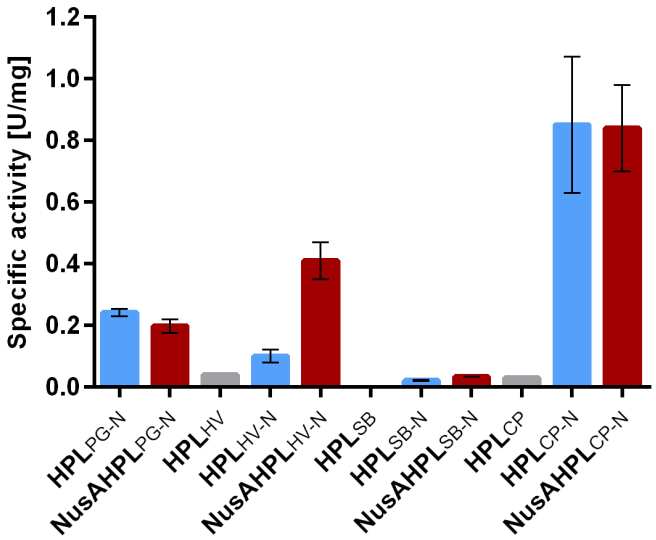

Fig. 17 Comparison of specific activities of HPL (grey bars), truncated HPL-N (blue bars) and fusion NusAHPL-N (red bars) proteins from *P. guajava* (PG), *H. vulgare* (HV), *S. bicolor* (SB) and *C. papaya* (CP). Activities were measured in the soluble fractions of the enzymes in triplicate.

3.2.3. Optimization of expression and solubilization of HPL_{CP-N}

Many HPLs have been reported to be membrane-associated, including guava HPL_{PG} [84]. Based on the high sequence identity with HPL_{CP}, we suspect that the papaya enzyme is also a membrane protein. Limited solubility and formation of inclusion bodies of membrane-associated enzymes is an issue, which deserves optimization. Membrane proteins are often incorporated into the cytoplasmic membrane of *E. coli* using the sec-translocon. The sec-translocon, however, is rapidly saturated, resulting in misfolded proteins that form inclusion bodies [172]. To improve the expression of HPL_{CP-N}, cultivation was tested using the C41(DE3) and Lemo21(DE3) strains, which are both designed to improve membrane protein expression [171, 172]. The level of proteins expressed with Lemo21(DE3) was described to be adjustable by the addition of different concentrations of L-rhamnose, thereby affecting the level of lysozyme, which acts as an inhibitor of T7 RNA polymerase. Around 369 $U \cdot l^{-1}$ were obtained in Lemo21(DE3) cultivation with no added L-rhamnose and even less activity was measured in cultivations with L-rhamnose (Fig. 18). 603 $U \cdot l^{-1}$ were found in the soluble fraction of C41(DE3). In contrast, around 1541 $U \cdot l^{-1}$ were measured from expressions with the initial used BL21(DE3) strain. Moreover, no increase in soluble protein bands were visible on SDS-PAGE from expressions in C41(DE3) and Lemo21(DE3) (Fig. A18 & Fig. A19). For this reason, the initially used BL21(DE3) strain was kept for further experiments.

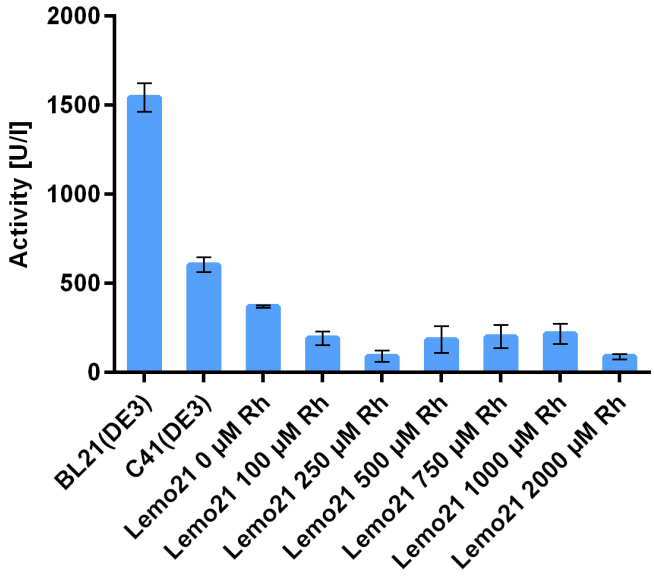

Fig. 18 Evaluation of the optimal expression strain for $HPL_{CP\text{-}N}$ production. Activity was measured photometrically in the soluble fraction in triplicate after cultivation at 25 °C in TB + δ-aminolevulinic acid and ammonium ferric citrate. The expression strains BL21(DE3), C41(DE3) and Lemo21(DE3) with varying L-rhamnose (Rh) concentrations were tested.

In further experiments, the cultivation conditions for the expression of $HPL_{CP\text{-}N}$ were optimized. For this purpose, cultivation was performed with temperatures ranging from 15 to 37 °C and activity was determined photometrically (Fig. 19). The highest HPL activity was observed for expressions at 25 °C (Fig. 19a) and was therefore used for all further experiments. In addition, the cultivation media LB, TB and ZYM5052 were tested with and without the addition of the supplements ammonium ferric citrate as iron source and δ-aminolevulinic acid (ALA) as heme precursor. Cultivation with LB medium reached around 441 $U \cdot l^{-1}$, whereas 1541 $U \cdot l^{-1}$ were obtained in cultivation with TB medium containing δ-aminolevulinic acid and 2694 $U \cdot l^{-1}$ in the autoinductive medium ZYM5052 containing δ-aminolevulinic acid (Fig. 19b). Consequently, further cultivations for $HPL_{CP\text{-}N}$ expression were carried out in ZYM5052 medium containing δ-aminolevulinic acid.

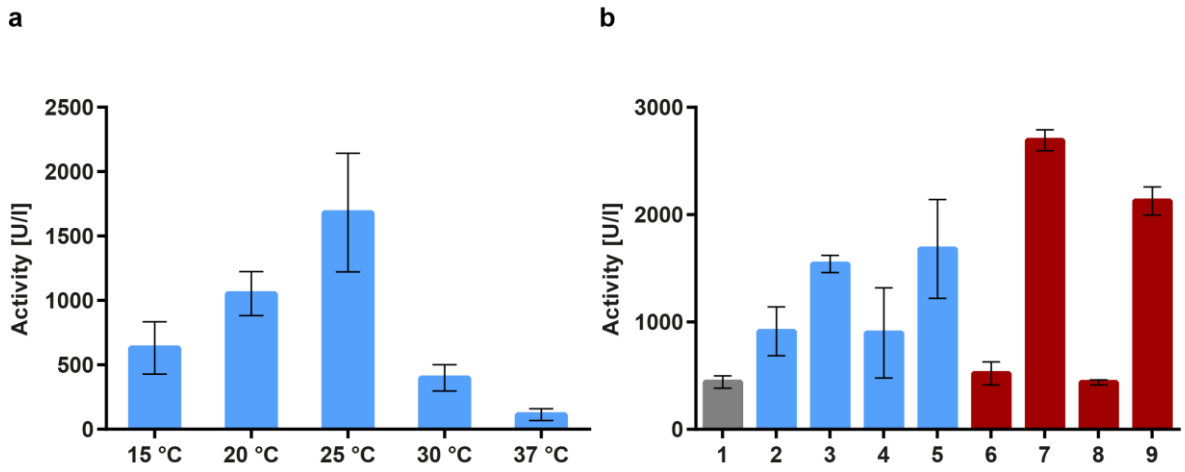

Fig. 19 Evaluation of optimal cultivation temperature (**a**) and cultivation medium (**b**) for $HPL_{CP\text{-}N}$ expression. Activity was measured photometrically in the soluble fraction in triplicate. (**a**) Activity measurements after cultivation in TB + δ-aminolevulinic acid (ALA) + ammonium ferric citrate (Fe) between 15 to 37 °C. (**b**) Activity measurements after cultivation at 25 °C in different cultivation media with 1: LB (grey bars), 2: TB (blue bars), 3: TB + ALA, 4: TB + Fe, 5: TB + ALA + Fe, 6: ZYM5052 (red bars), 7: ZYM5052 + ALA, 8: ZYM5052 + Fe, 9: ZYM5052 + ALA + Fe. Figure modified and reproduced from [175] with permission from Springer Nature.

A buffer screening was performed to optimize the solubility and activity of papaya $HPL_{CP\text{-}N}$. For this purpose, different buffer substances, pH values, as well as the addition of salts and detergents were tested (Fig. 20). The cell pellets were dissolved in the appropriate buffer and enzyme assays were performed in the same buffer. 50 mM Tris buffer pH 7.5 containing 50 mM NaCl was used as starting buffer and gradually each component was exchanged and its influence on solubility and activity was tested photometrically. The highest activity was measured when the pH value was reduced to pH 6, the buffer substance was exchanged to 50 mM potassium phosphate and the salt concentration was increased to 1 M. However, increased activities were only measured in the crude extract but not in the soluble fraction. To preserve the activity from the crude extract into the soluble fraction, the addition of a detergent was shown to be essential. Here, the best activities were measured upon addition of 0.2 % Triton X-100. By combining the best buffer components (50 mM potassium phosphate buffer pH 6 containing 1 M NaCl and 0.2 % Triton X-100), the activity of $HPL_{CP\text{-}N}$ in the soluble fraction was increased 60-fold (Fig. 20).

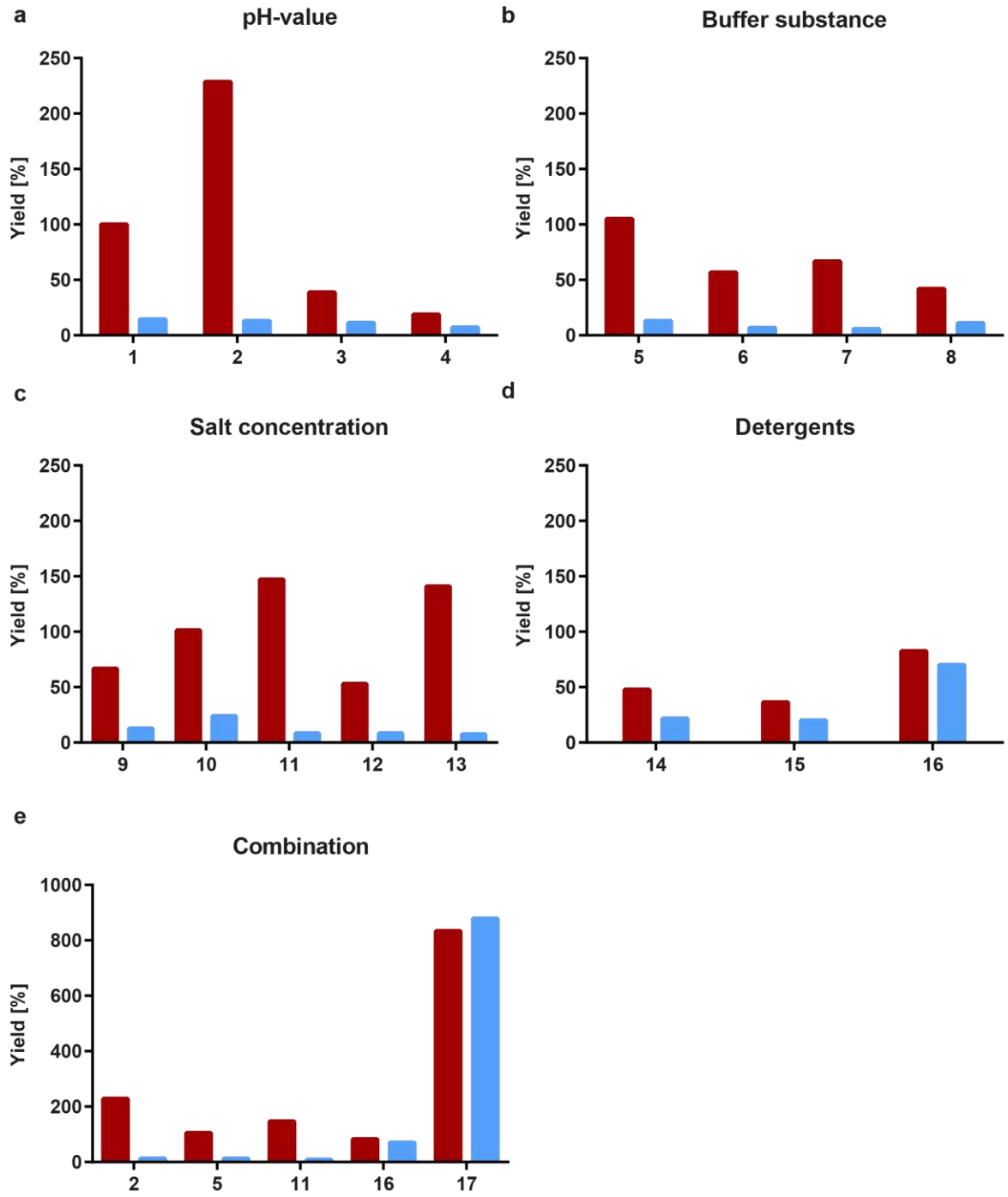

Fig. 20 Evaluation of optimal buffer for $HPL_{CP\text{-}N}$ solubilization and activity assay. The initially used 50 mM Tris buffer pH 7 containing 0.05 M NaCl (1) was set to 100 % and effects were subsequently evaluated in a one-factor-at-a-time approach. (**a**) pH values with (1) 50 mM Tris pH 7, (2) 50 mM potassium phosphate pH 6, (3) 50 mM Tris pH 8 and (4) 50 mM Tris pH 9; (**b**) Buffer substances with (5) 50 mM potassium phosphate, (6) 50 mM HEPES, (7) 50 mM MOPS and (8) 50 mM Bis-Tris; (**c**) Salt concentrations with (9) no salt, (10) 0.5 M NaCl, (11) 1 M NaCl, (12) 0.1 M KCl and (13) 1 M KCl; (**d**) Detergents with (14) 0.2 % Brij®, (15) 0.2 % Tween-20 and (16) 0.2 % Triton X-100. (**e**) The best buffer conditions of (**a**) – (**d**) were combined to buffer (17) with 50 mM potassium phosphate pH 6 containing 1 M NaCl and 0.2 % Triton X-100. Activity measurements were performed with the crude extract (red) and the soluble fraction (blue) in the same buffer used for solubilization. Figure modified and reproduced from [175] with permission from Springer Nature.

3.2.4. Fermentation, purification and biochemical characterization of HPL_{CP-N}

To obtain large quantities of the enzyme for purification, HPL_{CP-N} was expressed in a 3 l bioreactor containing 1.5 l ZYM5052 with δ-aminolevulinic acid. In a typical fermentation process, around 7174 U were obtained with a specific activity of 1.15 $U \cdot mg^{-1}$ in the crude extract and 1.27 $U \cdot mg^{-1}$ in the soluble fraction (Table 10). HPL_{CP-N} was purified by metal affinity chromatography using a HisTrap™ FastFlow column with bound nickel ions from Cytiva (USA). First, purification was performed using 50 mM potassium phosphate buffer pH 6 containing 1 M NaCl and 40 mM imidazole as binding buffer. After loading the soluble fraction onto the column, non-specific proteins were washed with 40 mM imidazole and HPL_{CP-N} was eluted with 500 mM imidazole. Active HPL_{CP-N} was eluted and a specific activity of 1.91 $U \cdot mg^{-1}$ was measured in the eluate fraction (Fig. A20). However, several non-specifically bound proteins were present in the eluate fraction as well that negatively influenced purity and specific activity. To optimize the purification process, a linear gradient of 40 to 500 mM imidazole was tested to determine the optimal imidazole concentration for the washing steps and HPL elution (Fig. A21). In addition, 0.1 % Triton X-100 was added to the buffers to ensure solubility of HPL. Many non-specific proteins were washed from the column at an imidazole concentration of around 100 mM and HPL_{CP-N} was eluted at an imidazole concentration of about 250 mM with a specific activity of 17.9 $U \cdot mg^{-1}$ (Fig. A21). Yet, some residual activity was measured after elution with an imidazole concentration of 500 mM. In further purification processes, stepwise washing steps of 40 mM and 100 mM imidazole were applied prior to elution of HPL_{CP-N} with 500 mM imidazole (Fig. 21a). Although the eluate fraction was still not completely pure, a strong enrichment was achieved. During a typical purification process, the specific activity increased almost 16-fold from 1.15 $U \cdot mg^{-1}$ in the crude extract to 18.21 $U \cdot mg^{-1}$ in the eluate (Table. 10). A Western Blot was performed with a monoclonal Anti-His antibody (Thermo Fisher Scientific, USA), confirming the presence of the His6-tagged HPL in the eluate fraction (Fig. 21b).

Table 10 Fermentation and purification process of HPL_{CP-N} determined with activity assays. Cells were cultivated with a volume of 1.5 l ZYM5052+δ-aminolevulinic acid in a 3 l bioreactor. Table reproduced from [175] with permission from Springer Nature.

	Total Activity [U]	**Volume [ml]**	**Volumetric activity [$U \cdot ml^{-1}$]**	**Protein concentration [$mg \cdot ml^{-1}$]**	**Specific activity [$U \cdot mg^{-1}$]**
Crude extract	7174	600	11.96	10.41	1.15
Soluble fraction	5722	600	9.54	7.53	1.27
Eluate	2447	120	20.39	1.12	18.21

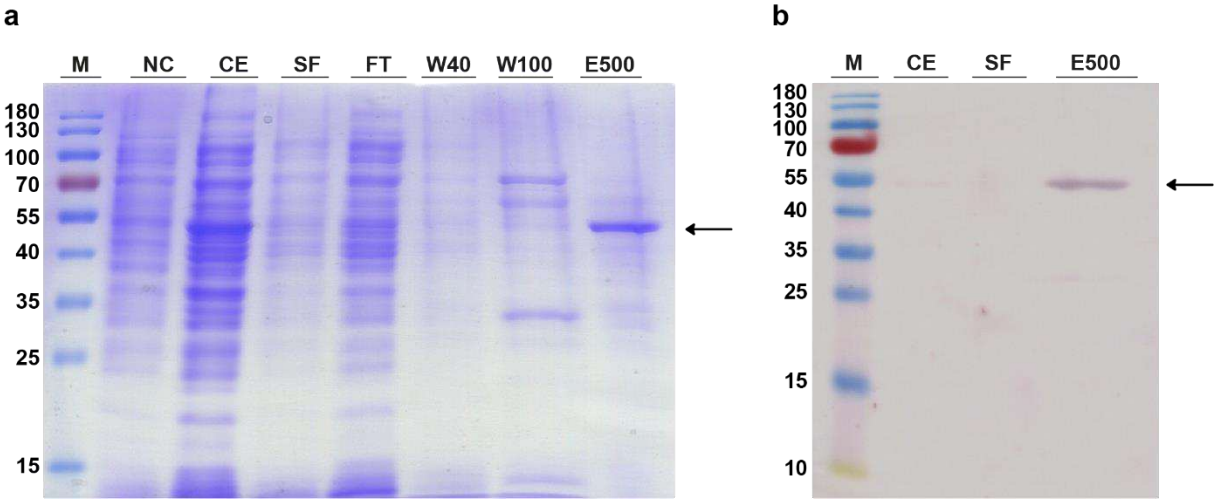

Fig. 21 Purification process of $HPL_{CP\text{-}N}$, determined by SDS-PAGE (**a**) and Western Blot (**b**). M: protein marker with sizes in kDa, NC: negative control, CE: crude extract, SF: soluble fraction, FT: flow through, W40: washing fraction with 40 mM imidazole, W100: washing fraction with 100 mM imidazole and E: elution with 500 mM imidazole. Figure modified and reproduced from [175] with permission from Springer Nature.

The native molecular weight of $HPL_{CP\text{-}N}$ was determined by size exclusion chromatography, using a 200 Increase 10/300 Superdex™ (Cytiva, USA) gel filtration column. The column was calibrated with the gel filtration markers kit for protein molecular weights of 29,000-700,000 Da (Sigma-Aldrich, USA) (Fig. 22). The molecular weight of the $HPL_{CP\text{-}N}$ in its native state was determined to be 225.9 kDa. Since the calculated molecular weight of the truncated and His6-tagged $HPL_{CP\text{-}N}$ is 53 kDa, it can be assumed that $HPL_{CP\text{-}N}$ is a tetramer.

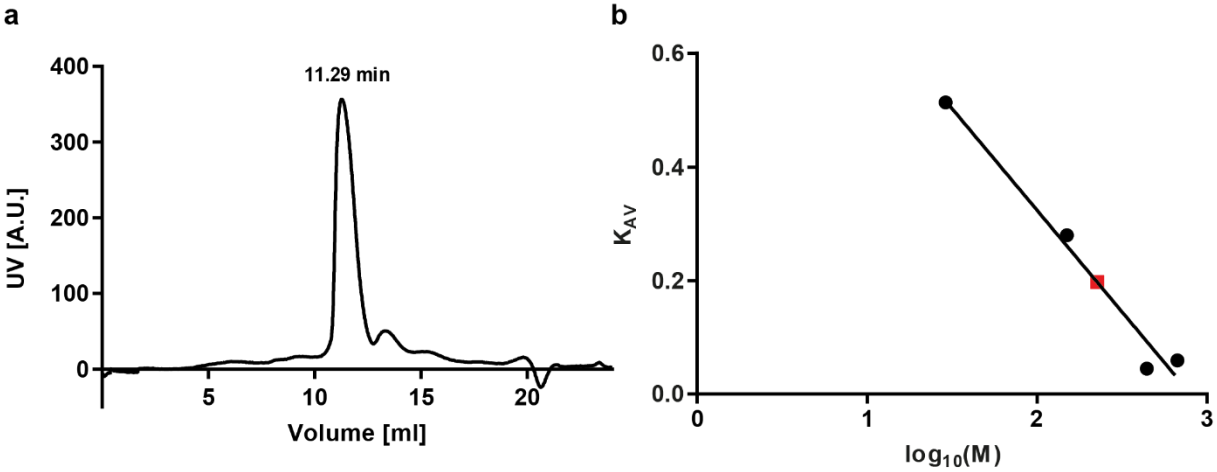

Fig. 22 Determination of molecular weight of native $HPL_{CP\text{-}N}$ by gel filtration (**a**) after calibration with carboanydrase (29 kDa), alcohol dehydrogenase (150 kDa), apoferritin (443 kDa) and thyroglobulin (669 kDa) (**b**). The distribution coefficients K_{AV} of the calibration proteins (black circles ●) were drawn against the logarithm of their known molecular weight. Based on the calculated formula (y = -0.3582x + 1.04), $HPL_{CP\text{-}N}$ (red square ■) with a K_{AV} of 0.197 obtained a $log_{10}(M)$ of 2.354, corresponding to a molecular weight of 225.9 kDa. Figure (b) reproduced from [175] with permission from Springer Nature.

The pH dependency of purified HPL_{CP-N} was determined photometrically in the range from pH 6 to pH 9 (Fig. 23). Highest activity was measured at pH 6, while 40 % of the activity was still retained at pH 9.

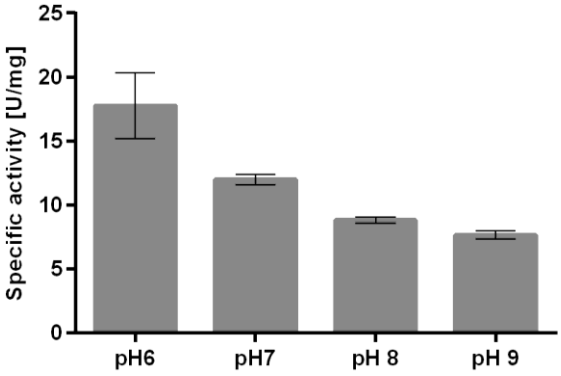

Fig. 23 Determination of pH dependence of purified HPL_{CP-N} from pH 6 to 9. Activity was measured photometrically in triplicate. Figure reproduced from [175] with permission from Springer Nature.

For comparison of the substrate affinities and catalytic efficiencies of HPL_{CP-N} for 13(*S*)-HPODE and 13(*S*)-HPOTE substrates, photometric enzyme assays were performed in triplicate using concentrations ranging from 0.005 to 0.1 mM of each hydroperoxide. Measured enzyme activities in ($mM \cdot min^{-1}$) were drawn against the initially applied substrate concentrations. Nonlinear regression was performed (Fig. 24) and the kinetic parameters K_m (Michaelis-Menten constant), v_{max} (maximum reaction rate) and k_{cat} (turnover number) were calculated using the GraphPad Prism 6.05 program (Table 11). The K_m value of HPL_{CP-N} is 140 µM for 13(*S*)-HPODE and 150 µM for 13(*S*)-HPOTE indicating a similar substrate affinity. HPL_{CP-N} shows a 1.55 fold higher catalytic efficiency (k_{cat}/K_m) towards 13(*S*)-HPOTE (4.23×10^6 $s^{-1} \cdot M^{-1}$) compared to 13(*S*)-HPODE (2.73×10^6 $s^{-1} \cdot M^{-1}$), showing a slight substrate preference for 13(*S*)-HPOTE.

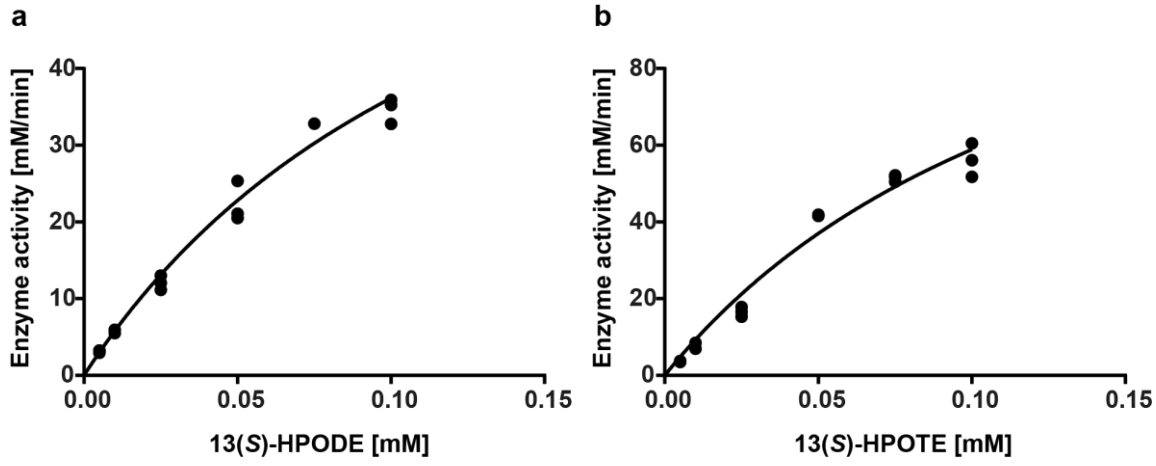

Fig. 24 Enzyme activity was measured in dependence of substrate concentrations ranging from 0.005 mM to 0.1 mM with (**a**) 13(*S*)-HPODE and (**b**) 13(*S*)-HPOTE. Diagrams were drawn with GraphPad Prism 6.05. Figure reproduced from [175] with permission from Springer Nature.

Table 11 Kinetic parameters of HPL_{CP-N} reaction with 13(*S*)-HPODE and 13(*S*)-HPOTE as substrates. Photometric activity assays were performed in triplicate and K_m, v_{max}, k_{cat} and catalytic efficiency k_{cat}/K_m were calculated with GraphPad Prism 6.05. Figure reproduced from [175] with permission from Springer Nature.

Substrates	K_m [µM]	V_{max} [µM·s^{-1}]	k_{cat} [s^{-1}]	k_{cat}/K_m [s^{-1}·M^{-1}]
13(*S*)-HPODE	140 ± 30	1452 ± 224	382	2.73×10^6
13(*S*)-HPOTE	150 ± 40	2408 ± 487	634	4.23×10^6

3.2.5. Monitoring of the HPL_{CP-N} reaction

Photometric analyses of the HPL reaction can only show the disappearance of the conjugated double bond system of the hydroperoxides, but does not give direct evidence of the reaction products. To monitor the formation of hexanal and 12-oxo-9(*Z*)-dodecenoic acid over the course of the HPL_{CP-N} reaction, GC-MS and GC-FID studies were conducted. For this purpose, reactions were typically carried out with 10 U·ml^{-1} of the soluble fraction of HPL_{CP-N} and 1 mM 13(*S*)-HPODE at 22 °C for up to 120 min. 12-Oxo-9(*Z*)-dodecenoic acid (peak at 11.9 min) and hexanal (peak at 2.3 min) were formed very rapidly within 10 sec after HPL_{CP-N} addition (Fig. 25). The major signals on mass spectra were 73 m/z and 103 m/z for hydrogenated and silylated 12-oxo-9(*Z*)-dodecenoic acid and 75 m/z and 159 m/z for hydrogenated and silylated hexanal (Fig. 26). This was confirmed by mass spectra of their reference standards (Fig. A22). Within the next 120 min, the peak for 12-oxo-9(*Z*)-dodecenoic acid at 11.9 min decreased and another small peak was detected at 12.2 min (Fig. 25). This peak correlates to a mass spectrum with main signals at 73 m/z and 129 m/z, corresponding to 12-oxo-10(*E*)-dodecenoic acid (traumatin), as confirmed with its reference standard (Fig. 26 & Fig. A22).

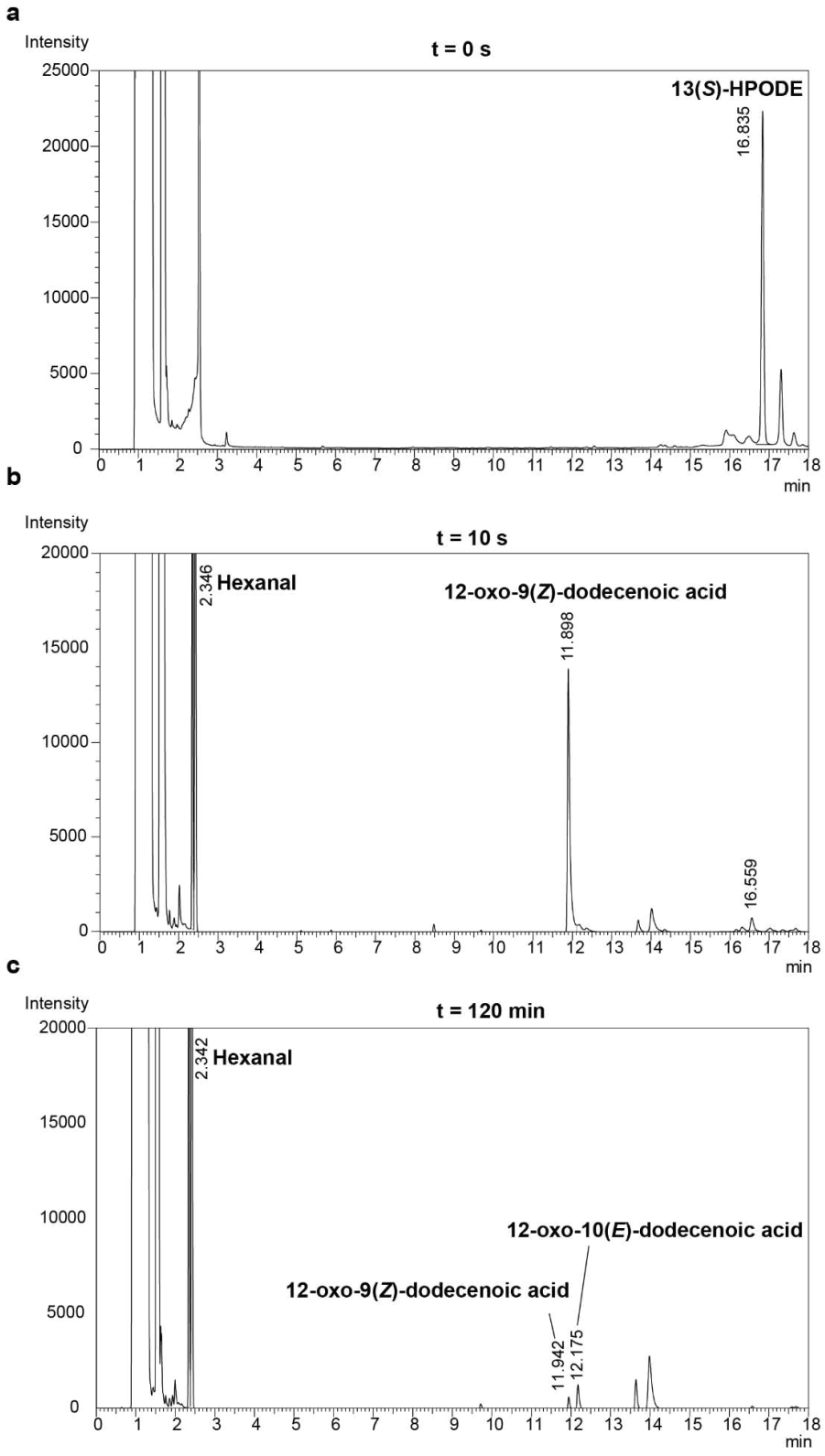

Fig. 25 GC-FID spectra of 13(*S*)-HPODE (**a**) and after incubation with soluble fraction of $HPL_{CP\text{-}N}$ at 22 °C for 10 sec (**b**) and for 120 min (**c**). Samples were hydrogenated with sodium borohydride and silylated with BSTFA-TMCS. Figure modified and reproduced from [175] with permission from Springer Nature.

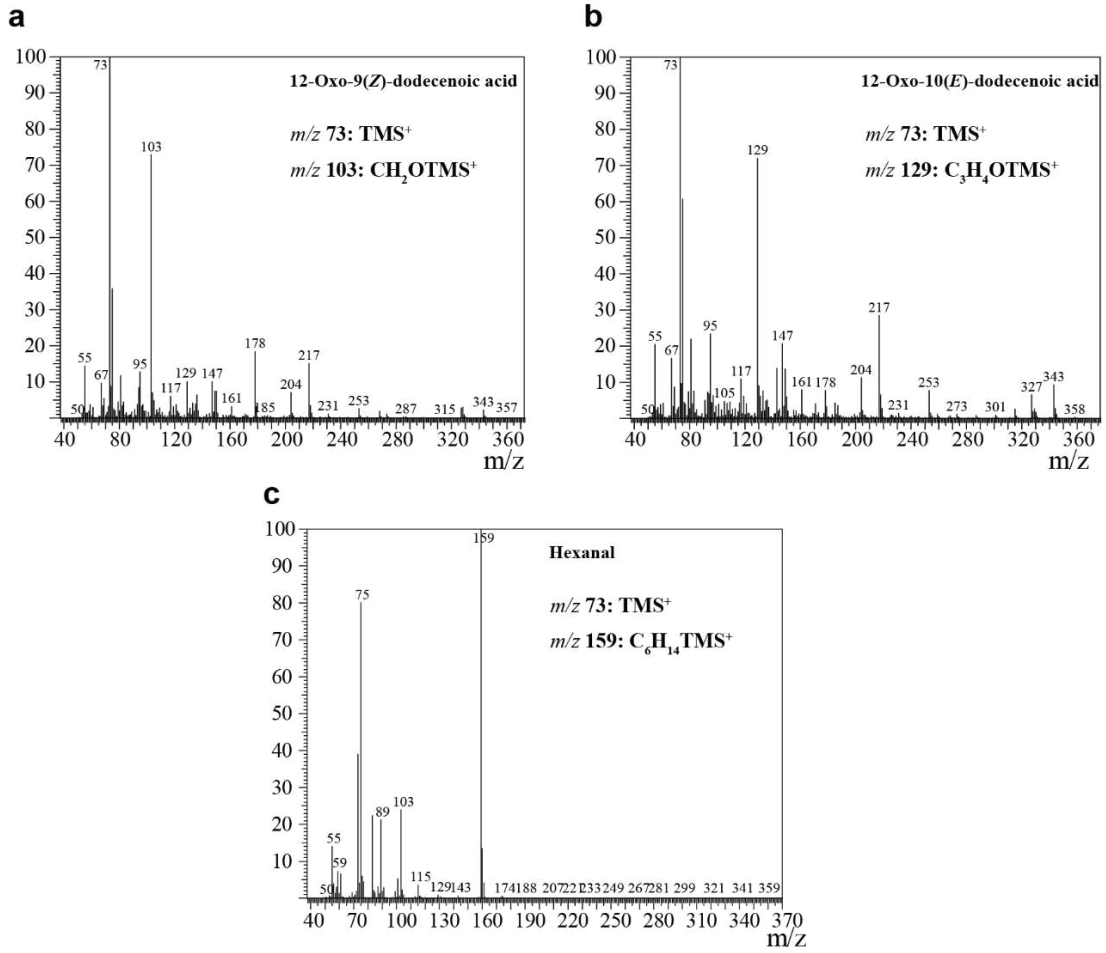

Fig. 26 Mass spectra of GC-peaks from 2.3 min (hexanal), 11.9 min (12-oxo-9(*Z*)-dodecenoic acid) and 12.2 min (12-oxo-10(*E*)-dodecenoic acid) retention time. Samples were hydrogenated with sodium borohydride and silylated with BSTFA-TMCS. Figure modified and reproduced from [175] with permission from Springer Nature.

Time-course experiments were carried out under different conditions to analyse the stability of the reaction products hexanal and 12-oxo-9(*Z*)-dodecenoic acid (Fig. 27). Reactions were performed with 1 mM 13(*S*)-HPODE as substrate and were run between 5 sec to 120 min prior to analysis by GC-FID. Calibration curves were generated with 12-hydroxydodecanoic acid and hexanal (Fig. A23). Since 12-oxo-9(*Z*)-dodecenoic acid was commercially available only in small quantities, 12-hydroxydodecanoic acid was used as calibration substance. Samples in which the soluble fraction was applied as enzyme source, after a very rapid formation of ~0.76 mM 12-oxo-9(*Z*)-dodecenoic acid within only 10 sec, the oxoacid concentration subsequently declined so that hardly any product remained after 120 min (Fig. 27a+b). In return, around 0.1 mM of the isomerization product traumatin was formed. To preserve the oxoacid from degradation and isomerization, reactions were performed at 0 °C on ice. This slightly slowed down the degradation of 12-oxo-9(*Z*)-dodecenoic acid, but still only about 28 % 12-oxo-9(*Z*)-dodecenoic acid yield was retained after 120 min of incubation. Furthermore, reactions were carried out with purified $HPL_{CP\text{-}N}$, which significantly slowed down the product degradation. A yield of 0.67 mM

12-oxo-9(*Z*)-dodecenoic acid was determined after 120 min reaction. In contrast to the oxo acid, hexanal was found to be more stable and good yields were measured in all three reaction setups (Fig. 27c). After 120 min incubation, yields of up to 81 % hexanal were observed.

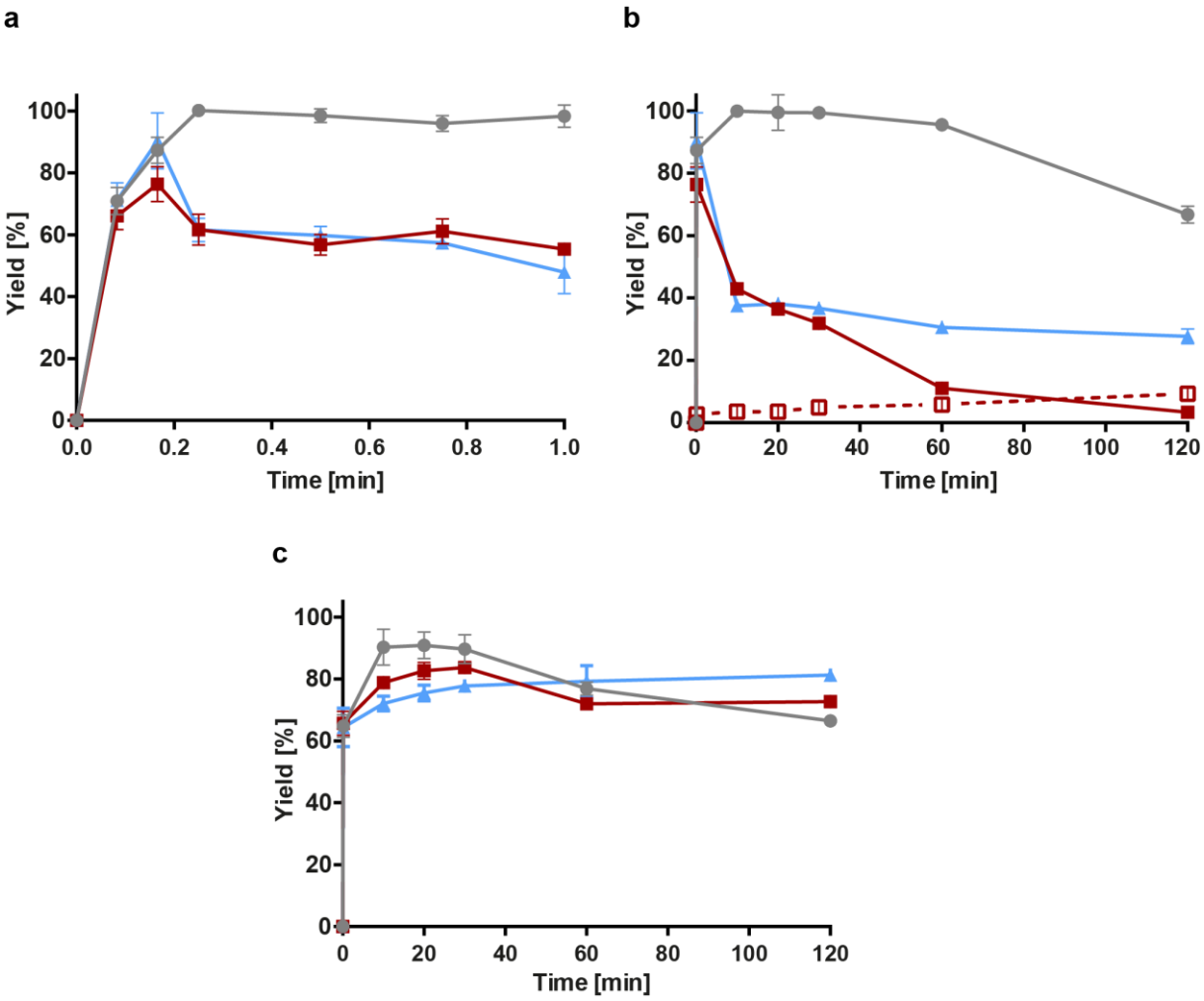

Fig. 27 Time-course experiments of $HPL_{CP\text{-}N}$ catalysis. The formation of 12-oxo-9(*Z*)-dodecenoic acid (**a+b**), 12-oxo-10(*E*)-dodecenoic acid (**b**) and hexanal (**c**) using 1 mM 13(*S*)-HPODE substrate at pH 6 was quantified with GC-FID. ● = 10 U·ml^{-1} of purified $HPL_{CP\text{-}N}$ at 22 °C; ■ = 10 U·ml^{-1} soluble fraction of $HPL_{CP\text{-}N}$ at 22 °C; ▲ = 10 U·ml^{-1} soluble fraction of $HPL_{CP\text{-}N}$ at 0 °C; □ with dotted red line = traumatin formation with 10 U·ml^{-1} soluble fraction of $HPL_{CP\text{-}N}$ at 22 °C. Figure modified and reproduced from [175] with permission from Springer Nature.

3.3. ω-Transaminases

3.3.1. Selection and cloning of ω-transaminases

Some ω-transaminases are known to accept long-chain aliphatic aldehydes as substrates, however, 12-oxododecenoic acid has not been tested yet. A literature and gene database survey was done to select potentially suitable ω-TAs for this reaction. ω-TA from *C. violaceum* (TR_{CV}; Acc. no.: WP_011135573.1) was selected as a well studied ω-TA which has already been shown to

aminate hydrophobic aldehydes such as 12-oxododecanoic acid [14]. ω-TA from *P. denitrificans* (TR_{PD}; Acc. no.: ABL72050.1) was demonstrated to aminate 6-oxohexanoic acid to 6-aminohexanoic acid [166] and has an identity of 38.81 % to TR_{CV} (Table 12). Two uncharacterized ω-TAs were identified using a BLAST search to find putative new homologs of TR_{CV}. Sequences from *A. denitrificans* (TR_{AD}; Acc. no.: WP_159877958.1) and *S. delicatus* (TR_{SD}; Acc. no.: WP_093738538.1) showed identities of 81.05 % (TR_{AD}) and 53.64 % (TR_{SD}) with respect to TR_{CV}. In addition, TR_2 (Acc. no.: MH588437) from *Acidihalobacter* sp. and TR_3 (Acc. no.: MF158202) and TR_6 (Acc. no.: MF158205) from uncultured *Rhodobacteraceae* bacteria can aminate bulky ketones and hexanal [168] and were incorporated in the substrate screening. They have an identity of 58.94 %, 34.54 % and 54.75 % with respect to TR_{CV}.

Table 12 Sequence identities of ω-TAs, calculated with BLAST [177]. Figure reproduced from [190] with permission from Springer Nature.

	TR_{AD}	**TR_{CV}**	**TR_{PD}**	**TR_{SD}**	**TR_2**	**TR_3**	**TR_6**
TR_{AD}	-	81.05	36.32	54.78	56.73	35.31	56.43
TR_{CV}	81.05	-	38.31	53.64	58.94	34.54	54.75
TR_{PD}	36.32	38.31	-	34.15	35.64	32.05	35.49
TR_{SD}	54.78	53.64	34.15	-	58.65	35.02	69.05
TR_2	56.73	58.94	35.64	58.65	-	36.93	60.05
TR_3	35.31	34.54	32.05	35.02	36.93	-	34.36
TR_6	56.43	54.75	35.49	69.05	60.05	34.36	-

The genes encoding TR_{CV}, TR_{AD}, TR_{PD} and TR_{SD} were designed with a His6-tag and were codon-optimized for expression in *E. coli* (Fig. A24-A27). They were cloned into the pET-21(b)+ expression vector by BioCat (Germany). Correct cloning was verified by DNA sequencing and restriction digestion (Fig. 28), which revealed the correct cloning of the ~1400 bp sized *ω-ta* genes. *Tr_2* (Fig. A28) that was cloned into the pRhokHi-2 vector as well as *tr_3* (Fig. A29) and *tr_6* (Fig. A30) that were cloned into the pBXCH vector, were expressed in *E. coli* MC1061 by the group of Prof. Dr. Manuel Ferrer [168].

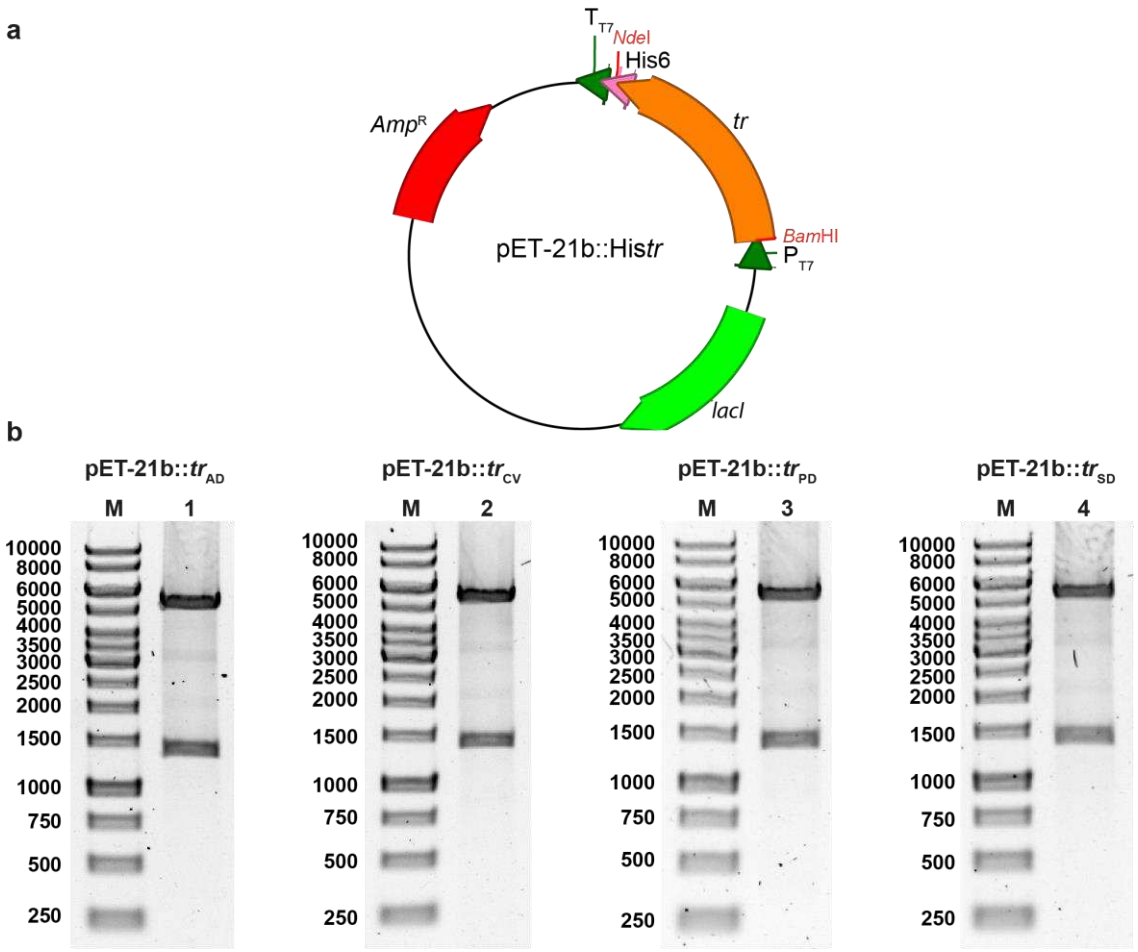

Fig. 28 Expression vector pET-21b::His*tr* (**a**) for expression of *A. denitrificans* (AD), *C. violaceum* (CV), *P. denitrificans* (PD) and *S. delicatus* (SD) ω-TAs and agarose gels of restriction digests of pET-21b::His*tr* (**b**) with *Nde*I and *Bam*HI. M: DNA ladder marker with sizes in bp.

3.3.2. Expression, purification and substrate specificity of ω-TAs

E. coli BL21(DE3) was transformed with the respective vectors and the ω-TAs were expressed in TB medium containing ampicillin at 20 °C for 24 h under continuous shaking. Expression of the enzymes was verified by SDS-PAGE (Fig. 29a). Strong protein bands were observed in the crude extracts and soluble fractions at ~50 kDa, which correspond with the calculated molecular weights of the ω-TAs. The His-tagged ω-TAs were purified with metal affinity chromatography and only minor impurities were visible in the TR_{PD} and TR_{SD} fractions on SDS-PAGE (Fig. 29b). Up to 80 mg of purified TR_{CV} were yielded from 50 ml of cultivation medium, while 41 mg TR_{AD}, 17 mg TR_{SD} and 13 mg TR_{PD} were obtained. Affinity-purified TR_2, TR_3 and TR_6 were provided by Prof. Dr. Manuel Ferrer and were included in the following experiments.

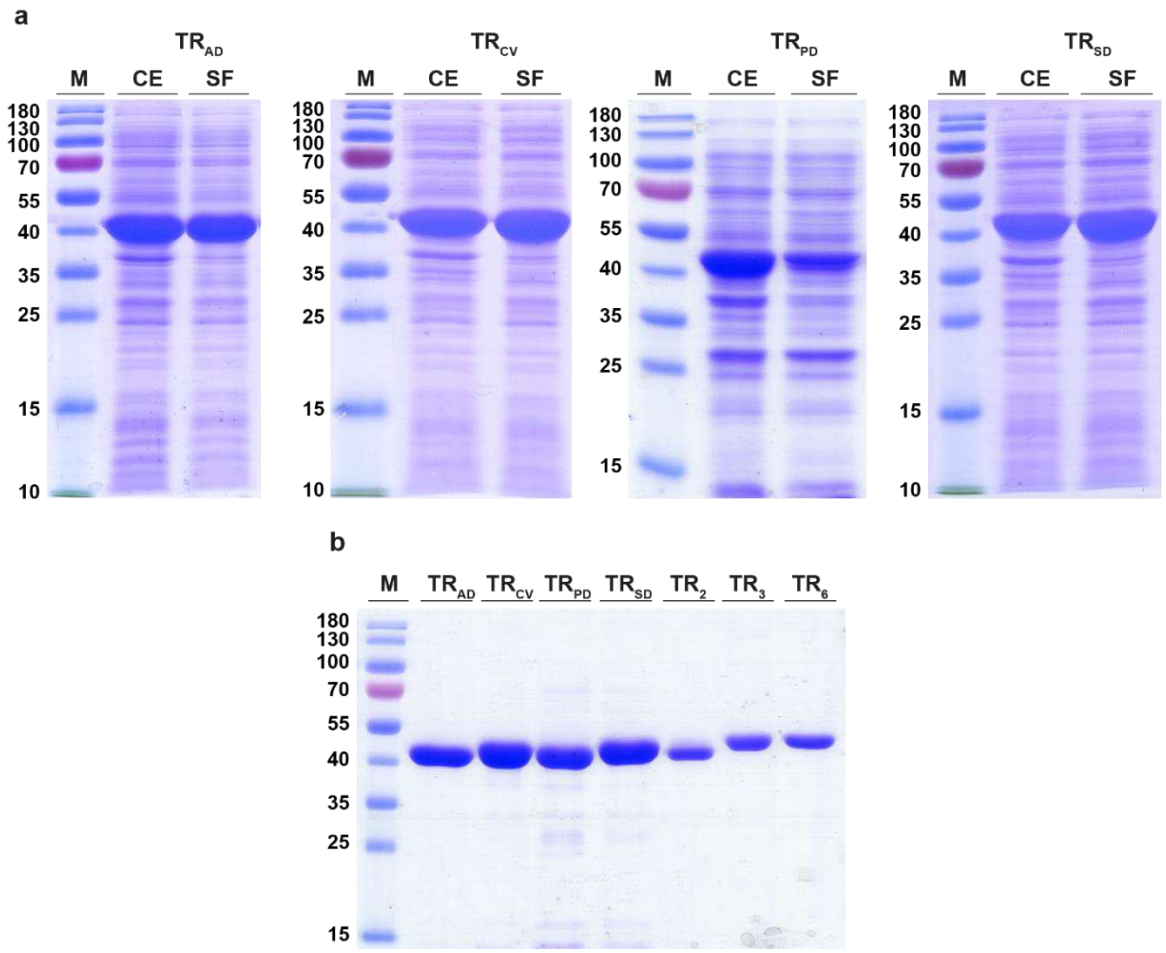

Fig. 29 Evaluation of overexpression (**a**) and purification (**b**) of ω-TAs. (**a**) SDS-PAGE of CE: crude extract and SF: soluble fraction with M: protein marker with sizes in kDa. (**b**) Eluate fractions of ω-TAs after metal affinity purification. ω-TAs from *A. denitrificans* (AD), *C. violaceum* (CV), *P. denitrificans* (PD), *S. delicatus* (SD), *Acidihalobacter* sp. (TR_2) and uncultured *Rhodobacteraceae* bacteria (TR_3 & TR_6) were used. Figure reproduced from [190] with permission from Springer Nature.

A coupled photometric enzyme assay was developed using purified ω-TA, a lactate dehydrogenase, an aldehyde as substrate, L-alanine, pyridoxal-5-phosphate and NADH (Fig. 30a). Transaminase reaction releases pyruvate, which is reduced by LDH under NADH consumption. The decrease of NADH was monitored at 340 nm, which is proportional to the transamination reaction. To ensure the functionality of the enzyme assay, negative controls were conducted with reactions successively omitting substrate, enzyme and cofactor. Only weak background responses were measured so that the functionality was proven. All ω-TAs were expressed as functionally active enzymes when measured with the reference substrate hexanal (Fig. 30b). Highest specific activity was measured with TR_{AD} with 1.17 U·mg^{-1}, followed by TR_6 with 1.01 U·mg^{-1} and TR_{SD} with 0.87 U·mg^{-1}. Furthermore, the ability of the ω-TAs to aminate the unsaturated oxoacids 12-oxo-9(*Z*)-dodecenoic acid and 12-oxo-10(*E*)-dodecenoic acid was tested in the coupled photometric assay. All ω-TAs were active on both, the 9(*Z*) and the 10(*E*) isoform (Fig. 30b). This demonstrates that the double bond, located in close proximity to the aldehyde, did not interfere

with the enzyme reaction. For most ω-TAs, the specific activities towards the 9(*Z*) and 10(*E*) isoforms differed only slightly, so that the position of the double bond can be neglected. TR_{PD} and TR_6, however, showed significantly lower specific activities towards 12-oxo-10(*E*)-dodecenoic acid than towards the 9(*Z*) isomer. Highest specific activities were obtained by TR_{AD} with 0.62 U·mg^{-1} for 12-oxo-9(*Z*)-dodecenoic acid and 0.52 U·mg^{-1} for 12-oxo-10(*E*)-dodecenoic acid.

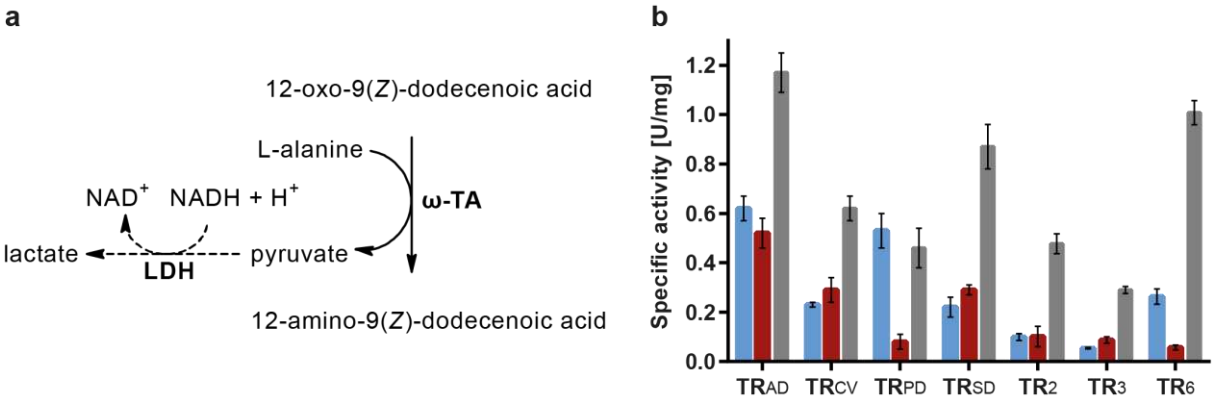

Fig. 30 Coupled enzymatic activity assay with a ω-TA and LDH. The decrease of absorbance was measured at 340 nm, correlating to the conversion of NADH to NAD$^+$. (**a**) Reaction scheme of the activity assay. (**b**) Comparison of specific activities of ω-TAs for the substrates hexanal (grey), 12-oxo-9(*Z*)-dodecenoic acid (blue bars) and 12-oxo-10(*E*)-dodecenoic acid (red bars). Activities were measured photometrically with purified enzyme in triplicate. ω-TAs from *A. denitrificans* (AD), *C. violaceum* (CV), *P. denitrificans* (PD) and *S. delicatus* (SD), *Acidihalobacter* sp. (TR_2) and uncultured *Rhodobacteraceae* bacteria (TR_3 & TR_6) were used. Figure reproduced from [190] with permission from Springer Nature.

3.3.3. Monitoring of the TR_{AD} reaction

The formation of 12-aminododecenoic acid was monitored exemplarily with TR_{AD}. The reaction was quantified by HPLC coupled to an evaporative light scattering detector (Fig. 31a). The substrate 12-oxododecenoic acid was not visible with the ELSD. L-alanine, which was added in excess and its ketone product pyruvate showed the same elution volume so that only 12-aminododecenoic acid was quantified. For this, a standard curve was prepared using commercially available 12-aminododecanoic acid at various concentrations (Fig. A31). In time-dependent reactions, a maximum yield of 47 % 12-aminododecenoic acid was obtained after one hour incubation at 22 °C (Fig. 31b), when 2.5 mM 12-oxo-9(*Z*)-dodecenoic acid was added as substrate. Within the next four hours, it was not possible to increase the yield, indicating that an equilibrium was reached with the given substrate and cosubstrate concentrations.

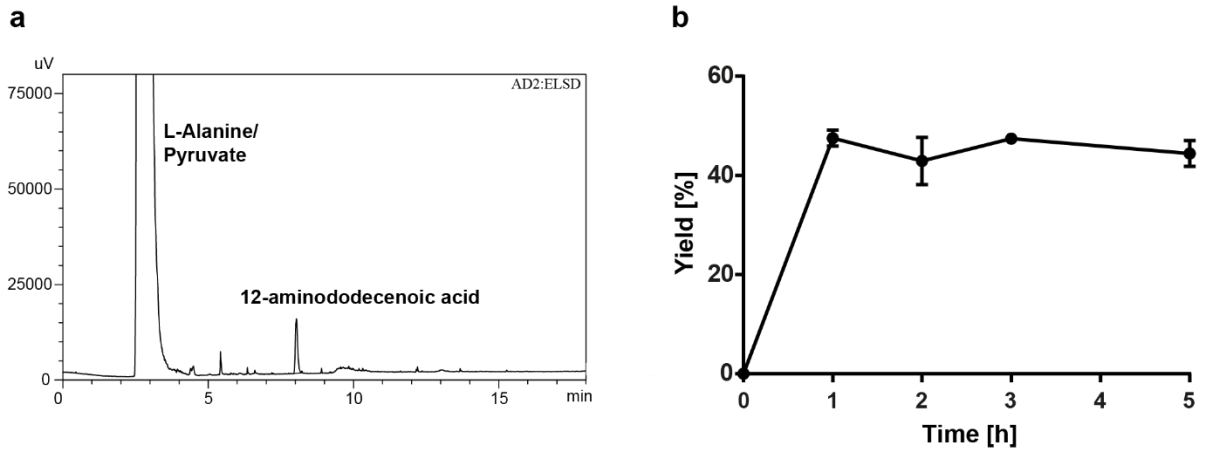

Fig. 31 Analysis of TR_{AD} catalyzed synthesis of 12-aminododecenoic acid, monitored with HPLC-ELSD. (**a**) ELSD chromatogram of TR_{AD} reaction after 1 h incubation at 22 °C. (**b**) Yield of 12-aminododecenoic acid after 1 to 5 h incubation with TR_{AD}. Reactions were done in triplicate and quantified with HPLC-ELSD analysis. Figure modified and reproduced from [190] with permission from Springer Nature.

The mass spectrum of 12-aminododecenoic acid obtained from 12-oxo-9(*Z*)-dodecenoic acid transformation exhibited a major signal at 214 m/z, correlating to the molecular weight of 214 g·mol^{-1} of its protonated form (Fig. 32a). 12-Aminododecanoic acid was used as reference standard, since the unsaturated form was not commercially available. Here, the major signal was 216 m/z, which is in accordance to the molecular weight of 216 g·mol^{-1} for the protonated molecule (Fig. 32c). The aldehydes 12-oxo-10(*E*)-dodecenoic acid and hexanal were tested as substrates as well. For the 10(*E*) isoform, a similar mass spectrum was obtained than for the 9(Z) isomer with a major signal at 214 m/z (Fig. 32b). When hexanal was used as substrate, hexylamine was detected in the mass spectrum with a substrate peak at 102 m/z in agreement with the molecular weight of 102 g·mol^{-1} for the protonated molecule (Fig. 32d). Hexylamine was used as reference standard, which gave an identical spectrum (Fig. 32e). The formation of 12-aminododecenoic acid was comparatively analyzed with the other six ω-TAs and the formation of 12-aminododecenoic acid was confirmed in all cases.

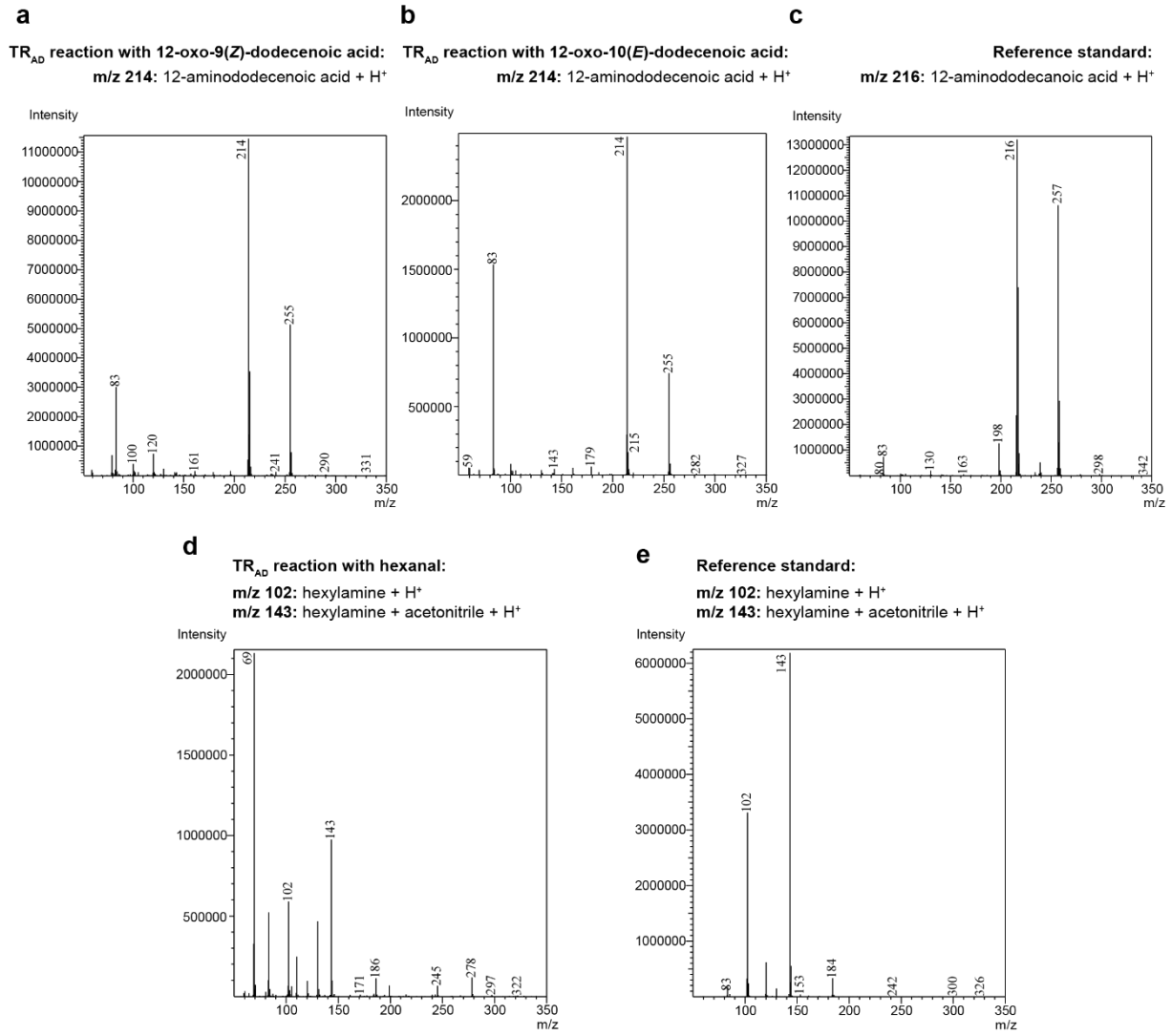

Fig. 32 Mass spectra analyses of TR_{AD} enzyme reactions. 12-Aminododecenoic acid was formed by TR_{AD} reaction with 12-oxo-9(*Z*)-dodecenoic acid (**a**) and 12-oxo-10(*E*)-dodecenoic acid (**b**), and was compared to a reference spectrum of 12-amindodecanoic acid (**c**). Hexylamine was formed by TR_{AD} reaction with hexanal (**d**) and compared to a reference spectrum of hexylamine (**e**). Figure modified and reproduced from [190] with permission from Springer Nature.

For many ω-TAs, an unfavorable L-alanine-pyruvate equilibrium has been described [140], requiring an excess of L-alanine. In TR_{AD} reactions, L-alanine concentrations of 10 to 50 mM were tested, corresponding to a five- to twentyfold excess over the 2.5 mM 12-oxo-9(*Z*)-dodecenoic acid used. With increasing L-alanine concentration, only slightly increased conversion of 12-oxo-9(*Z*)-dodecenoic acid was observed (Fig. 33a). Some ω-TAs were described as being more active at higher temperatures of up to 35 °C or in the presence of dimethyl sulfoxide (DMSO) [168]. In contrast, TR_{AD} activity did not increase with higher temperature (Fig. 33b). At 35 °C, only 28 % 12-aminododecenoic acid was formed within one hour, whereas around 47 % was obtained at 22 °C. Moreover, the yield of 12-aminododecenoic acid decreased from 47 % for samples without DMSO to 38 % for samples with 20 % DMSO (Fig. 33c). Hence, further experiments were conducted without added DMSO. The optimum pH and the optimum salt concentration were

analyzed photometrically with pH values ranging from pH 6 to 9 and salt concentrations ranging from 0 to 500 mM NaCl. Highest ω-TA activity was reached at pH 7.5 in the presence of 50 mM NaCl (Fig. 33d+e).

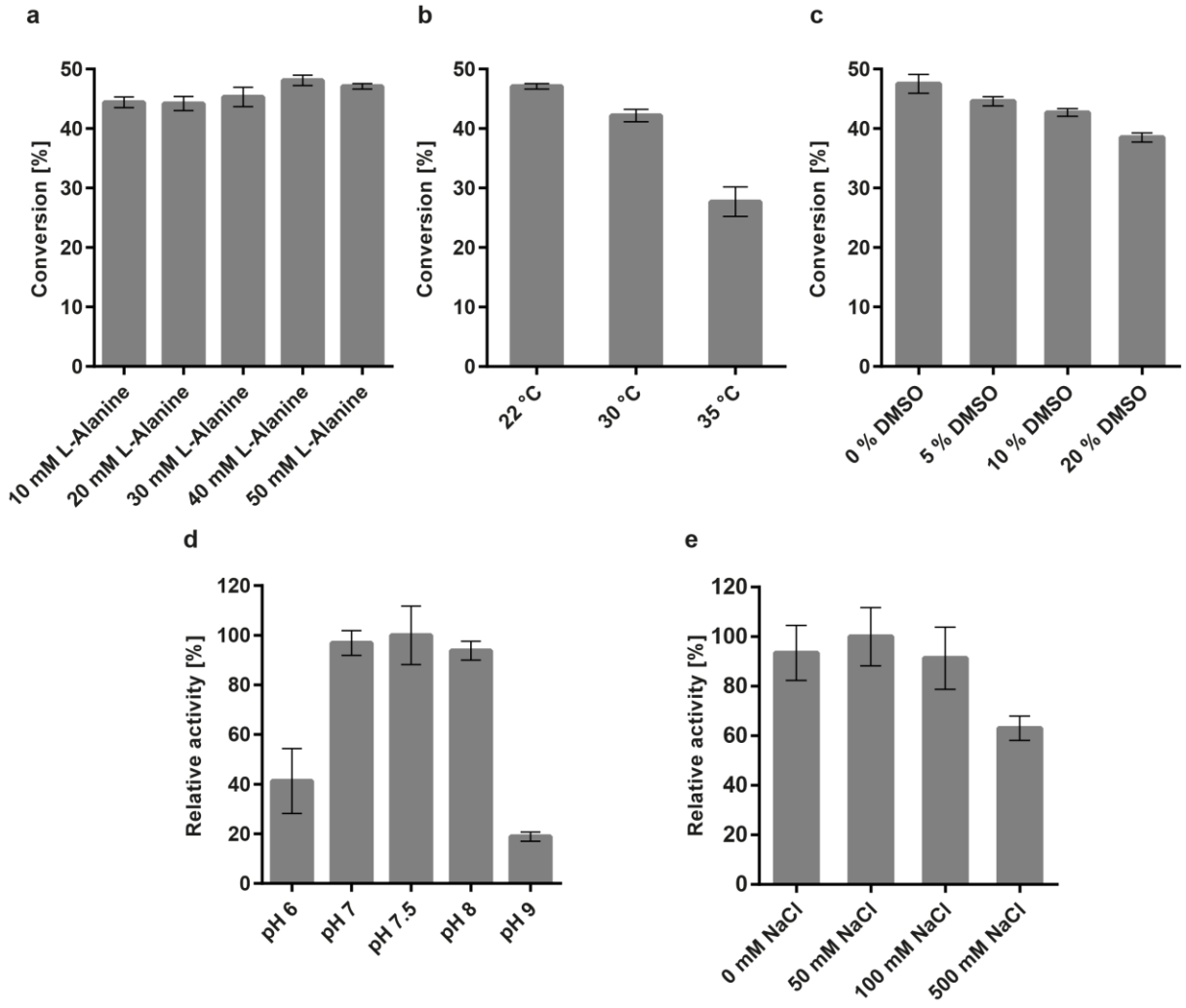

Fig. 33 Analysis of reaction conditions for TR_{AD} catalysis. (**a**) L-Alanine concentration, (**b**) reaction temperature and (**c**) DMSO addition were analyzed by HPLC-ELSD quantification. (**d**) Optimum pH value and (**e**) salt concentration were analyzed photometrically and highest relative activities were set to 100 %. Figure modified and reproduced from [190] with permission from Springer Nature.

3.4. Development of enzyme cascades for the synthesis of 12-oxo- and 12-aminododecenoic acid

Enzyme cascades can simplify the synthesis of polymer intermediates by saving time and reducing the necessity for purification steps. In this thesis, several one-pot reactions were conducted with either lipase, lipoxygenase and hydroperoxide lyase or lipoxygenase, hydroperoxide lyase and ω-transaminase. Commercially available LOX-1 showed 40-fold higher specific activity compared to purified LOX-1 from heterologously expressed samples. For this reason, the commercially

LOX-1 was used in one-pot reactions. In addition, Amano lipase from *P. fluorescens*, selected in an enzyme screening by Valentin Gala Marti [167], was obtained commercially. $HPL_{CP\text{-}N}$ and TR_{AD} were expressed and purified as described in the previous chapters and used for the one-pot reactions.

3.4.1. Coupling of lipase, LOX and HPL in one-pot reactions

First, one-pot reactions were carried out with LOX-1 and $HPL_{CP\text{-}N}$. Small-scale reactions were conducted at pH 7.5 with no active oxygen supply. Though LOX-1 has a pH optimum of 9 [167] and $HPL_{CP\text{-}N}$ a pH optimum of 6, both enzymes showed sufficient activity at pH 7.5. Triton X-100 was added since both LOX-1 [167] and $HPL_{CP\text{-}N}$ exhibited increased solubility and activity upon detergent addition. Time-dependent one-pot reactions were performed with initial linoleic acid concentrations of 1, 2.5 and 5 mM (Fig. 34). For this, LOX-1 was either incubated for 1 to 5 hours before analysis or incubated for 1 to 5 hours before $HPL_{CP\text{-}N}$ was added for further 15 min. Samples were analyzed by GC-FID quantification after calibration with linoleic acid, 13(*S*)-HPODE and 12-hydroxydodecanoic acid (Fig. A23). 80 % of linoleic acid was converted to 13(*S*)-HPODE within three hours when 1 mM linoleic acid was applied (Fig. 34a). Of these, up to 68 % 12-oxo-9(*Z*)-dodecenoic acid was synthesized after additional 15 min $HPL_{CP\text{-}N}$ incubation (Fig. 34b). Higher concentrations of linoleic acid led to a decrease in conversion, probably caused by oxygen depletion.

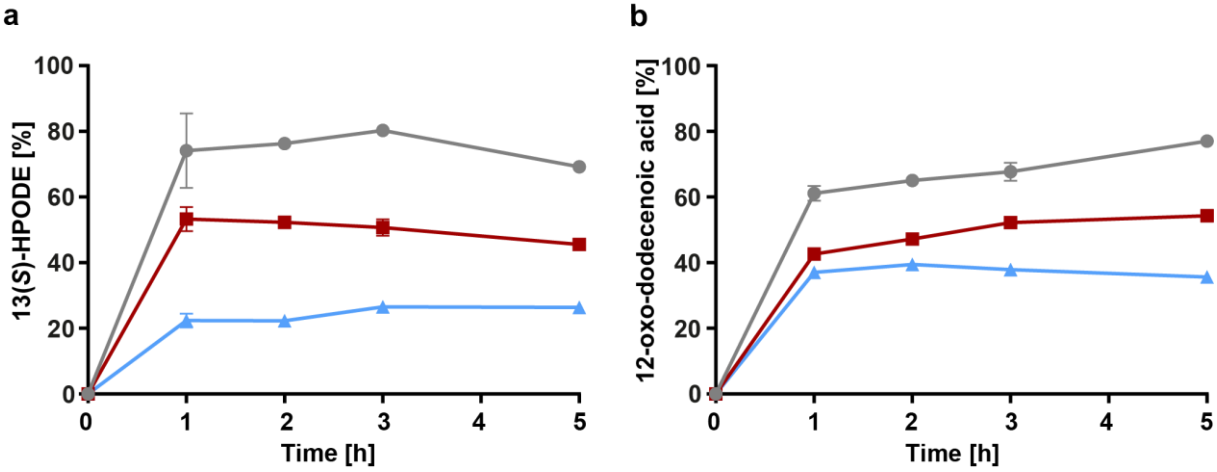

Fig. 34 Time-course of one-pot enzymatic reactions with LOX-1 and $HPL_{CP\text{-}N}$. (**a**) LOX-1 reactions were incubated for 1-5 hours with 1 (●), 2.5 (■) and 5 (▲) mM linoleic acid and the yield of 13(*S*)-HPODE was analyzed by GC-FID analyses. (**b**) After pre-incubation of LOX-1 for 1-5 hours, an equal volume of $HPL_{CP\text{-}N}$ was added for 15 min and 12-oxo-9(*Z*)-dodecenoic acid was analyzed by GC-FID analyses. The yield is given in percentage (%) of 12-oxododecenoic acid based on the 13(*S*)-HPODE yield from (**a**). Experiments were performed in triplicate. Figure modified and reproduced from [175] with permission from Springer Nature.

Comparison between simultaneous and consecutive addition of LOX-1 and HPL_{CP-N} revealed that the consecutive reaction setup resulted in significantly higher product yields (Fig. 35a). When LOX-1 and HPL_{CP-N} were added simultaneously and incubated for three hours before analysis, only low yields of 12-oxo-9(*Z*)-dodecenoic acid (9.3 % based on initial added concentration of linoleic acid) were obtained. In contrast, a pre-incubation of LOX-1 for three hours before HPL_{CP-N} catalysis for additional 15 min led to an overall yield of 62 % 12-oxo-9(*Z*)-dodecenoic acid. Consequently, the consecutive addition of enzymes seems to be the preferable reaction setup for the coupled LOX – HPL reaction.

Furthermore, one-pot reactions were carried out with Amano lipase from *P. fluorescens*, LOX-1 and HPL_{CP-N} with safflower as substrate. Control reactions were performed with lipase only, resulting in a yield of 66 % of released linoleic acid, as well as coupled lipase and LOX reactions, yielding 50 % 13(*S*)-HPODE (Fig. 35b). Three-enzyme one-pot reactions were performed either simultaneously or consecutively. In a simultaneous reaction, all three enzymes were added in the beginning, resulting in only low 12-oxo-9(*Z*)-dodecenoic acid yield (2 %). In a consecutive reaction setup, lipase was applied in the beginning and LOX-1 was added in 12 portions over three hours before HPL_{CP-N} was added for further 1 or 15 min. Around 42 % 12-oxo-9(*Z*)-dodecenoic acid was measured after 1 min HPL reaction, which declined rapidly thereafter.

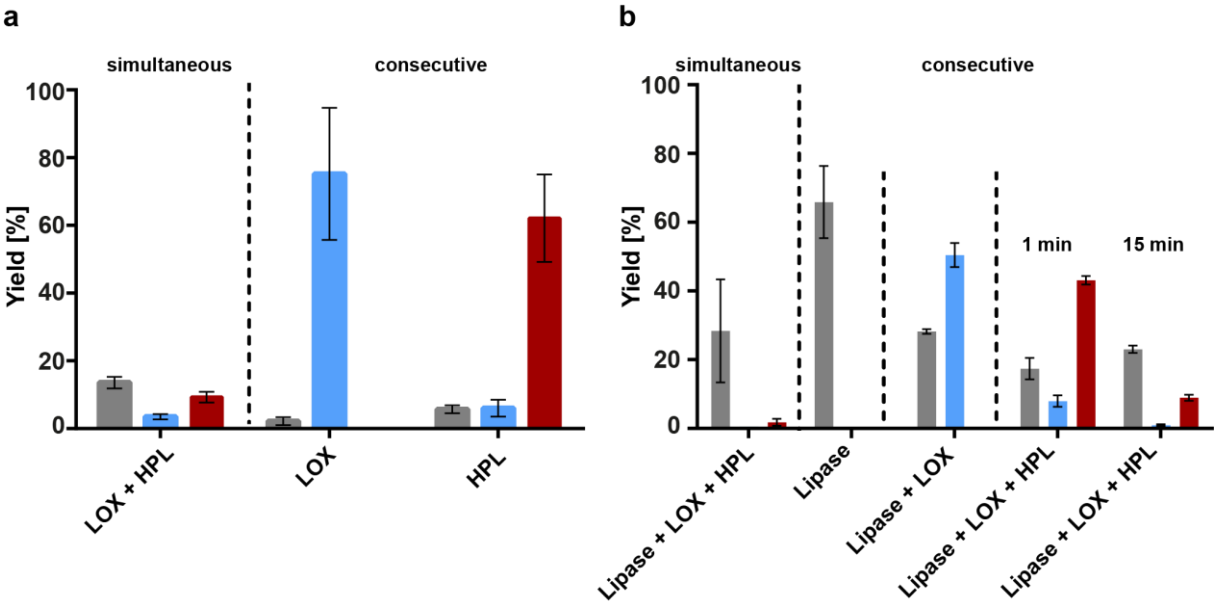

Fig. 35 Determination of optimal reaction setup with either simultaneous or consecutive enzyme addition in (**a**) one-pot reactions containing LOX-1 and HPL_{CP-N} and (**b**) one-pot reactions with Amano lipase from *P. fluorescens*, LOX-1 and HPL_{CP-N}. Grey bars: linoleic acid, blue bars: 13(*S*)-HPODE and red bars: 12-oxo-9(*Z*)-dodecenoic acid. Yield (%) based on a substrate concentration of (**a**) 0.5 mM linoleic acid or (**b**) safflower oil equivalent to 0.67 mM linoleic acid. Figure modified and reproduced from [175] with permission from Springer Nature.

3.4.2. Synthesis of 12-aminododecenoic acid from linoleic acid by coupling LOX, HPL and ω-TA

One-pot reactions with LOX, HPL and ω-TA were developed for the cascade synthesis of 12-aminododecenoic acid. Enzyme activity was measured photometrically in the same coupled photometric assay used for ω-TA alone (chapter 3.3.2) with LDH and NADH monitoring. Here, coupling of HPL and ω-TA demanded 13(*S*)-HPODE as substrate, while linoleic acid was used as substrate in the LOX, HPL and ω-TA cascade reaction (Fig. 36a). A decrease in absorbance of NADH at 340 nm can only occur, when the cascade reactions work in parallel. Control reactions were performed by sequentially omitting each enzyme, substrate and cosubstrate. Only low background activity was measured, so that the functionality of the assay can be confirmed. All ω-TAs were active in the one-pot reactions (Fig. 36b). In combined photometric enzyme assays with $HPL_{CP\text{-}N}$, ω-TA and LDH, highest conversion was measured with TR_{CV} obtaining 31.6 nmol·min^{-1}·ml^{-1}, followed by TR_{AD} and TR_2 with 30.8 nmol·min^{-1}·ml^{-1} and 23.7 nmol·min^{-1}·ml^{-1}. In combined LOX-1, $HPL_{CP\text{-}N}$, ω-TA and LDH assays, highest conversion of NADH was measured with TR_{AD} exhibiting 5.6 nmol·min^{-1}·ml^{-1}, followed by TR_{CV} and TR_2 with 4.9 nmol·min^{-1}·ml^{-1}.

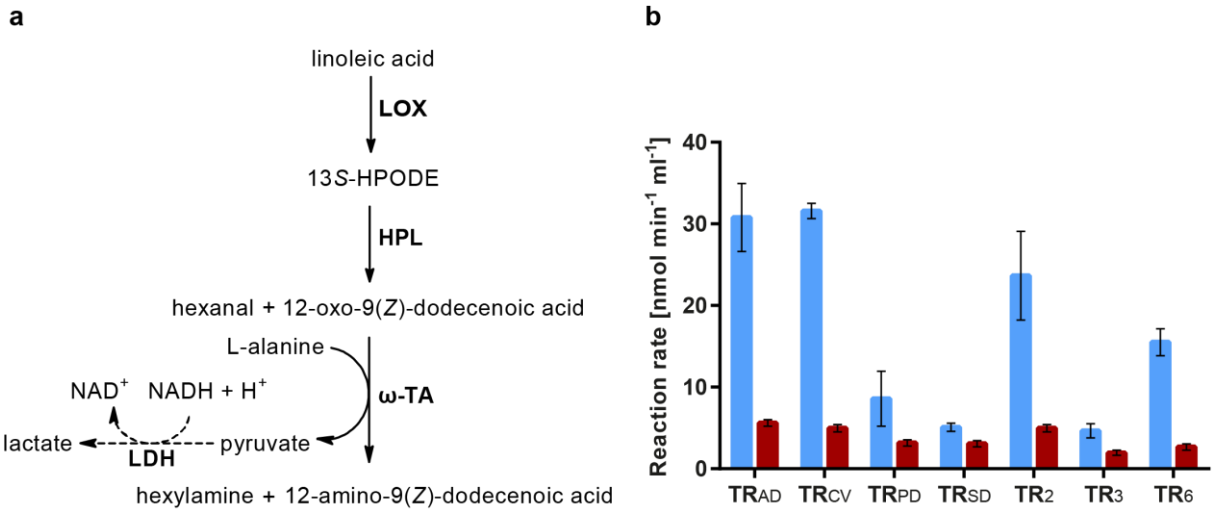

Fig. 36 Coupled photometric enzyme assay with lipoxygenase (LOX), hydroperoxide lyase (HPL), ω-transaminase (ω-TA) and lactate dehydrogenase (LDH). (**a**) Reaction scheme of photometric activity assay. (**b**) Conversion of NADH to NAD$^+$, determined photometrically with LDH in reactions with a ω-TA and $HPL_{CP\text{-}N}$ (blue bars) or with a ω-TA, $HPL_{CP\text{-}N}$ and LOX-1 (red bars). Figure reproduced from [190] with permission from Springer Nature.

Since only monitoring of an overall reaction is possible with the photometric assay, direct verification of 12-aminododecenoic formation was conducted with LC analysis. For these reactions, TR_{AD} was used exemplarily with $HPL_{CP\text{-}N}$ in small-scale with either 1 or 2.5 mM 13(*S*)-HPODE as substrate in 50 mM potassium phosphate buffer pH 7.5 containing 0.5 M NaCl. Combined $HPL_{CP\text{-}N}$ – TR_{AD} reactions were run either simultaneously or consecutively (Fig. 37a).

For simultaneous enzyme addition, $HPL_{CP\text{-}N}$ and TR_{AD} were incubated simultaneously for one hour before analysis. For consecutive enzyme addition, $HPL_{CP\text{-}N}$ was pre-incubated with 13(*S*)-HPODE for 5 min before TR_{AD} was added and incubated for an additional hour. In a third reaction setup, TR_{AD} was applied in the beginning and $HPL_{CP\text{-}N}$ was added in 6 portions every 10 min for the period of one hour. Highest yield of 12-aminododecenoic acid was obtained with stepwise addition of HPL, reaching a yield of 59 % for reactions with 1 mM substrate (Fig. 37a). When 2.5 mM substrate was added, a yield of 49 % 12-aminododecenoic acid was achieved.

Moreover, three-enzyme reactions were carried out with LOX-1, $HPL_{CP\text{-}N}$ and TR_{AD} with linoleic acid as substrate. The enzymes were again added either simultaneously or consecutively (Fig. 37b). In a simultaneous reaction, all enzymes were applied in the beginning and reaction was run for 3 h before analysis. The reaction time was prolonged compared to the two-enzyme reactions as LOX-1 reaction was shown to be much slower than $HPL_{CP\text{-}N}$ and TR_{AD} reaction [167]. For consecutive enzyme addition, LOX-1 was pre-incubated with linoleic acid for three hours before $HPL_{CP\text{-}N}$ was added for 5 min and TR_{AD} for an additional hour. In a second consecutive enzyme addition approach, LOX-1 was added in the beginning and pre-incubated with linoleic acid for three hours. Then, TR_{AD} was added and $HPL_{CP\text{-}N}$ was applied in portions every 10 min for one hour. The highest yield of 12-aminododecenoic acid was obtained in the third reaction setup with 12.1 % 12-aminododecenoic acid. Though yields are still low, the feasibility of the three-enzyme reaction to produce polymer precursor 12-aminododecenoic acid was successfully proven.

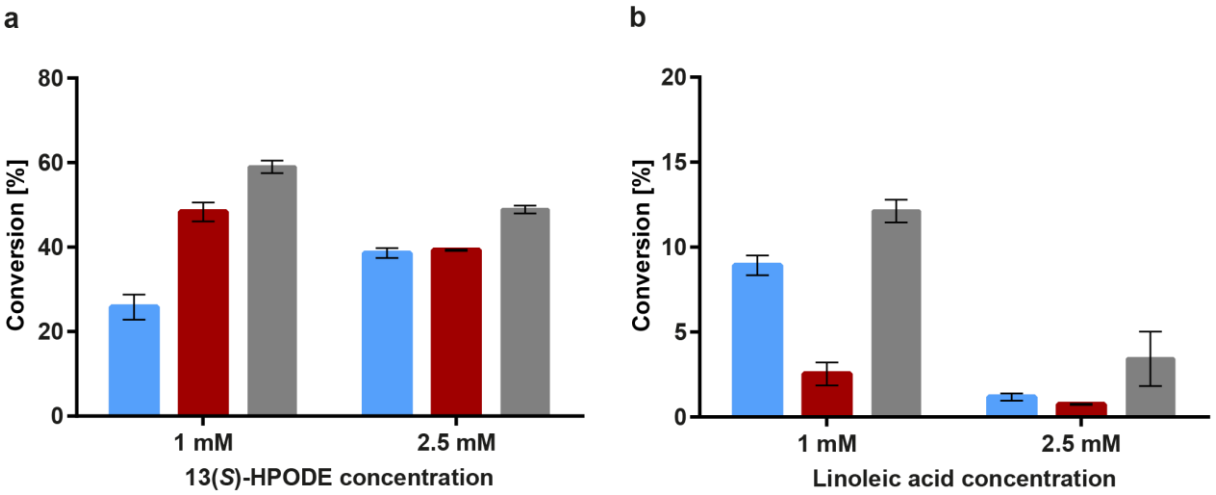

Fig. 37 Comparison of optimal one-pot reaction setups with coupled $HPL_{CP\text{-}N}$ and TR_{AD} (**a**) and coupled LOX-1, $HPL_{CP\text{-}N}$ and TR_{AD} (**b**) cascade reaction. (**a**) One-pot reactions with $HPL_{CP\text{-}N}$ and TR_{AD} with 1 and 2.5 mM 13(*S*)-HPODE as substrate. Reactions were performed simultaneously (blue bars) or consecutively by $HPL_{CP\text{-}N}$ addition before TR_{AD} addition (red bar), or TR_{AD} addition before $HPL_{CP\text{-}N}$ dosage in portions. (**b**) One-pot reactions with LOX-1, $HPL_{CP\text{-}N}$ and TR_{AD} with 1 and 2.5 mM linoleic acid as substrate. Reactions were performed simultaneously (blue bars) or consecutively by LOX-1 addition before $HPL_{CP\text{-}N}$ and then TR_{AD} addition, or LOX-1 addition before TR_{AD} addition and $HPL_{CP\text{-}N}$ dosage in portions. Figure reproduced from [190] with permission from Springer Nature.

4. Discussion

The synthesis of nylon-12 and other polyamides is still mostly based on petroleum-derived naphtha. To circumvent the dependence on crude oil, several attempts have been made to develop bio-based processes for the synthesis of polyamide precursor 12-aminododecanoic acid [11, 13, 14]. However, these routes depend on lauric acid, which is derived from palm kernel and coconut oil. These oils are highly demanded by e.g. the detergent and cleaning industry for surfactant production [191, 192]. A growing world population increases the need for these tropical oils, which puts pressure on the available agricultural area and threatens pristine rainforests [17]. Therefore, the aim of this work was to develop a novel enzymatic route for 12-aminododecenoic acid synthesis from linoleic acid, derived from vegetable oils from moderate to subtropical climate zones. In contrast to 12-aminododecanoic acid, the building block of saturated nylon-12, 12-aminododecenoic acid can be used as monomer for unsaturated nylon-12. Unsaturated polyamides are interesting polymers, as the double bonds can promote polymer crosslinking [193]. In recent years, several unsaturated polyamides derived from natural fatty acids have been described and their potential for utilization as thermoactive sealants, high-temperature resistant materials or barrier films has been proposed [194]. Unsaturated 12-aminododecenoic acid can also be hydrogenated to 12-aminododecanoic acid. For this, double bond hydrogenation could be performed with ene-reductases, which are capable in reducing unsaturated double bonds [195]. In this work, the enzymes LOX, HPL and ω-TA were successfully cloned, expressed and purified. Finally, one-pot enzyme reactions were performed, demonstrating the feasibility of this biocatalytic route.

4.1. Expression of recombinant LOX-1 and comparison with soybean flour and commercially LOX-1 preparations

Soybean LOX-1 is a well-characterized 13(*S*)-specific lipoxygenase that can be obtained either from soybean seeds or by heterologous expression in *E. coli* [59, 65, 196]. Although lipoxygenase is available in high quantities in soybeans, the presence of many different isozymes with distinct regioselectivities makes purification from plant extracts tedious [197]. For this reason, we wanted to express LOX-1 heterologously in expression vectors containing the synthetic gene for LOX-1 with a His6-tag.

Soluble and active LOX-1 was expressed in *E. coli* at temperatures ranging from 10 to 37 °C. The highest activity was measured at 15 °C (1357 $U \cdot l^{-1}$) and the lowest activity was measured at 37 °C (16 $U \cdot l^{-1}$), hence, an 85-fold increase in activity was achieved by lowering the temperature. In accordance, high yields of active LOX enzyme at low temperatures have been reported in

literature. The highest activity of rice LOX, for example, was observed at expression temperatures of 15 °C, whereas the highest activity of cucumber LOX was measured at expression temperatures of 8 °C [69, 198]. Previous expression of soybean LOX-1 also revealed best cultivation temperature of 15 °C [65], which is in agreement with our results. Lower cultivation temperatures result in slower protein expression and folding, which may enhance proper folding. Shirano et al. observed less formation of inclusion bodies of rice lipoxygenase after lowering the expression temperature, probably due to less misfolded protein [198].

Changing the cultivation medium from LB to TB further increased the activity 8.4-fold to 11,447 $U \cdot l^{-1}$, which may be explained by higher nutrient supply. TB provides almost 5 times more yeast extract, twice as much tryptone and contains glycerol as additional carbon source. This led to higher cell densities and more active enzyme. Furthermore, TB medium is buffered, ensuring a constant pH. Despite higher LOX-1 activities, no clear overexpression band was visible in the crude extract and soluble fraction on SDS-PAGE. Previous overexpression experiments by other groups also failed in yielding strong protein bands when prokaryotic expression hosts were used [65, 199].

A specific activity of around 2.8 $U \cdot mg^{-1}$ LOX-1 was obtained in the crude extract, when expression in TB medium at 15 °C was applied. Steczko et al. obtained a higher specific activity of 5.6 $U \cdot mg^{-1}$ LOX-1 by the addition of 3 % ethanol to the cultivation medium (Table 13) [65]. Ethanol is thought to be a trigger for heat shock proteins that can promote proper protein folding [65, 200]. However, the addition of ethanol did not lead to higher specific activities in our work. Other plant LOXs heterologously expressed in bacteria (mostly *E. coli*) achieved specific activities of around 1.35 $U \cdot mg^{-1}$ (*Pisum sativum* LOX) or 12.7 $U \cdot mg^{-1}$ of (*O. sativa* LOX) [196, 199]. In contrast, bacterial *Anabaena sp.* PCC 7120 LOX yielded higher activities of 56.7 $U \cdot mg^{-1}$ [202] (Table 13). It may be beneficial that this LOX is bacterial and therefore closer related to *E. coli*, which was used as expression host. Consequently, it may be advantageous for eukaryotic LOXs to use eukaryotic expression systems such as yeasts. The fungal Mn-LOX from *G. graminis* was shown to be highly glycosylated, so that expression in bacteria did not yield functional active enzyme. In contrast, expression in the yeast *P. pastoris* resulted in high amount of soluble enzyme, reaching up to 30 $mg \cdot l^{-1}$[72]. Almost the entire enzyme was secreted into the supernatant facilitating purification. Plant LOX were also expressed in yeast cells. *L. esculentum* LOX, for example, was expressed in *P. pastoris* and secreted into the cultivation medium, reaching specific activities of 90 $U \cdot mg^{-1}$ in the enriched supernatant [203]. In contrast, secretion of heterologously expressed pea seed LOX was not successful in expression experiments with *S. cerevisiae* and most enzyme remained inactively inside the cells [204]. Surprisingly, the same enzyme was actively expressed in *E. coli* [201]. In summary, expression in yeast cells can improve heterologous expression of eukaryotic LOXs, but in some cases, bacterial expression systems seem to be superior.

Table 13 Comparison of specific activities of lipoxygenases (LOX). CE: crude extract, SEC: size exclusion chromatography and IEX: ion exchange chromatography.

Enzyme	Specific activity [U·mg^{-1}]	Purification step	Enzyme origin	Expression system	Reference
LOX-1	2.8	CE	*G. max*	*E. coli*	This work
LOX-1	5.6	CE	*G. max*	*E. coli*	[65]
L-2 LOX	12.7	CE	*O. sativa*	*E. coli*	[198]
Pea 9-/13-LOXN2	1.35	CE	*P. sativum*	*E. coli*	[201]
ana-LOX	56.7	Supernatant	*Anabaena sp.* PCC 7120	*Bacillus subtilis*	[202]
Mn-LO	18	Secreted	*G. graminis*	*P. pastoris*	[72]
TomloxD	90	Enriched supernatant	*L. esculentum*	*P. pastoris*	[203]
LOX-1	150	Affinity purification	*G. max*	*E. coli*	This work
LOX-1	193	SEC purification	*G. max*	*E. coli*	[65]
L-2 LOX	402	IEX purification	*O. sativa*	*E. coli*	[198]
ana-LOX	442	Affinity purification	*Anabaena sp.* PCC 7120	*Bacillus subtilis*	[202]
LOX in soybean flour	51	Enriched flour	*G. max*	-	[167]
SIGMA LOX-1	6000	Enriched	*G. max*	-	Sigma-Aldrich

Metal affinity purification was performed for LOX-1 purification. Around 150 U·mg^{-1} were obtained in the eluate fraction, corresponding to a 54-fold increase in specific activity compared to the crude extract. In comparison, Steczko et al. obtained 193 U·mg^{-1} LOX-1 through purification with ion exchange chromatography (IEX) followed by size exclusion chromatography (SEC) [65] (Table 13). Furthermore, 402 U·mg^{-1} were determined for *O. sativa* LOX, when purified with IEX and 442 U·mg^{-1} of *Anabaena sp*. PCC 7120 LOX were obtained after affinity purification [198, 202]. However, it must be considered that after purification of *Anabaena sp*. PCC 7120 only a yield of 5 % of the initial activity was retained [202].

LOX-1 was found to be decomposed into several degradation fragments, which was proven by Western blot using a specific LOX-1 antibody. Especially, a second strong protein band at around 70 kDa was visible on SDS-PAGE. Fragmentation of the enzyme resulted in a decrease of full-length active enzyme by more than half. Often degradation of recombinant expressed proteins is caused by endogenous proteases [205] and several protease inhibitors have been developed for prevention. In this work, the addition of PMSF, a serine protease or a protease inhibitor mix (cOmplete™ Mini, EDTA-free Protease Inhibitor Cocktail from Roche) was tested. However, no decline in degradation could be observed. Similarly, proteolysis of heterologous expressed *Magnaporthe salvinii* 9(*S*)-LOX could not be prevented by the addition of protease inhibitors [206].

Around 51 U·mg^{-1} lipoxygenase activity were observed in soybean flour extracts [167] and around 6000 U·mg^{-1} lipoxygenase activity in a commercial LOX-1 preparation from soybean (Sigma-Aldrich) (Table 13). In contrast, the highest activity for LOX-1 after expression under optimized conditions and purification was 150 U·mg^{-1}. Thus, it seems that LOX-1 expression in *E. coli* does not yield sufficient amounts of active enzyme. For this reason, all further experiments towards the design of enzyme cascades were performed with commercial Sigma LOX-1.

4.2. Cloning and expression of plant-derived hydroperoxide lyases

Hydroperoxide lyases are plant enzymes that can either be obtained by purification from plant material or by heterologous expression. However, in contrast to lipoxygenases, HPLs are only expressed in small quantities in plants and are often membrane-associated [94]. In addition, similar enzymes of the CYP74 enzyme family such as allene oxide synthases are present in the plants, making separation of the structurally related enzymes difficult [39]. For this reason, purification of HPL from plant material is often tedious and results in low yields. Hence, heterologous expression of HPLs is often preferred over the use of plant material extraction and was also followed in this work.

Four HPLs were selected for cloning and expression: HPL from guava, papaya, barley and sorghum. A phylogenetic tree of known HPLs and the HPLs analyzed in this work was constructed to illustrate the evolutionary relationship of HPLs (Fig. 38). Within the CYP74 protein family, the CYP74B subgroup comprises 13-HPLs, whereas the CYP74C subgroup comprises 9/13-HPLs and 9-HPLs [39]. The phylogenetic tree shows that all HPLs expressed in this work belong to the CYP74B subgroup of 13-HPLs, which are predicted to cleave 13(*S*)-HPODE and 13(*S*)-HPOTE. Within the CYP74B subgroup, a division into two groups was recognized, one solely containing HPLs from dicotyledons (e.g., HPL_{PG} and HPL_{CP}) and the other one only containing HPLs from

monocotyledons (e.g., HPL_{HV} and HPL_{SB}). This explains the high sequence identities of HPL_{CP} with HPL_{PG} and HPL_{SB} with HPL_{HV}.

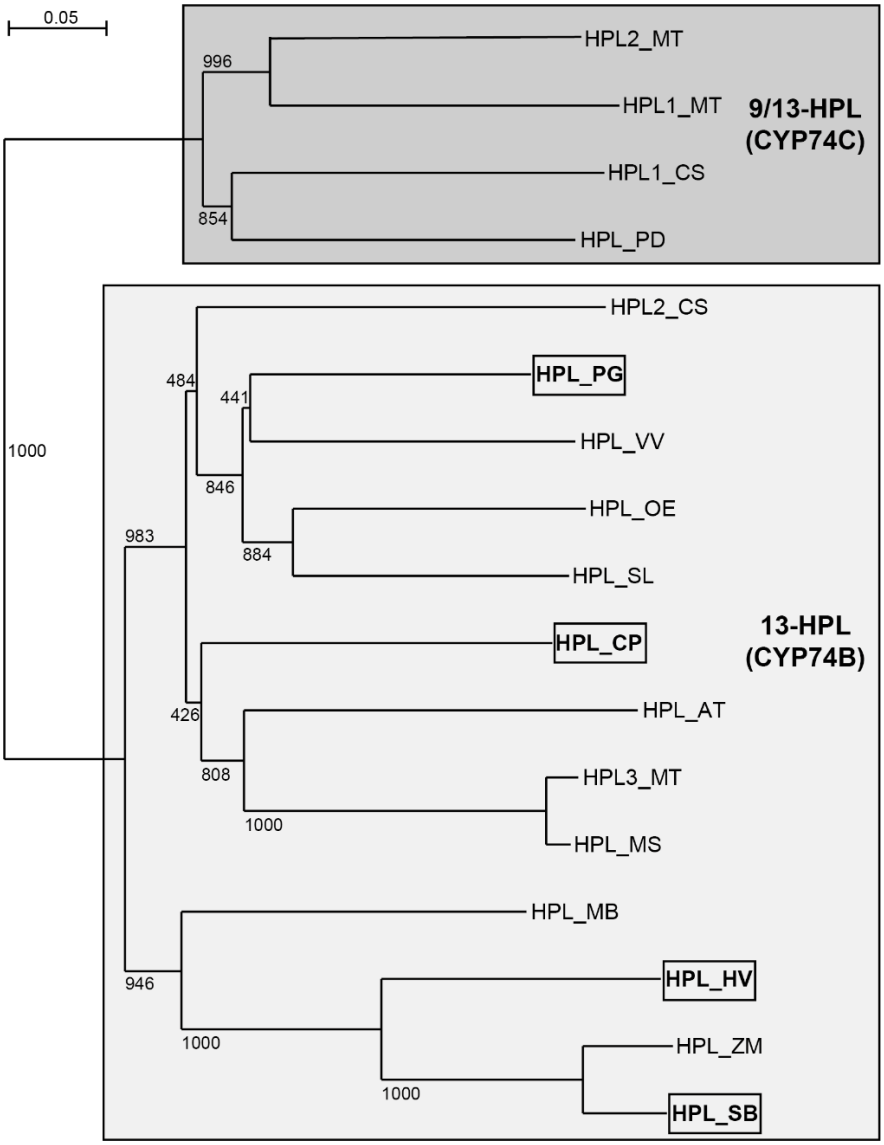

Fig. 38 Phylogenetic tree of HPL sequences with known HPLs from literature and HPLs analyzed in this work (marked in boxes). A multiple alignment was performed with ClustalX and a neighbor-joining tree was drawn with NJplot. The bootstrap value was set to 1000. The incorporated HPLs including their accession numbers were: MT: *Medicago truncatula* (1: CAC86898.1, 2: CAC86899.1, 3: AAY30368.1); CS: *Cucumis sativus* (1: AHC08715.1, 2: XP_004144503.1); PD: *Prunus dulcis* (CAE18065.1); PG: *P. guajava* (AAK15070.1); VV: *Vitis vinifera* (NP_001268011.1); OE: *O. europaea* (ACD43482.1); SL: *Solanum lycopersicum* (NP_001234420.2); CP: *C. papaya* (XP_021890218.1); AT: *A. thaliana* (AAC69871.1); MS: *M. sativa* (CAB54847.1); MB: *Musa balbisiana* (THU49863.1); HV: *H. vulgare* (CAC82980.1); SB: *S. biocolor* (OQU84187.1) and ZM: *Zea mays* (AAS47027.1). Figure modified and reproduced from [175] with permission from Springer Nature.

Expression was performed with full-length HPLs, N-terminally truncated HPLs and NusA – HPL fusion proteins. Full-length HPLs showed almost no activity, which is consistent with no or only low activity described for other full-length HPLs [97, 103]. The N-terminus was considered to be either a transit peptide or part of a post-translational regulation mechanism [97, 98]. An increase

in activity was found for many HPLs upon deletion of the N-terminal sequence [103, 207] and was confirmed in this work for papaya, barley and sorghum HPL. For papaya HPL, the initial specific activity was increased 28.3-fold by the deletion of the N-terminus (Table 14). Fusion proteins can improve the solubility of enzymes by enhancing proper folding of the target proteins [188, 189]. For guava HPL, for example, the activity was improved by N-terminal truncation and fusion with the maltose binding protein MBP [103]. In this work, fusion of N-terminally truncated guava, sorghum and papaya HPL to NusA did not result in increased activity. Only barley HPL showed a 4-fold higher activity as NusA – HPL fusion protein (Table 14). Since the overall activity of papaya $HPL_{CP\text{-}N}$ was highest (0.85 U·mg^{-1}), this HPL was selected for further experiments. The NusA fusion protein showed a similar activity, however, the N-terminally truncated enzyme was preferred to avoid undesired interference of the NusA protein in HPL characterization studies.

Compared with other HPLs that are heterologously expressed in bacterial hosts (mainly *E. coli*), $HPL_{CP\text{-}N}$ exhibited a relatively high specific activity (Table 14). In contrast, HPL from *Camellia sinensis* obtained a specific activity of 0.2 U·mg^{-1} and HPL from *Cucumis melo* showed a specific activity of 0.51 U·mg^{-1} in the soluble fraction [208]. HPL from *M. sativa* had a specific activity of 0.62 U·mg^{-1} in the soluble fraction and 5.42 U·mg^{-1} in the solubilized membrane fraction, indicating enzyme insertion into the cytoplasmic membrane during expression in *E. coli* [97]. As described for LOX expression, expression of eukaryotic HPLs in a prokaryotic expression strain may be difficult and therefore several attempts have been made to express HPLs in yeast. For secreted *L. esculentum* HPL, around 0.38 U·mg^{-1} were obtained after expression with *P. pastoris*, whereas for *Citrullus lanatus* HPL around 1.19 U·mg^{-1} were obtained after expression in *S. cerevisiae* [108, 153]. Furthermore, *C. lanatus* was expressed in *N. tabacum*, reaching a specific activity of 1.47 U·mg^{-1} in leaf extracts [110].

Table 14 Comparison of enzymatic activities of hydroperoxide lyases (HPL). SF: soluble fraction.

Enzyme	Specific activity [U·mg^{-1}]	Purification step	Enzyme origin	Expression system	Reference
HPL_{CP}	0.03	SF	*C. papaya*	*E. coli*	This work
$HPL_{CP\text{-}N}$	0.85	SF	*C. papaya*	*E. coli*	This work
$NusAHPL_{CP\text{-}N}$	0.84	SF	*C. papaya*	*E. coli*	This work
$HPL_{HV\text{-}N}$	0.1	SF	*H. vulgare*	*E. coli*	This work
$NusAHPL_{HV\text{-}N}$	0.41	SF	*H. vulgare*	*E. coli*	This work
$HPL_{PG\text{-}N}$	0.24	SF	*P. guajava*	*E. coli*	This work
$NusAHPL_{PG\text{-}N}$	0.2	SF	*P. guajava*	*E. coli*	This work
$HPL_{SB\text{-}N}$	0.02	SF	*S. bicolor*	*E. coli*	This work
$NusAHPL_{SB\text{-}N}$	0.03	SF	*S. bicolor*	*E. coli*	This work

Enzyme	Specific activity [U·mg^{-1}]	Purification step	Enzyme origin	Expression system	Reference
CsHPL	0.2	SF	*C. sinensis*	*E. coli*	[209]
CmHPL	0.51	SF	*C. melo*	*E. coli*	[208]
CYP74Bv2-N	0.62	SF	*M. sativa*	*E. coli*	[97]
CYP74Bv2-N	5.42	Solubilized membrane fraction	*M. sativa*	*E. coli*	[97]
LeHPL	0.37	Secretion	*L. esculentum*	*P. pastoris*	[108]
CaHPL	0.15	Cellular extract	*Capsicum annum*	*Y. lipolytica*	[210]
ClHPL	1.19	SF	*C. lanatus*	*S. cerevisiae*	[153]
ClHPL	1.47	Leaf extracts	*C. lanatus*	*N. tabacum*	[110]
HPL$_{CP-N}$	18.21	Affinity purification	*C. papaya*	*E. coli*	This work
CYP74Bv2-N	200	Affinity purification	*M. sativa*	*E. coli*	[97]
OeHPLwt	16.98	Affinity purification	*O. europaea*	*E. coli*	[105]
HvHPL	1407	Affinity purification	*H. vulgare*	*E. coli*	[107]
CaHPL	2.94	Affinity purification	*C. annum*	*Y. lipolytica*	[210]

Expression of membrane proteins often leads to inclusion bodies and this was also observed for HPL$_{CP-N}$, which might be a membrane protein like guava HPL$_{PG}$ [84]. Membrane proteins are often incorporated into the cytoplasmic membrane of *E. coli*. However, during strong overexpression, the sec translocon, which is important for membrane incorporation of membrane proteins and for translocation of secretory proteins, is rapidly saturated. This leads to misfolded proteins that precipitate as inclusion bodies [172]. Consequently, overexpression of the desired protein should be slowed down to avoid saturation of the sec translocon and to obtain more properly folded protein. Tijet et al. circumvented this problem by omitting the inducer IPTG, resulting in less inclusion bodies and more active guava HPL [84]. Specific derivatives of *E. coli* BL21(DE3) have been developed for improved membrane protein expression and a positive effect was shown in many examples [171, 172, 211]. The Walker strains C41(DE3) and C43(DE3) possess mutations in the *lac*UV5 promoter region, which controls the expression of T7 RNA polymerase, which in

turn transcribes the target gene [171, 172]. By slowing down the expression, the toxicity of the targeted membrane proteins was reduced, resulting in more correct folded proteins. Lemo21(DE3) is another derivative of BL21(DE3) with adjustable T7 RNA polymerase to optimize the expression level of membrane proteins [172, 211]. Despite many positive examples [211], no increase in active $HPL_{CP\text{-}N}$ was achieved by expression in C41(DE3) and Lemo21(DE3) compared with expression in BL21(DE3).

In contrast, a higher level of active $HPL_{CP\text{-}N}$ was achieved by changing the cultivation medium. A six-fold higher volumetric activity was obtained with the autoinductive medium ZYM5052 containing δ-aminolevulinic acid compared to the initially used LB medium. The increase in activity can be attributed to higher cell density achieved by higher nutrient content. In contrast to LB, ZYM5052 contains a trace metal mix and additional magnesium supply. Moreover, ZYM5052 is buffered and contains glycerol as additional carbon source. Although the complex medium TB contains five times the amount of yeast extract and twice the amount of tryptone compared to ZYM5052, lower yields of active $HPL_{CP\text{-}N}$ were obtained. Hence, the addition of the trace metal solution as well as induction with lactose instead of IPTG seem to trigger HPL expression. The addition of δ-aminolevulinic acid as heme-precursor increased the activity, which can be explained by the fact that HPL is a heme-containing enzyme and therefore adequate supply must be ensured. This was also observed for HPLs from olive, bell pepper or sugar beet [104, 105, 207].

4.3. Purification and characterization of papaya $HPL_{CP\text{-}N}$

Proteins that are incorporated into membranes can be extracted by the addition of detergents, which mimic a membrane surrounding [96, 97, 212]. Several HPLs, e.g. from barrel medic, barley or guava have been described to show higher activity in the soluble fraction when a detergent such as Triton X-100, Brij99 or emulphogene was added [84, 107, 114]. For $HPL_{CP\text{-}N}$, a buffer without detergent resulted in only 14 % recovery of activity in the soluble fraction, whereas 85 % of activity was recovered with a buffer containing the detergent Triton X-100. In addition to the positive effect of detergents, the addition of a high salt concentration significantly increased the activity of $HPL_{CP\text{-}N}$. This effect has already been described for barley, olive or mint leaf HPLs [107, 112, 213].

Purification of histidine-tagged $HPL_{CP\text{-}N}$ was performed chromatographically. Although several purification conditions were tested, it was not possible to elute a completely pure $HPL_{CP\text{-}N}$ enzyme. This might be a result of the relatively low overexpression of soluble $HPL_{CP\text{-}N}$, which makes enrichment difficult. Problems with affinity purification were also reported for other HPLs. For example, heterologously expressed HPLs from *Vitis vinifera* or *O. sativa* could not be enriched to yield pure elution bands [77, 214]. Purification of $HPL_{CP\text{-}N}$ might be improved by additional

purification steps such as a size exclusion chromatography. However, due to low amounts of active $HPL_{CP\text{-}N}$ obtained after affinity purification, further purification steps were not incorporated. Instead, the enzyme was used with an estimated purity of 70 % for the enzyme cascade developments. A specific activity of 18.21 $U \cdot mg^{-1}$ was measured in the eluate fraction. In comparison, 16.98 $U \cdot mg^{-1}$ were reported for purified *O. europaea* HPL [105], 2.94 $U \cdot mg^{-1}$ for purified *C. annum* HPL [210] and 200 $U \cdot mg^{-1}$ for purified *M. sativa* HPL [97] (Table 14). Koeduka et al. even reached 1407 $U \cdot mg^{-1}$ for purified full-length barley HPL [107]. These activities are surprisingly high, since we only obtained very low activity for full-length barley HPL in the crude extract (0.04 $U \cdot mg^{-1}$) and therefore decided not to purify the enzyme.

The native molecular weight of $HPL_{CP\text{-}N}$ correlates with the tertiary structure of a tetramer upon comparison to its calculated molecular weight. This corresponds to the published tetrameric structures of HPLs from soybean, guava or sunflower [84, 85, 215]. In contrast, a trimeric confirmation was predicted for HPLs from tomato leaves and green bells [86, 216].

Many HPLs have a strong preference for 13(*S*)-HPOTE compared to 13(*S*)-HPODE as substrate. HPL from *Solanum tuberosum*, for example, possesses a 28-fold higher catalytic efficiency (k_{cat}/K_m) with 13(*S*)-HPOTE than with 13(*S*)-HPODE [111]. HPL from *Medicago truncatula* shows a 5.3-fold higher and HPL from *O. europaea* a 5.5-fold higher catalytic efficiency [105, 114]. In this work, $HPL_{CP\text{-}N}$ was found to exhibit only a 1.5-fold higher catalytic efficiency for 13(*S*)-HPOTE compared to 13(*S*)-HPODE. Compared to other HPLs, the relative catalytic efficiency for 13(*S*)-HPODE is high, making papaya HPL a suitable enzyme for the biocatalytic route starting from linoleic acid.

The reaction of HPL was found to proceed very rapidly, leading to hexanal and unstable 12-oxo-9(*Z*)-dodecenoic acid. Time-dependent experiments showed that a maximum of 12-oxo-9(*Z*)-dodecenoic acid was reached within 10 sec, when the soluble fraction was used as $HPL_{CP\text{-}N}$ source. Over the next 120 min, it declined almost completely, while its isoform 12-oxo-10(*E*)-dodecenoic acid, also known as traumatin, increased to 10 % of the initial substrate concentration. Part of the other 90 % 12-oxo-9(*Z*)-dodecenoic acid might be degraded into smaller products, converted to 12,12-dihydroxy-9(*Z*)-dodecenoic acid as described by Grechkin et al. [74] or react with amine residues of proteins forming Schiff bases.

Traumatin, as well as its derivative traumatic acid are plant wound hormones [26], whereas 12-oxo-9(*Z*)-dodecenoic acid is believed to be the transient intermediate for the synthesis of its 10(*E*) isoform. Grechkin and Hamberg suggested a keto-enol tautomerism as mechanism for 12-oxo-10(*E*)-dodecenoic acid formation [83]. For alfalfa HPL, a 3*Z*:2*E*-enal isomerase was proposed as isomerization factor for the formation of traumatin [100]. We could demonstrate that the decrease of 12-oxo-9(*Z*)-dodecenoic acid significantly slowed down when purified enzyme

was used instead of the protein-rich soluble fraction. For this reason, we suggest that high protein concentrations can also lead to non-selective formation of traumatin (Fig. 39). A Schiff base may be formed with lysine residues of protein rich fractions and traumatin formation may proceed via imine-enamine tautomerism. Hence, fast reaction setup and enzyme purification is necessary to achieve high yields of 12-oxo-9(*Z*)-dodecenoic acid.

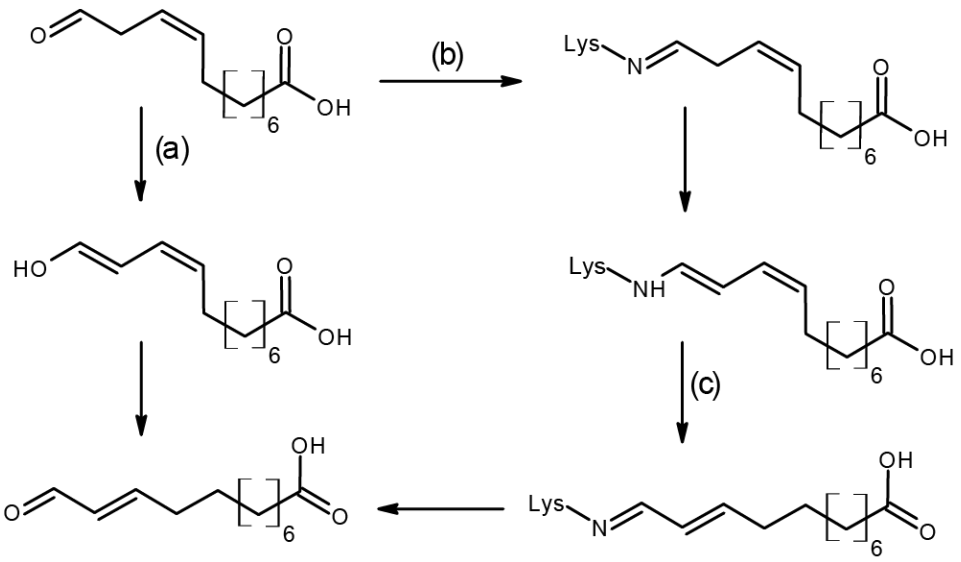

Fig. 39 Formation of 12-oxo-10(*E*)-dodecenoic acid (traumatin). Traumatin might be either built through (**a**) keto-enol tautomerism or (**b**) Schiff base formation, exemplified with a lysine residue (Lys), followed by (**c**) imine-enamine tautomerism. Figure reproduced from [175] with permission from Springer Nature.

4.4. Comparison of ω-TAs for the amination of 12-oxododecenoic acid and hexanal

ω-Transaminases can convert a variety of aldehydes and ketones, including 12-oxododecanoic acid to 12-aminododecanoic [13, 165, 217]. In contrast, the unsaturated form has not yet been tested as substrate. In this work, seven ω-TAs were screened for their ability to transaminate the unsaturated 12-oxo-9(*Z*)-dodecenoic acid and 12-oxo-10(*E*)-dodecenoic acid. For this, ω-TAs from *C. violaceum* (TR_{CV}) and *P. denitrificans* (TR_{PD}) were chosen since they have been proved to convert aliphatic medium- to long-chain aldehydes [14, 166]. TR_{AD} from *A. denitrificans* and TR_{SD} from *S. delicatus* were identified with a BLAST search for putative new homologs of TR_{CV}. The affinity-purified ω-TAs from *Acidihalobacter* sp. (TR_2) and uncultured *Rhodobacteraceae* bacterium (TR_3 and TR_6) were obtained from Prof. Manuel Ferrer (CSIC Madrid, Spain) and have previously been shown to be active on hexanal [168].

The ω-transaminases were analyzed based on their sequences and outlined in a phylogenetic tree together with known ω-TAs from literature to determine phylogenetic relations (Fig. 40). The diagram shows that the ω-TAs used in this work are widely distributed among the ω-TAs. TR_{CV}

and TR_{AD}, both belonging to the *Chromobacteriaceae* family are related close to each other and share a sequence identity of 81 % (Table 12, Fig. 40). In contrast, TR_{PD}, TR_{SD}, TR_3 and TR_6 that all belong to the *Rhodobacteraceae* family are phylogenetically more distant to each other. TR_3, for example, only shares a sequence identity of 32 % to TR_{PD}, 35 % to TR_{SD} and 34 % to TR_6. TR_2 belongs to the *Ectothiorhodospiraceae* family and shares sequence identities between 35 to 60 % to the other ω-TAs studied. Furthermore, ω-TAs differ in terms of their amino acid sequences in the binding pockets. Rausch et al. predicted 17 amino acids to be involved in substrate binding, including 12 in the large (L)-pocket, four in the small (S)-pocket and a highly conserved lysine for PLP binding [124]. A multiple sequence alignment was performed (Fig. A32), revealing that TR_{AD} shares all 17 amino acids with TR_{CV}, whereas TR_{SD}, TR_{PD}, TR_2 and TR_6 share 14 and TR_3 shares only ten amino acids. This is in consistency with the results of the phylogenetic analyses demonstrating that TR_{CV} is most closely related to TR_{AD} (Table 12, Fig. 40). TR_{SD}, TR_2 and TR_6 are phylogenetically more distant to TR_{CV} and share approximately 55 % sequence identity, whereas TR_{PD} and TR_3 share approximately 35 % sequence identity to TR_{CV}.

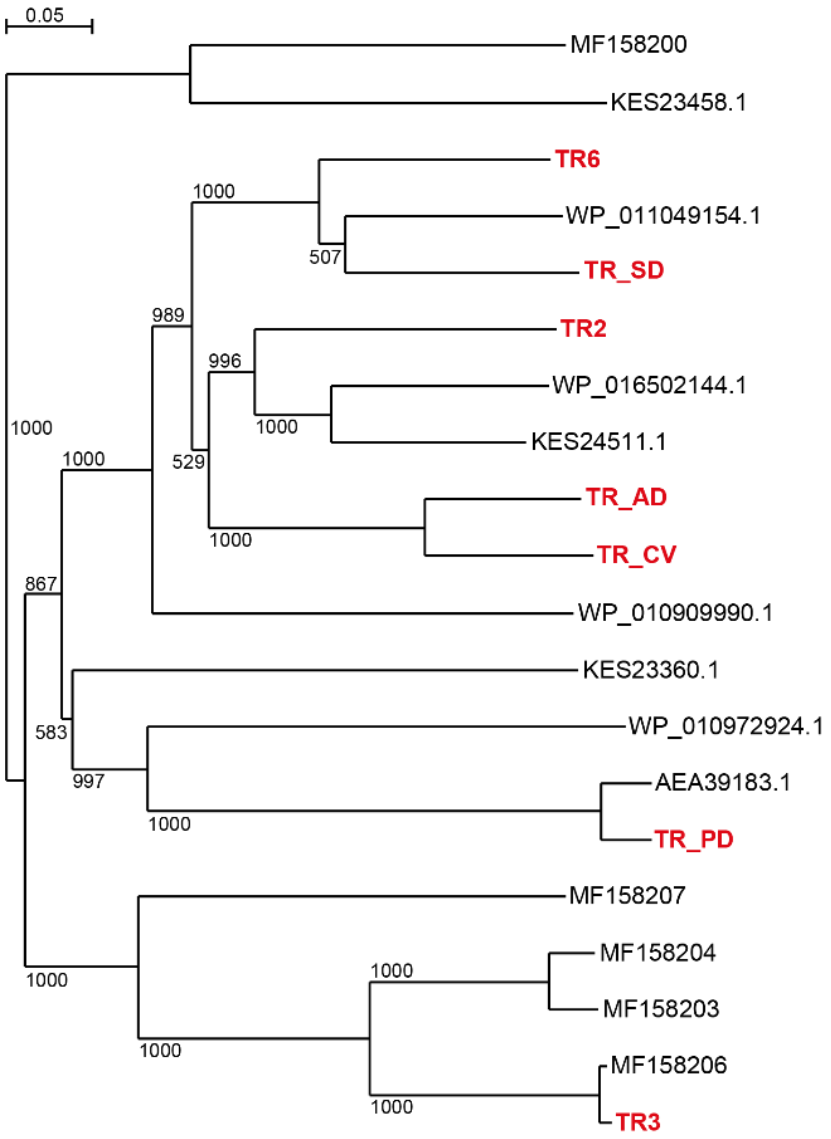

Fig. 40 Phylogenetic neighbor-joining tree of ω-transaminases, tested in this study (marked in red). A neighbor-joining tree was drawn with NJplot with a bootstrap value of 1000. The following ω-TAs were selected for the tree: TR_AD: *A. denitrificans* (WP_159877958.1); TR_CV: *C. violaceum* (WP_011135573.1); TR_PD: *P. denitrificans* (ABL72050.1); TR_SD: *S. delicatus* (WP_093738538.1); TR1: *Pseudomonas* sp. (MF158200); TR2: *Acidihalobacter* sp. (MH588437); TR3: uncultured *Rhodobacteraceae* bacterium (MF158202); TR4: uncultured *Rhodobacteraceae* bacterium (MF158203); TR5: uncultured *Rhodobacteraceae* bacterium (MF158204); TR6: uncultured *Rhodobacteraceae* bacterium (MF158205); TR7: uncultured *Rhodobacteraceae* bacterium (MF158206); TR8: *Amphritea* sp. (MF158207); TR from *Pseudomonas* sp. AAC (KES23458.1, KES23360.1 and KES24511.1); TR from *Mesorhizobium loti* (WP_010909990.1); TR from *Vibrio fluvialis* (AEA39183.1); TR from *P. putida* (WP_016502144.1); TR from *Agrobacterium tumefaciens* (WP_010972924.1) and TR from *S. pomeroyi* (WP_011049154.1). Figure reproduced from [190] with permission from Springer Nature.

TR_{AD}, TR_{CV}, TR_{PD} and TR_{SD} were successfully expressed in *E. coli* and purified by affinity chromatography. In contrast to LOX and HPL, strong overexpression and high purity of the eluted proteins were obtained. This could be due to the different origin of the enzymes. While lipoxygenase and hydroperoxide lyases studied are plant enzymes, the ω-TAs studied are of

bacterial origin and hence closer related to the *E. coli* expression host. High protein concentrations of the pure ω-TAs were obtained in the eluate fractions with 2.1 mg·ml^{-1} for TR_{PD}, 2.8 mg·ml^{-1} for TR_{SD}, 5.1 mg·ml^{-1} for TR_{AD} and 13.9 mg·ml^{-1} for TR_{CV}. Expression of other bacterial ω-TAs was frequently performed in *E. coli*, often resulting in highly overexpressed soluble enzyme [135, 168, 218]. In addition, purification of bacterial ω-TAs appears to be comparatively simple, mostly resulting in pure eluates [168, 218].

According to photometrical analysis, all purified ω-TAs were active with the aliphatic aldehyde hexanal and 12-oxododecenoic in its 9(*Z*) and 10(*E*) configuration. The highest activities were measured for six of the seven ω-TAs with the substrate hexanal. Only TR_{PD} showed slightly higher activity with 12-oxo-9(*Z*)-dodecenoic acid. Since the double bond of the oxo acids is located near the aldehyde group, it was not clear whether the ω-TAs would accept it as a substrate. We have now demonstrated that the double bond does not affect the reactivity of the ω-TAs and the 9(*Z*) or 10(*E*) configuration does not influence activity of most ω-TAs significantly. Only in the case of TR_{PD} and TR_6, significantly higher activities toward the 9(*Z*) isomer than toward the 10(*E*) isomer were found. Previous work has been done for the conversion of the saturated 12-oxododecanoic acid to 12-aminododecanoic acid in enzyme cascades [13, 164, 217]. However, no specific activities for the sole reaction were given for comparison with our work. Coscolín et al. have measured the specific activities for hexanal from ten ω-TAs, including TR_2, TR_3 and TR_6 with 0.63 U·mg^{-1}, 0.97 U·mg^{-1} and 0.42 U·mg^{-1}. These measurements differ from this work where the enzymes exhibited 0.47 U·mg^{-1}, 0.29 U·mg^{-1} and 1.01 U·mg^{-1}. However, it must be considered that Coscolín et al. used 2-(4-nitrophenyl)ethan-1-amine as amine donor and reactions were conducted at 40 °C, whereas the reactions of this work were performed with L-alanine as amine donor and were carried out at 22 °C. Hence, a comparison is only possible to a limited extent. In this work, highest specific activity toward hexanal as well as 12-oxododecenoic acid in both the 9(*Z*)- and 10(*E*) configuration was measured for *A. denitrificans* TR_{AD}. This enzyme, which has not yet been characterized, thus appears to be well suited for the transamination of aliphatic aldehydes.

Only an indirect proof of reaction was possible with the photometric assay. For direct analysis of 12-aminododecenoic acid formation, further methods of the product were required. Since 12-Aminododecenoic acid is poorly soluble, both in aqueous solutions and in organic solvents, the development of a suitable analytical method was difficult. The GC analysis previously conducted for monitoring of the HPL reaction did not work for the ω-TA reaction. 12-Aminododecenoic acid remained in the aqueous phase during solvent extraction. Evaporation of the aqueous phase and further dissolution in a solvent also failed. Consequently, a new analytical method was developed using HPLC and LC-MS. Here, 100 µl of the reaction mixture was diluted directly in 900 µl of an

acetonitrile:water mixture, bypassing solvent extraction. This way, the formation of 12-aminododecenoic acid and hexylamine could be verified by HPLC and LC-MS analyses.

Around 47 % 12-aminododecenoic acid was obtained after 1 hour reactions with TR_{AD}. However, the yield could not be increased by prolonged reaction times of up to five hours. Changing the incubation temperature or adding DMSO, both of which have been described as enhancers of the enzyme reaction [168], failed to increase the yield of 12-aminododecenoic acid. This indicates that an equilibrium was reached under the given substrate and cosubstrate concentrations. That is a common problem in ω-TA reactions, often caused by an undesirable equilibrium between L-alanine and pyruvate, so that the theoretical yield of 100 % cannot be achieved [141]. Several methods have been developed in recent years to circumvent this issue. The amine donor can be added in high stoichiometric excess, the carbonyl by-product can be removed or the carbonyl by-product can be reaminated to the amine donor [140, 219]. Although, a 20-fold higher amount of L-alanine was applied compared to the aldehyde substrate (50 mM compared to 2.5 mM), only around 50 % of 12-aminododecenoic acid were obtained. Hence, future experiments might be performed to establish an alanine regeneration system.

4.5. Challenges and opportunities of enzyme cascades targeting 12-oxo- and 12-aminododecenoic acid synthesis

The use of enzyme cascades offers many advantages over separate enzyme reactions. These include reduced process and purification steps and a shift of unfavorable reaction equilibria towards the desired product [220]. In the past, lipases, lipoxygenases, hydroperoxide lyases and ω-transaminases have been applied in enzyme cascades. Lipoxygenases were successfully coupled with lipases for combined oil hydrolysis with subsequent hydroperoxidation [167, 221, 222]. Furthermore, LOX and HPL were used in tandem for the synthesis of green note aromas [151, 152]. One-pot reactions have been conducted with *Nicotiana benthamiana* 9-LOX and watermelon 9/13-HPL, yielding 64 % of C_9-aldehydes from linoleic acid [151]. Furthermore, a *Y. lipolytica* double mutant was engineered with soybean lipoxygenase and green bell pepper hydroperoxide lyase for the synthesis of hexanal, reaching a concentration of 189 $mg \cdot l^{-1}$ [223]. In another attempt, Otte et al. combined 9-LOX and 9/13-HPL for the synthesis of 9-oxononanoic acid [208]. Furthermore, they developed an *E. coli* whole-cell biocatalyst in which the cascade was extended with endogenous oxidoreductases for oxidation of the C_9 aldehyde to azelaic acid. The dicarboxylic acid is an interesting polyamide and polyester building block [224]. Moreover, one-pot reactions were performed with ω-TAs for the synthesis of polyamide precursors. For example, an alcohol dehydrogenase was coupled with a Baeyer-Villiger monooxygenase, an esterase and a ω-TA from *Silicibacter pomeroyi* for the conversion of 12-hydroxystearic acid to

11-aminoundecanoic acid [13]. Furthermore, Schrewe et al. developed an engineered biocatalyst using the alkane monooxygenase AlkBGT with a ω-TA for the synthesis of 12-aminododecanoic acid methyl ester [14]. In addition, an alanine regeneration system was applied to ensure sufficient cosubstrate supply and the outer membrane protein AlkL as well as the alcohol dehydrogenase AlkJ were overexpressed for enhanced substrate uptake and increased alcohol oxidation [11, 15].

Despite the variety of one-pot reactions and whole-cell reactions, to our knowledge, coupling of oxylipin pathway enzymes with a ω-TA has not been shown before. Issues for the enzyme cascade developments were the differences of the enzymes regarding optimum reaction conditions, a limited availability of HPL and low stability of the highly reactive intermediates. HPL could only be obtained in limited amounts, so the cascade reactions were conducted on a small scale. For this reason, no active O_2 gassing was applied, resulting in a limitation of the LOX reaction. Consequently, a decrease in 13(*S*)-HPODE yield from 80 to 27 % was detected when the substrate concentration was increased from 1 to 5 mM linoleic acid. This was probably caused by O_2 deficiency as described before [167]. For all coupled one-pot reactions, a consecutive addition of enzymes was preferable over simultaneous addition. This was previously reported for one-pot reactions with 9(*S*)-LOX from *S. tuberosum* and 9/13-HPL from *Cucumis melo* for the synthesis of 9-oxononanoic acid and 3(*Z*)-nonenal [208]. Again, the yield was significantly increased by consecutive addition of enzymes instead of simultaneous addition. 12-Oxo-9(*Z*)-dodecenoic acid is unstable and rapidly converted to 12-oxo-10(*E*)-dodecenoic acid [74], especially in presence of high protein concentration. Hence, in cascade reactions, lipase and LOX-1 were pre-incubated with the substrate before addition of $HPL_{CP\text{-}N}$ only 1 to 15 min prior analysis. Like this, the yield of 12-oxo-9(*Z*)-dodecenoic acid could be preserved. This reaction setup is also favorable for the HPL enzyme, since it gets deactivated very quickly [107]. Thus, addition of high HPL concentration for fast catalysis is preferable to addition of low concentration and slow catalysis. For further transamination, a rapid conversion of 12-oxo-9(*Z*)-dodecenoic acid to 12-aminododecenoic acid is important. In one-pot reactions with TR_{AD}, this was achieved by a prior addition of TR_{AD} and a stepwise addition of $HPL_{CP\text{-}N}$ gradually, thereby circumventing the fast degradation of the products.

In general, three-enzyme cascade reactions resulted in lower yields than two-enzyme reactions. For a coupled lipase – LOX – HPL reaction, the yield of 12-oxo-9(*Z*)-dodecenoic acid was 32 % lower than for a coupled LOX – HPL reaction. The same was observed for coupled ω-transaminase reactions, where the yield of 12-aminododecenoic acid was reduced by 80 % from a coupled HPL – ω-TA reaction to a coupled LOX – HPL – ω-TA reaction. To further optimize the three-enzyme reactions and to establish a four-enzyme reaction with lipase – LOX – HPL – ω-TA, the reactions should be optimized to obtain higher yields. This could be achieved, for example, by larger

reaction setups with external O_2 addition to increase the conversion rate of the lipoxygenase reaction. Moreover, whole-cell biocatalysts could be developed to circumvent the problems of *in-vitro* one-pot enzyme reactions. For this, the use of *Y. lipolytica* yeast as expression strain could be beneficial because it can grow on fatty acids and oils and use them as sole carbon source [225]. Moreover, the addition of an alanine and PLP regeneration system could promote high synthesis of 12-aminodeocenoic acid by bypassing the unfavorable balance of alanine and pyruvate. Whole-cell biocatalysts with the alkane monooxygenase AlkBGT and ω-TA from *C. violaceum* yielded up to 96.5 % 12-aminododecanoic acid after implementation of a cofactor regeneration system [11, 15]. Hence, his could also promote the yield of 12-aminododecenoic acid in LOX, HPL and ω-TA cascades.

5. References

1. PlascticsEurope (2021). Plastics-the Facts 2021- An analysis of European plastics production, demand and waste data. Retrieved November 11, 2022, from https://plasticseurope.org/wp-content/uploads/2021/12/Plastics-the-Facts-2021-web-final.pdf.
2. Rosenboom, J. G., Langer, R. & Traverso, G. (2022). Bioplastics for a circular economy. *Nature Reviews Materials 2022 7:2*, *7*, 117–137. https://doi.org/10.1038/s41578-021-00407-8.
3. Zhou, Y., Wu, S. & Bornscheuer, U. T. (2021). Recent advances in (chemo)enzymatic cascades for upgrading bio-based resources. *Chemical Communications*, *57*, 10661–10674. https://doi.org/10.1039/D1CC04243B.
4. Bell, E. L., Finnigan, W., France, S. P., Green, A. P., Hayes, M. A., Hepworth, L. J., Lovelock, S. L., Niikura, H., Osuna, S., Romero, E., Ryan, K. S., Turner, N. J. & Flitsch, S. L. (2021). Biocatalysis. *Nature Reviews Methods Primers 2021 1:1*, *1*, 1–21. https://doi.org/10.1038/s43586-021-00044-z.
5. Chinthapalli, R., Skoczinski, P., Carus, M., Baltus, W., De Guzman, D., Käb, H., Raschka, A. & Ravenstijn, J. (2019). Biobased building blocks and polymers—global capacities, production and trends, 2018–2023. *Industrial Biotechnology*, *15*, 237–241. https://doi.org/10.1089/IND.2019.29179.RCH.
6. Nanda, S., Patra, B. R., Patel, R., Bakos, J. & Dalai, A. K. (2021). Innovations in applications and prospects of bioplastics and biopolymers: a review. *Environmental Chemistry Letters 2021 20:1*, *20*, 379–395. https://doi.org/10.1007/S10311-021-01334-4.
7. Arikan, E. B. & Ozsoy, H. D. (2015). A review: investigation of bioplastics. *Journal of Civil Engineering and Architecture*, *9*, 188–192. https://doi.org/10.17265/1934-7359/2015.02.007.
8. Luengo, J. M., García, B., Sandoval, A., Naharro, G. & Olivera, E. R. (2003). Bioplastics from microorganisms. *Current Opinion in Microbiology*, *6*, 251–260. https://doi.org/10.1016/S1369-5274(03)00040-7.
9. Chung, H., Yang, J. E., Ha, J. Y., Chae, T. U., Shin, J. H., Gustavsson, M. & Lee, S. Y. (2015). Bio-based production of monomers and polymers by metabolically engineered microorganisms. *Current Opinion in Biotechnology*, *36*, 73–84. https://doi.org/10.1016/j.copbio.2015.07.003.

10. Karau, A., Sieber, V., Haas, T., Haeger, H., Grammann, K., Buehler, B., Blank, L., Schmid, A., Jach, G., Lalla, B., Mueller, A., Schullehner, K., Welters, P., Eggert, T. & Weckbecker, A. (2015, April 21). ω-Aminocarboxylic acids, ω-aminocarboxylic acid esters, or recombinant cells which produce lactams thereof. U.S. Patent No. 9,012,227B2.
11. Ladkau, N., Assmann, M., Schrewe, M., Julsing, M. K., Schmid, A. & Bühler, B. (2016). Efficient production of the nylon 12 monomer ω-aminododecanoic acid methyl ester from renewable dodecanoic acid methyl ester with engineered *Escherichia coli*. *Metabolic Engineering*, *36*, 1–9. https://doi.org/10.1016/j.ymben.2016.02.011.
12. GlobeNewswire. (2019). Polyamide market to reach USD 38.30 billion by 2026. Retrieved November 17, 2022, from https://www.globenewswire.com/news-release/2019/07/15/1882593/0/en/Polyamide-Market-To-Reach-USD-38-30-Billion-By-2026-Reports-And-Data.html.
13. Song, J.-W., Lee, J.-H., Bornscheuer, U. T. & Park, J.-B. (2014). Microbial synthesis of medium-chain α,ω-dicarboxylic acids and ω-aminocarboxylic acids from renewable long-chain fatty acids. *Advanced Synthesis & Catalysis*, *356*, 1782–1788. https://doi.org/10.1002/adsc.201300784.
14. Schrewe, M., Ladkau, N., Bühler, B. & Schmid, A. (2013). Direct terminal alkylamino-functionalization via multistep biocatalysis in one recombinant whole-cell catalyst. *Advanced Synthesis & Catalysis*, *355*, 1693–1697. https://doi.org/10.1002/adsc.201200958.
15. Ge, J., Yang, X., Yu, H. & Ye, L. (2020). High-yield whole cell biosynthesis of Nylon 12 monomer with self-sufficient supply of multiple cofactors. *Metabolic Engineering*, *62*, 172–185. https://doi.org/10.1016/j.ymben.2020.09.006.
16. Dislich, C., Keyel, A. C., Salecker, J., Kisel, Y., Meyer, K. M., Auliya, M., Barnes, A. D., Corre, M. D., Darras, K., Faust, H., Hess, B., Klasen, S., Knohl, A., Kreft, H., Meijide, A., Nurdiansyah, F., Otten, F., Pe'er, G., Steinebach, S., Tarigan, S., Tölle, M. H., Tscharntke, T. & Wiegand, K. (2017). A review of the ecosystem functions in oil palm plantations, using forests as a reference system. *Biological Reviews*, *92*, 1539–1569. https://doi.org/10.1111/BRV.12295.
17. Qaim, M., Sibhatu, K. T., Siregar, H. & Grass, I. (2020). Environmental, economic, and social consequences of the oil palm boom. *Annual Review of Resource Economics*, *12*, 321–344. https://doi.org/10.1146/annurev-resource-110119-024922.
18. Howe, G. A. & Schilmiller, A. L. (2002). Oxylipin metabolism in response to stress. *Current Opinion in Plant Biology*, *5*, 230–236. https://doi.org/10.1016/S1369-5266(02)00250-9.
19. Feussner, I. & Wasternack, C. (2002). The lipoxygenase pathway. *Annual Review of Plant Biology*, *53*, 275–297. https://doi.org/10.1146/annurev.arplant.53.100301.135248.

20. Cohen, Y., Gisi, U. & Niderman, T. (1993). Local and systemic protection against *Phytophthora infestans* induced in potato and tomato plants by jasmonic acid and jasmonic methyl ester. *Phytopathology*, *83*, 1054–1062. https://doi.org/10.1094/PHYTO-83-1054.
21. Sivasankar, S., Sheldrick, B. & Rothstein, S. J. (2000). Expression of allene oxide synthase determines defense gene activation in tomato. *Plant Physiology*, *122*, 1335–1342. https://doi.org/10.1104/PP.122.4.1335.
22. Wasternack, C. & Hause, B. (2013). Jasmonates: Biosynthesis, perception, signal transduction and action in plant stress response, growth and development. An update to the 2007 review in Annals of Botany. *Annals of Botany*, *111*, 1021–1058. https://doi.org/10.1093/aob/mct067.
23. Croft, K. P. C., Jüttner, F. & Slusarenko, A. J. (1993). Volatile products of the lipoxygenase pathway evolved from *Phaseolus vulgaris* (L.) leaves inoculated with *Pseudomonas syringae pv phaseolicola*. *Plant Physiology*, *101*, 13–24. https://doi.org/10.1104/pp.101.1.13.
24. Finidori-Logli, V., Bagnères, A. G. & Clément, J. L. (1996). Role of plant volatiles in the search for a host by parasitoid *Diglyphus isaea* (Hymenoptera: Eulophidae). *Journal of Chemical Ecology 1996 22:3*, *22*, 541–558. https://doi.org/10.1007/BF02033654.
25. Bate, N. J. & Rothstein, S. J. (1998). C6-volatiles derived from the lipoxygenase pathway induce a subset of defense-related genes. *Plant Journal*, *16*, 561–569. https://doi.org/10.1046/j.1365-313X.1998.00324.x.
26. Zimmerman, D. C. & Coudron, C. A. (1979). Identification of traumatin, a wound hormone, as 12-Oxo- trans -10-dodecenoic Acid. *Plant Physiology*, *63*, 536–541. https://doi.org/10.1104/pp.63.3.536.
27. Weber, H., Chételat, A., Caldelari, D. & Farmer, E. E. (1999). Divinyl ether fatty acid synthesis in late blight-diseased potato leaves. *Plant Cell*, *11*, 485–493. https://doi.org/10.1105/tpc.11.3.485.
28. Hamberg, M. (1999). An epoxy alcohol synthase pathway in higher plants: Biosynthesis of antifungal trihydroxy oxylipins in leaves of potato. *Lipids 1999 34:11*, *34*, 1131–1142. https://doi.org/10.1007/S11745-999-0464-7.
29. Namai, T., Kato, T., Yamaguchi, Y. & Hirukawa, T. (1993). Anti-rice blast activity and resistance induction of C-18 oxygenated fatty acids. *Bioscience, Biotechnology, and Biochemistry*, *57*, 611–613. https://doi.org/10.1271/BBB.57.611.
30. Kuhn, H., Wiesner, R., Rathmann, J. & Schewe, T. (1991). Formation of ketodienoic fatty acids by the pura pea lipoxygenase-1. *Eicosanoids*, *4*, 9–14. Retrieved from http://www.ncbi.nlm.nih.gov/pubmed/1905562
31. Nanda, S. & Yadav, J. S. (2003). Lipoxygenase biocatalysis: a survey of asymmetric oxygenation. *Journal of Molecular Catalysis B: Enzymatic*, *26*, 3–28. https://doi.org/10.1016/S1381-1177(03)00146-2.

32. Haeggström, J. Z. & Funk, C. D. (2011, October 12). Lipoxygenase and leukotriene pathways: Biochemistry, biology, and roles in disease. *Chemical Reviews*. American Chemical Society. https://doi.org/10.1021/cr200246d.

33. Oliw, E. H. (2002). Plant and fungal lipoxygenases. *Prostaglandins and Other Lipid Mediators*, *68–69*, 313–323. https://doi.org/10.1016/S0090-6980(02)00037-0.

34. Hansen, J., Garreta, A., Benincasa, M., Fusté, M. C., Busquets, M. & Manresa, A. (2013). Bacterial lipoxygenases, a new subfamily of enzymes? A phylogenetic approach. *Applied Microbiology and Biotechnology*, *97*, 4737–4747. https://doi.org/10.1007/s00253-013-4887-9.

35. Andreou, A., Brodhun, F. & Feussner, I. (2009). Biosynthesis of oxylipins in non-mammals. *Progress in Lipid Research*, *48*, 148–170. https://doi.org/10.1016/j.plipres.2009.02.002.

36. Biringer, R. G. (2020). The enzymology of human eicosanoid pathways: the lipoxygenase branches. *Molecular Biology Reports 2020 47:9*, *47*, 7189–7207. https://doi.org/10.1007/S11033-020-05698-8.

37. Sugio, A., Østergaard, L. H., Matsui, K. & Takagi, S. (2018). Characterization of two fungal lipoxygenases expressed in *Aspergillus oryzae*. *Journal of Bioscience and Bioengineering*, *126*, 436–444. https://doi.org/10.1016/J.JBIOSC.2018.04.005.

38. Joo, Y. C. & Oh, D. K. (2012). Lipoxygenases: Potential starting biocatalysts for the synthesis of signaling compounds. *Biotechnology Advances*, *30*, 1524–1532. https://doi.org/10.1016/J.BIOTECHADV.2012.04.004.

39. Stolterfoht, H., Rinnofner, C., Winkler, M. & Pichler, H. (2019). Recombinant lipoxygenases and hydroperoxide lyases for the synthesis of green leaf volatiles. *Journal of Agricultural and Food Chemistry*, *67*, 13367–13392. https://doi.org/10.1021/acs.jafc.9b02690.

40. Andreou, A. & Feussner, I. (2009). Lipoxygenases – Structure and reaction mechanism. *Phytochemistry*, *70*, 1504–1510. https://doi.org/10.1016/j.phytochem.2009.05.008.

41. Heshof, R., Jylhä, S., Haarmann, T., Jørgensen, A. L. W., Dalsgaard, T. K. & De Graaff, L. H. (2014). A novel class of fungal lipoxygenases. *Applied Microbiology and Biotechnology*, *98*, 1261–1270. https://doi.org/10.1007/s00253-013-5392-x.

42. Wennman, A., Jernerén, F., Magnuson, A. & Oliw, E. H. (2015). Expression and characterization of manganese lipoxygenase of the rice blast fungus reveals prominent sequential lipoxygenation of α-linolenic acid. *Archives of Biochemistry and Biophysics*, *583*, 87–95. https://doi.org/10.1016/J.ABB.2015.07.014.

43. Hörnsten, L., Su, C., Osbourn, A. E., Hellman, U. & Oliw, E. H. (2002). Cloning of the manganese lipoxygenase gene reveals homology with the lipoxygenase gene family. *European Journal of Biochemistry*, *269*, 2690–2697. https://doi.org/10.1046/J.1432-1033.2002.02936.X.

44. Lõhelaid, H., Järving, R., Valmsen, K., Varvas, K., Kreen, M., Järving, I. & Samel, N. (2008). Identification of a functional allene oxide synthase-lipoxygenase fusion protein in the soft coral *Gersemia fruticosa* suggests the generality of this pathway in octocorals. *Biochimica et Biophysica Acta (BBA) - General Subjects*, *1780*, 315–321. https://doi.org/10.1016/J.BBAGEN.2007.10.010.

45. Teder, T., Lõhelaid, H. & Samel, N. (2017). Structural and functional insights into the reaction specificity of catalase-related hydroperoxide lyase: A shift from lyase activity to allene oxide synthase by site-directed mutagenesis. *PLOS ONE*, *12*, e0185291. https://doi.org/10.1371/JOURNAL.PONE.0185291.

46. Zheng, Y., Boeglin, W. E., Schneider, C. & Brash, A. R. (2008). A 49-kDa mini-lipoxygenase from *Anabaena* sp. PCC 7120 retains catalytically complete functionality. *Journal of Biological Chemistry*, *283*, 5138–5147. https://doi.org/10.1074/jbc.M705780200.

47. Andreou, A., Göbel, C., Hamberg, M. & Feussner, I. (2010). A bisallylic mini-lipoxygenase from Cyanobacterium *Cyanothece* sp. that has an iron as cofactor. *Journal of Biological Chemistry*, *285*, 14178–14186. https://doi.org/10.1074/jbc.M109.094771.

48. Andreou, A. Z., Vanko, M., Bezakova, L. & Feussner, I. (2008). Properties of a mini 9R-lipoxygenase from *Nostoc* sp. PCC 7120 and its mutant forms. *Phytochemistry*, *69*, 1832–1837. https://doi.org/10.1016/J.PHYTOCHEM.2008.03.002.

49. Gardner, H. W. (1989). Soybean lipoxygenase-1 enzymically forms both (9S)- and (13S)-hydroperoxides from linoleic acid by a pH-dependent mechanism. *Biochimica et Biophysica Acta - Lipids and Lipid Metabolism*, *1001*, 274–281. https://doi.org/10.1016/0005-2760(89)90111-2.

50. Sellhorn, G. E., Youn, B., Webb, B. N., Gloss, L. M., Kang, C. & Grimes, H. D. (2011). Biochemical characterization, kinetic analysis and molecular modeling of recombinant vegetative lipoxygenases from soybean. *International Journal of Biology*, *3*. https://doi.org/10.5539/ijb.v3n1p44.

51. Newcomer, M. E. & Brash, A. R. (2015). The structural basis for specificity in lipoxygenase catalysis. *Protein Science*, *24*, 298–309. https://doi.org/10.1002/pro.2626.

52. May, C., Höhne, M., Gnau, P., Schwennesen, K. & Kindl, H. (2000). The N-terminal β-barrel structure of lipid body lipoxygenase mediates its binding to liposomes and lipid bodies. *European Journal of Biochemistry*, *267*, 1100–1109. https://doi.org/10.1046/J.1432-1327.2000.01105.X.

53. Minor, W., Steczko, J., Stec, B., Otwinowski, Z., Bolin, J. T., Walter, R. & Axelrod, B. (1996). Crystal structure of soybean lipoxygenase L-1 at 1.4 Å resolution. *Biochemistry*, *35*, 10687–10701. https://doi.org/10.1021/bi960576u.

54. Ivanov, I., Heydeck, D., Hofheinz, K., Roffeis, J., O'Donnell, V. B., Kuhn, H. & Walther, M. (2010). Molecular enzymology of lipoxygenases. *Archives of Biochemistry and Biophysics*, *503*, 161–174. https://doi.org/10.1016/j.abb.2010.08.016.

55. Hayward, S., Cilliers, T. & Swart, P. (2017). Lipoxygenases: from isolation to application. *Comprehensive Reviews in Food Science and Food Safety*, *16*, 199–211. https://doi.org/10.1111/1541-4337.12239.

56. Skrzypczak-Jankun, E., Bross, R. A., Carroll, R. T., Dunham, W. R. & Funk, J. O. (2001). Three-dimensional structure of a purple lipoxygenase. *Journal of the American Chemical Society*, *123*, 10814–10820. https://doi.org/10.1021/ja011759t.

57. Goddard, T. D., Huang, C. C., Meng, E. C., Pettersen, E. F., Couch, G. S., Morris, J. H. & Ferrin, T. E. (2017). UCSF ChimeraX: Meeting modern challenges in visualization and analysis. *Protein Science*, *27*, 14–25. https://doi.org/10.1002/PRO.3235.

58. Zoia, L., Perazzini, R., Crestini, C. & Argyropoulos, D. S. (2011). Understanding the radical mechanism of lipoxygenases using 31P NMR spin trapping. *Bioorganic & Medicinal Chemistry*, *19*, 3022–3028. https://doi.org/10.1016/J.BMC.2011.02.046.

59. Fauconnier, M. L. & Marlier, M. (1996). An efficient procedure for the production of fatty acid hydroperoxides from hydrolyzed flax seed oil and soybean lipoxygenase. *Biotechnology Techniques*, *10*, 839–844. https://doi.org/10.1007/BF00154668.

60. Drouet, P., Thomas, D. & Legoy, M. D. (1994). Production of 13(S)-hydroperoxy-9(Z),11(E)-octadecadienoic acid using soybean lipoxygenase 1 in a biphasic octane-water system. *Tetrahedron Letters*, *35*, 3923–3926. https://doi.org/10.1016/S0040-4039(00)76703-7.

61. Ramadoss, C. S. & Axelrod, B. (1982). High-performance liquid chromatographic separation of lipoxygenase isozymes in crude soybean extracts. *Analytical Biochemistry*, *127*, 25–31. https://doi.org/10.1016/0003-2697(82)90139-7.

62. Németh, Á. S., Szajáni, B., Márczy, J. S. & Simon, M. L. (1998). A simple and rapid method enhancing of lipoxygenase-1 to lipoxygenase-2+lipoxygenase-3 isoenzyme activity ratio in soybean meal extracts. *Biotechnology Techniques 1998 12:5*, *12*, 389–392. https://doi.org/10.1023/A:1008830532629.

63. Aanangi, R., Kotapati, K. V., Palaka, B. K., Kedam, T., Kanika, N. D. & Ampasala, D. R. (2016). Purification and characterization of lipoxygenase from mung bean (*Vigna radiata* L.) germinating seedlings. *3 Biotech*, *6*, 1–8. https://doi.org/10.1007/s13205-016-0427-5.

64. Mandal, S., Dahuja, A., Kar, A. & Santha, I. M. (2014). In vitro kinetics of soybean lipoxygenase with combinatorial fatty substrates and its functional significance in off flavour development. *Food Chemistry*, *146*, 394–403. https://doi.org/10.1016/J.FOODCHEM.2013.08.100.

65. Steczko, J., Donoho, G. A., Dixon, J. E., Sugimoto, T. & Axelrod, B. (1991). Effect of ethanol and low-temperature culture on expression of soybean lipoxygenase L-1 in *Escherichia coli*. *Protein Expression and Purification*, *2*, 221–227. https://doi.org/10.1016/1046-5928(91)90075-T.

66. Schiller, D., Contreras, C., Vogt, J., Dunemann, F., Defilippi, B. G., Beaudry, R. & Schwab, W. (2015). A dual positional specific lipoxygenase functions in the generation of flavor compounds during climacteric ripening of apple. *Horticulture Research*, *2*. https://doi.org/10.1038/hortres.2015.3.

67. Heshof, R., van Schayck, J. P., Tamayo-Ramos, J. A. & de Graaff, L. H. (2014). Heterologous expression of *Gaeumannomyces graminis* lipoxygenase in *Aspergillus nidulans*. *AMB Express*, *4*, 1–6. https://doi.org/10.1186/s13568-014-0065-4.

68. Kelle, S., Zelena, K., Krings, U., Linke, D. & Berger, R. G. (2014). Expression of soluble recombinant lipoxygenase from *Pleurotus sapidus* in *Pichia pastoris*. *Protein Expression and Purification*, *95*, 233–239. https://doi.org/10.1016/j.pep.2014.01.004.

69. Feussner, I., Bachmann, A., Höhne, M. & Kindl, H. (1998). All three acyl moieties of trilinolein are efficiently oxygenated by recombinant His-tagged lipid body lipoxygenase in vitro. *FEBS Letters*, *431*, 433–436. https://doi.org/10.1016/S0014-5793(98)00808-4.

70. Brodhun, F., Cristobal-Sarramian, A., Zabel, S., Newie, J., Hamberg, M. & Feussner, I. (2013). An iron 13S-lipoxygenase with an α-linolenic acid specific hydroperoxidase activity from *Fusarium oxysporum*. *PLOS ONE*, *8*, e64919. https://doi.org/10.1371/JOURNAL.PONE.0064919.

71. Lu, X., Zhang, J., Liu, S., Zhang, D., Xu, Z., Wu, J., Li, J., Du, G. & Chen, J. (2013). Overproduction, purification, and characterization of extracellular lipoxygenase of *Pseudomonas aeruginosa* in *Escherichia coli*. *Applied Microbiology and Biotechnology*, *97*, 5793–5800. https://doi.org/10.1007/S00253-012-4457-6/FIGURES/6.

72. Cristea, M., Engström, Å., Su, C., Hörnsten, L. & Oliw, E. H. (2005). Expression of manganese lipoxygenase in *Pichia pastoris* and site-directed mutagenesis of putative metal ligands. *Archives of Biochemistry and Biophysics*, *434*, 201–211. https://doi.org/10.1016/J.ABB.2004.10.026.

73. Hughes, R. K., De Domenico, S. & Santino, A. (2009). Plant Cytochrome CYP74 family: biochemical features, endocellular localisation, activation mechanism in plant defence and improvements for industrial applications. *ChemBioChem*, *10*, 1122–1133. https://doi.org/10.1002/cbic.200800633.

74. Grechkin, A. N. & Hamberg, M. (2004). The "heterolytic hydroperoxide lyase" is an isomerase producing a short-lived fatty acid hemiacetal. *Biochimica et Biophysica Acta - Molecular and Cell Biology of Lipids*, *1636*, 47–58. https://doi.org/10.1016/j.bbalip.2003.12.003.

75. Mita, G., Quarta, A., Fasano, P., Paolis, A. De, Sansebastiano, G. P. Di, Perrotta, C., Iannacone, R., Belfield, E., Hughes, R., Tsesmetzis, N., Casey, R. & Santino, A. (2005). Molecular cloning and characterization of an almond 9-hydroperoxide lyase, a new CYP74 targeted to lipid bodies1. *Journal of Experimental Botany*, 2321–2333. https://doi.org/https://doi.org/10.1093/jxb/eri225.

76. Howe, G. A., Lee, G. I., Itoh, A., Li, L. & DeRocher, A. E. (2000). Cytochrome P450-dependent metabolism of oxylipins in tomato. cloning and expression of allene oxide synthase and fatty acid hydroperoxide lyase. *Plant Physiology*, *123*, 711–724. https://doi.org/10.1104/PP.123.2.711.

77. Kuroda, H., Oshima, T., Kaneda, H. & Takashio, M. (2014). Identification and functional analyses of two cDNAs that encode fatty acid 9-/13-hydroperoxide lyase (CYP74C) in rice. *OUP*, *69*, 1545–1554. https://doi.org/10.1271/BBB.69.1545.

78. Matsui, K. (2006). Green leaf volatiles: hydroperoxide lyase pathway of oxylipin metabolism. *Current Opinion in Plant Biology*, *9*, 274–280. https://doi.org/10.1016/j.pbi.2006.03.002.

79. Rustgi, S., Springer, A., Kang, C., von Wettstein, D., Reinbothe, C., Reinbothe, S. & Pollmann, S. (2019). Allene oxide synthase and hydroperoxide lyase, two non-canonical cytochrome P450s in *Arabidopsis thaliana* and their different roles in plant defense. *International Journal of Molecular Sciences*, *20*, 3064. https://doi.org/10.3390/ijms20123064.

80. Toporkova, Y. Y., Smirnova, E. O., Gorina, S. S., Mukhtarova, L. S. & Grechkin, A. N. (2018). Detection of the first higher plant epoxyalcohol synthase: Molecular cloning and characterisation of the CYP74M2 enzyme of spikemoss *Selaginella moellendorffii*. *Phytochemistry*, *156*, 73–82. https://doi.org/10.1016/j.phytochem.2018.08.010.

81. Nelson, D. R. (1999). Cytochrome P450 and the individuality of species. *Archives of Biochemistry and Biophysics*, *369*, 1–10. https://doi.org/10.1006/ABBI.1999.1352.

82. Brash, A. R. (2009). Mechanistic aspects of CYP74 allene oxide synthases and related cytochrome P450 enzymes. *Phytochemistry*, *70*, 1522–1531. https://doi.org/10.1016/J.PHYTOCHEM.2009.08.005.

83. Grechkin, A. N., Brühlmann, F., Mukhtarova, L. S., Gogolev, Y. V. & Hamberg, M. (2006). Hydroperoxide lyases (CYP74C and CYP74B) catalyze the homolytic isomerization of fatty acid hydroperoxides into hemiacetals. *Biochimica et Biophysica Acta (BBA) - Molecular and Cell Biology of Lipids*, *1761*, 1419–1428. https://doi.org/10.1016/J.BBALIP.2006.09.002.

84. Tijet, N., Wäspi, U., Gaskin, D. J. H., Hunziker, P., Muller, B. L., Vulfson, E. N., Slusarenko, A., Brash, A. R. & Whitehead, I. M. (2000). Purification, molecular cloning, and expression of the gene encoding fatty acid 13-hydroperoxide lyase from guava fruit (*Psidium guajava*). *Lipids*, *35*, 709–720. https://doi.org/10.1007/s11745-000-0577-z.

85. Itoh, A. & Vick, B. A. (1999). The purification and characterization of fatty acid hydroperoxide lyase in sunflower. *Biochimica et Biophysica Acta - Molecular and Cell Biology of Lipids*, *1436*, 531–540. https://doi.org/10.1016/S0005-2760(98)00161-1.

86. Shibata, Y., Matsui, K., Kajiwara, T. & Hatanaka, A. (1995). Purification and properties of fatty acid hydroperoxide lyase from green bell pepper fruits. *Plant and Cell Physiology*, *36*, 147–156. https://doi.org/10.1093/OXFORDJOURNALS.PCP.A078731.

87. Shibata, Y., Matsui, K., Kajiwara, T. & Hatanaka, A. (1995). Fatty acid hydroperoxide lyase is a heme protein. *Biochemical and Biophysical Research Communications*, *207*, 438–443. https://doi.org/10.1006/bbrc.1995.1207.

88. Li, L., Chang, Z., Pan, Z., Fu, Z. Q. & Wang, X. (2008). Modes of heme binding and substrate access for cytochrome P450 CYP74A revealed by crystal structures of allene oxide synthase. *Proceedings of the National Academy of Sciences of the United States of America*, *105*, 13883–13888. https://doi.org/10.1073/pnas.0804099105.

89. Lee, D. S., Nioche, P., Hamberg, M. & Raman, C. S. (2008). Structural insights into the evolutionary paths of oxylipin biosynthetic enzymes. *Nature*, *455*, 363–368. https://doi.org/10.1038/nature07307.

90. Waterhouse, A., Bertoni, M., Bienert, S., Studer, G., Tauriello, G., Gumienny, R., Heer, F. T., De Beer, T. A. P., Rempfer, C., Bordoli, L., Lepore, R. & Schwede, T. (2018). SWISS-MODEL: homology modelling of protein structures and complexes. *Nucleic Acids Research*, *46*, W296–W303. https://doi.org/10.1093/NAR/GKY427.

91. Toporkova, Y. Y., Gogolev, Y. V., Mukhtarova, L. S. & Grechkin, A. N. (2008). Determinants governing the CYP74 catalysis: Conversion of allene oxide synthase into hydroperoxide lyase by site-directed mutagenesis. *FEBS Letters*, *582*, 3423–3428. https://doi.org/10.1016/j.febslet.2008.09.005.

92. Stumpe, M., Bode, J., Göbel, C., Wichard, T., Schaaf, A., Frank, W., Frank, M., Reski, R., Pohnert, G. & Feussner, I. (2006). Biosynthesis of C9-aldehydes in the moss *Physcomitrella patens*. *Biochimica et Biophysica Acta (BBA) - Molecular and Cell Biology of Lipids*, *1761*, 301–312. https://doi.org/10.1016/J.BBALIP.2006.03.008.

93. Toporkova, Y. Y., Askarova, E. K., Gorina, S. S., Mukhtarova, L. S. & Grechkin, A. N. (2022). Oxylipin biosynthesis in spikemoss *Selaginella moellendorffii*: Identification of allene oxide synthase (CYP74L2) and hydroperoxide lyase (CYP74L1). *Phytochemistry*, *195*, 113051. https://doi.org/10.1016/J.PHYTOCHEM.2021.113051.

94. Poltronieri, P., De Domenico, S., Bonsegna, S. & Santino, A. (2018). Oxylipins and green leaf volatiles: Application of enzymes from plant origin to produce flavors and antifungal aldehydes. In *Enzymes in Food Biotechnology: Production, Applications, and Future Prospects* (pp. 551–567). Elsevier. https://doi.org/10.1016/B978-0-12-813280-7.00032-3.

95. De Domenico, S., Tsesmetzis, N., Di Sansebastiano, G. Pietro, Hughes, R. K., Casey, R. & Santino, A. (2007). Subcellular localisation of *Medicago truncatula* 9/13-hydroperoxide lyase reveals a new localisation pattern and activation mechanism for CYP74C enzymes. *BMC Plant Biology*, *7*, 1–13. https://doi.org/10.1186/1471-2229-7-58.

96. Riley, J. C. M., Willemot, C. & Thompson, J. E. (1996). Lipoxygenase and hydroperoxide lyase activities in ripening tomato fruit. *Postharvest Biology and Technology*, *7*, 97–107. https://doi.org/10.1016/0925-5214(95)00032-1.

97. Noordermeer, M. A., van Dijken, A. J. H., Smeekens, S. C. M., Veldink, G. A. & Vliegenthart, J. F. G. (2000). Characterization of three cloned and expressed 13-hydroperoxide lyase isoenzymes from alfalfa with unusual N-terminal sequences and different enzyme kinetics. *European Journal of Biochemistry*, *267*, 2473–2482. https://doi.org/10.1046/j.1432-1327.2000.01283.x.

98. Bate, N. J., Sivasankar, S., Moxon, C., Riley, J. M. C., Thompson, J. E. & Rothstein, S. J. (1998). Molecular characterization of an *Arabidopsis* gene encoding hydroperoxide lyase, a Cytochrome P-450 that is wound inducible. *Plant Physiology*, *117*, 1393–1400. https://doi.org/10.1104/PP.117.4.1393.

99. Padilla, M. N., Hernández, M. L., Pérez, A. G., Sanz, C. & Martínez-Rivas, J. M. (2010). Isolation, expression, and characterization of a 13-hydroperoxide lyase gene from olive fruit related to the biosynthesis of the main virgin olive oil aroma compounds. *Journal of Agricultural and Food Chemistry*, *58*, 5649–5657. https://doi.org/10.1021/jf9045396.

100. Noordermeer, M. A., Veldink, G. A. & Vliegenthart, J. F. G. (1999). Alfalfa contains substantial 9-hydroperoxide lyase activity and a 3Z:2E-enal isomerase. *FEBS Letters*, *443*, 201–204. https://doi.org/10.1016/S0014-5793(98)01706-2.

101. Salas, J. J. & Sánchez, J. (1999). Hydroperoxide lyase from olive (*Olea europaea*) fruits. *Plant Science*, *143*, 19–26. https://doi.org/10.1016/S0168-9452(99)00027-8.

102. Gigot, C., Ongena, M., Fauconnier, M. L., Wathelet, J. P., du Jardin, P. & Thonart, P. (2010). The lipoxygenase metabolic pathway in plants: Potential for industrial production of natural green leaf volatiles. *Biotechnology, Agronomy, Society and Environment*, *14*, 451–460. Retrieved from https://popups.uliege.be/1780-4507/index.php?id=5669

103. Brühlmann, F., Bosijokovic, B., Ullmann, C., Auffray, P., Fourage, L. & Wahler, D. (2013). Directed evolution of a 13-hydroperoxide lyase (CYP74B) for improved process performance. *Journal of Biotechnology*, *163*, 339–345. https://doi.org/10.1016/J.JBIOTEC.2012.11.005.

104. Delcarte, J., Fauconnier, M. L., Jacques, P., Matsui, K., Thonart, P. & Marlier, M. (2003). Optimisation of expression and immobilized metal ion affinity chromatographic purification of recombinant (His)6-tagged cytochrome P450 hydroperoxide lyase in *Escherichia coli*. *Journal of Chromatography B: Analytical Technologies in the Biomedical and Life Sciences*, *786*, 229–236. https://doi.org/10.1016/S1570-0232(02)00815-2.

105. Jacopini, S., Mariani, M., de Caraffa, V. B.-B., Gambotti, C., Vincenti, S., Desjobert, J.-M., Muselli, A., Costa, J., Berti, L. & Maury, J. (2016). Olive recombinant hydroperoxide lyase, an efficient biocatalyst for synthesis of green leaf volatiles. *Applied Biochemistry and Biotechnology*, *179*, 671–683. https://doi.org/10.1007/s12010-016-2023-x.

106. Matsui, K., Miyahara, C., Wilkinson, J., Hiatt, B., Knauf, V. & Kajiwara, T. (2000). Fatty acid hydroperoxide lyase in tomato fruits: cloning and properties of a recombinant enzyme expressed in *Escherichia coli*. *Bioscience, Biotechnology, and Biochemistry*, *64*, 1189–1196. https://doi.org/10.1271/bbb.64.1189.

107. Koeduka, T., Stumpe, M., Kajiwara, T. & Feussner, I. (2003). Kinetics of barley FA hydroperoxide lyase are modulated by salts and detergents. *Lipids*, *38*, 1167–1172. https://doi.org/10.1007/s11745-003-1175-9.

108. Atwal, A. S., Bisakowski, B., Richard, S., Robert, N. & Lee, B. (2005). Cloning and secretion of tomato hydroperoxide lyase in *Pichia pastoris*. *Process Biochemistry*, *40*, 95–102. https://doi.org/10.1016/J.PROCBIO.2003.11.042.

109. Bourel, G., Nicaud, J. M., Nthangeni, B., Santiago-Gomez, P., Belin, J. M. & Husson, F. (2004). Fatty acid hydroperoxide lyase of green bell pepper: cloning in *Yarrowia lipolytica* and biogenesis of volatile aldehydes. *Enzyme and Microbial Technology*, *35*, 293–299. https://doi.org/10.1016/J.ENZMICTEC.2003.12.014.

110. Fukushige, H. & Hildebrand, D. F. (2005). Watermelon (*Citrullus lanatus*) hydroperoxide lyase greatly increases C 6 aldehyde formation in transgenic leaves. *Journal of Agricultural and Food Chemistry*, *53*, 2046–2051. https://doi.org/10.1021/jf048391e.

111. Mu, W., Xue, Q., Jiang, B. & Hua, Y. (2012). Molecular cloning, expression, and enzymatic characterization of *Solanum tuberosum* hydroperoxide lyase. *European Food Research and Technology*, *234*, 723–731. https://doi.org/10.1007/s00217-012-1685-z.

112. Jacopini, S., Vincenti, S., Mariani, M., Brunini-Bronzini de Caraffa, V., Gambotti, C., Desjobert, J. M., Muselli, A., Costa, J., Tomi, F., Berti, L. & Maury, J. (2017). Activation and stabilization of olive recombinant 13-hydroperoxide lyase using selected additives. *Applied Biochemistry and Biotechnology*, *182*, 1000–1013. https://doi.org/10.1007/s12010-016-2377-0.

113. Long, Z., Kong, X., Zhang, C. & Hua, Y. (2010). Stability of hydroperoxide lyase activity from *Amaranthus tricolor* (*Amaranthus mangostanus* L.) leaves: influence of selected additives. *Journal of the Science of Food and Agriculture*, *90*, 729–734. https://doi.org/10.1002/JSFA.3874.

114. Hughes, R. K., Belfield, E. J. & Casey, R. (2006). CYP74C3 and CYP74A1, plant cytochrome P450 enzymes whose activity is regulated by detergent micelle association, and proposed new rules for the classification of CYP74 enzymes. *Biochemical Society Transactions*, *34*, 1223–1227. https://doi.org/10.1042/BST0341223.

115. Matsui, K., Toyota, H., Kajiwara, T., Kakuno, T. & Hatanaka, A. (1991). Fatty acid hydroperoxide cleaving enzyme, hydroperoxide lyase, from tea leaves. *Phytochemistry*, *30*, 2109–2113. https://doi.org/10.1016/0031-9422(91)83596-D.

116. Guo, F. & Berglund, P. (2017). Transaminase biocatalysis: optimization and application. *Green Chemistry*, *19*, 333–360. https://doi.org/10.1039/C6GC02328B.

117. Mathew, S. & Yun, H. (2012). ω-Transaminases for the production of optically pure amines and unnatural amino acids. *ACS Catalysis*, *2(6)*, 993-1001. https://doi.org/10.1021/cs300116n.

118. Braunstein, A. E. & Kritzmann, M. G. (1937). Formation and breakdown of amino-acids by inter-molecular transfer of the amino group. *Nature 1937 140:3542*, 503–504. https://doi.org/10.1038/140503b0.

119. Rudat, J., Brucher, B. R. & Syldatk, C. (2012). Transaminases for the synthesis of enantiopure beta-amino acids. *AMB Express, 2,* 1-10. https://doi.org/10.1186/2191-0855-2-11.

120. Patil, M. D., Grogan, G., Bommarius, A. & Yun, H. (2018). Recent advances in ω-transaminase-mediated biocatalysis for the enantioselective synthesis of chiral amines. *Catalysts 2018, 8,* 254. https://doi.org/10.3390/CATAL8070254.

121. Höhne, M., Schätzle, S., Jochens, H., Robins, K. & Bornscheuer, U. T. (2010). Rational assignment of key motifs for function guides in silico enzyme identification. *Nature Chemical Biology 2010 6:11*, 807–813. https://doi.org/10.1038/nchembio.447.

122. Kelly, S. A., Pohle, S., Wharry, S., Mix, S., Allen, C. C. R., Moody, T. S. & Gilmore, B. F. (2018). Application of ω-transaminases in the pharmaceutical industry. *Chemical Reviews, 118, 1*, 349–367. https://doi.org/10.1021/acs.chemrev.7b00437.

123. Steffen-Munsberg, F., Vickers, C., Kohls, H., Land, H., Mallin, H., Nobili, A., Skalden, L., van den Bergh, T., Joosten, H. J., Berglund, P., Höhne, M. & Bornscheuer, U. T. (2015). Bioinformatic analysis of a PLP-dependent enzyme superfamily suitable for biocatalytic applications. *Biotechnology Advances*, *33*, 566–604. https://doi.org/10.1016/J.BIOTECHADV.2014.12.012.

124. Rausch, C., Lerchner, A., Schiefner, A. & Skerra, A. (2013). Crystal structure of the ω-aminotransferase from *Paracoccus denitrificans* and its phylogenetic relationship with other class III amino- transferases that have biotechnological potential. *Proteins: Structure, Function and Bioinformatics*, *81*, 774–787. https://doi.org/10.1002/prot.24233.

125. Humble, M. S., Cassimjee, K. E., Hãkansson, M., Kimbung, Y. R., Walse, B., Abedi, V., Federsel, H. J., Berglund, P. & Logan, D. T. (2012). Crystal structures of the *Chromobacterium violaceum* ω-transaminase reveal major structural rearrangements upon binding of coenzyme PLP. *The FEBS Journal*, *279*, 779–792. https://doi.org/10.1111/J.1742-4658.2012.08468.X.

126. Shin, J. S. & Kim, B. G. (2002). Exploring the active site of amine:pyruvate aminotransferase on the basis of the substrate structure-reactivity relationship: How the enzyme controls substrate specificity and stereoselectivity. *Journal of Organic Chemistry*, *67*, 2848–2853. https://doi.org/10.1021/jo016115i.

127. Iwasaki, A., Yamada, Y., Kizaki, N., Ikenaka, Y. & Hasegawa, J. (2006). Microbial synthesis of chiral amines by (R)-specific transamination with *Arthrobacter* sp. KNK168. *Applied Microbiology and Biotechnology*, *69*, 499–505. https://doi.org/10.1007/s00253-005-0002-1.

128. Łyskowski, A., Gruber, C., Steinkellner, G., Schü Rmann, M., Schwab, H., Gruber, K. & Steiner, K. (2014). Crystal structure of an (R)-selective ω-transaminase from *Aspergillus terreus*. *PLOS ONE*, *9*, e87350. https://doi.org/10.1371/JOURNAL.PONE.0087350.

129. Thomsen, M., Skalden, L., Palm, G. J., Höhne, M., Bornscheuer, U. T. & Hinrichs, W. (2014). Crystallographic characterization of the (R)-selective amine transaminase from *Aspergillus fumigatus*. *Acta Crystallographica Section D: Biological Crystallography*, *70*, 1086–1093. https://doi.org/10.1107/S1399004714001084.

130. Percudani, R. & Peracchi, A. (2009). The B6 database: A tool for the description and classification of vitamin B6-dependent enzymatic activities and of the corresponding protein families. *BMC Bioinformatics*, *10*, 273. https://doi.org/10.1186/1471-2105-10-273.

131. Grishin, N. V., Phillips, M. A. & Goldsmith, E. J. (1995). Modeling of the spatial structure of eukaryotic ornithine decarboxylases. *Protein Science*, *4*, 1291–1304. https://doi.org/10.1002/PRO.5560040705.

132. Slabu, I., Galman, J. L., Lloyd, R. C. & Turner, N. J. (2017). Discovery, engineering, and synthetic application of transaminase biocatalysts. *ACS Catalysis*, *7*, 8263–8284. https://doi.org/10.1021/acscatal.7b02686.

133. Meng, Q., Ramírez-Palacios, C., Wijma, H. J. & Janssen, D. B. (2022). Protein engineering of amine transaminases. *Frontiers in Catalysis*, *2*, 25. https://doi.org/10.3389/FCTLS.2022.1049179.

134. Malik, M. S., Park, E. S. & Shin, J. S. (2012). Features and technical applications of ω-transaminases. *Applied Microbiology and Biotechnology*, *94*, 1163–1171. https://doi.org/10.1007/s00253-012-4103-3.

135. Cassimjee, K. E., Humble, M. S., Miceli, V., Colomina, C. G. & Berglund, P. (2011). Active site quantification of an Ω-Transaminase by performing a half transamination reaction. *ACS Catalysis*, *1*, 1051–1055. https://doi.org/10.1021/cs200315h.

136. Voss, M., Das, D., Genz, M., Kumar, A., Kulkarni, N., Kustosz, J., Kumar, P., Bornscheuer, U. T. & Höhne, M. (2018). In silico based engineering approach to improve transaminases for the conversion of bulky substrates. *ACS Catalysis*, *8*, 11524–11533. https://doi.org/10.1021/acscatal.8b03900.

137. Steffen-Munsberg, F., Vickers, C., Thontowi, A., Schätzle, S., Meinhardt, T., Svedendahl Humble, M., Land, H., Berglund, P., Bornscheuer, U. T. & Höhne, M. (2013). Revealing the structural basis of promiscuous amine transaminase activity. *ChemCatChem*, *5*, 154–157. https://doi.org/10.1002/cctc.201200545.

138. Soda, K., Yoshimura, T. & Esaki, N. (2001). Stereospecificity for the hydrogen transfer of pyridoxal enzyme reactions. *The Chemical Record*, *1*, 373–384. https://doi.org/10.1002/TCR.1021.

139. Höhne, M. & Bornscheuer, U. T. (2009). Biocatalytic routes to optically active amines. *ChemCatChem*, *1*, 42–51. https://doi.org/10.1002/CCTC.200900110.

140. Fuchs, M., Farnberger, J. E. & Kroutil, W. (2015). The industrial age of biocatalytic transamination. *European Journal of Organic Chemistry*, *2015*, 6965–6982. https://doi.org/10.1002/EJOC.201500852.

141. Shin, J. S. & Kim, B. G. (1999). Asymmetric synthesis of chiral amines with ω-transaminase. *Biotechnology and Bioengineering*, *65*, 206–211. https://doi.org/10.1002/(SICI)1097-0290(19991020)65:2<206::AID-BIT11>3.0.CO;2-9.

142. Sattler, J. H., Fuchs, M., Tauber, K., Mutti, F. G., Faber, K., Pfeffer, J., Haas, T. & Kroutil, W. (2012). Redox self-sufficient biocatalyst network for the amination of primary alcohols. *Angewandte Chemie International Edition*, *51*, 9156–9159. https://doi.org/10.1002/ANIE.201204683.

143. Cato, L., Halmos, A. L. & Small, D. M. (2006). Measurement of lipoxygenase in Australian white wheat flour: the effect of lipoxygenase on the quality properties of white salted noodles. *Journal of the Science of Food and Agriculture*, *86*, 1670–1678. https://doi.org/10.1002/JSFA.2539.

144. Frazier, P. J., Brimblecombe, F. A., Daniels, N. W. R. & Russell Eggitt, P. W. (1977). The effect of lipoxygenase action on the mechanical development of doughs from fat-extracted and reconstituted wheat flours. *Journal of the Science of Food and Agriculture*, *28*, 247–254. https://doi.org/10.1002/JSFA.2740280305.

145. Salmon, S., Shi, C. & Liu, J. (2006). Treatment of fabrics, fibers, or yarns. US Patent US20060042020A1.

146. de Roos, A. L., Dijk, A. & Folkertsma, B. (2006). Bleaching of dairy products. US Patent US 20060127533 A1.

147. Wu, Z., Robinson, D. S., Hughes, R. K., Casey, R., Hardy, D. & West, S. I. (1999). Co-oxidation of β-carotene catalyzed by soybean and recombinant pea lipoxygenases. *Journal of Agricultural and Food Chemistry*, *47*, 4899–4906. https://doi.org/10.1021/jf9901690.

148. Heshof, R., de Graaff, L. H., Villaverde, J. J., Silvestre, A. J. D., Haarmann, T., Dalsgaard, T. K. & Buchert, J. (2016). Industrial potential of lipoxygenases. *Critical Reviews in Biotechnology*, *36*, 665–674. https://doi.org/10.3109/07388551.2015.1004520.

149. Faubion, J. & Hoseney, R. (1984). Lipoxygenase: Its biochemistry and role in breadmaking. *Cereal Chemistry*, *58*, 175–180.

150. Permyakova, M. D. & Trufanov, V. A. (2011). Effect of soybean lipoxygenase on baking properties of wheat flour. *Applied Biochemistry and Microbiology 2011 47:3*, *47*, 315–320. https://doi.org/10.1134/S0003683811030100.

151. Huang, F. C. & Schwab, W. (2011). Cloning and characterization of a 9-lipoxygenase gene induced by pathogen attack from *Nicotiana benthamiana* for biotechnological application. *BMC Biotechnology*, *11*, 1–15. https://doi.org/10.1186/1472-6750-11-30.

152. Fukushige, H. & Hildebrand, D. F. (2005). A simple and efficient system for green note compound biogenesis by use of certain lipoxygenase and hydroperoxide lyase sources. *Journal of Agricultural and Food Chemistry*, *53*, 6877–6882. https://doi.org/10.1021/jf047954j.

153. Buchhaupt, M., Guder, J. C., Etschmann, M. M. W. & Schrader, J. (2012). Synthesis of green note aroma compounds by biotransformation of fatty acids using yeast cells coexpressing lipoxygenase and hydroperoxide lyase. *Applied Microbiology and Biotechnology*, *93*, 159–168. https://doi.org/10.1007/s00253-011-3482-1.

154. Vincenti, S., Mariani, M., Alberti, J.-C., Jacopini, S., Brunini-Bronzini de Caraffa, V., Berti, L. & Maury, J. (2019). Biocatalytic synthesis of natural green leaf volatiles using the lipoxygenase metabolic pathway. *Catalysts*, *9*, 873. https://doi.org/10.3390/catal9100873.

155. Hubert, J., Münzbergová, Z., Nesvorná, M., Poltronieri, P. & Santino, A. (2008). Acaricidal effects of natural six-carbon and nine-carbon aldehydes on stored-product mites. *Experimental and Applied Acarology*, *44*, 315–321. https://doi.org/10.1007/s10493-008-9146-x.

156. Jabłońska-Trypuć, A., Pankiewicz, W. & Czerpak, R. (2016). Traumatic acid reduces oxidative stress and enhances collagen biosynthesis in cultured human skin fibroblasts. *Lipids*, *51*, 1021–1035. https://doi.org/10.1007/s11745-016-4174-5.

157. Jabłońska-Trypuć, A., Krętowski, R., Wołejko, E., Wydro, U. & Butarewicz, A. (2019). Traumatic acid toxicity mechanisms in human breast cancer MCF-7 cells. *Regulatory Toxicology and Pharmacology*, *106*, 137–146. https://doi.org/10.1016/j.yrtph.2019.04.023.

158. Adams, J. P., Brown, M. J. B., Diaz-Rodriguez, A., Lloyd, R. C. & Roiban, G. D. (2019). Biocatalysis: a pharma perspective. *Advanced Synthesis & Catalysis*, *361*, 2421–2432. https://doi.org/10.1002/ADSC.201900424.

159. Ghislieri, D. & Turner, N. J. (2014). Biocatalytic approaches to the synthesis of enantiomerically pure chiral amines. *Topics in Catalysis*, *57*, 284–300. https://doi.org/10.1007/s11244-013-0184-1.

160. Savile, C. K., Janey, J. M., Mundorff, E. C., Moore, J. C., Tam, S., Jarvis, W. R., Colbeck, J. C., Krebber, A., Fleitz, F. J., Brands, J., Devine, P. N., Huisman, G. W. & Hughes, G. J. (2010). Biocatalytic asymmetric synthesis of chiral amines from ketones applied to sitagliptin manufacture. *Science*, *329*, 305–309. https://doi.org/10.1126/science.1188934.

161. Fuchs, M., Koszelewski, D., Tauber, K., Kroutil, W. & Faber, K. (2010). Chemoenzymatic asymmetric total synthesis of (S)-Rivastigmine using ω-transaminases. *Chemical Communications*, *46*, 5500–5502. https://doi.org/10.1039/C0CC00585A.

162. Koszelewski, D., Pressnitz, D., Clay, D. & Kroutil, W. (2009). Deracemization of mexiletine biocatalyzed by ω-transaminases. *Organic Letters*, *11*, 4810–4812. https://doi.org/10.1021/ol901834x.

163. Bea, H. S., Park, H. J., Lee, S. H. & Yun, H. (2011). Kinetic resolution of aromatic β-amino acids by ω-transaminase. *Chemical Communications*, *47*, 5894–5896. https://doi.org/10.1039/c1cc11528f.

164. Sung, S., Jeon, H., Sarak, S., Ahsan, M. M., Patil, M. D., Kroutil, W., Kim, B. G. & Yun, H. (2018). Parallel anti-sense two-step cascade for alcohol amination leading to ω-amino fatty acids and α,ω-diamines. *Green Chemistry*, *20*, 4591–4595. https://doi.org/10.1039/c8gc02122h.

165. Ahsan, M. M., Jeon, H., P. Nadarajan, S., Chung, T., Yoo, H.-W., Kim, B.-G., Patil, M. D. & Yun, H. (2018). Biosynthesis of the nylon 12 monomer, ω-aminododecanoic acid with novel CYP153A, AlkJ, and ω-TA enzymes. *Biotechnology Journal*, *13*, 1700562. https://doi.org/10.1002/biot.201700562.

166. Sattler, J. H., Fuchs, M., Mutti, F. G., Grischek, B., Engel, P., Pfeffer, J., Woodley, J. M. & Kroutil, W. (2014). Introducing an in situ capping strategy in systems biocatalysis to access 6-aminohexanoic acid. *Angewandte Chemie*, *126*, 14377–14381. https://doi.org/10.1002/ange.201409227.

167. Gala Marti, V., Coenen, A. & Schörken, U. (2021). Synthesis of linoleic acid 13-hydroperoxides from safflower oil utilizing lipoxygenase in a coupled enzyme system with in-situ oxygen generation. *Catalysts*, *11*, 1119. https://doi.org/10.3390/catal11091119.

168. Coscolín, C., Katzke, N., García-Moyano, A., Navarro-Fernández, J., Almendral, D., Martínez-Martínez, M., Bollinger, A., Bargiela, R., Gertler, C., Chernikova, T. N., Rojo, D., Barbas, C., Tran, H., Golyshina, O. V., Koch, R., Yakimov, M. M., Bjerga, G. E. K., Golyshin, P. N., Jaeger, K.-E. & Ferrer, M. (2019). Bioprospecting reveals class III ω-transaminases converting bulky ketones and environmentally relevant polyamines. *Applied and Environmental Microbiology*, *85,* e02404-18. https://doi.org/10.1128/AEM.02404-18.

169. Berlyn, M. K. (1998). Linkage map of *Escherichia coli* K-12, edition 10: the traditional map. *Microbiology and molecular biology reviews : MMBR*, *62*, 814–984.

170. Studier, F. W. & Moffatt, B. A. (1986). Use of bacteriophage T7 RNA polymerase to direct selective high-level expression of cloned genes. *Journal of Molecular Biology*, *189*, 113–130. https://doi.org/10.1016/0022-2836(86)90385-2.

171. Miroux, B. & Walker, J. E. (1996). Over-production of proteins in *Escherichia coli*: mutant hosts that allow synthesis of some membrane proteins and globular proteins at high levels. *Journal of Molecular Biology*, *260*, 289–298. Retrieved from http://citeseerx.ist.psu.edu/viewdoc/download?doi=10.1.1.598.4870&rep=rep1&type=pdf.

172. Wagner, S., Klepsch, M. M., Schlegel, S., Appel, A., Draheim, R., Tarry, M., Högbom, M., Van Wijk, K. J., Slotboom, D. J., Persson, J. O. & De Gier, J. W. (2008). Tuning *Escherichia coli* for membrane protein overexpression. *Proceedings of the National Academy of Sciences of the United States of America*, *105*, 14371–14376. https://doi.org/10.1073/pnas.0804090105.

173. Bertani, G. (1951). Studies on lysogenesis. I. The mode of phage liberation by lysogenic *Escherichia coli*. *Journal of bacteriology*, *62*, 293–300. Retrieved from http://www.ncbi.nlm.nih.gov/pubmed/14888646.

174. Studier, F. W. (2005). Protein production by auto-induction in high density shaking cultures. *Protein expression and purification*, *41*, 207–234. https://doi.org/10.1016/j.pep.2005.01.016.

175. Coenen, A., Gala Marti, V., Müller, K., Sheremetiev, M., Finamore, L. & Schörken, U. (2022). Synthesis of polymer precursor 12-oxododecenoic acid utilizing recombinant papaya hydroperoxide lyase in an enzyme cascade. *Applied Biochemistry and Biotechnology*, *194*, 6194–6212. https://doi.org/10.1007/s12010-022-04095-0.

176. National Center for Biotechnology Information (NCBI)[Internet]. Bethesda (MD): National Library of Medicine (US), National Center for Biotechnology Information; 1988 – cited 2023 Jan 11. Retrieved from https://www.ncbi.nlm.nih.gov/.

177. Altschul, S. F., Gish, W., Miller, W., Myers, E. W. & Lipman, D. J. (1990). Basic local alignment search tool. *Journal of Molecular Biology*, *215*, 403–410. https://doi.org/10.1016/S0022-2836(05)80360-2.

178. Sievers, F., Wilm, A., Dineen, D., Gibson, T. J., Karplus, K., Li, W., Lopez, R., McWilliam, H., Remmert, M., Söding, J., Thompson, J. D. & Higgins, D. G. (2011). Fast, scalable generation of high-quality protein multiple sequence alignments using Clustal Omega. *Molecular Systems Biology*, *7*, 539. https://doi.org/10.1038/MSB.2011.75.

179. Thompson, J., Gibson, T. J., Plewniak, F., Jeanmougin, F. & Higgins, D. G. (1997). The CLUSTAL_X windows interface: flexible strategies for multiple sequence alignment aided by quality analysis tools. *Nucleic Acids Research*, *25*, 4876–4882. https://doi.org/10.1093/nar/25.24.4876.

180. Perrière, G. & Gouy, M. (1996). WWW-query: An on-line retrieval system for biological sequence banks. *Biochimie*, *78*, 364–369. https://doi.org/10.1016/0300-9084(96)84768-7.

181. Berman, H. M., Westbrook, J., Feng, Z., Gilliland, G., Bhat, T. N., Weissig, H., Shindyalov, I. N. & Bourne, P. E. (2000). The Protein Data Bank. *Nucleic Acids Research*, *28*, 235–242. https://doi.org/10.1093/NAR/28.1.235.

182. Kuwayama, H., Obara, S., Morio, T., Katoh, M., Urushihara, H. & Tanaka, Y. (2002). PCR-mediated generation of a gene disruption construct without the use of DNA ligase and plasmid vectors. *Nucleic Acids Research*, *30*, E2. https://doi.org/10.1093/nar/30.2.e2.

183. Hanahan, D. (1983). Studies on transformation of *Escherichia coli* with plasmids. *Journal of Molecular Biology*, *166*, 557–580. https://doi.org/10.1016/S0022-2836(83)80284-8.

184. Davis, M. W. & Jorgensen, E. M. (2022). ApE, A plasmid editor: a freely available DNA manipulation and visualization program. *Frontiers in Bioinformatics*, *2,* 818619. https://doi.org/10.3389/FBINF.2022.818619.

185. Bradford, M. M. (1976). A rapid and sensitive method for the quantitation of microgram quantities of protein utilizing the principle of protein-dye binding. *Analytical Biochemistry*, *72*, 248–254. https://doi.org/10.1016/0003-2697(76)90527-3.

186. Laemmli, U. K. (1970). Cleavage of structural proteins during the assembly of the head of bacteriophage T4. *Nature*, *227*, 680–685. https://doi.org/10.1038/227680a0.

187. Davis, G. D., Elisee, C., Mewham, D. M. & Harrison, R. G. (1999). New fusion protein systems designed to give soluble expression in *Escherichia coli*. *Biotechnology and Bioengineering*, *65*, 382–388. https://doi.org/10.1002/(SICI)1097-0290(19991120)65:4<382::AID-BIT2>3.0.CO;2-I.

188. Nallamsetty, S. & Waugh, D. S. (2006). Solubility-enhancing proteins MBP and NusA play a passive role in the folding of their fusion partners. *Protein Expression and Purification*, *45*, 175–182. https://doi.org/10.1016/j.pep.2005.06.012.

189. De Marco, V., Stier, G., Blandin, S. & De Marco, A. (2004). The solubility and stability of recombinant proteins are increased by their fusion to NusA. *Biochemical and Biophysical Research Communications*, *322*, 766–771. https://doi.org/10.1016/j.bbrc.2004.07.189.

190. Coenen, A., Ferrer, M., Jaeger, K.-E. & Schörken, U. (2023). Synthesis of 12-aminododecenoic acid by coupling transaminase to oxylipin pathway enzymes. *Applied Microbiology and Biotechnology*, Manuscript accepted.

191. Behr, A. & Gomes, J. P. (2010). The refinement of renewable resources: New important derivatives of fatty acids and glycerol. *European Journal of Lipid Science and Technology*, *112*, 31–50. https://doi.org/10.1002/EJLT.200900091.

192. Knaut, J. & Richtler, H. J. (1985). Trends in industrial uses of palm and lauric oils. *Journal of the American Oil Chemists' Society*, *62*, 317–327. https://doi.org/10.1007/BF02541398.

193. Pryde, E. H. (1979). Unsaturated Polyamides. *Journal of Macromolecular Science, Part C*, *17*, 1–35. https://doi.org/10.1080/00222357908080903.

194. Radzik, P., Leszczyńska, A. & Pielichowski, K. (2020, January 1). Modern biopolyamide-based materials: synthesis and modification. *Polymer Bulletin*. Springer. https://doi.org/10.1007/s00289-019-02718-x.

195. Toogood, H. S. & Scrutton, N. S. (2018). Discovery, characterization, engineering, and applications of ene-reductases for industrial biocatalysis. *ACS Catalysis*, *8*, 3532–3549. https://doi.org/10.1021/acscatal.8b00624.

196. Elshof, M. B. W., Janssen, M., Veldink, G. A. & Vliegenthart, J. F. G. (1996). Biocatalytic large-scale production of 13(S)-hydroperoxy-9(Z), 11(E) octadecadienoic acid from hydrolysed safflower oil by a crude soybean-flour extract as lipoxygenase source. *Recueil des Travaux Chimiques des Pays-Bas*, *115*, 499–504. https://doi.org/10.1002/RECL.19961151109.

197. Baysal, T. & Demirdöven, A. (2007). Lipoxygenase in fruits and vegetables: A review. *Enzyme and Microbial Technology*, *40*, 491–496. https://doi.org/10.1016/J.ENZMICTEC.2006.11.025.

198. Shirano, Y. & Shibata, D. (1990). Low temperature cultivation of *Escherichia coli* carrying a rice lipoxygenase L-2 cDNA produces a soluble and active enzyme at a high level. *FEBS Letters*, *271*, 128–130. https://doi.org/10.1016/0014-5793(90)80388-Y.

199. Palmieri-Thiers, C., Canaan, S., Brunini, V., Lorenzi, V., Tomi, F., Desseyn, J. L., Garscha, U., Oliw, E. H., Berti, L. & Maury, J. (2009). A lipoxygenase with dual positional specificity is expressed in olives (*Olea europaea* L.) during ripening. *Biochimica et Biophysica Acta (BBA) - Molecular and Cell Biology of Lipids*, *1791*, 339–346. https://doi.org/10.1016/J.BBALIP.2009.02.012.

200. Neidhardt, F. C., VanBogelen, R. A. & Vaughn, V. (1984). The genetics and regulation of heat-shock proteins. *Annual review of genetics*, *18*, 295–329. https://doi.org/10.1146/annurev.ge.18.120184.001455.

201. Veronico, P., Giannino, D., Melillo, M. T., Leone, A., Reyes, A., Kennedy, M. W. & Bleve-Zacheo, T. (2006). A novel lipoxygenase in pea roots. Its function in wounding and biotic stress. *Plant Physiology*, *141*, 1045–1055. https://doi.org/10.1104/PP.106.081679.

202. Zhang, C., Tao, T., Ying, Q., Zhang, D., Lu, F., Bie, X. & Lu, Z. (2012). Extracellular production of lipoxygenase from *Anabaena* sp. PCC 7120 in *Bacillus subtilis* and its effect on wheat protein. *Applied Microbiology and Biotechnology*, *94*, 949–958. https://doi.org/10.1007/s00253-012-3895-5.

203. Hu, T., Qv, X., Hu, Z., Chen, G. & Chen, Z. (2011). Expression, molecular characterization and detection of lipoxygenase activity of tomloxD from tomato. *African Journal of Biotechnology*, *10*, 490–498. https://doi.org/10.5897/AJB10.1386.

204. Knust, B. & von Wettstein, D. (1992). Expression and secretion of pea-seed lipoxygenase isoenzymes in *Saccharomyces cerevisiae*. *Applied Microbiology and Biotechnology 1992 37:3*, *37*, 342–351. https://doi.org/10.1007/BF00210990.

205. Rozkov, A. & Enfors, S. O. (2004). Analysis and control of proteolysis of recombinant proteins in *Escherichia coli*. In: Physiological stress responses in bioprocesses. *Advances in biochemical engineering/biotechnology 89,* 163–195. Springer, Berlin, Heidelberg. https://doi.org/10.1007/b95567.

206. Wennman, A. & Oliw, E. H. (2013). Secretion of two novel enzymes, manganese 9S-lipoxygenase and epoxy alcohol synthase, by the rice pathogen *Magnaporthe salvinii*. *Journal of lipid research*, *54*, 762–775. https://doi.org/10.1194/JLR.M033787.

207. Gigot, C., Ongena, M., Fauconnier, M. L., Muhovski, Y., Wathelet, J. P., Du Jardin, P. & Thonart, P. (2012). Optimization and scaling up of a biotechnological synthesis of natural green leaf volatiles using *Beta vulgaris* hydroperoxide lyase. *Process Biochemistry*, *47*, 2547–2551. https://doi.org/10.1016/j.procbio.2012.07.018.

208. Otte, K. B., Kirtz, M., Nestl, B. M. & Hauer, B. (2013). Synthesis of 9-oxononanoic acid, a precursor for biopolymers. *ChemSusChem*, *6*, 2149–2156. https://doi.org/10.1002/cssc.201300183.

209. Deng, W. W., Wu, Y. L., Li, Y. Y., Tan, Z. & Wei, C. L. (2016). Molecular cloning and characterization of hydroperoxide lyase gene in the leaves of tea plant (*Camellia sinensis*). *Journal of Agricultural and Food Chemistry*, *64*, 1770–1776. https://doi.org/10.1021/acs.jafc.5b05748.

210. Santiago-Gómez, M. P., Kermasha, S., Nicaud, J. M., Belin, J. M. & Husson, F. (2010). Predicted secondary structure of hydroperoxide lyase from green bell pepper cloned in the yeast *Yarrowia lipolytica*. *Journal of Molecular Catalysis B: Enzymatic*, *65*, 63–67. https://doi.org/10.1016/j.molcatb.2010.01.009.

211. Schlegel, S., Löfblom, J., Lee, C., Hjelm, A., Klepsch, M., Strous, M., Drew, D., Slotboom, D. J. & De Gier, J. W. (2012). Optimizing membrane protein overexpression in the *Escherichia coli* strain Lemo21(DE3). *Journal of Molecular Biology*, *423*, 648–659. https://doi.org/10.1016/J.JMB.2012.07.019.

212. Hughes, R. K., Belfield, E. J., Muthusamay, M., Khan, A., Rowe, A., Harding, S. E., Fairhurst, S. A., Bornemann, S., Ashton, R., Thorneley, R. N. F. & Casey, R. (2006). Characterization of *Medicago truncatula* (barrel medic) hydroperoxide lyase (CYP74C3), a water-soluble detergent-free cytochrome P450 monomer whose biological activity is defined by monomer–micelle association. *Biochemical Journal*, *395*, 641–652. https://doi.org/10.1042/BJ20051667.

213. Akacha, N. B., Karboune, S., Gargouri, M. & Kermasha, S. (2010). Activation and stabilization of the hydroperoxide lyase enzymatic extract from mint leaves (*Mentha spicata*) using selected chemical additives. *Applied Biochemistry and Biotechnology*, *160*, 901–911. https://doi.org/10.1007/s12010-009-8625-9.

214. Zhu, B. Q., Xu, X. Q., Wu, Y. W., Duan, C. Q. & Pan, Q. H. (2012). Isolation and characterization of two hydroperoxide lyase genes from grape berries HPL isogenes in *Vitis vinifera* grapes. *Molecular Biology Reports*, *39*, 7443–7455. https://doi.org/10.1007/s11033-012-1577-0.

215. Olias, J. M., Rios, J., Vaile, M., Zamora, R., Sanz, L. C. & Axelrod, B. (1990). Fatty acid hydroperoxide lyase in germinating soybean seedlings. *Journal of Agricultural and Food Chemistry*, *38*, 624–630. https://doi.org/10.1021/jf00093a009.

216. Fauconnier, M. L., Perez, A. G., Sanz, C. & Marlier, M. (1997). Purification and characterization of tomato leaf (*Lycopersicon esculentum* Mill.) hydroperoxide lyase. *Journal of Agricultural and Food Chemistry*, *45*, 4232–4236. https://doi.org/10.1021/jf9701042.

217. Ahsan, M. M., Patil, M. D., Jeon, H., Sung, S., Chung, T. & Yun, H. (2018). Biosynthesis of nylon 12 monomer, ω-aminododecanoic acid using artificial self-sufficient P450, AlkJ and ω-TA. *Catalysts 2018, Vol. 8, Page 400*, *8*, 400. https://doi.org/10.3390/CATAL8090400.

218. Shin, J. S., Yun, H., Jang, J. W., Park, I. & Kim, B. G. (2003). Purification, characterization, and molecular cloning of a novel amine:pyruvate transaminase from *Vibrio fluvialis* JS17. *Applied Microbiology and Biotechnology*, *61*, 463–471. https://doi.org/10.1007/s00253-003-1250-6.

219. Höhne, M., Kühl, S., Robins, K. & Bornscheuer, U. T. (2008). Efficient asymmetric synthesis of chiral amines by combining transaminase and pyruvate decarboxylase. *ChemBioChem*, *9*, 363–365. https://doi.org/10.1002/CBIC.200700601.

220. Song, J. W., Seo, J. H., Oh, D. K., Bornscheuer, U. T. & Park, J. B. (2020). Design and engineering of whole-cell biocatalytic cascades for the valorization of fatty acids. *Catalysis Science & Technology*, *10*, 46–64. https://doi.org/10.1039/C9CY01802F.

221. Gargouri, M. & Legoy, M. D. (1997). Bienzymatic reaction for hydroperoxide production in a multiphasic system. *Enzyme and Microbial Technology*, *21*, 79–84. https://doi.org/10.1016/S0141-0229(96)00229-3.

222. Wang, J., Li, K., He, Y., Liu, X., Wang, P., Xu, L., Yan, J. & Yan, Y. (2021). Bi-enzyme directed self-assembled system toward biomimetic synthesis of fatty acid hydroperoxides like soybean. *Composites Part B: Engineering*, *222*, 109091. https://doi.org/10.1016/J.COMPOSITESB.2021.109091.

223. Małajowicz, J. & Kozłowska, M. (2021). Factors affecting the yield in formation of fat-derived fragrance compounds by *Yarrowia lipolytica* yeast. *Applied Sciences 2021, Vol. 11, Page 9843*, *11*, 9843. https://doi.org/10.3390/APP11219843.

224. Otte, K. B., Kittelberger, J., Kirtz, M., Nestl, B. M. & Hauer, B. (2014). Whole-cell one-pot biosynthesis of azelaic acid. *ChemCatChem*, *6*, 1003–1009. https://doi.org/10.1002/cctc.201300787.

225. Nicaud, J. M. (2012). *Yarrowia lipolytica*. *Yeast*, *29*, 409–418. https://doi.org/10.1002/YEA.2921.

6. Appendix

>LOX-1

MHHHHHHFSAGHKIKGTVVLMPKNELEVNPDGSAVDNLNAFLGRSVSLQLISATKADAHGKGKVGKDTFLEGINT
SLPTLGAGESAFNIHFEWDGSMGIPGAFYIKNYMQVEFFLKSLTLEAISNQGTIRFVCNSWVYNTKLYKSVRIFFAN
HTYVPSETPAPLVSYREEELKSLRGNGTGERKEYDRIYDYDVYNDLGNPDKSEKLARPVLGGSSTFPYPRRGRTGRG
PTVTDPNTEKQGEVFYVPRDENLGHLKSKDALEIGTKSLSQIVQPAFESAFDLKSTPIEFHSFQDVHDLYEGGIKLPR
DVISTIIPLPVIKELYRTDGQHILKFPQPHVVQVSQSAWMTDEEFAREMIAGVNPCVIRGLEEFPPKSNLDPAIYGDQ
SSKITADSLDLDGYTMDEALGSRRLFMLDYHDIFMPYVRQINQLNSAKTYATRTILFLREDGTLKPVAIELSLPHSA
GDLSAAVSQVVLPAKEGVESTIWLLAKAYVIVNDSCYHQLMSHWLNTHAAMEPFVIATHRHLSVLHPIYKLLTPHY
RNNMNINALARQSLINANGIIETTFLPSKYSVEMSSAVYKNWVFTDQALPADLIKRGVAIKDPSTPHGVRLLIEDYP
YAADGLEIWAAIKTWVQEYVPLYYARDDDVKNDSELQHWWKEAVEKGHGDLKDKPWWPKLQTLEDLVEVCLIII
WIASALHAAVNFGQYPYGGLIMNRPTASRRLLPEKGTPEYEEMINNHEKAYLRTITSKLPTLISLSVIEILSTHASDE
VYLGQRDNPHWTSDSKALQAFQKFGNKLKEIEEKLVRRNNDPSLQGNRLGPVQLPYTLLYPSSEEGLTFRGIPNSIS
I*

>*lox-1* codon-optimized

CATATGCATCATCATCATCACCATTTTAGTGCAGGTCATAAAATTAAGGGTACAGTGGTGCTGATGCCGAAAAAT
GAACTGGAAGTTAATCCGGATGGTAGTGCCGTTGATAATCTGAATGCATTTCTGGGCCGTAGTGTGAGCCTGCAG
CTGATTAGTGCCACCAAAGCCGATGCCCATGGTAAAGGCAAAGTTGGCAAAGATACCTTTCTGGAAGGCATTAAT
ACCAGCCTGCCGACCCTGGGTGCCGGTGAAAGTGCCTTTAATATTCATTTTGAATGGGATGGTAGCATGGGTATT
CCGGGTGCCTTTTATATTAAGAATTATATGCAGGTGGAGTTCTTTCTGAAAAGCCTGACCCTGGAAGCCATTAGC
AATCAGGGTACAATTCGCTTTGTGTGTAATAGTTGGGTGTATAATACCAAACTGTATAAAAGCGTTCGCATTTTC
TTTGCCAATCATACCTATGTTCCGAGTGAAACCCCGGCCCCGCTGGTTAGTTATCGCGAAGAAGAACTGAAAAGC
TTACGCGGTAATGGCACCGGCGAACGTAAAGAATATGATCGCATCTATGATTATGACGTTTATAATGATCTGGGT
AATCCGGATAAAAGCGAAAAACTGGCCCGCCCGGTGCTGGGTGGTAGTAGCACCTTTCCGTATCCGCGCCGCGGCC
GTACCGGTAGAGGTCCTACCGTGACCGATCCGAATACCGAAAAACAGGGCGAAGTTTTCTATGTTCCGCGCGATG
AAAATCTGGGCCATCTGAAAAGTAAAGATGCACTGGAAATTGGTACAAAAAGTCTGAGCCAGATTGTTCAGCCGG
CCTTTGAAAGTGCCTTCGATCTGAAAAGTACCCCGATTGAATTTCATAGCTTTCAGGATGTTCATGATCTGTATG
AAGGCGGTATTAAGCTGCCGCGCGATGTGATTAGCACCATTATTCCGCTGCCGGTTATTAAGGAACTGTATCGCA
CCGATGGTCAGCATATTCTGAAATTTCCGCAGCCGCATGTTGTTCAGGTGAGCCAGAGCGCCTGGATGACCGATG
AAGAATTTGCCCGCGAAATGATTGCCGGTGTTAATCCGTGCGTGATTCGCGGTCTGGAAGAATTTCCGCCGAAAA
GCAATCTGGACCCTGCAATCTATGGCGATCAGAGCAGTAAAATTACCGCAGATAGTCTGGATCTGGATGGTTATA
CCATGGATGAAGCCCTGGGTAGCCGCCGCCTGTTTATGCTGGATTATCATGATATTTTCATGCCGTATGTGCGTCA
GATTAATCAGCTGAATAGTGCAAAAACCTATGCCACCCGCACCATTCTGTTTCTGCGTGAAGATGGCACCCTGAA
ACCGGTTGCCATTGAACTGAGCCTGCCGCATAGCGCAGGTGACCTGAGTGCAGCCGTGAGCCAGGTTGTGCTGCCG
GCAAAAGAAGGTGTTGAAAGTACCATTTGGCTGCTGGCAAAAGCCTATGTTATTGTGAATGATAGCTGCTATCAT
CAGCTGATGAGCCATTGGCTGAATACCCATGCCGCCATGGAACCGTTTGTTATTGCAACCCATCGCCATCTGAGTG
TGCTGCATCCGATCTATAAACTGCTGACCCCGCATTATCGCAATAATATGAATATTAACGCCCTGGCCCGTCAGAG
TTTAATTAATGCCAATGGTATTATCGAGACCACCTTTCTGCCGAGCAAATATAGCGTTGAAATGAGCAGCGCCGT
TTATAAAAATTGGGTTTTTACCGATCAGGCACTGCCGGCAGATCTGATTAAGCGTGGCGTTGCAATTAAGGACCC
TAGTACCCCGCATGGCGTGCGTCTGCTGATTGAAGATTATCCGTATGCCGCCGATGGTCTGGAAATTTGGGCCGCC
ATTAAGACCTGGGTTCAGGAATATGTGCCGCTGTATTATGCACGCGATGATGATGTTAAAAATGATAGTGAACTG
CAGCATTGGTGGAAAGAAGCCGTGGAAAAAGGTCATGGTGACCTGAAAGATAAACCGTGGTGGCCGAAACTGCAG
ACCCTGGAAGATCTGGTGGAAGTTTGTCTGATTATTATTTGGATTGCAAGCGCACTGCATGCAGCCGTGAATTTT
GGTCAGTATCCGTATGGTGGCCTGATTATGAATCGCCCGACCGCCAGTCGCCGCCTGCTGCCTGAAAAAGGCACCC
CGGAATATGAAGAAATGATTAATAATCACGAGAAGGCATATCTGCGCACCATTACCAGCAAACTGCCGACCTTAA
TTAGTCTGAGCGTGATTGAAATTCTGAGCACCCATGCCAGCGATGAAGTGTATCTGGGCCAGCGTGATAATCCGC
ATTGGACCAGCGATAGTAAAGCACTGCAGGCATTTCAGAAATTTGGTAATAAGCTGAAAGAGATTGAGGAAAAA
CTGGTTCGCCGTAATAATGATCCGAGCCTGCAGGGTAATCGTCTGGGCCCGGTTCAGCTGCCGTATACCCTGCTGT
ATCCGAGCAGTGAAGAAGGCTTAACCTTTCGTGGCATTCCGAATAGTATTAGTATTTAAGGATCC

Fig. A 1 LOX-1 protein sequence and codon-optimized *lox-1* gene sequence with His6-tag marked in grey and restriction sites underlined.

```
HPL_CP      MMMKLMNISPTMSSPSSPPSSSPLASNSISTPPSSALPLRTIPGSYGWPLLGPLSDRLDY      60
AOS_AT      -----------------------------------LPIRNIPGNYGLPIVGPIKDRWDY      24
                                               **:*.***.** *::**:.** **

HPL_CP      FWFQGPETFFRKRMEKNKSSVFRTNVPPSFPFFLDVNPNVIAVLDVKSFSHLFDLEIVEK      120
AOS_AT      FYDQGAEEFFKSRIRKYNSTVYRVNMPPGA--FIAENPQVVALLDGKSFPVLFDVDKVEK      82
             *: ** * **:.*:.* :*:*:*.*:**.   *:  **:*:*:** ***  ***:: ***

HPL_CP      KDVLVGSFVPSTRFTGDVRVGVYLDTAEPKHSEVKNLTMELLQRGSKVWQSELLSNLDKM      180
AOS_AT      KDLFTGTYMPSTELTGGYRILSYLDPSEPKHEKLKNLLFFLLKSSRNRIFPEFQATYSEL      142
             **::.*:::***.:**. *:  *** :****.::*** : **: . :    *: :. .::

HPL_CP      WDMVEATVAEKGKATYLGPLQQCIFNFIMKALAGIDPAVSPQIANSGYIMLDRWLFLQLL      240
AOS_AT      FDSLEKELSLKGKADFGGSSDGTAFNFLARAFYGTNPADTKLKADAPG-LITKWVLFNLH      201
             :* :*  :: **** : *  :   ***: :*: * :** :   *::   :: :*::::*

HPL_CP      PTVNIGILQPLEEIFLHSWAYPFFLVRNDYKNLYDFIKQNGKEVLQIAETKFGLTEEETI      300
AOS_AT      PLLSIGLPRVIEEPLIHTFSLPPALVKSDYQRLYEFFLESAGEILVEAD-KLGISREEAT      260
             * :.**: : :** ::*::: *  **:.**:.**:*: :.. *:*  *: *:*::.**:

HPL_CP      HNLLFVIGFNAFGGFSVFLPSLLDAISSDQTGLQDKLKKEVREHSVPGSG-LDFETMSKM      359
AOS_AT      HNLLFATCFNTWGGMKILFPNMVKRIGRAGHQVHNRLAEEIRSVIKSNGGELTMGAIEKM      320
             *****.  **::**:.:::*.::. *.     ::::* :*:*.    ..* * : ::.**

HPL_CP      ELVKSVVYEALRFKPPVPTQYGRARKDFRLTSHDSVYDIKKGELLCGFQPLVMRDPEVFD      419
AOS_AT      ELTKSVVYECLRFEPPVTAQYGRAKKDLVIESHDAAFKVKAGEMLYGYQPLATRDPKIFD      380
             **.******.***:*** :*****:**: : ***:.:.:* **:* *:***. ***::**

HPL_CP      EPEKFKPDRFLG-EGSKLLSYLYWSNGPQTGSPSESNKQCAAKEVVPLTACLVVAHLFLR      478
AOS_AT      RADEFVPERFVGEEGEKLLRHVLWSNGPETETPTVGNKQCAGKDFVVLVARLFVIEIFRR      440
             . ::* *:**:* **.*** :: *****:* :*: .*****.*:.* *.* *.* .:* *

HPL_CP      YEKISGGSGSITALEKTK      496
AOS_AT      YD----------------      442
             *:
```

Fig. A 2 Alignment of *A. thaliana* AOS_{AT} (PDB number: 3CLI) as template and *C. papaya* HPL_{CP} model. The alignment was performed with the Swiss-model program [90] to generate a protein structure model for HPL_{CP} on the basis of the crystal structure of AOS_{AT}.

>HPL_{PG}

MARVVMSNMSPAMSSTYPPSLSPPSSPRPTTLPVRTIPGSYGWPLLGPISDRLDYFWFQGPETFFRKRIEKYKSTVF
RANVPPCFPFFSNVNPNVVVVLDCESFAHLFDMEIVEKSNVLVGDFMPSVKYTGNIRVCAYLDTSEPQHAQVKNFA
MDILKRSSKVWESEVISNLDTMWDTIESSLAKDGNASVIFPLQKFLFNFLSKSIIGADPAASPQVAKSGYAMLDRWL
ALQLLPTINIGVLQPLVEIFLHSWAYPFALVSGDYNKLYQFIEKEGREAVERAKAEFGLTHQEAIHNLLFILGFNAFG
GFSIFLPTLLSNILSDTTGLQDRLRKEVRAKGGPALSFASVKEMELVKSVVYETLRLNPPVPFQYARARKDFQLKSH
DSVFDVKKGELLCGYQKVVMTDPKVFDEPESFNSDRFVQNSELLDYLYWSNGPQTGTPTESNKQCAAKDYVTLTA
CLFVAYMFRRYNSVTGSSSSITAVEKANHHHHHH*

>*hpl_{PG}* codon-optimized

CATATGGCGAGGGTCGTGATGAGCAACATGTCGCCGGCCATGTCGTCCACCTACCCCCCGTCTCTGTCCCCGCCGT
CGTCGCCGCGGCCGACCACCCTGCCTGTTCGCACCATTCCGGGTAGCTATGGTTGGCCGCTGCTGGGTCCGATTAG
TGATCGTCTGGATTATTTTTGGTTTCAGGGCCCGGAAACCTTTTTCCGCAAACGCATTGAAAAATATAAGAGCAC
CGTTTTTCGCGCCAATGTGCCGCCGTGTTTTCCGTTTTTCAGCAATGTTAATCCGAATGTTGTTGTGGTGCTGGAT
TGCGAAAGCTTTGCCCATCTGTTTGATATGGAAATTGTTGAAAAGAGCAACGTTCTGGTTGGCGATTTTATGCCG
AGCGTTAAATATACCGGTAATATTCGCGTGTGCGCCTATCTGGATACCAGCGAACCGCAGCATGCACAGGTTAAA
AATTTTGCCATGGATATTCTGAAGCGTAGTAGCAAAGTTTGGGAAAGCGAAGTTATTAGTAATCTGGATACCATG
TGGGATACCATTGAAAGCAGCCTGGCCAAAGATGGCAATGCAAGTGTTATTTTTCCGCTGCAGAAATTTCTGTTT
AATTTTCTGAGTAAGAGCATCATTGGTGCAGATCCGGCAGCAAGCCCGCAGGTGGCCAAAAGCGGCTATGCAATG
CTGGATCGTTGGCTGGCACTGCAGCTGCTGCCGACCATTAATATTGGTGTTCTGCAGCCGCTGGTTGAAATTTTTC
TGCATAGCTGGGCATATCCGTTTGCACTGGTTAGCGGTGACTATAATAAGCTGTATCAGTTTATTGAGAAGGAAG
GTCGTGAAGCCGTGGAACGTGCAAAAGCCGAATTTGGTCTGACCCATCAGGAAGCCATTCATAATCTGCTGTTTA
TTCTGGGTTTTAATGCATTTGGCGGCTTTAGTATTTTTCTGCCGACCCTGCTGAGTAATATTCTGAGTGATACCAC
CGGCCTGCAGGATCGTCTGCGCAAAGAAGTTCGCGCAAAAGGCGGTCCGGCCCTGAGCTTTGCCAGCGTGAAAGA
AATGGAACTGGTGAAAAGCGTTGTGTATGAAACCCTGCGCCTGAATCCGCCGGTGCCGTTTCAGTATGCACGTGC
CCGCAAAGATTTTCAGCTGAAAAGCCATGATAGCGTTTTTGATGTGAAAAAAGGCGAACTGCTGTGTGGTTATCA
GAAAGTGGTTATGACCGATCCGAAAGTGTTTGATGAACCGGAAAGTTTTAATAGTGATCGCTTTGTTCAGAATAG
CGAACTGCTGGATTATCTGTATTGGAGCAATGGTCCGCAGACCGGTACACCGACCGAAAGCAATAAGCAGTGTGC
CGCAAAAGATTATGTGACCCTGACCGCCTGCCTGTTTGTTGCCTATATGTTTCGTCGTTATAATAGCGTGACCGGT
AGCAGCAGCAGCATTACCGCAGTTGAAAAAGCCAATCATCATCATCATCACCATTAAGGATCC

Fig. A 3 Guava HPL_{PG} protein sequence and codon-optimized *hpl_{PG}* gene sequence with His6-tag marked in grey and restriction sites underlined. The N-terminal sequence that was truncated in the "–N"-enzyme is written in red.

>HPL_{CP}

MMMKLMNISPTMSSPSSPPSSSPLASNSISTPPSSALPLRTIPGSYGWPLLGPLSDRLDYFWFQGPETFFRKRMEKN
KSSVFRTNVPPSFPFFLDVNPNVIAVLDVKSFSHLFDLEIVEKKDVLVGSFVPSTRFTGDVRVGVYLDTAEPKHSEVK
NLTMELLQRGSKVWQSELLSNLDKMWDMVEATVAEKGKATYLGPLQQCIFNFIMKALAGIDPAVSPQIANSGYIM
LDRWLFLQLLPTVNIGILQPLEEIFLHSWAYPFFLVRNDYKNLYDFIKQNGKEVLQIAETKFGLTEEETIHNLLFVIG
FNAFGGFSVFLPSLLDAISSDQTGLQDKLKKEVREHSVPGSGLDFETMSKMELVKSVVYEALRFKPPVPTQYGRARK
DFRLTSHDSVYDIKKGELLCGFQPLVMRDPEVFDEPEKFKPDRFLGEGSKLLSYLYWSNGPQTGSPSESNKQCAAK
EVVPLTACLVVAHLFLRYEKISGGSGSITALEKTKHHHHHH*

>*hpl_{CP}* codon-optimized

CATATGATGATGAAGCTGATGAATATCAGTCCGACCATGAGTAGCCCGAGCAGCCCGCCGAGTAGTAGCCCGCTG
GCCAGTAATAGCATTAGCACCCCGCCGAGCAGTGCACTGCCGCTGCGTACCATTCCGGGCAGCTATGGCTGGCCGC
TGCTGGGTCCGCTGAGCGATCGCCTGGATTATTTTTGGTTTCAGGGTCCGGAAACCTTTTTCCGTAAACGCATGGA
AAAGAATAAGAGCAGCGTTTTTCGTACCAATGTGCCGCCGAGCTTTCCGTTTTTCCTGGATGTGAATCCGAATGT
TATTGCCGTTCTGGATGTTAAAAGCTTTAGCCATCTGTTTGATCTGGAAATTGTGGAAAAGAAAGATGTGCTGGT
GGGTAGCTTTGTGCCGAGTACCCGTTTTACCGGCGATGTGCGCGTTGGTGTTTATCTGGATACCGCCGAACCGAAA
CATAGCGAAGTGAAAAATCTGACAATGGAACTGCTGCAGCGTGGCAGTAAAGTGTGGCAGAGTGAACTGCTGAGT
AATCTGGATAAAATGTGGGATATGGTGGAAGCCACCGTGGCCGAAAAAGGTAAAGCAACCTATCTGGGTCCGTTA
CAGCAGTGCATTTTTAATTTTATTATGAAGGCCCTGGCCGGTATTGATCCGGCAGTTAGCCCGCAGATTGCCAAT
AGCGGTTATATTATGCTGGATCGCTGGCTGTTTCTGCAGCTGCTGCCGACCGTGAATATTGGCATTCTGCAGCCGC
TGGAAGAAATTTTTCTGCATAGTTGGGCATATCCGTTTTTCTTAGTGCGTAATGATTATAAAAACCTGTACGATT
TCATCAAGCAGAATGGCAAAGAAGTGCTGCAGATTGCCGAAACCAAATTTGGTCTGACCGAAGAAGAAACCATTC
ATAATCTGCTGTTTGTTATTGGCTTTAATGCATTTGGTGGCTTTAGTGTTTTTCTGCCGAGTTTACTGGATGCAA
TTAGCAGTGATCAGACCGGTCTGCAGGATAAACTGAAAAAAGAAGTTCGTGAACATAGCGTTCCGGGTAGCGGCC
TGGATTTTGAAACCATGAGCAAAATGGAACTGGTGAAAAGCGTGGTTTATGAAGCCCTGCGTTTTAAACCGCCGG
TTCCGACCCAGTATGGTCGTGCCCGCAAAGATTTTCGCCTGACCAGTCATGATAGTGTGTATGATATTAAGAAGG
GTGAACTGCTGTGTGGCTTTCAGCCGCTGGTTATGCGTGATCCGGAAGTTTTTGATGAACCGGAAAAATTCAAAC
CGGATCGTTTTCTGGGCGAAGGTAGCAAACTGCTGAGCTATCTGTATTGGAGTAATGGTCCGCAGACCGGTAGTC
CGAGTGAAAGCAATAAGCAGTGTGCAGCAAAAGAAGTGGTGCCGCTGACCGCCTGTCTGGTGGTTGCACATCTGT
TTCTGCGTTATGAAAAAATTAGTGGCGGTAGTGGTAGCATTACCGCCCTGGAAAAAACCAAACATCATCATCATC
ACCATTAAGGATCC

Fig. A 4 Papaya HPL_{CP} protein sequence and codon-optimized *hpl_{CP}* gene sequence with His6-tag marked in grey and restriction sites underlined. The N-terminal sequence that was truncated in the "–N"-enzyme is written in red. Figure modified and reproduced from [175] with permission from Springer Nature.

>HPL_{Hv}

MLPSFSPAVTAAAMAPPPPKPIPGGYGAPVLGPLRDRLDYFWFQGPEEFFRRRAAQHRSTVFRANIPPTFPFFVGIN
PRVIAIVDTAAFTALFDPELVDKRDCLIGPYNPSDSFTGGTRVGVYLDTEEPEHERTKAFAMDLLRRSSRVWAPEFL
EGVDGMLAAIESDLAAGKEGGASFLVPLQRCIFRFLCRSVASADPAAEGLVDRYGLFILDVWLGLQLLPTQKVGAIP
QPLEELLLHSFPFPSILAKPGYDLLYRFVAKHGAESVAVGVTNHGMSEKDAINNILFLLGFNAFGGFSVFLPFLILQIG
KDAALRARLRDEVRAALDQHDGEVGFASVKGMPLVRSTVYEVLRMNPPVPLQFGRARRDFVLRSHGGEGFSVAGG
EMLCGYQPLAMRDPEVFERPEEFVADRFVGAGGEALLRYVYWSNGPETGEPALGNKQCAAKDVVIATACMLVAEL
FRRYDDFECTGTAFTSLKKRPQPQPSSHHHHHH*

>*hpl_{Hv}* codon-optimized

CATATGCTGCCGAGCTTTAGCCCGGCAGTTACCGCAGCAGCAATGGCTCCGCCGCCGCCTAAACCGATTCCGGGCG
GTTATGGTGCACCGGTTCTGGGCCCGCTGCGTGATCGCCTGGATTATTTTTGGTTTCAGGGCCCGGAAGAATTTTT
CCGTCGCCGCGCAGCACAGCATCGTAGCACCGTTTTTCGTGCAAATATTCCGCCGACCTTTCCGTTTTTCGTTGGT
ATTAATCCGCGTGTTATTGCCATTGTGGATACCGCAGCATTCACTGCCCTGTTTGATCCGGAACTGGTTGATAAAC
GCGATTGTCTGATTGGCCCGTATAATCCGAGCGATAGCTTTACCGGCGGTACACGCGTTGGTGTTTATCTGGATAC
CGAAGAACCGGAACATGAACGTACCAAAGCCTTTGCAATGGATCTGCTGCGTCGTAGTAGCCGCGTTTGGGCCCCG
GAATTTCTGGAAGGTGTTGATGGCATGCTGGCAGCCATTGAAAGCGATCTGGCCGCAGGCAAAGAAGGTGGTGCC
AGTTTTCTGGTGCCGCTGCAGCGCTGCATTTTTCGTTTTCTGTGTCGTAGTGTTGCCAGCGCAGATCCGGCAGCAG
AAGGCTTAGTTGATCGCTATGGCCTGTTTATTCTGGATGTTTGGCTGGGTCTGCAGCTGCTGCCGACCCAGAAAG
TTGGTGCAATTCCGCAGCCGCTGGAAGAACTGCTGCTGCATAGCTTTCCGTTTCCGAGCATTCTGGCCAAACCGGG
TTATGATCTGCTGTATCGTTTTGTGGCAAAACATGGCGCCGAAAGTGTTGCCGTTGGTGTTACCAATCATGGCAT
GAGTGAAAAAGATGCAATTAATAATATCCTGTTCCTGCTGGGTTTTAATGCATTTGGCGGCTTTAGCGTTTTTCT
GCCGTTTCTGATTCTGCAGATTGGCAAAGATGCCGCCCTGCGCGCCCGTCTGCGCGACGAGGTGAGAGCAGCACTG
GATCAGCATGATGGCGAAGTGGGTTTTGCAAGTGTTAAAGGCATGCCGCTGGTTCGTAGCACCGTGTATGAAGTG
CTGCGCATGAATCCGCCGGTTCCGCTGCAGTTTGGTCGTGCCCGTCGTGATTTTGTGCTGCGCAGTCATGGTGGTG
AAGGTTTTAGCGTGGCCGGTGGTGAAATGCTGTGTGGCTATCAGCCGCTGGCCATGCGCGATCCGGAAGTTTTTG
AACGTCCGGAAGAATTCGTGGCCGATCGTTTTGTGGGTGCAGGCGGCGAAGCCCTGCTGCGTTATGTTTATTGGA
GCAATGGTCCGGAAACCGGCGAACCGGCCCTGGGTAATAAGCAGTGTGCCGCCAAAGATGTGGTTATTGCAACCG
CCTGTATGCTGGTTGCCGAACTGTTTCGTCGCTATGATGATTTTGAATGCACCGGCACCGCCTTTACCAGCCTGAA
AAAACGCCCGCAGCCGCAGCCGAGCAGTCATCATCATCATCACCATTAAGGATCC

Fig. A 5 Barley HPL_{HV} protein sequence and codon-optimized *hpl_{HV}* gene sequence with His6-tag marked in grey and restriction sites underlined. The N-terminal sequence that was truncated in the "–N"-enzyme is written in red.

>HPL_{SB}

MLPSFVSPTASASVTPPPRPIPGSHGPPVLGPLRDRLDYFWFQSQDEFFRKRAAAHRSTVFRTNIPPTFPFFVGIDP
RVVAIVDAAAFTALFDPDLVDKRDILIGPYNPGTGFTGGTRVGVYLDTQEAEHTRIKTFAMDLLHRSARSWPAEFR
AGVGAMLDAVDADFAANKASSASYLVPLQQCIFRFLCKAFAGADPSADWLVDNFGFTILDIWLALQILPTQKVGVV
QPLEELLIHSFPLPSFLIWPGYYLLYRFVEKHGAEAVAYAETQHGISKKDAINNILFVLGFNAFGGFSVFLPFLVAKVG
DAADAAGLRPRLRDEVRRAMDKAKDADAEFGFAAVRESMPLVRSTVYEMLRMQPPVPLQFGRARRDFVLQSHGG
AAYQVSKGEVLCGYQPLAMRDPEVFDRPEEFVPERFLGDDGARLLQHLFWSNGPETEQPAPGNKQCAAKEVVVD
TACMLLAELFRRYDDFVVEGTSFTKLVKRQPSPSLSPAAAAGAGAQQHHHHHH*

>*hpl_{SB}* codon-optimized

CATATGCTGCCGAGCTTTGTTAGTCCGACCGCAAGTGCCAGCGTGACCCCGCCTCCGCGTCCTATTCCGGGTAGCC
ATGGCCCGCCGGTTCTGGGTCCGCTGCGTGATCGTCTGGATTATTTTTGGTTTCAGAGCCAAGATGAATTTTTCCG
TAAACGTGCAGCCGCACATCGCAGCACCGTTTTTCGTACCAATATTCCGCCGACCTTTCCGTTTTTCGTGGGCATT
GATCCGCGTGTGGTGGCCATTGTTGATGCAGCCGCATTCACTGCACTGTTTGATCCGGATCTGGTTGATAAACGCG
ATATTCTGATTGGCCCGTATAATCCGGGTACAGGCTTTACCGGCGGCACCCGCGTGGGCGTTTATCTGGATACCCA
GGAAGCAGAACATACCCGTATTAAGACCTTTGCCATGGATCTGCTGCATCGCAGCGCCCGCAGCTGGCCTGCAGAA
TTTCGTGCCGGTGTGGGCGCAATGCTGGATGCAGTTGATGCCGATTTTGCAGCAAATAAGGCAAGTAGTGCCAGT
TATCTGGTGCCGCTGCAGCAGTGTATTTTTCGTTTTCTGTGCAAAGCCTTTGCAGGCGCAGATCCGAGCGCAGATT
GGCTGGTTGATAATTTTGGCTTTACCATTCTGGATATTTGGCTGGCACTGCAGATTCTGCCGACCCAGAAAGTTG
GCGTGGTTCAGCCGCTGGAAGAACTGCTGATTCATAGTTTTCCGCTGCCGAGCTTCCTGATTTGGCCGGGCTATTA
TCTGCTGTATCGTTTTGTGGAAAAACATGGTGCCGAAGCAGTGGCATACGCTGAAACCCAGCATGGTATTAGTAA
AAAAGATGCCATTAACAACATCCTGTTTGTTCTGGGCTTTAATGCCTTTGGTGGCTTTAGTGTGTTTCTGCCGTTT
CTGGTGGCAAAAGTTGGCGATGCAGCCGATGCCGCCGGTCTGCGTCCGAGACTGCGTGATGAAGTGCGTCGTGCCA
TGGATAAAGCAAAAGATGCCGATGCCGAATTTGGCTTTGCCGCCGTTCGCGAAAGCATGCCGCTGGTTCGCAGTA
CCGTGTATGAAATGCTGCGCATGCAGCCGCCGGTGCCGCTGCAATTTGGCCGCGCTCGCCGTGATTTTGTTCTGCA
GAGCCATGGCGGCGCAGCATATCAGGTGAGCAAAGGCGAAGTGCTGTGCGGTTATCAGCCGCTGGCAATGCGTGA
TCCGGAAGTGTTTGATCGCCCGGAAGAATTTGTGCCGGAACGCTTTCTGGGCGATGATGGCGCCCGCCTGCTGCAG
CATCTGTTTTGGAGTAATGGTCCGGAAACCGAACAGCCGGCACCGGGCAATAAGCAGTGCGCCGCCAAAGAAGTG
GTGGTTGATACCGCCTGCATGCTGCTGGCAGAACTGTTTCGTCGTTATGATGATTTTGTTGTTGAAGGCACCAGC
TTTACCAAACTGGTGAAACGTCAGCCGAGCCCGAGCCTGAGCCCGGCAGCAGCAGCTGGTGCCGGTGCTCAGCAGC
ATCATCATCATCACCATTAAGGATCC

Fig. A 6 Sorghum HPL_{SB} protein sequence and codon-optimized *hpl_{SB}* gene sequence with His6-tag marked in grey and restriction sites underlined. The N-terminal sequence that was truncated in the "–N"-enzyme is written in red.

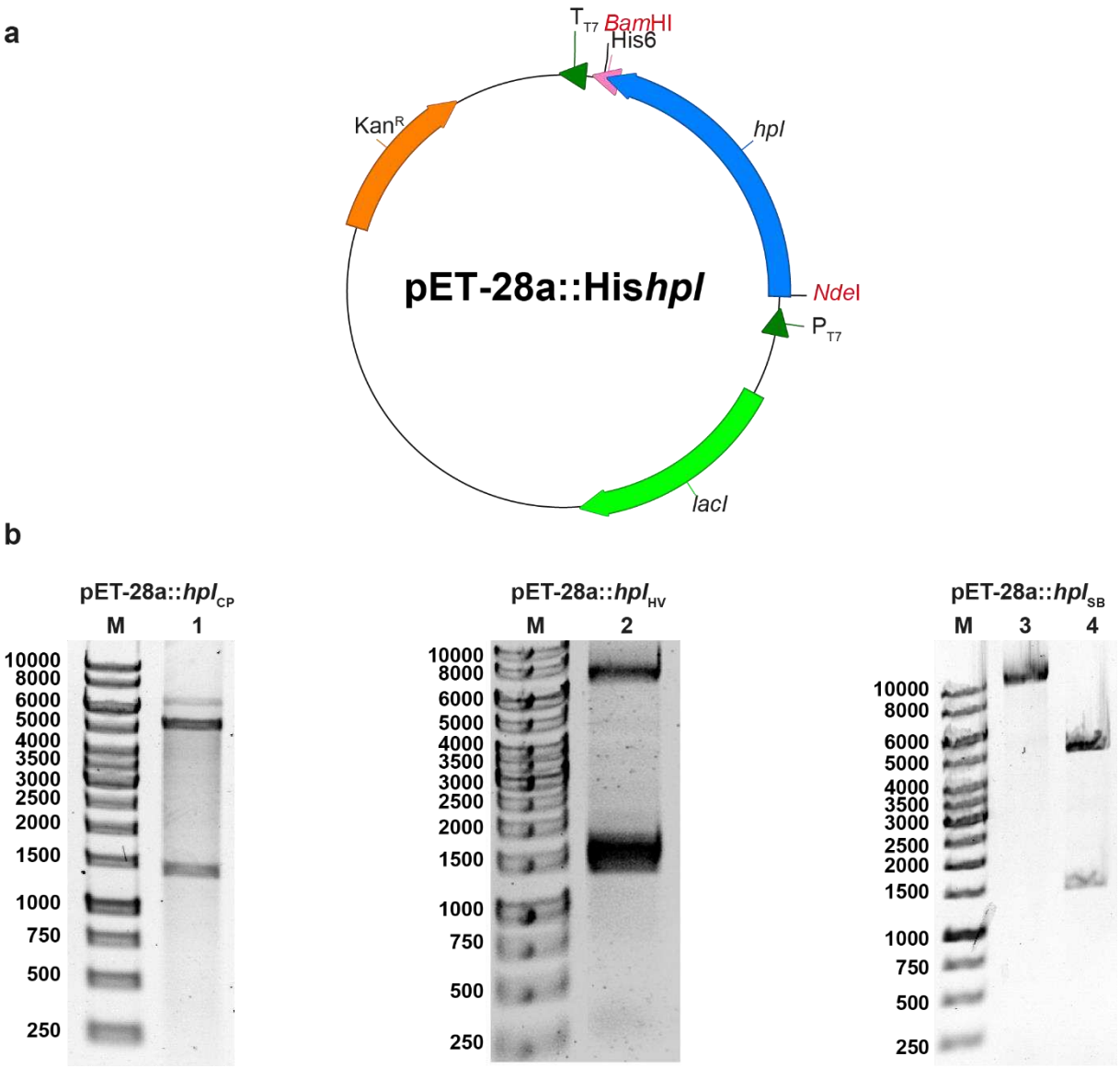

Fig. A 7 Expression vector pET-28a::His*hpl* (**a**) for expression of HPL_{PG} = *P. guajava*, HPL_{CP} = *C. papaya,* HPL_{HV} = *H. vulgare* and HPL_{SB} = *S. bicolor* and agarose gels of restriction digests of pET-28a::His*hpl* (**b**) with *Nde*I and *Bam*HI. M: DNA ladder marker with sizes in bp.

```
                    ....|....| ....|....| ....|....| ....|....| ....|....|
                             10         20         30         40         50
S.lycopersicum      ---------- ---------- ---MNSAPLS TPAPVTLPVR SIPGSYGLPL
O.europaea          ---------- MMAKMTGSPS VTPLSPPSPS PPSPSSLPLR AIPGGYGWPV
V.vinifera          ---------M LSSTVMSVSP GVPTPSSLTP PSPPSSSPVR AIPGSYGWPV
P.guajava           -----MARVV MSNMSPAMSS TYPPSLSPPS SPRPTTLPVR TIPGSYGWPL
C.papaya            MMMKLMNISP TMSSPSSPPS SSPLASNSIS TPPSSALPLR TIPGSYGWPL
A.thaliana          ------MLLR TMAATSPRPP PSTSLTSQQP PSPPSQLPLR TMPGSYGWPL
M.sativa            ---------- ----MSLPPP IPPPSLATPP KARPTELPIR QIPGSHGWPL
M.balbisiana        ---------- ---------- -MAMMWSLAS ATAVTTLPTR PIPGSYGPPL
H.vulgare           ---------- ---------- MLPSFSPAVT AAAMAPPPPK PIPGGYGAPV
S.bicolor           ---------- ---------- -MLPSFVSPT ASASVTPPPR PIPGSHGPPV

                    ....|....| ....|....| ....|....| ....|....| ....|....|
                             60         70         80         90        100
S.lycopersicum      VGPIADRLDY FWFQKPENFF TKRMEKHKST VFRTNVPPCF PFFGSVNPNV
O.europaea          VGPIIDRLNY FWFQGPPTFF KKRMEKYKST VFRTNVPPTF PWFLGVNPNV
V.vinifera          LGPIADRLDY FWFQGPETFF RKRIDKYKST VFRTNVPPSF PFFVGVNPNV
P.guajava           LGPISDRLDY FWFQGPETFF RKRIEKYKST VFRANVPPCF PFFSNVNPNV
C.papaya            LGPLSDRLDY FWFQGPETFF RKRMEKNKSS VFRTNVPPSF PFFLDVNPNV
A.thaliana          VGPLSDRLDY FWFQGPDKFF RTRAEKYKST VFRTNIPPTF PFFGNVNPNI
M.sativa            LGPLSDRLDY FWFQKPENFF RTRMEKYKST VFRTNVPPTF PFFTNVNPNI
M.balbisiana        VGPLKDRLDY FWFQGPETFF RSRMATHKST VFRTNMPPTF PFFVGVDPRV
H.vulgare           LGPLRDRLDY FWFQGPEEFF RRRAAQHRST VFRANIPPTF PFFVGINPRV
S.bicolor           LGPLRDRLDY FWFQSQDEFF RKRAAAHRST VFRTNIPPTF PFFVGIDPRV

                    ....|....| ....|....| ....|....| ....|....| ....|....|
                            110        120        130        140        150
S.lycopersicum      VAVLDVKSFS HLFDMEIVEK ANVLVGDFMP SVVYTGDMRV CAYLDTSEPK
O.europaea          IAVLDVKSFS HLFDMEIVEK ANVLVGDFMP SVKYTGDFRV CAYLDTSEAK
V.vinifera          IAVLDCKSFS FLFDMDVVEK KNVLVGDFMP SVKYTGDIRV CAYLDTAETQ
P.guajava           VVVLDCESFA HLFDMEIVEK SNVLVGDFMP SVKYTGNIRV CAYLDTSEPQ
C.papaya            IAVLDVKSFS HLFDLEIVEK KDVLVGSFVP STRFTGDVRV GVYLDTAEPK
A.thaliana          VAVLDVKSFS HLFDMDLVDK RDVLIGDFRP SLGFYGGVCV GVNLDTTEPK
M.sativa            IAVLDCKSFS HLFDMDLVDK RDVLVGDFVP SVEFTGNIRV GVYQDVSEPQ
M.balbisiana        VTVLDCTSFS ALFDLEVVEK NNILIGDYMP SLSFTGDTRV VVYLDPSEPD
H.vulgare           IAIVDTAAFT ALFDPELVDK RDCLIGPYNP SDSFTGGTRV GVYLDTEEPE
S.bicolor           VAIVDAAAFT ALFDPDLVDK RDILIGPYNP GTGFTGGTRV GVYLDTQEAE

                    ....|....| ....|....| ....|....| ....|....| ....|....|
                            160        170        180        190        200
S.lycopersicum      HAQIKNFSQD ILKRGSKTWV PTLLKELDTM FTTFEADLSK S--NTASLLP
O.europaea          HTQIKNFSLD ILKRSSTIWV PSLISSLDSM WDKIDADVAN S--GSASSFL
V.vinifera          HARVKSFAMD ILKRSSSIWA SEVVASLDTM WDTIDAGVAK S--NSASYIK
P.guajava           HAQVKNFAMD ILKRSSKVWE SEVISNLDTM WDTIESSLAK D--GNASVIF
C.papaya            HSEVKNLTME LLQRGSKVWQ SELLSNLDKM WDMVEATVAE K--GKATYLG
A.thaliana          HAKIKGFAME TLKRSSKVWL QELRSNLNIF WGTIESEISK N--GAASYIF
M.sativa            HAKAKNFSMN ILKQSSSIWV PELISNLDIF LDQIEATLSN S--SSASYFS
M.balbisiana        HARVKSFCLE LLRRGAKTWV SSFLSNLDVM LATIEQGISK D--GSAGLFG
H.vulgare           HERTKAFAMD LLRRSSRVWA PEFLEGVDGM LAAIESDLAA GKEGGASFLV
S.bicolor           HTRIKTFAMD LLHRSARSWP AEFRAGVGAM LDAVDADFAA NKASSASYLV
```

```
                    ....|....| ....|....| ....|....| ....|....| ....|....|
                            210        220        230        240        250
S.lycopersicum      ALQKFLFNFF SLTILGADPS VSPEIANSGY IFLDSWLAIQ LAPTVSIGVL
O.europaea          PMQQFLFRFL TRCIVGADPS TSPEIASSGH IMLDKWLGIQ ILPTVNIGIL
V.vinifera          PLQRFIFHFL TKCLVGADPA VSPEIAESGY VMLDKWVFLQ LLPTISVNFL
P.guajava           PLQKFLFNFL SKSIIGADPA ASPQVAKSGY AMLDRWLALQ LLPTINIGVL
C.papaya            PLQQCIFNFI MKALAGIDPA VSPQIANSGY IMLDRWLFLQ LLPTVNIGIL
A.thaliana          PLQRCIFSFL CASLAGVDAS VSPDIAENGW KTINTWLALQ VIPTAKLGVV
M.sativa            PLQKFLFTFL SKVLARADPS LDPKIAESGS SMLNKWLAVQ LLPTVSVGTI
M.balbisiana        PLQKCIFAFL CKSIIGADPS VSPDVGENGF VMLDKWLALQ LLPTVKVGAI
H.vulgare           PLQRCIFRFL CRSVASADPA AEGLVDRYGL FILDVWLGLQ LLPTQKVGAI
S.bicolor           PLQQCIFRFL CKAFAGADPS ADWLVDNFGF TILDIWLALQ ILPTQKVGVV

                    ....|....| ....|....| ....|....| ....|....| ....|....|
                            260        270        280        290        300
S.lycopersicum      QP-LEEILVH SFAYPFFLVK GNYEKLVQFV KNEAKEVLSR AQTEFQLTEQ
O.europaea          QP-LEELFLH SFSYPFWLVK GDYNKLVQFV EKEGKEVIQR AQTEFNLTEQ
V.vinifera          QP-LEEIFLH SFAYPFFLVK GDYRKLYDFV EQHGQAVLQR GETEFNLSKE
P.guajava           QP-LVEIFLH SWAYPFALVS GDYNKLYQFI EKEGREAVER AKAEFGLTHQ
C.papaya            QP-LEEIFLH SWAYPFFLVR NDYKNLYDFI KQNGKEVLQI AETKFGLTEE
A.thaliana          PQPLEEILLH TWPYPSLLIA GNYKKLYNFI DENAGDCLRL GQEEFRLTRD
M.sativa            QP-LEEIFLH SFSYPYALVS GDYKNLYNFI KQHGKEVIKN G-TEFGLSED
M.balbisiana        PQPLEEILLH SFPLPFFLVS RDYRKLYEFV EKQGQEVVQR AETEHGLSKH
H.vulgare           XQPLEELLLH SFPFPSILAK PGYDLLYRFV AKHGAESVAV GVTNHGMSEK
S.bicolor           -QPLEELLIH SFPLPSFLIW PGYYLLYRFV EKHGAEAVAY AETQHGISKK

                    ....|....| ....|....| ....|....| ....|....| ....|....|
                            310        320        330        340        350
S.lycopersicum      EAIHNLLFIL GFNAFGGFSI FLPTLLGNLG DEKNADMQEK LRKEVRDKVG
O.europaea          EAIHNLLFIL GFNAFGGFTI FFLALLSAIG DQKSTGLHEK LRDEVRQKSG
V.vinifera          ETTHNLLFVL GFNAFGGFTI FFPSLLSALS GK--PELQAK LREEVRSKIK
P.guajava           EAIHNLLFIL GFNAFGGFSI FLPTLLSNIL SDT-TGLQDR LRKEVRAKGG
C.papaya            ETIHNLLFVI GFNAFGGFSV FLPSLLDAIS SDQ-TGLQDK LKKEVR-EHS
A.thaliana          EAIQNLLFVL GFNAYGGFSV FLPSLIGRIT GDN-SGLQER IRTEVRRVCG
M.sativa            EAIHNLLFVL GFNSYGGFSI FLPKLIESIT NGP-TGLQEK LRKEAREKGG
M.balbisiana        DAINNILFVL GFNAFGGFSV FFPTLLTTIG RDK-TGLREK LKDEVRRVMK
H.vulgare           DAINNILFLL GFNAFGGFSV FLPFLILQIG ------KDAA LRARLRDEVR
S.bicolor           DAINNILFVL GFNAFGGFSV FLPFLVAKVG DAA---DAAG LRPRLRDEVR

                    ....|....| ....|....| ....|....| ....|....| ....|....|
                            360        370        380        390        400
S.lycopersicum      VNP------- -ENLSFESVK EMELVQSFVY ETLRLSPPVP SQYARARKDF
O.europaea          SNS------- -NTLSFESVK DMELVQSFVY ETLRLNPPVP SQFARARKDF
V.vinifera          PGT------- -N-LTFESVK DLELVHSVVY ETLRLNPPVP LQYARARKDF
P.guajava           ---------- -PALSFASVK EMELVKSVVY ETLRLNPPVP FQYARARKDF
C.papaya            VPG------- -SGLDFETMS KMELVKSVVY EALRFKPPVP TQYGRARKDF
A.thaliana          SG-------- -SDLNFKTVN EMELVKSVVY ETLRFNPPVP LQFARARKDF
M.sativa            ---------- -STLGFDSLK ELELINSVVY ETLRMNPPVP LQFGRARKDF
M.balbisiana        SRGE------ -KRPSFETVR EMELVRSTVY EVLRLNPPVP LQYGRARTDF
H.vulgare           AALD---QHD GEVGFASVKG -MPLVRSTVY EVLRMNPPVP LQFGRARRDF
S.bicolor           RAMDKAKDAD AEFGFAAVRE SMPLVRSTVY EMLRMQPPVP LQFGRARRDF
```

```
                    ....|....| ....|....| ....|....| ....|....| ....|....|
                            410        420        430        440        450
S.lycopersicum      KLSSHDS-VY EIKKGELLCG YQPLVMKDPK VFDE-PEKFV LERFTKEKG-
O.europaea          KLTSHDA-VY EIKKGELLCG YQPLVMKDAK VFEESPATFL YDRFTREKGG
V.vinifera          QLSSHDS-VF EIKKGDLLCG FQKVAMTDPK IFDD-PETFV PDRFTKEKG-
P.guajava           QLKSHDS-VF DVKKGELLCG YQKVVMTDPK VFDE-PESFN SDRFVQNSE-
C.papaya            RLTSHDS-VY DIKKGELLCG FQPLVMRDPE VFDE-PEKFK PDRFLGEGS-
A.thaliana          QISSHDA-VF EVKKGELLCG YQPLVMRDAN VFDE-PEEFK PDRYVGETG-
M.sativa            QLSSYDS-AF NVKKGELLCG FQKLVMRDPV VFDE-PEQFK PERFTKEKG-
M.balbisiana        TLNSHDA-AF KVQKGELLCG YQPLVMRDPA VFDD-PETFA PERFMGSGK-
H.vulgare           VLRSHGGEGF SVAGGEMLCG YQPLAMRDPE VFER-PEEFV ADRFVGAGG-
S.bicolor           VLQSHGGAAY QVSKGEVLCG YQPLAMRDPE VFDR-PEEFV PERFLGDDG-

                    ....|....| ....|....| ....|....| ....|....| ....|....|
                            460        470        480        490        500
S.lycopersicum      KELLNYLFWS NGPQTGRPTE SNKQCAAKDM VTLTASLIVA YIFQKYDSVS
O.europaea          TELLNYLYWS NGPQTGSATA ANKQCAAKEI VPLTAALFVA YLFQRYDDIT
V.vinifera          RELLNYLFWS NGPQTGSPSD RNKQCAAKDY VTMTAVLFVT HMFQRYDSVT
P.guajava           --LLDYLYWS NGPQTGTPTE SNKQCAAKDY VTLTACLFVA YMFRRYNSVT
C.papaya            -KLLSYLYWS NGPQTGSPSE SNKQCAAKEV VPLTACLVVA HLFLRYEKIS
A.thaliana          SELLNYLYWS NGPQTGTPSA SNKQCAAKDI VTLTASLLVA DLFLRYDTIT
M.sativa            AELLNYLYWS NGPQTGSPTV SNKQCAGKDI VTFTAALIVA HLLRRYDLIK
M.balbisiana        -ELLKYIFWS NGPETGTPTP ANKQCAAKDY VVETACLLMA EIFNRYDEFV
H.vulgare           EALLRYVYWS NGPETGEPAL GNKQCAAKDV VIATACMLVA ELFRRYDDFE
S.bicolor           ARLLQHLFWS NGPETEQPAP GNKQCAAKEV VVDTACMLLA ELFRRYDDFV

                    ....|....| ....|....| ....|....|
                            510        520        530
S.lycopersicum      FSSGSLTSVK KAS------- ----------
O.europaea          ISSGSITAVE KSK------- ----------
V.vinifera          ASGSSITAVE KAN------- ----------
P.guajava           GSSSSITAVE KAN------- ----------
C.papaya            GGSGSITALE KTK------- ----------
A.thaliana          GDSGSIKAVV KAK------- ----------
M.sativa            GDGSSITALQ KAK------- ----------
M.balbisiana        CADDAISVTK LERATERE-- ----------
H.vulgare           CTGTAFTSLK KRPQPQPSS- ----------
S.bicolor           VEGTSFTKLV KRQPSPSLSP AAAAGAGAQQ
```

Fig. A 8 Multiple sequence alignment of HPL sequences obtained with ClustalΩ [178].

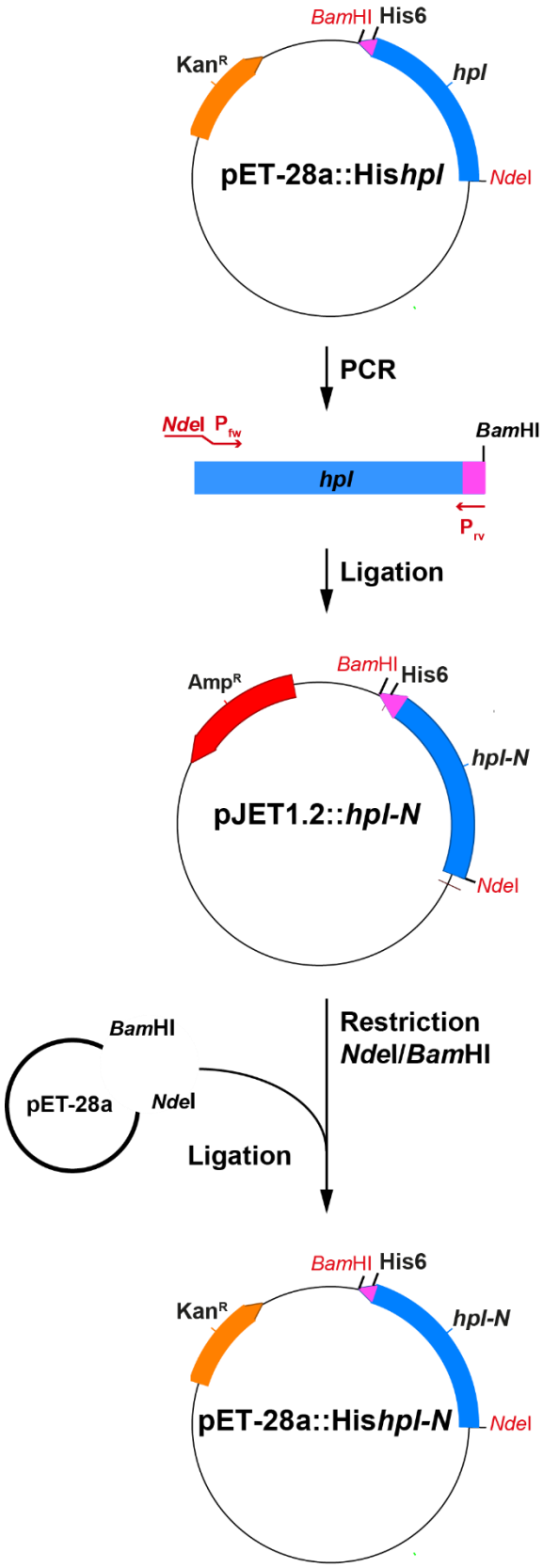

Fig. A 9 Scheme for the cloning of N-terminal truncated HPLs. A PCR was performed using the pET-28::His*hpl* vector as template with specific primers truncating the sequence coding for the unconserved N-terminus. The PCR fragment was ligated into the cloning vector pJET1.2 for amplification. The amplified fragments were restricted with *Bam*HI and *Nde*I and ligated into the expression vector pET-28a(+). P: primer.

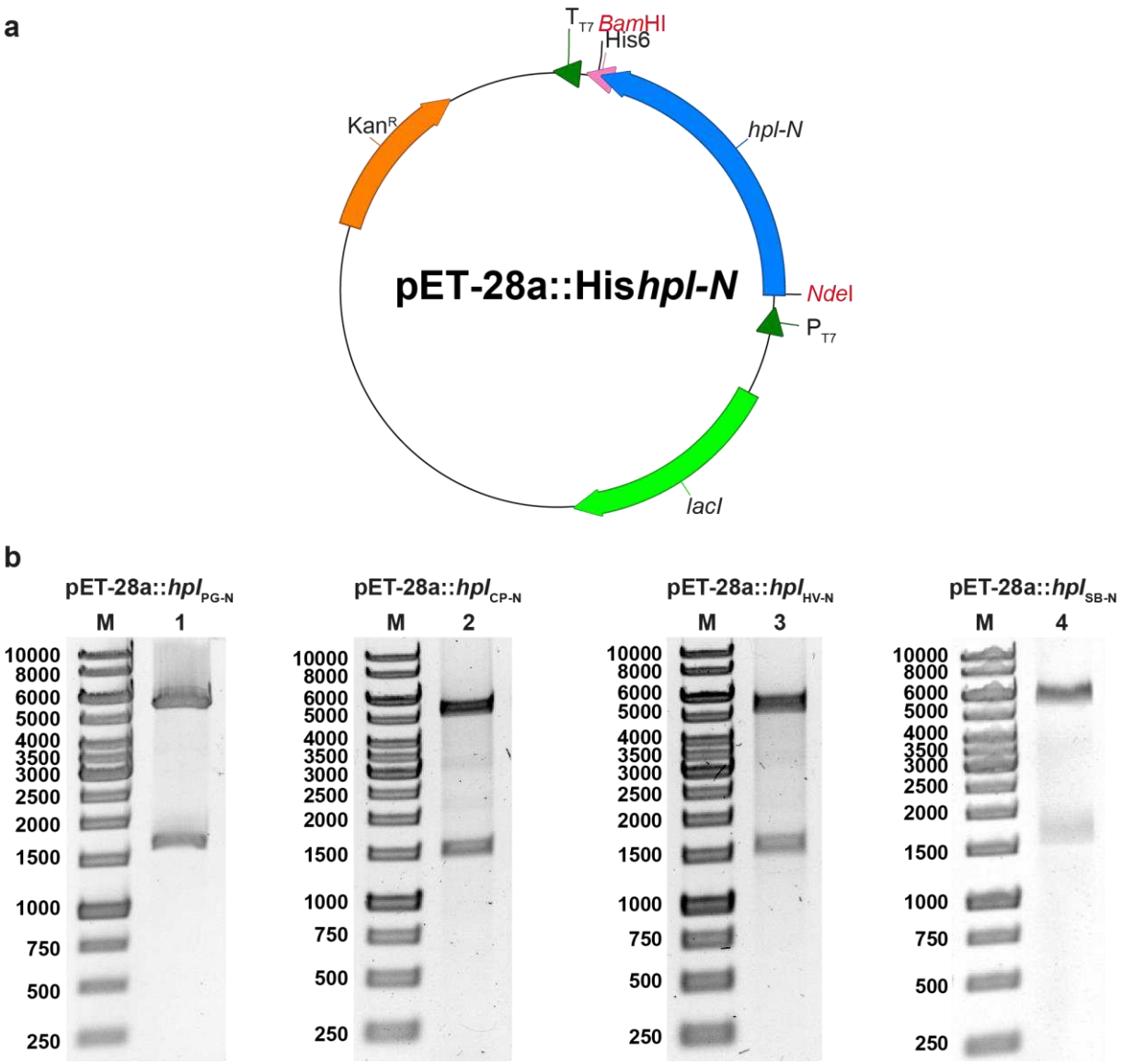

Fig. A 10 Expression vector pET-28a::His*hpl-N* (**a**) for expression of N-terminal truncated HPL_{PG-N} = *P. guajava*, HPL_{CP-N} = *C. papaya,* HPL_{HV-N} = *H. vulgare* and HPL_{SB-N} = *S. bicolor* and agarose gels of restriction digests of pET-28a::His*hpl-N* (**b**) with *Nde*I and *Bam*HI. M: DNA ladder marker with sizes in bp.

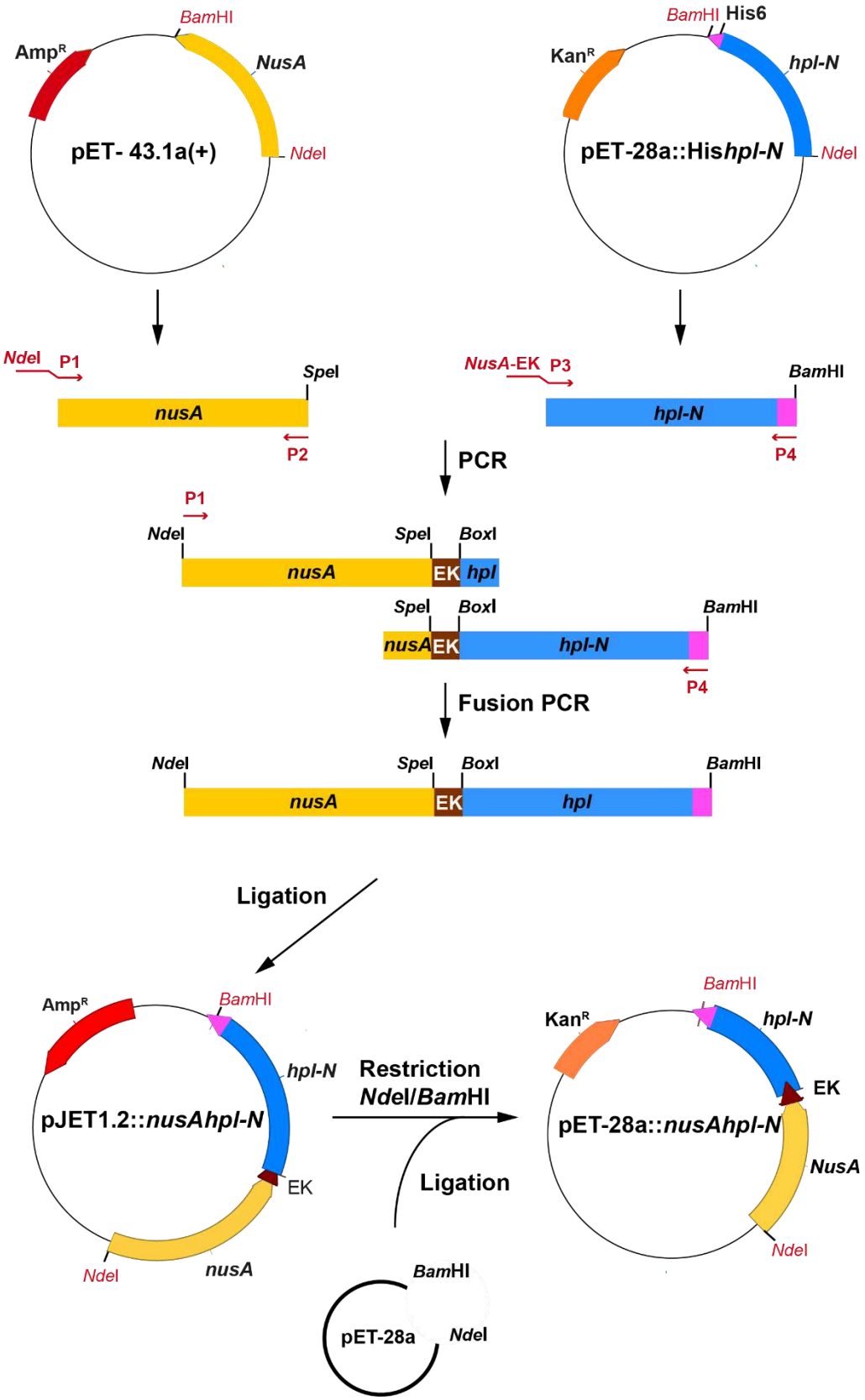

Fig. A 11 Scheme for the cloning of NusA – HPL fusion proteins. A PCR was performed to amplify the *nusA* and the *hpl-N* sequences with overlapping fragments. Subsequently, a fusion PCR was conducted for ligating the *nusA* and the *hpl-N* sequences. The fusion fragments were ligated into the cloning vector pJET1.2 for amplification. Then, they were restricted with *Bam*HI and *Nde*I and ligated into the expression vector pET-28a(+). P1-4: primers, EK: sequence coding for enterokinase cleavage site.

>NusA

MNKEILAVVEAVSNEKALPREKIFEALESALATATKKKYEQEIDVRVQIDRKSGDFDTFRRWLVVDEVTQPTKEITL
EAARYEDESLNLGDYVEDQIESVTFDRITTQTAKQVIVQKVREAERAMVVDQFREHEGEIITGVVKKVNRDNISLDL
GNNAEAVILREDMLPRENFRPGDRVRGVLYSVRPEARGAQLFVTRSKPEMLIELFRIEVPEIGEEVIEIKAAARDPGS
RAKIAVKTNDKRIDPVGACVGMRGARVQAVSTELGGERIDIVLWDDNPAQFVINAMAPADVASIVVDEDKHTMDI
AVEAGNLAQAIGRNGQNVRLASQLSGWELNVMTVDDLQAKHQAEAHAAIDTFTKYLDIDEDFATVLVEEGFSTLE
ELAYVPMKELLEIEGLDEPTVEALRERAKNALATIAQAQEESLGDNKPADDLLNLEGVDRDLAFKLAARGVCTLED
LAEQGIDDLADIEGLTDEKAGALIMAARNICWFGDE

>*nusA*

ATGAACAAAGAAATTTTGGCTGTAGTTGAAGCCGTATCCAATGAAAAGGCGCTACCTCGCGAGAAGATTTTCGAA
GCATTGGAAAGCGCGCTGGCGACAGCAACAAAGAAAAAATATGAACAAGAGATCGACGTCCGCGTACAGATCGAT
CGCAAAAGCGGTGATTTTGACACTTTCCGTCGCTGGTTAGTTGTTGATGAAGTCACCCAGCCGACCAAGGAAATC
ACCCTTGAAGCCGCACGTTATGAAGATGAAAGCCTGAACCTGGGCGATTACGTTGAAGATCAGATTGAGTCTGTT
ACCTTTGACCGTATCACTACCCAGACGGCAAAACAGGTTATCGTGCAGAAAGTGCGTGAAGCCGAACGTGCGATG
GTGGTTGATCAGTTCCGTGAACACGAAGGTGAAATCATCACCGGCGTGGTGAAAAAAGTAAACCGCGACAACATC
TCTCTGGATCTGGGCAACAACGCTGAAGCCGTGATCCTGCGCGAAGATATGCTGCCGCGTGAAAACTTCCGCCCTG
GCGACCGCGTTCGTGGCGTGCTCTATTCCGTTCGCCCGGAAGCGCGTGGCGCGCAACTGTTCGTCACTCGTTCCAA
GCCGGAAATGCTGATCGAACTGTTCCGTATTGAAGTGCCAGAAATCGGCGAAGAAGTGATTGAAATTAAAGCAGC
GGCTCGCGATCCGGGTTCTCGTGCGAAAATCGCGGTGAAAACCAACGATAAACGTATCGATCCGGTAGGTGCTTG
CGTAGGTATGCGTGGCGCGCGTGTTCAGGCGGTGTCTACTGAACTGGGTGGCGAGCGTATCGATATCGTCCTGTG
GGATGATAACCCGGCGCAGTTCGTGATTAACGCAATGGCACCGGCAGACGTTGCTTCTATCGTGGTGGATGAAGA
TAAACACACCATGGACATCGCCGTTGAAGCCGGTAATCTGGCGCAGGCGATTGGCCGTAACGGTCAGAACGTGCG
TCTGGCTTCGCAACTGAGCGGTTGGGAACTCAACGTGATGACCGTTGACGACCTGCAAGCTAAGCATCAGGCGGA
AGCGCACGCAGCGATCGACACCTTCACCAAATATCTCGACATCGACGAAGACTTCGCGACTGTTCTGGTAGAAGA
AGGCTTCTCGACGCTGGAAGAATTGGCCTATGTGCCGATGAAAGAGCTGTTGGAAATCGAAGGCCTTGATGAGCC
GACCGTTGAAGCACTGCGCGAGCGTGCTAAAAATGCACTGGCCACCATTGCACAGGCCCAGGAAGAAAGCCTCGG
TGATAACAAACCGGCTGACGATCTGCTGAACCTTGAAGGGGTAGATCGTGATTTGGCATTCAAACTGGCCGCCCG
TGGCGTTTGTACGCTGGAAGATCTCGCCGAACAGGGCATTGATGATCTGGCTGATATCGAAGGGTTGACCGACGA
AAAAGCCGGAGCACTGATTATGGCTGCCCGTAATATTTGCTGGTTCGGTGACGAA

Fig. A 12 NusA protein sequence and *nusA* gene sequence.

>NusAHPL$_{CP-N}$

MNKEILAVVEAVSNEKALPREKIFEALESALATATKKKYEQEIDVRVQIDRKSGDFDTFRRWLVVDEVTQPTKEITL
EAARYEDESLNLGDYVEDQIESVTFDRITTQTAKQVIVQKVREAERAMVVDQFREHEGEIITGVVKKVNRDNISLDL
GNNAEAVILREDMLPRENFRPGDRVRGVLYSVRPEARGAQLFVTRSKPEMLIELFRIEVPEIGEEVIEIKAAARDPGS
RAKIAVKTNDKRIDPVGACVGMRGARVQAVSTELGGERIDIVLWDDNPAQFVINAMAPADVASIVVDEDKHTMDI
AVEAGNLAQAIGRNGQNVRLASQLSGWELNVMTVDDLQAKHQAEAHAAIDTFTKYLDIDEDFATVLVEEGFSTLE
ELAYVPMKELLEIEGLDEPTVEALRERAKNALATIAQAQEESLGDNKPADDLLNLEGVDRDLAFKLAARGVCTLED
LAEQGIDDLADIEGLTDEKAGALIMAARNICWFGDEATSDDDDKSVLPLRTIPGSYGWPLLGPLSDRLDYFWFQGP
ETFFRKRMEKNKSSVFRTNVPPSFPFFLDVNPNVIAVLDVKSFSHLFDLEIVEKKDVLVGSFVPSTRFTGDVRVGVY
LDTAEPKHSEVKNLTMELLQRGSKVWQSELLSNLDKMWDMVEATVAEKGKATYLGPLQQCIFNFIMKALAGIDP
AVSPQIANSGYIMLDRWLFLQLLPTVNIGILQPLEEIFLHSWAYPFFLVRNDYKNLYDFIKQNGKEVLQIAETKFGLT
EEETIHNLLFVIGFNAFGGFSVFLPSLLDAISSDQTGLQDKLKKEVREHSVPGSGLDFETMSKMELVKSVVYEALRFK
PPVPTQYGRARKDFRLTSHDSVYDIKKGELLCGFQPLVMRDPEVFDEPEKFKPDRFLGEGSKLLSYLYWSNGPQTG
SPSESNKQCAAKEVVPLTACLVVAHLFLRYEKISGGSGSITALEKTKHHHHHH

>*nusAhpl*$_{CP-N}$

CATATGAACAAAGAAATTTTGGCTGTAGTTGAAGCCGTATCCAATGAAAAGGCGCTACCTCGCGAGAAGATTTTC
GAAGCATTGGAAAGCGCGCTGGCGACAGCAACAAAGAAAAAATATGAACAAGAGATCGACGTCCGCGTACAGATC
GATCGCAAAAGCGGTGATTTTGACACTTTCCGTCGCTGGTTAGTTGTTGATGAAGTCACCCAGCCGACCAAGGAA
ATCACCCTTGAAGCCGCACGTTATGAAGATGAAAGCCTGAACCTGGGCGATTACGTTGAAGATCAGATTGAGTCT
GTTACCTTTGACCGTATCACTACCCAGACGGCAAAACAGGTTATCGTGCAGAAAGTGCGTGAAGCCGAACGTGCG
ATGGTGGTTGATCAGTTCCGTGAACACGAAGGTGAAATCATCACCGGCGTGGTGAAAAAAGTAAACCGCGACAAC
ATCTCTCTGGATCTGGGCAACAACGCTGAAGCCGTGATCCTGCGCGAAGATATGCTGCCGCGTGAAAACTTCCGCC
CTGGCGACCGCGTTCGTGGCGTGCTCTATTCCGTTCGCCCGGAAGCGCGTGGCGCGCAACTGTTCGTCACTCGTTC
CAAGCCGGAAATGCTGATCGAACTGTTCCGTATTGAAGTGCCAGAAATCGGCGAAGAAGTGATTGAAATTAAAGC
AGCGGCTCGCGATCCGGGTTCTCGTGCGAAAATCGCGGTGAAAACCAACGATAAACGTATCGATCCGGTAGGTGC
TTGCGTAGGTATGCGTGGCGCGCGTGTTCAGGCGGTGTCTACTGAACTGGGTGGCGAGCGTATCGATATCGTCCT
GTGGGATGATAACCCGGCGCAGTTCGTGATTAACGCAATGGCACCGGCAGACGTTGCTTCTATCGTGGTGGATGA
AGATAAACACACCATGGACATCGCCGTTGAAGCCGGTAATCTGGCGCAGGCGATTGGCCGTAACGGTCAGAACGT
GCGTCTGGCTTCGCAACTGAGCGGTTGGGAACTCAACGTGATGACCGTTGACGACCTGCAAGCTAAGCATCAGGC
GGAAGCGCACGCAGCGATCGACACCTTCACCAAATATCTCGACATCGACGAAGACTTCGCGACTGTTCTGGTAGA
AGAAGGCTTCTCGACGCTGGAAGAATTGGCCTATGTGCCGATGAAAGAGCTGTTGGAAATCGAAGGCCTTGATGA
GCCGACCGTTGAAGCACTGCGCGAGCGTGCTAAAAATGCACTGGCCACCATTGCACAGGCCCAGGAAGAAAGCCTC
GGTGATAACAAACCGGCTGACGATCTGCTGAACCTTGAAGGGGTAGATCGTGATTTGGCATTCAAACTGGCCGCC
CGTGGCGTTTGTACGCTGGAAGATCTCGCCGAACAGGGCATTGATGATCTGGCTGATATCGAAGGGTTGACCGAC
GAAAAAGCCGGAGCACTGATTATGGCTGCCCGTAATATTTGCTGGTTCGGTGACGAAGCGACTAGTGATGACGAC
GACAAGAGTGTCCTGCCGCTGCGTACCATTCCGGGCAGCTATGGCTGGCCGCTGCTGGGTCCGCTGAGCGATCGCC
TGGATTATTTTTGGTTTCAGGGTCCGGAAACCTTTTTCCGTAAACGCATGGAAAAGAATAAGAGCAGCGTTTTTC
GTACCAATGTGCCGCCGAGCTTTCCGTTTTTCCTGGATGTGAATCCGAATGTTATTGCCGTTCTGGATGTTAAAA
GCTTTAGCCATCTGTTTGATCTGGAAATTGTGGAAAAGAAAGATGTGCTGGTGGGTAGCTTTGTGCCGAGTACCC
GTTTTACCGGCGATGTGCGCGTTGGTGTTTATCTGGATACCGCCGAACCGAAACATAGCGAAGTGAAAAATCTGA
CAATGGAACTGCTGCAGCGTGGCAGTAAAGTGTGGCAGAGTGAACTGCTGAGTAATCTGGATAAAATGTGGGATA
TGGTGGAAGCCACCGTGGCCGAAAAAGGTAAAGCAACCTATCTGGGTCCGTTACAGCAGTGCATTTTTAATTTTA
TTATGAAGGCCCTGGCCGGTATTGATCCGGCAGTTAGCCCGCAGATTGCCAATAGCGGTTATATTATGCTGGATC
GCTGGCTGTTTCTGCAGCTGCTGCCGACCGTGAATATTGGCATTCTGCAGCCGCTGGAAGAAATTTTTCTGCATAG
TTGGGCATATCCGTTTTTCTTAGTGCGTAATGATTATAAAAACCTGTACGATTTCATCAAGCAGAATGGCAAAGA
AGTGCTGCAGATTGCCGAAACCAAATTTGGTCTGACCGAAGAAGAAACCATTCATAATCTGCTGTTTGTTATTGG
CTTTAATGCATTTGGTGGCTTTAGTGTTTTTCTGCCGAGTTTACTGGATGCAATTAGCAGTGATCAGACCGGTCT
GCAGGATAAACTGAAAAAAGAAGTTCGTGAACATAGCGTTCCGGGTAGCGGCCTGGATTTTGAAACCATGAGCAA
AATGGAACTGGTGAAAAGCGTGGTTTATGAAGCCCTGCGTTTTAAACCGCCGGTTCCGACCCAGTATGGTCGTGC
CCGCAAAGATTTTCGCCTGACCAGTCATGATAGTGTGTATGATATTAAGAAGGGTGAACTGCTGTGTGGCTTTCA
GCCGCTGGTTATGCGTGATCCGGAAGTTTTTGATGAACCGGAAAAATTCAAACCGGATCGTTTTCTGGGCGAAGG
TAGCAAACTGCTGAGCTATCTGTATTGGAGTAATGGTCCGCAGACCGGTAGTCCGAGTGAAAGCAATAAGCAGTG
TGCAGCAAAAGAAGTGGTGCCGCTGACCGCCTGTCTGGTGGTTGCACATCTGTTTCTGCGTTATGAAAAAATTAG
TGGCGGTAGTGGTAGCATTACCGCCCTGGAAAAAACCAAACATCATCATCATCACCATTAAGGATCC

Fig. A 13 NusAHPL$_{CP-N}$ fusion protein sequence and *nusAhpl*$_{CP-N}$ fusion gene sequence with His6-tag marked in grey and restriction sites underlined. Enterokinase cleavage site is marked blue.

>NusAHPL$_{PG-N}$

MNKEILAVVEAVSNEKALPREKIFEALESALATATKKKYEQEIDVRVQIDRKSGDFDTFRRWLVVDEVTQPTKEITL
EAARYEDESLNLGDYVEDQIESVTFDRITTQTAKQVIVQKVREAERAMVVDQFREHEGEIITGVVKKVNRDNISLDL
GNNAEAVILREDMLPRENFRPGDRVRGVLYSVRPEARGAQLFVTRSKPEMLIELFRIEVPEIGEEVIEIKAAARDPGS
RAKIAVKTNDKRIDPVGACVGMRGARVQAVSTELGGERIDIVLWDDNPAQFVINAMAPADVASIVVDEDKHTMDI
AVEAGNLAQAIGRNGQNVRLASQLSGWELNVMTVDDLQAKHQAEAHAAIDTFTKYLDIDEDFATVLVEEGFSTLE
ELAYVPMKELLEIEGLDEPTVEALRERAKNALATIAQAQEESLGDNKPADDLLNLEGVDRDLAFKLAARGVCTLED
LAEQGIDDLADIEGLTDEKAGALIMAARNICWFGDEATSDDDDKSLPVRTIPGSYGWPLLGPISDRLDYFWFQGPE
TFFRKRIEKYKSTVFRANVPPCFPFFSNVNPNVVVVLDCESFAHLFDMEIVEKSNVLVGDFMPSVKYTGNIRVCAYL
DTSEPQHAQVKNFAMDILKRSSKVWESEVISNLDTMWDTIESSLAKDGNASVIFPLQKFLFNFLSKSIIGADPAASP
QVAKSGYAMLDRWLALQLLPTINIGVLQPLVEIFLHSWAYPFALVSGDYNKLYQFIEKEGREAVERAKAEFGLTHQ
EAIHNLLFILGFNAFGGFSIFLPTLLSNILSDTTGLQDRLRKEVRAKGGPALSFASVKEMELVKSVVYETLRLNPPVPF
QYARARKDFQLKSHDSVFDVKKGELLCGYQKVVMTDPKVFDEPESFNSDRFVQNSELLDYLYWSNGPQTGTPTES
NKQCAAKDYVTLTACLFVAYMFRRYNSVTGSSSSITAVEKANHHHHHH

>*nusAhpl*$_{PG-N}$

CATATGAACAAAGAAATTTTGGCTGTAGTTGAAGCCGTATCCAATGAAAAGGCGCTACCTCGCGAGAAGATTTTC
GAAGCATTGGAAAGCGCGCTGGCGACAGCAACAAAGAAAAAATATGAACAAGAGATCGACGTCCGCGTACAGATC
GATCGCAAAAGCGGTGATTTTGACACTTTCCGTCGCTGGTTAGTTGTTGATGAAGTCACCCAGCCGACCAAGGAA
ATCACCCTTGAAGCCGCACGTTATGAAGATGAAAGCCTGAACCTGGGCGATTACGTTGAAGATCAGATTGAGTCT
GTTACCTTTGACCGTATCACTACCCAGACGGCAAAACAGGTTATCGTGCAGAAAGTGCGTGAAGCCGAACGTGCG
ATGGTGGTTGATCAGTTCCGTGAACACGAAGGTGAAATCATCACCGGCGTGGTGAAAAAAGTAAACCGCGACAAC
ATCTCTCTGGATCTGGGCAACAACGCTGAAGCCGTGATCCTGCGCGAAGATATGCTGCCGCGTGAAAACTTCCGCC
CTGGCGACCGCGTTCGTGGCGTGCTCTATTCCGTTCGCCCGGAAGCGCGTGGCGCGCAACTGTTCGTCACTCGTTC
CAAGCCGGAAATGCTGATCGAACTGTTCCGTATTGAAGTGCCAGAAATCGGCGAAGAAGTGATTGAAATTAAAGC
AGCGGCTCGCGATCCGGGTTCTCGTGCGAAAATCGCGGTGAAAACCAACGATAAACGTATCGATCCGGTAGGTGC
TTGCGTAGGTATGCGTGGCGCGCGTGTTCAGGCGGTGTCTACTGAACTGGGTGGCGAGCGTATCGATATCGTCCT
GTGGGATGATAACCCGGCGCAGTTCGTGATTAACGCAATGGCACCGGCAGACGTTGCTTCTATCGTGGTGGATGA
AGATAAACACACCATGGACATCGCCGTTGAAGCCGGTAATCTGGCGCAGGCGATTGGCCGTAACGGTCAGAACGT
GCGTCTGGCTTCGCAACTGAGCGGTTGGGAACTCAACGTGATGACCGTTGACGACCTGCAAGCTAAGCATCAGGC
GGAAGCGCACGCAGCGATCGACACCTTCACCAAATATCTCGACATCGACGAAGACTTCGCGACTGTTCTGGTAGA
AGAAGGCTTCTCGACGCTGGAAGAATTGGCCTATGTGCCGATGAAAGAGCTGTTGGAAATCGAAGGCCTTGATGA
GCCGACCGTTGAAGCACTGCGCGAGCGTGCTAAAAATGCACTGGCCACCATTGCACAGGCCCAGGAAGAAAGCCTC
GGTGATAACAAACCGGCTGACGATCTGCTGAACCTTGAAGGGGTAGATCGTGATTTGGCATTCAAACTGGCCGCC
CGTGGCGTTTGTACGCTGGAAGATCTCGCCGAACAGGGCATTGATGATCTGGCTGATATCGAAGGGTTGACCGAC
GAAAAAGCCGGAGCACTGATTATGGCTGCCCGTAATATTTGCTGGTTCGGTGACGAAGCGACTAGTGATGACGAC
GACAAGAGTGTCCTGCCTGTTCGCACCATTCCGGGTAGCTATGGTTGGCCGCTGCTGGGTCCGATTAGTGATCGTC
TGGATTATTTTTGGTTTCAGGGCCCGGAAACCTTTTTCCGCAAACGCATTGAAAAATATAAGAGCACCGTTTTTC
GCGCCAATGTGCCGCCGTGTTTTCCGTTTTTCAGCAATGTTAATCCGAATGTTGTTGTGGTGCTGGATTGCGAAA
GCTTTGCCCATCTGTTTGATATGGAAATTGTTGAAAAGAGCAACGTTCTGGTTGGCGATTTTATGCCGAGCGTTA
AATATACCGGTAATATTCGCGTGTGCGCCTATCTGGATACCAGCGAACCGCAGCATGCACAGGTTAAAAATTTTG
CCATGGATATTCTGAAGCGTAGTAGCAAAGTTTGGGAAAGCGAAGTTATTAGTAATCTGGATACCATGTGGGATA
CCATTGAAAGCAGCCTGGCCAAAGATGGCAATGCAAGTGTTATTTTTCCGCTGCAGAAATTTCTGTTTAATTTTC
TGAGTAAGAGCATCATTGGTGCAGATCCGGCAGCAAGCCCGCAGGTGGCCAAAAGCGGCTATGCAATGCTGGATC
GTTGGCTGGCACTGCAGCTGCTGCCGACCATTAATATTGGTGTTCTGCAGCCGCTGGTTGAAATTTTTCTGCATAG
CTGGGCATATCCGTTTGCACTGGTTAGCGGTGACTATAATAAGCTGTATCAGTTTATTGAGAAGGAAGGTCGTGA
AGCCGTGGAACGTGCAAAAGCCGAATTTGGTCTGACCCATCAGGAAGCCATTCATAATCTGCTGTTTATTCTGGG
TTTTAATGCATTTGGCGGCTTTAGTATTTTTCTGCCGACCCTGCTGAGTAATATTCTGAGTGATACCACCGGCCTG
CAGGATCGTCTGCGCAAAGAAGTTCGCGCAAAAGGCGGTCCGGCCCTGAGCTTTGCCAGCGTGAAAGAAATGGAA
CTGGTGAAAAGCGTTGTGTATGAAACCCTGCGCCTGAATCCGCCGGTGCCGTTTCAGTATGCACGTGCCCGCAAAG
ATTTTCAGCTGAAAAGCCATGATAGCGTTTTTGATGTGAAAAAAGGCGAACTGCTGTGTGGTTATCAGAAAGTGG
TTATGACCGATCCGAAAGTGTTTGATGAACCGGAAAGTTTTAATAGTGATCGCTTTGTTCAGAATAGCGAACTGC
TGGATTATCTGTATTGGAGCAATGGTCCGCAGACCGGTACACCGACCGAAAGCAATAAGCAGTGTGCCGCAAAAG
ATTATGTGACCCTGACCGCCTGCCTGTTTGTTGCCTATATGTTTCGTCGTTATAATAGCGTGACCGGTAGCAGCAG
CAGCATTACCGCAGTTGAAAAAGCCAATCATCATCATCATCACCATTAAGGATCC

Fig. A 14 NusAHPL$_{PG-N}$ fusion protein sequence and *nusAhpl*$_{PG-N}$ fusion gene sequence with His6-tag marked in grey and restriction sites underlined. Enterokinase cleavage site is marked blue.

>NusAHPL$_{HV-N}$

MNKEILAVVEAVSNEKALPREKIFEALESALATATKKKYEQEIDVRVQIDRKSGDFDTFRRWLVVDEVTQPTKEITL
EAARYEDESLNLGDYVEDQIESVTFDRITTQTAKQVIVQKVREAERAMVVDQFREHEGEIITGVVKKVNRDNISLDL
GNNAEAVILREDMLPRENFRPGDRVRGVLYSVRPEARGAQLFVTRSKPEMLIELFRIEVPEIGEEVIEIKAAARDPGS
RAKIAVKTNDKRIDPVGACVGMRGARVQAVSTELGGERIDIVLWDDNPAQFVINAMAPADVASIVVDEDKHTMDI
AVEAGNLAQAIGRNGQNVRLASQLSGWELNVMTVDDLQAKHQAEAHAAIDTFTKYLDIDEDFATVLVEEGFSTLE
ELAYVPMKELLEIEGLDEPTVEALRERAKNALATIAQAQEESLGDNKPADDLLNLEGVDRDLAFKLAARGVCTLED
LAEQGIDDLADIEGLTDEKAGALIMAARNICWFGDEATSDDDDKSVPPPKPIPGGYGAPVLGPLRDRLDYFWFQGP
EEFFRRRAAQHRSTVFRANIPPTFPFFVGINPRVIAIVDTAAFTALFDPELVDKRDCLIGPYNPSDSFTGGTRVGVYL
DTEEPEHERTKAFAMDLLRRSSRVWAPEFLEGVDGMLAAIESDLAAGKEGGASFLVPLQRCIFRFLCRSVASADPA
AEGLVDRYGLFILDVWLGLQLLPTQKVGAIPQPLEELLLHSFPFPSILAKPGYDLLYRFVAKHGAESVAVGVTNHGM
SEKDAINNILFLLGFNAFGGFSVFLPFLILQIGKDAALRARLRDEVRAALDQHDGEVGFASVKGMPLVRSTVYEVLR
MNPPVPLQFGRARRDFVLRSHGGEGFSVAGGEMLCGYQPLAMRDPEVFERPEEFVADRFVGAGGEALLRYVYWS
NGPETGEPALGNKQCAAKDVVIATACMLVAELFRRYDDFECTGTAFTSLKKRPQPQPSSHHHHHH

>*nusAhpl*$_{HV-N}$

CATATGAACAAAGAAATTTTGGCTGTAGTTGAAGCCGTATCCAATGAAAAGGCGCTACCTCGCGAGAAGATTTTC
GAAGCATTGGAAAGCGCGCTGGCGACAGCAACAAAGAAAAAATATGAACAAGAGATCGACGTCCGCGTACAGATC
GATCGCAAAAGCGGTGATTTTGACACTTTCCGTCGCTGGTTAGTTGTTGATGAAGTCACCCAGCCGACCAAGGAA
ATCACCCTTGAAGCCGCACGTTATGAAGATGAAAGCCTGAACCTGGGCGATTACGTTGAAGATCAGATTGAGTCT
GTTACCTTTGACCGTATCACTACCCAGACGGCAAAACAGGTTATCGTGCAGAAAGTGCGTGAAGCCGAACGTGCG
ATGGTGGTTGATCAGTTCCGTGAACACGAAGGTGAAATCATCACCGGCGTGGTGAAAAAAGTAAACCGCGACAAC
ATCTCTCTGGATCTGGGCAACAACGCTGAAGCCGTGATCCTGCGCGAAGATATGCTGCCGCGTGAAAACTTCCGCC
CTGGCGACCGCGTTCGTGGCGTGCTCTATTCCGTTCGCCCGGAAGCGCGTGGCGCGCAACTGTTCGTCACTCGTTC
CAAGCCGGAAATGCTGATCGAACTGTTCCGTATTGAAGTGCCAGAAATCGGCGAAGAAGTGATTGAAATTAAAGC
AGCGGCTCGCGATCCGGGTTCTCGTGCGAAAATCGCGGTGAAAACCAACGATAAACGTATCGATCCGGTAGGTGC
TTGCGTAGGTATGCGTGGCGCGCGTGTTCAGGCGGTGTCTACTGAACTGGGTGGCGAGCGTATCGATATCGTCCT
GTGGGATGATAACCCGGCGCAGTTCGTGATTAACGCAATGGCACCGGCAGACGTTGCTTCTATCGTGGTGGATGA
AGATAAACACACCATGGACATCGCCGTTGAAGCCGGTAATCTGGCGCAGGCGATTGGCCGTAACGGTCAGAACGT
GCGTCTGGCTTCGCAACTGAGCGGTTGGGAACTCAACGTGATGACCGTTGACGACCTGCAAGCTAAGCATCAGGC
GGAAGCGCACGCAGCGATCGACACCTTCACCAAATATCTCGACATCGACGAAGACTTCGCGACTGTTCTGGTAGA
AGAAGGCTTCTCGACGCTGGAAGAATTGGCCTATGTGCCGATGAAAGAGCTGTTGGAAATCGAAGGCCTTGATGA
GCCGACCGTTGAAGCACTGCGCGAGCGTGCTAAAAATGCACTGGCCACCATTGCACAGGCCCAGGAAGAAAGCCTC
GGTGATAACAAACCGGCTGACGATCTGCTGAACCTTGAAGGGGTAGATCGTGATTTGGCATTCAAACTGGCCGCC
CGTGGCGTTTGTACGCTGGAAGATCTCGCCGAACAGGGCATTGATGATCTGGCTGATATCGAAGGGTTGACCGAC
GAAAAAGCCGGAGCACTGATTATGGCTGCCCGTAATATTTGCTGGTTCGGTGACGAAGCGACTAGTGATGACGAC
GACAAGAGTGTCCCGCCGCCTAAACCGATTCCGGGCGGTTATGGTGCACCGGTTCTGGGCCCGCTGCGTGATCGCC
TGGATTATTTTTGGTTTCAGGGCCCGGAAGAATTTTTCCGTCGCCGCGCAGCACAGCATCGTAGCACCGTTTTTCG
TGCAAATATTCCGCCGACCTTTCCGTTTTTCGTTGGTATTAATCCGCGTGTTATTGCCATTGTGGATACCGCAGCA
TTCACTGCCCTGTTTGATCCGGAACTGGTTGATAAACGCGATTGTCTGATTGGCCCGTATAATCCGAGCGATAGCT
TTACCGGCGGTACACGCGTTGGTGTTTATCTGGATACCGAAGAACCGGAACATGAACGTACCAAAGCCTTTGCAA
TGGATCTGCTGCGTCGTAGTAGCCGCGTTTGGGCCCCGGAATTTCTGGAAGGTGTTGATGGCATGCTGGCAGCCAT
TGAAAGCGATCTGGCCGCAGGCAAAGAAGGTGGTGCCAGTTTTCTGGTGCCGCTGCAGCGCTGCATTTTTCGTTT
TCTGTGTCGTAGTGTTGCCAGCGCAGATCCGGCAGCAGAAGGCTTAGTTGATCGCTATGGCCTGTTTATTCTGGA
TGTTTGGCTGGGTCTGCAGCTGCTGCCGACCCAGAAAGTTGGTGCAATTCCGCAGCCGCTGGAAGAACTGCTGCTG
CATAGCTTTCCGTTTCCGAGCATTCTGGCCAAACCGGGTTATGATCTGCTGTATCGTTTTGTGGCAAAACATGGCG
CCGAAAGTGTTGCCGTTGGTGTTACCAATCATGGCATGAGTGAAAAAGATGCAATTAATAATATCCTGTTCCTGC
TGGGTTTTAATGCATTTGGCGGCTTTAGCGTTTTTCTGCCGTTTCTGATTCTGCAGATTGGCAAAGATGCCGCCCT
GCGCGCCCGTCTGCGCGACGAGGTGAGAGCAGCACTGGATCAGCATGATGGCGAAGTGGGTTTTGCAAGTGTTAA
AGGCATGCCGCTGGTTCGTAGCACCGTGTATGAAGTGCTGCGCATGAATCCGCCGGTTCCGCTGCAGTTTGGTCGT
GCCCGTCGTGATTTTGTGCTGCGCAGTCATGGTGGTGAAGGTTTTAGCGTGGCCGGTGGTGAAATGCTGTGTGGC
TATCAGCCGCTGGCCATGCGCGATCCGGAAGTTTTTGAACGTCCGGAAGAATTCGTGGCCGATCGTTTTGTGGGT
GCAGGCGGCGAAGCCCTGCTGCGTTATGTTTATTGGAGCAATGGTCCGGAAACCGGCGAACCGGCCCTGGGTAAT
AAGCAGTGTGCCGCCAAAGATGTGGTTATTGCAACCGCCTGTATGCTGGTTGCCGAACTGTTTCGTCGCTATGAT
GATTTTGAATGCACCGGCACCGCCTTTACCAGCCTGAAAAAACGCCCGCAGCCGCAGCCGAGCAGTCATCATCATC
ATCACCATTAAGGATCC

Fig. A 15 NusAHPL$_{HV-N}$ fusion protein sequence and *nusAhpl*$_{HV-N}$ fusion gene sequence with His6-tag marked in grey and restriction sites underlined. Enterokinase cleavage site is marked blue.

>NusAHPL$_{SB-N}$

MNKEILAVVEAVSNEKALPREKIFEALESALATATKKKYEQEIDVRVQIDRKSGDFDTFRRWLVVDEVTQPTKEITL
EAARYEDESLNLGDYVEDQIESVTFDRITTQTAKQVIVQKVREAERAMVVDQFREHEGEIITGVVKKVNRDNISLDL
GNNAEAVILREDMLPRENFRPGDRVRGVLYSVRPEARGAQLFVTRSKPEMLIELFRIEVPEIGEEVIEIKAAARDPGS
RAKIAVKTNDKRIDPVGACVGMRGARVQAVSTELGGERIDIVLWDDNPAQFVINAMAPADVASIVVDEDKHTMDI
AVEAGNLAQAIGRNGQNVRLASQLSGWELNVMTVDDLQAKHQAEAHAAIDTFTKYLDIDEDFATVLVEEGFSTLE
ELAYVPMKELLEIEGLDEPTVEALRERAKNALATIAQAQEESLGDNKPADDLLNLEGVDRDLAFKLAARGVCTLED
LAEQGIDDLADIEGLTDEKAGALIMAARNICWFGDEATSDDDDKSVVPPPRPIPGSHGPPVLGPLRDRLDYFWFQS
QDEFFRKRAAAHRSTVFRTNIPPTFPFFVGIDPRVVAIVDAAAFTALFDPDLVDKRDILIGPYNPGTGFTGGTRVGV
YLDTQEAEHTRIKTFAMDLLHRSARSWPAEFRAGVGAMLDAVDADFAANKASSASYLVPLQQCIFRFLCKAFAGA
DPSADWLVDNFGFTILDIWLALQILPTQKVGVVQPLEELLIHSFPLPSFLIWPGYYLLYRFVEKHGAEAVAYAETQH
GISKKDAINNILFVLGFNAFGGFSVFLPFLVAKVGDAADAAGLRPRLRDEVRRAMDKAKDADAEFGFAAVRESMPL
VRSTVYEMLRMQPPVPLQFGRARRDFVLQSHGGAAYQVSKGEVLCGYQPLAMRDPEVFDRPEEFVPERFLGDDGA
RLLQHLFWSNGPETEQPAPGNKQCAAKEVVVDTACMLLAELFRRYDDFVVEGTSFTKLVKRQPSPSLSPAAAAGA
GAQQHHHHHH

>*nusAhpl*$_{SB-N}$

CATATGAACAAAGAAATTTTGGCTGTAGTTGAAGCCGTATCCAATGAAAAGGCGCTACCTCGCGAGAAGATTTTC
GAAGCATTGGAAAGCGCGCTGGCGACAGCAACAAAGAAAAAATATGAACAAGAGATCGACGTCCGCGTACAGATC
GATCGCAAAAGCGGTGATTTTGACACTTTCCGTCGCTGGTTAGTTGTTGATGAAGTCACCCAGCCGACCAAGGAA
ATCACCCTTGAAGCCGCACGTTATGAAGATGAAAGCCTGAACCTGGGCGATTACGTTGAAGATCAGATTGAGTCT
GTTACCTTTGACCGTATCACTACCCAGACGGCAAAACAGGTTATCGTGCAGAAAGTGCGTGAAGCCGAACGTGCG
ATGGTGGTTGATCAGTTCCGTGAACACGAAGGTGAAATCATCACCGGCGTGGTGAAAAAAGTAAACCGCGACAAC
ATCTCTCTGGATCTGGGCAACAACGCTGAAGCCGTGATCCTGCGCGAAGATATGCTGCCGCGTGAAAACTTCCGCC
CTGGCGACCGCGTTCGTGGCGTGCTCTATTCCGTTCGCCCGGAAGCGCGTGGCGCGCAACTGTTCGTCACTCGTTC
CAAGCCGGAAATGCTGATCGAACTGTTCCGTATTGAAGTGCCAGAAATCGGCGAAGAAGTGATTGAAATTAAAGC
AGCGGCTCGCGATCCGGGTTCTCGTGCGAAAATCGCGGTGAAAACCAACGATAAACGTATCGATCCGGTAGGTGC
TTGCGTAGGTATGCGTGGCGCGCGTGTTCAGGCGGTGTCTACTGAACTGGGTGGCGAGCGTATCGATATCGTCCT
GTGGGATGATAACCCGGCGCAGTTCGTGATTAACGCAATGGCACCGGCAGACGTTGCTTCTATCGTGGTGGATGA
AGATAAACACACCATGGACATCGCCGTTGAAGCCGGTAATCTGGCGCAGGCGATTGGCCGTAACGGTCAGAACGT
GCGTCTGGCTTCGCAACTGAGCGGTTGGGAACTCAACGTGATGACCGTTGACGACCTGCAAGCTAAGCATCAGGC
GGAAGCGCACGCAGCGATCGACACCTTCACCAAATATCTCGACATCGACGAAGACTTCGCGACTGTTCTGGTAGA
AGAAGGCTTCTCGACGCTGGAAGAATTGGCCTATGTGCCGATGAAAGAGCTGTTGGAAATCGAAGGCCTTGATGA
GCCGACCGTTGAAGCACTGCGCGAGCGTGCTAAAAATGCACTGGCCACCATTGCACAGGCCCAGGAAGAAAGCCTC
GGTGATAACAAACCGGCTGACGATCTGCTGAACCTTGAAGGGGTAGATCGTGATTTGGCATTCAAACTGGCCGCC
CGTGGCGTTTGTACGCTGGAAGATCTCGCCGAACAGGGCATTGATGATCTGGCTGATATCGAAGGGTTGACCGAC
GAAAAAGCCGGAGCACTGATTATGGCTGCCCGTAATATTTGCTGGTTCGGTGACGAAGCGACTAGTGATGACGAC
GACAAGAGTGTCGTCCCGCCTCCGCGTCCTATTCCGGGTAGCCATGGCCCGCCGGTTCTGGGTCCGCTGCGTGATC
GTCTGGATTATTTTTGGTTTCAGAGCCAAGATGAATTTTTCCGTAAACGTGCAGCCGCACATCGCAGCACCGTTTT
TCGTACCAATATTCCGCCGACCTTTCCGTTTTTCGTGGGCATTGATCCGCGTGTGGTGGCCATTGTTGATGCAGCC
GCATTCACTGCACTGTTTGATCCGGATCTGGTTGATAAACGCGATATTCTGATTGGCCCGTATAATCCGGGTACA
GGCTTTACCGGCGGCACCCGCGTGGGCGTTTATCTGGATACCCAGGAAGCAGAACATACCCGTATTAAGACCTTTG
CCATGGATCTGCTGCATCGCAGCGCCCGCAGCTGGCCTGCAGAATTTCGTGCCGGTGTGGGCGCAATGCTGGATGC
AGTTGATGCCGATTTTGCAGCAAATAAGGCAAGTAGTGCCAGTTATCTGGTGCCGCTGCAGCAGTGTATTTTTCG
TTTTCTGTGCAAAGCCTTTGCAGGCGCAGATCCGAGCGCAGATTGGCTGGTTGATAATTTTGGCTTTACCATTCTG
GATATTTGGCTGGCACTGCAGATTCTGCCGACCCAGAAAGTTGGCGTGGTTCAGCCGCTGGAAGAACTGCTGATT
CATAGTTTTCCGCTGCCGAGCTTCCTGATTTGGCCGGGCTATTATCTGCTGTATCGTTTTGTGGAAAAACATGGTG
CCGAAGCAGTGGCATACGCTGAAACCCAGCATGGTATTAGTAAAAAAGATGCCATTAACAACATCCTGTTTGTTC
TGGGCTTTAATGCCTTTGGTGGCTTTAGTGTGTTTCTGCCGTTTCTGGTGGCAAAAGTTGGCGATGCAGCCGATG
CCGCCGGTCTGCGTCCGAGACTGCGTGATGAAGTGCGTCGTGCCATGGATAAAGCAAAAGATGCCGATGCCGAAT
TTGGCTTTGCCGCCGTTCGCGAAAGCATGCCGCTGGTTCGCAGTACCGTGTATGAAATGCTGCGCATGCAGCCGCC
GGTGCCGCTGCAATTTGGCCGCGCTCGCCGTGATTTTGTTCTGCAGAGCCATGGCGGCGCAGCATATCAGGTGAGC
AAAGGCGAAGTGCTGTGCGGTTATCAGCCGCTGGCAATGCGTGATCCGGAAGTGTTTGATCGCCCGGAAGAATTT
GTGCCGGAACGCTTTCTGGGCGATGATGGCGCCCGCCTGCTGCAGCATCTGTTTTGGAGTAATGGTCCGGAAACCG
AACAGCCGGCACCGGGCAATAAGCAGTGCGCCGCCAAAGAAGTGGTGGTTGATACCGCCTGCATGCTGCTGGCAG
AACTGTTTCGTCGTTATGATGATTTTGTTGTTGAAGGCACCAGCTTTACCAAACTGGTGAAACGTCAGCCGAGCC
CGAGCCTGAGCCCGGCAGCAGCAGCTGGTGCCGGTGCTCAGCAGCATCATCATCATCACCATTAAGGATCC

Fig. A 16 NusAHPL$_{SB\text{-}N}$ fusion protein sequence and *nusAhpl*$_{SB\text{-}N}$ fusion gene sequence with His6-tag marked in grey and restriction sites underlined. Enterokinase cleavage site is marked blue.

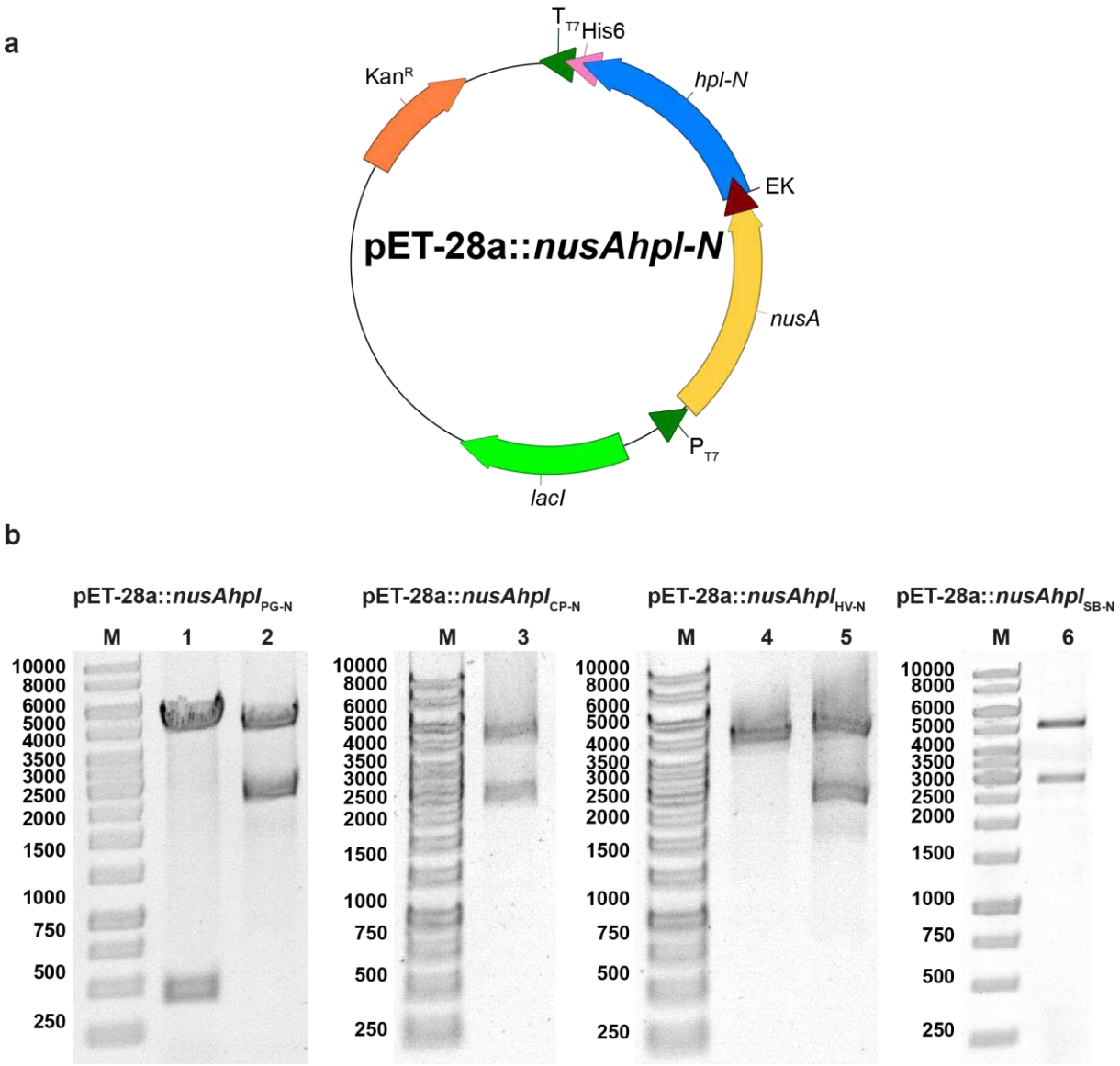

Fig. A 17 Expression vector pET-28a::*NusAhpl* (**a**) for expression of fusion proteins with NusA and HPL_{PG-N} = *P. guajava*, HPL_{CP-N} = *C. papaya,* HPL_{HV-N} = *H. vulgare* and HPL_{SB-N} = *S. bicolor* and agarose gels of restriction digests of pET-28a::*nusAhpl-N* (**b**) with *Nde*I and *Bam*HI. M: DNA ladder marker with sizes in bp.

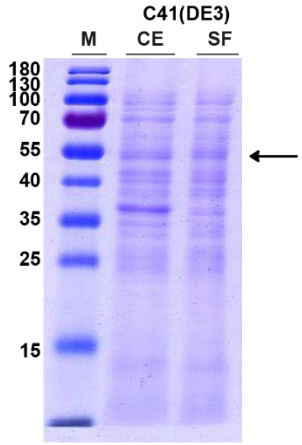

Fig. A 18 SDS-PAGE of HPL_{CP-N} expression in *E. coli* C41(DE3). M: protein marker with sizes in kDa, CE: crude extract and SF: soluble fraction.

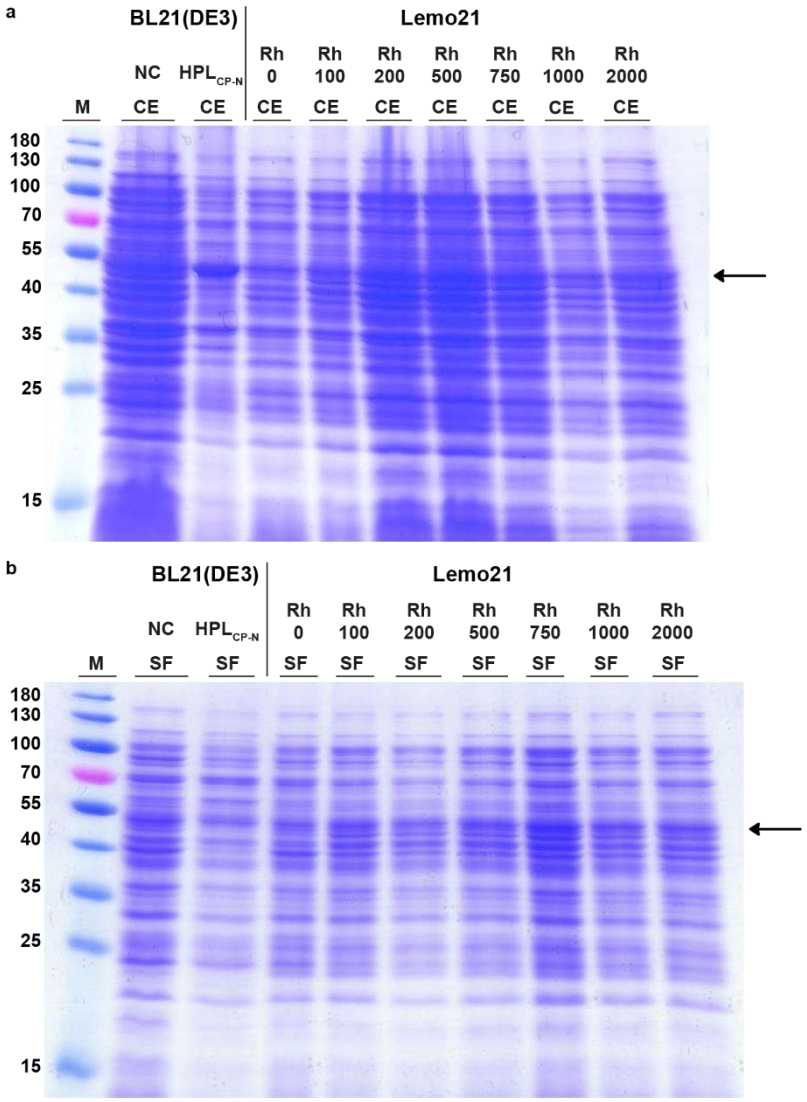

Fig. A 19 SDS-PAGEs of HPL_{CP-N} expression in *E. coli* Lemo21 and BL21(DE3) in the crude extract (**a**) and the soluble fraction (**b**). For expression with Lemo21, rhamnose (Rh) was added in concentrations ranging from 0 to 2000 µM. M: protein marker with sizes in kDa, NC: negative control, CE: crude extract and SF: soluble fraction.

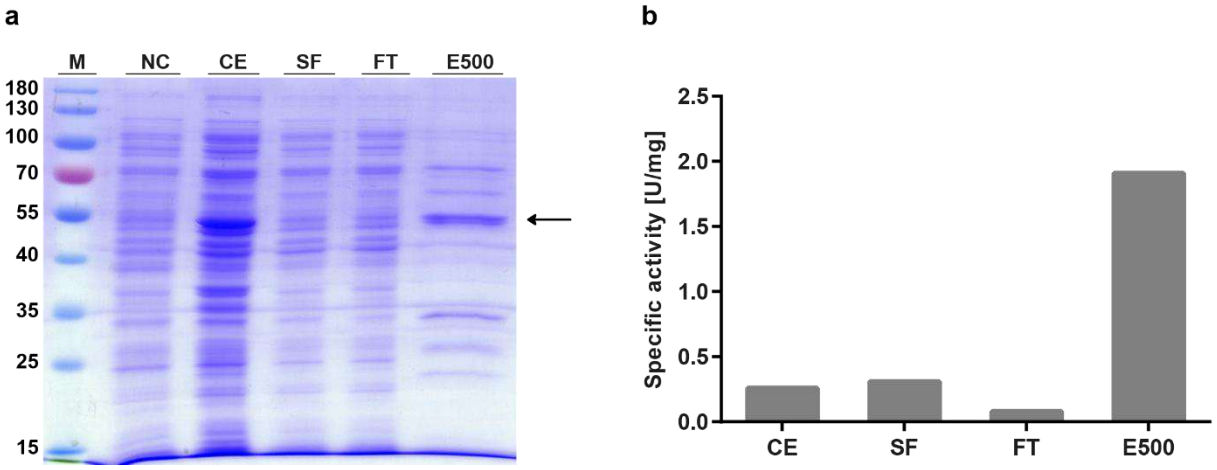

Fig. A 20 Initial purification process of HPL_{CP-N}, determined by SDS-PAGE (**a**) and photometrical enzyme assay (**b**). M: protein marker with sizes in kDa, NC: negative control, CE: crude extract, SF: soluble fraction, FT: flow through and E500: elution with 500 mM imidazole.

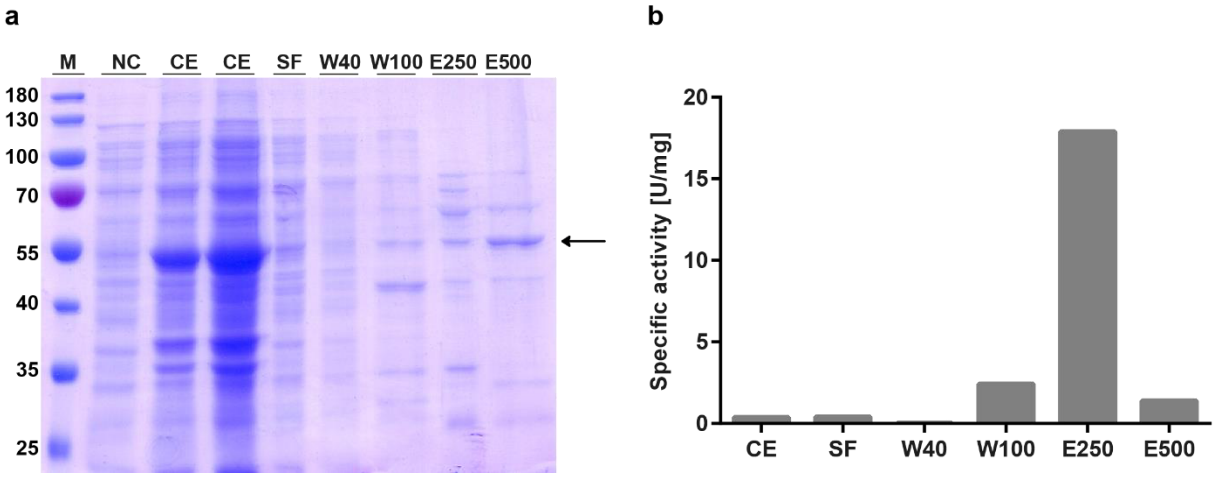

Fig. A 21 Purification process of HPL_{CP-N} purification using a gradient of imidazole for elution, determined by SDS-PAGE (**a**) and photometrical enzyme assay (**b**). M: protein marker with sizes in kDa, NC: negative control, CE: crude extract, SF: soluble fraction, W40: washing fraction with 40 mM imidazole, W100: washing fraction with 100 mM, E250: elution with 250 mM imidazole and E500: elution with 500 mM imidazole.

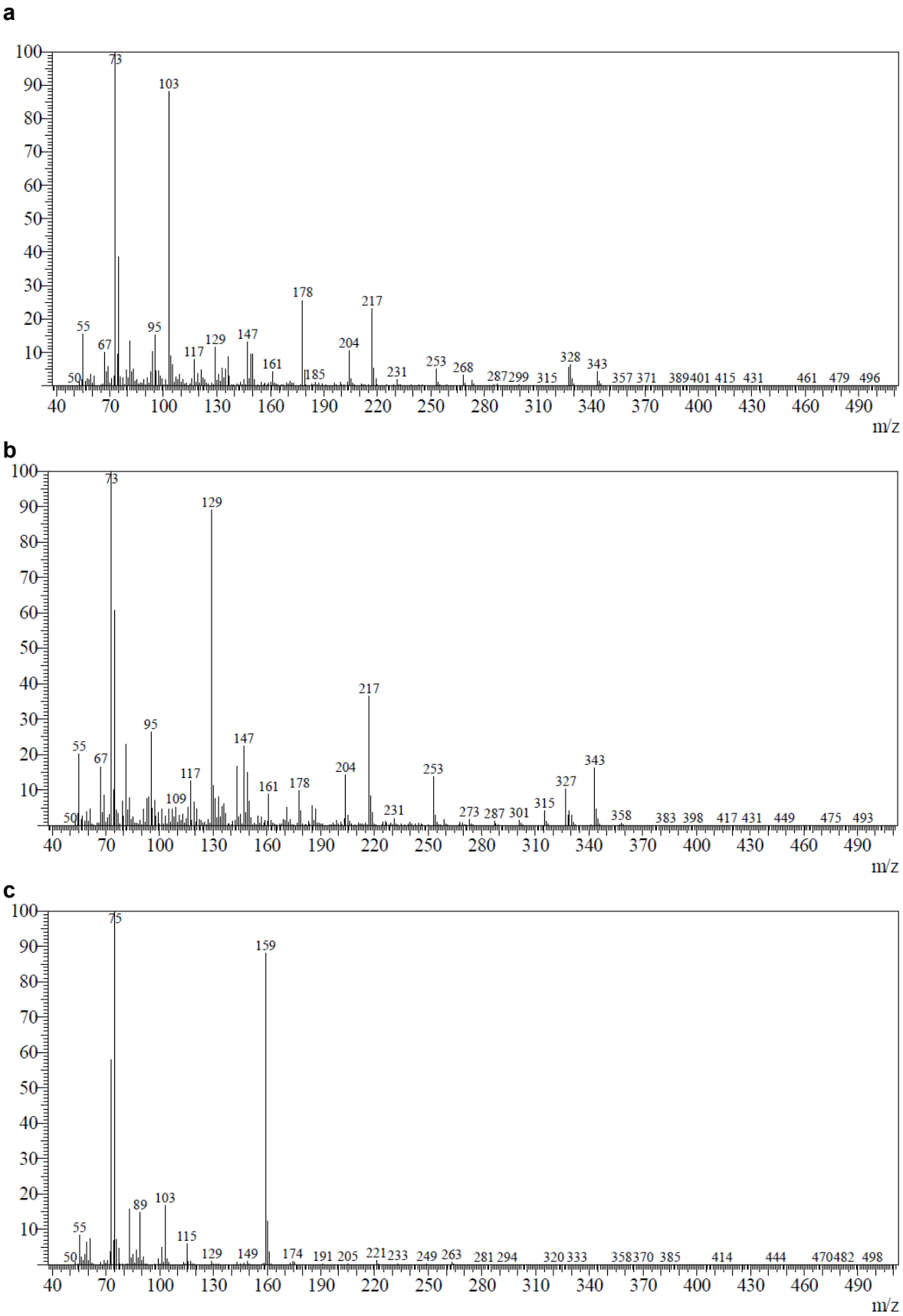

Fig. A 22 Mass spectra of reference standards analyzed with GC-MS of (**a**) 12-oxo-9(*Z*)-dodecenoic acid, (**b**) 12-oxo-10(*E*)-dodecenoic acid and (**c**) hexanal. Samples were hydrogenated with sodium borohydride and silylated with BSTFA-TMCS. Figure modified and reproduced from [175] with permission from Springer Nature.

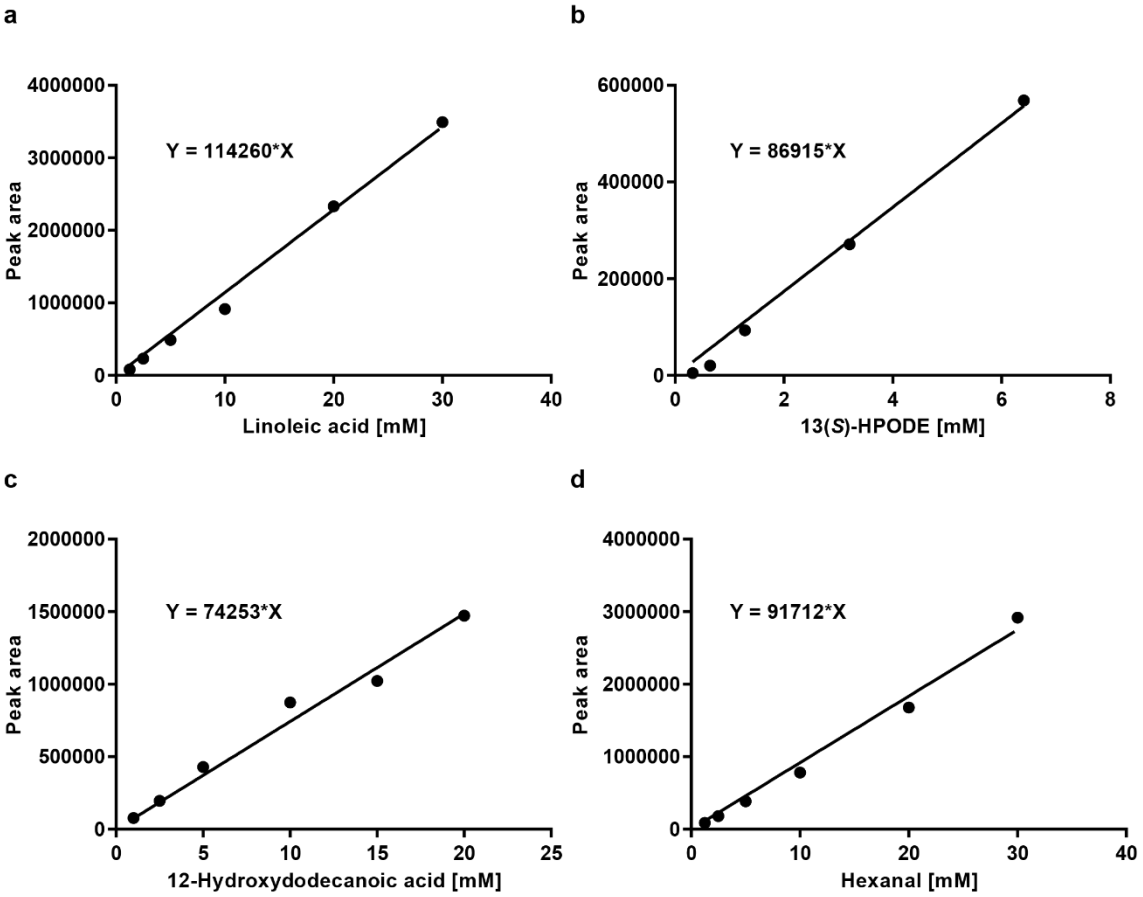

Fig. A 23 Calibration curves of hydrogenated and silylated linoleic acid (**a**), 13(*S*)-HPODE (**b**), 12-hydroxydodecanoic acid (**c**) and hexanal (**d**), measured on GC-FID. Linear regression was conducted with GraphPad Prism 6.05.

>TR_{CV}

MQKQRTTSQWRELDAAHHLHPFTDTASLNQAGARVMTRGEGVYLWDSEGNKIIDGMAGLWCVNVGYGRKDFAE
AARRQMEELPFYNTFFKTTHPAVVELSSLLAEVTPAGFDRVFYTNSGSESVDTMIRMVRRYWDVQGKPEKKTLIG
RWNGYHGSTIGGASLGGMKYMHEQGDLPIPGMAHIEQPWWYKHGKDMTPDEFGVVAARWLEEKILEIGADKVA
AFVGEPIQGAGGVIVPPATYWPEIERICRKYDVLLVADEVICGFGRTGEWFGHQHFGFQPDLFTAAKGLSSGYLPIGA
VFVGKRVAEGLIAGGDFNHGFTYSGHPVCAAVAHANVAALRDEGIVQRVKDDIGPYMQKRWRETFSRFEHVDDVR
GVGMVQAFTLVKNKAKRELFPDFGEIGTLCRDIFFRNNLIMRACGDHIVSAPPLVMTRAEVDEMLAVAERCLEEFE
QTLKARGLAHHHHHH*

>*tr_{CV}* codon-optimized

CATATGCAGAAACAGCGTACCACCAGTCAGTGGCGTGAACTGGATGCAGCCCATCATCTGCATCCGTTCACCGATA
CCGCCAGCCTGAATCAGGCCGGCGCCCGTGTGATGACCCGTGGTGAAGGTGTGTATCTGTGGGATAGTGAAGGTA
ATAAAATTATTGACGGTATGGCCGGTCTGTGGTGCGTGAATGTGGGCTATGGCCGTAAAGACTTCGCAGAAGCAG
CACGTCGCCAGATGGAAGAACTGCCGTTCTATAATACCTTCTTCAAAACCACCCATCCGGCAGTTGTTGAACTGAG
TAGTCTGCTGGCAGAAGTTACCCCGGCAGGCTTCGATCGTGTGTTCTATACCAATAGTGGTAGTGAAAGTGTGGA
TACCATGATTCGCATGGTGCGTCGTTATTGGGATGTGCAGGGCAAACCGGAAAAAAAAAACCTTAATTGGCCGTTG
GAATGGTTATCATGGTAGTACCATTGGTGGTGCAAGTCTGGGTGGTATGAAATATATGCATGAACAGGGCGATCT
GCCGATTCCGGGCATGGCACATATTGAACAGCCGTGGTGGTATAAACATGGCAAAGATATGACCCCGGATGAATT
CGGTGTTGTGGCAGCACGTTGGCTGGAAGAAAAAATTCTGGAAATTGGCGCCGATAAAGTTGCCGCCTTCGTGGG
CGAACCGATTCAGGGTGCAGGTGGTGTTATTGTTCCGCCGGCAACCTATTGGCCGGAAATTGAACGTATCTGTCG
CAAATATGATGTTCTGCTGGTGGCCGATGAAGTGATCTGTGGCTTCGGCCGCACCGGTGAATGGTTCGGTCATCA
GCACTTCGGCTTCCAGCCGGATCTGTTCACCGCCGCAAAAGGCCTGAGCAGCGGCTATCTGCCGATTGGCGCAGTG
TTCGTGGGTAAACGTGTTGCAGAAGGCCTGATTGCAGGTGGTGACTTCAATCATGGCTTCACCTATAGTGGCCAT
CCGGTGTGTGCCGCCGTGGCCCATGCAAATGTTGCCGCCCTGCGCGATGAAGGCATTGTTCAGCGCGTTAAAGATG
ATATTGGTCCGTATATGCAGAAACGTTGGCGTGAAACCTTCAGCCGCTTCGAACATGTTGATGATGTTCGCGGCG
TGGGTATGGTGCAGGCATTCACCCTGGTTAAAAATAAAGCAAAACGCGAACTGTTCCCGGACTTCGGTGAAATTG
GCACCCTGTGTCGTGATATCTTCTTCCGTAATAATCTGATTATGCGTGCCTGTGGCGATCATATTGTTAGCGCACC
GCCGCTGGTTATGACCCGCGCCGAAGTGGATGAAATGCTGGCAGTGGCAGAACGTTGCCTGGAAGAATTCGAACA
GACCCTGAAAGCACGCGGTCTGGCACATCATCATCATCACCATTAAGGATCC

Fig. A 24 Protein sequence of ω-transaminase TR_{CV} from *C. violaceum* and codon-optimized *tr_{CV}* gene sequence with His6-tag marked in grey and restriction sites underlined.

>TR_{SD}

MPSITNHLPTAELQALDSAHHMHPFTTNDELTQKGARVITRAKGIYLTDSEGNEILDAMAGLWCVNLG
YGREEMGQVAARQMNELPYYNTFFQTTHVPAIALAKELADLAPGDLNYVFFAGSGSEANDTNLRMVRT
YWAQKGKPEKSHVISRKNAYHGSSVGSASLGGMTPMHEQGGLPIPGIHHIGQPDWWAEGGDQSPEEFG
LARARELEDKILELGADNVAAFIGEPIQGAGGVVIPPSTYWPEIQRICDKHDVLLIADEVICGFGRTGNWF
GSQTMGIKPHIMTIAKGLSSGYAPIGGSIVCDEVAEVINACEFNHGYTYSGHPVCAAVALENLRIMQEENII
DHVQNVAAPALQEALNKLGEHPLVGGVNVSGLMASLPLTPHKESRAKFASDAGTAGYLCREHCFANNL
VMRHVGDRMIISPPLIITPEEIAIFADRATRALDATYADLKDKDLLKAASHHHHHH*

>*tr_{SD}* codon-optimized

CATATGCCGAGTATTACCAATCATCTGCCGACCGCCGAACTGCAGGCACTGGATAGCGCCCATCACATG
CATCCGTTCACCACCAATGATGAACTGACCCAGAAAGGTGCCCGTGTGATTACCCGTGCAAAAGGCATC
TATCTGACCGATAGTGAAGGCAATGAAATTCTGGATGCCATGGCCGGCCTGTGGTGTGTTAATCTGGG
CTATGGTCGCGAAGAAATGGGTCAGGTTGCAGCACGCCAGATGAATGAACTGCCGTATTATAATACCT
TCTTCCAGACCACCCATGTTCCGGCCATTGCACTGGCCAAAGAACTGGCCGATCTGGCCCCGGGTGATC
TGAATTATGTGTTCTTCGCCGGCAGCGGTAGCGAAGCCAATGATACCAATCTGCGTATGGTGCGTACCT
ATTGGGCACAGAAAGGCAAACCGGAAAAAAGTCATGTGATTAGTCGCAAAAATGCATATCATGGTAGC
AGTGTGGGTAGCGCCAGTCTGGGTGGTATGACCCCGATGCATGAACAGGGTGGTCTGCCGATTCCGGG
CATTCATCATATTGGTCAGCCGGATTGGTGGGCAGAAGGTGGTGATCAGAGTCCGGAAGAATTCGGCC
TGGCACGCGCACGTGAACTGGAAGATAAAATTCTGGAACTGGGCGCAGATAATGTGGCCGCATTCATT
GGCGAACCGATTCAGGGTGCAGGTGGTGTTGTGATTCCGCCGAGCACCTATTGGCCGGAAATTCAGCGC
ATCTGTGATAAACATGATGTTCTGCTGATTGCAGATGAAGTTATCTGTGGCTTCGGTCGCACCGGCAA
TTGGTTCGGTAGCCAGACCATGGGCATTAAACCGCATATTATGACCATTGCCAAAGGTCTGAGCAGCG
GCTATGCCCCGATTGGTGGCAGCATTGTGTGTGATGAAGTGGCCGAAGTGATTAATGCATGTGAATTC
AATCATGGCTATACCTATAGTGGTCATCCGGTGTGTGCCGCAGTTGCACTGGAAAATCTGCGTATTAT
GCAGGAAGAAAATATTATTGACCACGTTCAGAATGTGGCAGCACCGGCCCTGCAGGAAGCACTGAATA
AACTGGGTGAACATCCGCTGGTGGGTGGCGTTAATGTGAGTGGTCTGATGGCCAGCCTGCCGCTGACCC
CGCATAAAGAAAGTCGTGCAAAATTCGCAAGTGATGCCGGCACCGCAGGCTATCTGTGCCGTGAACAT
TGCTTCGCAAATAATCTGGTGATGCGTCATGTGGGCGATCGTATGATTATTAGTCCGCCGCTGATTAT
TACCCCGGAAGAAATTGCAATCTTCGCCGATCGCGCAACCCGTGCCCTGGATGCCACCTATGCAGATCT
GAAAGATAAAGATCTGCTGAAAGCAGCAAGCCATCATCATCATCACCATTAAGGATCC

Fig. A 25 Protein sequence of ω-transaminase TR_{SD} from *S. delicatus* and codon-optimized *tr_{SD}* gene sequence with His6-tag marked in grey and restriction sites underlined.

>TR_{AD}

MQNQRTTTEWRELDAAHHLHPFTDTNSLNQQGARVITKADGIYLYDSEGNKILDGMAGLWCVNIGYGRKDLPEV
AKQQMEQLAYYNTFFKTTHPAVVELSHLLAEVAPEGFKQVFYTNSGSESVDTMIRMVRRYWDVKGKKDKKTLIGR
WNGYHGSTIGGASLGGMTYMHEQGDLPIPGIVHVEQPWWYKHGKDMTPEEFGLAAAKWVEDKILEVGADKVAA
FVGEPIQGAGGVIVPPSTYWPEIQRICQKYDILLVADEVICGFGRTGEWFGQQVFGFKPDIFTTAKGLSSGYQPIGAVF
VNEKVATTLAEGGDFNHGFTYSGHPVAAAVAHANVKALRDEGIVDRVKNDTGPYMQKRWREVFGQFEHVDDVR
GVGLIQAFTLVKNKATRELFPNFGEIGTMCRDIFFKNNLIMRACGDHIVSAPPLVISKEEIDQMLETAAKCMVEFEK
QLKERGLVHHHHHH*

>*tr_{AD}* codon-optimized

CATATGCAGAATCAGCGTACCACCACCGAATGGCGTGAACTGGATGCAGCACATCATCTGCATCCGTTCACCGATA
CCAATAGTCTGAATCAGCAGGGTGCACGCGTGATTACCAAAGCCGATGGCATCTATCTGTATGATAGTGAAGGCA
ATAAAATCCTGGATGGTATGGCCGGCCTGTGGTGCGTTAATATTGGCTATGGCCGTAAAGATCTGCCGGAAGTTG
CAAAACAGCAGATGGAACAGCTGGCCTATTATAATACCTTCTTCAAAACCACCCATCCGGCAGTGGTTGAACTGA
GTCATCTGCTGGCCGAAGTTGCACCGGAAGGCTTCAAACAGGTGTTCTATACCAATAGTGGTAGTGAAAGTGTGG
ATACCATGATTCGCATGGTTCGCCGCTATTGGGATGTTAAAGGTAAAAAAGATAAGAAGACCCTGATTGGTCGCT
GGAATGGCTATCATGGTAGCACCATTGGTGGTGCAAGTCTGGGCGGTATGACCTATATGCATGAACAGGGTGATC
TGCCGATTCCGGGTATTGTGCATGTTGAACAGCCGTGGTGGTATAAACATGGCAAAGATATGACCCCGGAAGAAT
TCGGCCTGGCAGCAGCAAAATGGGTGGAAGATAAAATTCTGGAAGTGGGCGCCGATAAAGTTGCAGCATTCGTTG
GCGAACCGATTCAGGGTGCCGGCGGCGTGATTGTGCCGCCTAGTACCTATTGGCCGGAAATTCAGCGTATCTGTCA
GAAATATGATATTCTGCTGGTGGCAGATGAAGTGATCTGTGGCTTCGGTCGTACCGGTGAATGGTTCGGTCAGCA
GGTGTTCGGCTTCAAACCGGATATCTTCACCACCGCCAAAGGTCTGAGTAGTGGCTATCAGCCGATTGGTGCAGTG
TTCGTTAATGAAAAAGTTGCAACCACCCTGGCCGAAGGCGGCGACTTCAATCATGGCTTCACCTATAGCGGTCATC
CGGTTGCAGCCGCCGTTGCCCATGCCAATGTTAAAGCCCTGCGTGATGAAGGCATTGTTGATCGCGTTAAAAATG
ATACCGGCCCGTATATGCAGAAACGTTGGCGCGAAGTGTTCGGCCAGTTCGAACATGTGGATGATGTGCGCGGCG
TTGGCCTGATTCAGGCCTTCACCCTGGTGAAAAATAAAGCAACCCGCGAACTGTTCCCGAACTTCGGCGAAATTGG
TACCATGTGTCGCGATATCTTCTTCAAAAATAATCTGATTATGCGCGCCTGTGGCGATCATATTGTTAGCGCACCG
CCGCTGGTTATTAGTAAAGAAGAAATTGATCAGATGCTGGAAACCGCAGCAAAATGTATGGTGGAATTCGAAAA
ACAGCTGAAAGAACGTGGTCTGGTTCATCATCATCATCACCATTAAGGATCC

Fig. A 26 Protein sequence of ω-transaminase TR_{AD} from *A. denitrificans* and codon-optimized *tr_{AD}* gene sequence with His6-tag marked in grey and restriction sites underlined.

>TR_{PD}

MNQPQSWEARAETYSLYGFTDMPSVHQRGTVVVTHGEGPYIVDVHGRRYLDANSGLWNMVAGFDHKGLIEAAK
AQYDRFPGYHAFFGRMSDQTVMLSEKLVEVSPFDNGRVFYTNSGSEANDTMVKMLWFLHAAEGKPQKRKILTRW
NAYHGVTAVSASMTGKPYNSVFGLPLPGFIHLTCPHYWRYGEEGETEAQFVARLARELEDTITREGADTIAGFFAE
PVMGAGGVIPPAKGYFQAILPILRKYDIPMISDEVICGFGRTGNTWGCLTYDFMPDAIISSKNLTAGFFPMGAVILGP
DLAKRVEAAVEAIEEFPHGFTASGHPVGCAIALKAIDVVMNEGLAENVRRLAPRFEAGLKRIADRPNIGEYRGIGFM
WALEAVKDKPTKTPFDANLSVSERIANTCTDLGLICRPLGQSIVLCPPFILTEAQMDEMFEKLEKALDKVFAEVAH
HHHHH*

>*tr_{PD}* codon-optimized

CATATGAACCAGCCGCAGAGTTGGGAAGCCCGCGCAGAAACCTATAGTCTGTATGGCTTCACCGATATGCCGAGC
GTTCATCAGCGCGGCACCGTGGTTGTTACCCATGGTGAAGGCCCGTATATTGTGGATGTTCATGGCCGCCGTTATC
TGGATGCCAATAGCGGTCTGTGGAATATGGTTGCCGGCTTCGATCATAAAGGTCTGATTGAAGCAGCAAAAGCCC
AGTATGATCGCTTCCCGGGTTATCATGCCTTCTTCGGTCGTATGAGCGATCAGACCGTGATGCTGAGCGAAAAAC
TGGTTGAAGTGAGTCCGTTCGATAATGGTCGCGTGTTCTATACCAATAGCGGTAGCGAAGCCAATGATACCATGG
TGAAAATGCTGTGGTTCCTGCATGCAGCAGAAGGCAAACCGCAGAAACGTAAAATTCTGACCCGTTGGAATGCAT
ATCATGGTGTGACCGCCGTTAGCGCCAGTATGACCGGTAAACCGTATAATAGTGTGTTCGGCCTGCCGCTGCCGGG
CTTCATTCATCTGACCTGTCCGCATTATTGGCGTTATGGTGAAGAAGGCGAAACCGAAGCACAGTTCGTTGCCCGC
CTGGCCCGCGAACTGGAAGATACCATTACCCGCGAAGGCGCCGATACCATTGCAGGCTTCTTCGCCGAACCGGTTA
TGGGCGCCGGTGGTGTTATTCCGCCGGCCAAAGGCTACTTCCAGGCAATTCTGCCGATTCTGCGTAAATATGATAT
TCCGATGATTAGCGATGAAGTGATCTGTGGCTTCGGTCGTACCGGTAATACCTGGGGTTGCCTGACCTATGACTTC
ATGCCGGATGCAATTATTAGCAGCAAAAATCTGACCGCCGGCTTCTTCCCGATGGGTGCCGTTATTCTGGGTCCGG
ATCTGGCAAAACGTGTTGAAGCAGCAGTGGAAGCAATTGAAGAATTCCCGCATGGCTTCACCGCAAGTGGCCATC
CGGTTGGTTGTGCAATTGCCCTGAAAGCCATTGATGTGGTTATGAATGAAGGTCTGGCCGAAAATGTGCGTCGCC
TGGCCCCGCGCTTCGAAGCTGGTCTGAAACGCATTGCCGATCGCCCGAATATTGGCGAATATCGCGGTATTGGCTT
CATGTGGGCCCTGGAAGCCGTTAAAGATAAACCGACCAAAACACCGTTCGATGCCAATCTGAGTGTGAGCGAACG
CATTGCAAATACCTGTACCGATCTGGGCCTGATCTGTCGCCCGCTGGGTCAGAGTATTGTGCTGTGTCCGCCGTTC
ATTCTGACCGAAGCCCAGATGGATGAAATGTTCGAAAAACTGGAAAAAGCACTGGATAAAGTGTTCGCCGAAGTT
GCCCATCATCATCATCACCATTAAGGATCC

Fig. A 27 Protein sequence of ω-transaminase TR_{PD} from *P. denitrificans* and codon-optimized *tr_{PD}* gene sequence with His6-tag marked in grey and restriction sites underlined.

>TR2

MSQSQRSTADWQRLDAAHHLHPFTDYGELNTKGSRIITRAEGCYLWDSDGNQILDGMAGLWCVNIGYGRKELAE
VAYRQMQELPYYNNFFQCSHPPAIELSRLLSEVTPKHMNHVFFTGSGSDSNDTILRMVRYYWKLLGKPYKKVVISR
ENAYHGSTVAGASLSGMKAMHAQGDLPIPGIEHIEQPYHFGRAPDMDPAEFGRQAAQALERKIDEIGECNVAAFIA
EPIQGAGGVIIPPDSYWPEIKRICAERDILLIVDEVITGFGRLGTWFGSQYYDLQPDLMPIAKGLSSGYMPIGGVMVSD
RVAKVVIEEGGEFFHGYTYSGHPVAAAVAAENIRIMRDEGIIERAGAEIAPYLQARWRELGEHPLVGEARGVGMVA
ALELVKSKQPLERFEEPGKVGSLCRDLSVKNGLVMRAVGGTMIISPPLVLSREQVDELIDKARRTLDETHKAIGGAH
HHHHH*

>*tr2*

ATGAGTCAATCGCAACGCTCCACCGCAGACTGGCAGCGCCTCGACGCCGCCCACCACCTGCACCCGTTCACCGACT
ACGGCGAACTCAATACCAAGGGCTCGCGCATCATCACGCGTGCCGAAGGCTGTTACCTGTGGGATTCCGACGGCAA
CCAGATCCTGGACGGCATGGCCGGCCTGTGGTGCGTCAACATCGGCTACGGGCGCAAGGAACTCGCCGAAGTCGCC
TACAGGCAGATGCAGGAACTGCCCTACTACAACAACTTCTTCCAATGCAGCCATCCGCCGGCCATCGAGCTGTCGC
GGCTGCTGTCCGAGGTCACTCCCAAGCACATGAACCATGTGTTCTTCACCGGCTCGGGCTCGGACTCCAACGACAC
CATCCTGCGCATGGTGCGCTACTACTGGAAGCTGCTCGGCAAGCCCTACAAGAAGGTCGTCATCTCGCGTGAGAAC
GCCTACCACGGCAGCACCGTGGCCGGCGCCAGCCTGAGCGGCATGAAAGCCATGCACGCGCAGGGCGACCTGCCGA
TTCCCGGCATCGAACATATCGAACAGCCCTACCACTTCGGCCGCGCGCCGGACATGGACCCGGCCGAATTCGGCCG
CCAGGCCGCGCAGGCGCTGGAGCGCAAGATCGACGAGATCGGCGAGTGCAACGTCGCTGCCTTCATCGCCGAGCCC
ATCCAGGGCGCCGGCGGCGTGATCATCCCGCCGGACAGCTACTGGCCGGAGATCAAGCGCATCTGCGCCGAACGCG
ACATCCTGTTGATCGTCGACGAGGTCATCACCGGCTTCGGTCGCCTGGGCACCTGGTTCGGCTCGCAGTACTACGA
CCTCCAGCCGGATCTCATGCCCATCGCCAAGGGTCTGTCCTCGGGCTACATGCCGATCGGCGGCGTGATGGTTTCC
GACCGCGTGGCCAAGGTCGTCATCGAGGAAGGCGGCGAGTTCTTCCACGGCTATACCTACTCCGGCCATCCGGTGG
CGGCAGCGGTTGCCGCGGAGAACATCCGCATCATGCGCGACGAAGGCATCATCGAACGCGCCGGCGCGGAGATCGC
ACCGTACCTGCAGGCCCGCTGGCGCGAGCTGGGCGAGCATCCGCTGGTCGGCGAGGCGCGCGGCGTGGGCATGGTG
GCAGCCTTGGAACTGGTCAAATCCAAGCAGCCCCTGGAGCGCTTCGAGGAGCCCGGCAAGGTCGGCAGCCTGTGCC
GCGACCTGAGCGTCAAGAACGGCCTGGTGATGCGCGCGGTGGGCGGCACGATGATCATTTCGCCGCCGTTGGTTCT
CAGCCGCGAACAGGTCGACGAGCTCATCGACAAGGCCCGCAGGACGCTGGACGAAACGCACAAGGCGATCGGCGG
CGCCCATCATCATCATCACCATTGA

Fig. A 28 Protein sequence of ω-transaminase TR_2 from *Acidihalobacter* sp. and codon-optimized *tr_2* gene sequence with His6-tag marked in grey and restriction sites underlined.

>TR3
MKDENFLKENNARHLWHPMGAPGDLQANTPKIITGASGVSITDIDGHQTVDAVGGLWCVNLGYSNDVVKEAIAK
QLYDLPYYSAFAGTSNPPAIEASYAVREFFAEDGMGRVFFTSGGSDSVETALRLARQYHRLRGEPTRTKYISLKKGY
HGTHFGGASVNGNNRFRINYEPLLPGCFHLPSPYPYRNPFNETDPAQLAQNIAAAFEDEIAFQDANTIAAFIMEPIQ
GAGGVIVPDASFMGLMRDICDRHGILLISDEVITGFGRTGDWSGARHWGVKPDLMTTAKGITSGYFPVGACLLSEA
VAEVFEKDTSGEAAIYHGYTYSAHPVGAAAVVATLAETQRLDLKTNAAARGTQLFEGVKKLAEKHDIIGDVRGGHG
LMTGIEIVSDKAAKTPMDNETMKRIHQTAYEAGAMVRLGAHNVLMSPPLTISEAEVNTILTALDAGFSAAHHHHH
H*

>*tr3*

ATGAAAGACGAAAACTTCCTCAAGGAAAACAACGCCCGCCACCTCTGGCACCCGATGGGCGCCCCCGGTGATTTGC
AGGCCAACACGCCAAAAATCATCACCGGTGCCTCGGGCGTCTCGATCACCGACATTGACGGCCACCAAACCGTCGA
CGCCGTGGGCGGGCTCTGGTGCGTCAACCTCGGCTACTCCAACGACGTGGTGAAAGAGGCGATCGCCAAACAACTC
TACGATCTGCCCTACTACTCCGCCTTCGCCGGAACCTCGAACCCGCCCGCCATCGAAGCGTCCTACGCCGTGCGCGA
ATTCTTTGCCGAGGACGGCATGGGCCGCGTCTTCTTTACCTCCGGCGGCAGCGACAGCGTCGAAACCGCCCTGCGC
CTCGCGCGTCAGTATCACCGCCTGCGCGGCGAACCGACCCGCACCAAATATATCTCGCTCAAAAAAGGCTACCACG
GCACGCATTTCGGCGGTGCGTCGGTCAACGGCAACAACCGGTTCCGCATCAACTACGAACCGCTCCTGCCGGGCTG
CTTCCACCTGCCCTCGCCCTACCCCTACCGTAACCCCTTCAACGAAACCGATCCGGCCCAGCTCGCTCAGAACATCG
CCGCCGCGTTTGAAGACGAAATCGCCTTTCAGGACGCGAACACCATCGCCGCCTTCATCATGGAACCGATCCAAGG
CGCGGGCGGTGTCATCGTGCCGGACGCGAGTTTCATGGGCCTCATGCGCGACATCTGTGACCGCCACGGCATCCTG
CTGATCTCGGACGAAGTCATCACCGGCTTTGGCCGCACCGGCGACTGGTCCGGCGCACGTCACTGGGGCGTCAAAC
CCGACCTGATGACCACCGCCAAGGGCATCACCTCGGGCTATTTCCCCGTCGGCGCCTGCCTCCTGAGCGAAGCCGT
GGCCGAAGTCTTTGAAAAAGACACCAGCGGCGAAGCGGCTATCTATCACGGCTACACCTACTCGGCCCACCCGGTC
GGCGCGGCCGCCGTTGTGGCCACACTCGCCGAAACCCAACGCCTCGACCTCAAGACCAACGCTGCCGCCCGCGGCA
CCCAACTCTTTGAGGGCGTAAAGAAACTTGCCGAGAAACACGACATCATCGGCGATGTGCGCGGCGGCCATGGCCT
CATGACCGGGATCGAAATCGTCTCGGACAAAGCGGCCAAGACCCCGATGGACAACGAGACCATGAAACGCATCCA
CCAAACCGCCTACGAGGCCGGTGCCATGGTGCGTCTGGGCGCACATAACGTGCTCATGTCCCCGCCCCTGACCATC
TCCGAGGCCGAAGTGAACACGATCCTCACCGCCCTCGACGCAGGCTTCTCCGCCGCGCATCATCATCATCACCATT
AA

Fig. A 29 Protein sequence of ω-transaminase TR_3 from *Rhodobacteraceae* bacteria and codon-optimized *tr_3* gene sequence with His6-tag marked in grey and restriction sites underlined.

>TR6

MVQITNHMPTAELQALDAAHHMHPFTTQSELAERGARVITRAEGAYIYDSEGNKILDGMAGLWCVNIGYGRQELV
DVAARQMAELPYYNTFFMTTHVPAIALSAKLAELAPAHLNHVFYSSSGSEANDTNIRLVRTYWAEKGKPSKSIIISR
HNAYHGSTLGGASLGGMGGMHAQGGLPIPDIHHIDQPNWWAEGGDMDPAEFGLERAQQLEKAILKLGEDRVAAF
IAEPVQGAGGVIVPPETYWPEIQRICDKYEILLIADEVICGFGRTGNWFGSETVGWKPDIMTIAKGLSSGYQPIGGSIV
SDEIATVIGNCEFNHGYTYHAHPVAAAVALENLRILDEEGIVARVRDETGPYLAQKWAAMADHPMVGEASIVGMM
GSIALTPNKSTRATFKAEAGTVGYICRERCFANNLVMRHVGDRMIISPPLTLTRDEIDLLIERAWKSLDEGMAEVKK
QGLWQEGHHHHHH*

>*tr6*

ATGGTCCAGATCACCAACCACATGCCCACCGCCGAATTGCAGGCGCTGGATGCCGCGCACCACATGCACCCGTTTA
CCACGCAATCCGAACTGGCCGAACGTGGCGCGCGGGTCATCACCCGTGCCGAGGGCGCGTATATTTATGACTCCGA
GGGCAATAAAATTCTGGATGGCATGGCCGGTTTGTGGTGTGTCAACATCGGTTATGGTCGTCAGGAACTGGTCGA
TGTGGCGGCGCGCCAAATGGCGGAACTGCCCTATTACAACACGTTTTTCATGACCACCCATGTGCCCGCGATTGCC
CTGTCCGCCAAACTGGCCGAACTGGCGCCCGCGCATCTGAACCACGTGTTCTATTCCTCTTCGGGGTCCGAAGCGA
ACGATACCAACATCCGTTTGGTGCGCACCTATTGGGCCGAAAAGGGCAAGCCGTCGAAATCCATTATCATCAGCCG
CCACAACGCCTATCACGGGTCCACCCTTGGCGGTGCCAGCCTTGGCGGTATGGGCGGTATGCACGCACAGGGCGGC
CTGCCGATTCCCGATATTCATCATATTGATCAACCGAACTGGTGGGCCGAGGGCGGCGATATGGACCCTGCCGAAT
TTGGTCTGGAACGCGCGCAACAGCTGGAAAAGGCGATTCTGAAACTGGGCGAGGACCGCGTTGCCGCCTTTATCG
CCGAACCCGTGCAGGGGGCTGGTGGTGTGATCGTGCCGCCAGAAACCTATTGGCCGGAAATTCAGCGCATTTGCG
ACAAATACGAAATCCTGCTGATCGCAGACGAGGTGATCTGCGGTTTCGGGCGCACCGGCAACTGGTTCGGGTCTG
AAACCGTGGGCTGGAAACCCGACATCATGACCATCGCCAAGGGCCTGTCGTCAGGGTATCAGCCCATCGGCGGCTC
GATTGTGTCCGACGAAATCGCCACAGTGATTGGCAACTGCGAATTCAATCATGGTTATACCTATCATGCCCATCCG
GTGGCTGCTGCGGTGGCCTTGGAAAACCTGCGCATTCTGGACGAAGAGGGCATAGTCGCCCGTGTTAGAGACGAA
ACTGGCCCCTATCTGGCGCAGAAATGGGCGGCGATGGCCGACCACCCGATGGTGGGAGAGGCCAGCATCGTGGGC
ATGATGGGGTCTATTGCTTTGACCCCCAACAAATCAACCCGCGCCACGTTCAAGGCCGAGGCAGGCACCGTGGGTT
ACATCTGCCGCGAGCGTTGCTTTGCCAATAATCTGGTGATGCGCCATGTCGGCGACCGCATGATCATTTCACCGCC
GCTGACCCTGACCCGCGATGAGATCGACCTTTTGATTGAACGTGCATGGAAATCGCTGGACGAAGGCATGGCCGA
GGTCAAGAAACAGGGCCTGTGGCAAGAGGGACATCATCATCATCACCATTAG

Fig. A 30 Protein sequence of ω-transaminase TR_6 from *Rhodobacteraceae* bacteria and codon-optimized tr_6 gene sequence with His6-tag marked in grey and restriction sites underlined.

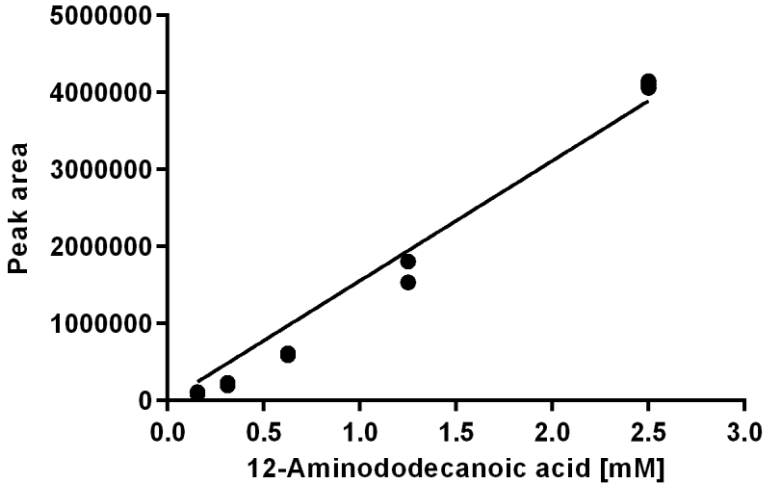

Fig. A 31 Calibration curve 12-aminododecanoic acid analyzed with HPLC-ELSD. Concentrations ranging from 0.15 to 2.5 mM were measured in triplicate and plotted against the peak area. Linear regression was performed with GraphPad Prism 6.05.

```
                ....|....| ....|....| ....|....| ....|....| ....|....|
                        10         20         30         40         50
TR3             ------MKDE NFLKENNARH LWHPMGAPGD LQANTPKIIT GASGVSITDI
TRPD            ------MNQP QSWEARAETY SLYGFTDMPS VHQRGTVVVT HGEGPYIVDV
TRSD            MPSITNHLPT AELQALDSAH HMHPFTTNDE LTQKGARVIT RAKGIYLTDS
TR6             MVQITNHMPT AELQALDAAH HMHPFTTQSE LAERGARVIT RAEGAYIYDS
TR2             --MSQSQRST ADWQRLDAAH HLHPFTDYGE LNTKGSRIIT RAEGCYLWDS
TRCV            ---MQKQRTT SQWRELDAAH HLHPFTDTAS LNQAGARVMT RGEGVYLWDS
TRAD            ---MQNQRTT TEWRELDAAH HLHPFTDTNS LNQQGARVIT KADGIYLYDS

                ....|....| ....|....| ....|....| ....|....| ....|....|
                        60         70         80         90        100
TR3             DGHQTVDAVG GLWCVNLGYS NDVVKEAIAK QLYDLPYYSA FAGTSNPPAI
TRPD            HGRRYLDANS GLWNMVAGFD HKGLIEAAKA QYDRFPGYHA FFGRMSDQTV
TRSD            EGNEILDAMA GLWCVNLGYG REEMGQVAAR QMNELPYYNT FFQTTHVPAI
TR6             EGNKILDGMA GLWCVNIGYG RQELVDVAAR QMAELPYYNT FFMTTHVPAI
TR2             DGNQILDGMA GLWCVNIGYG RKELAEVAYR QMQELPYYNN FFQCSHPPAI
TRCV            EGNKIIDGMA GLWCVNVGYG RKDFAEAARR QMEELPFYNT FFKTTHPAVV
TRAD            EGNKILDGMA GLWCVNIGYG RKDLPEVAKQ QMEQLAYYNT FFKTTHPAVV

                ....|....| ....|....| ....|....| ....|....| ....|....|
                       110        120        130        140        150
TR3             EASYAVREFF AEDGMGRVFF TSGGSDSVET ALRLARQYHR LRGEPTRTKY
TRPD            MLSEKLVEV- SPFDNGRVFY TNSGSEANDT MVKMLWFLHA AEGKPQKRKI
TRSD            ALAKELADL- APGDLNYVFF AGSGSEANDT NLRMVRTYWA QKGKPEKSHV
TR6             ALSAKLAEL- APAHLNHVFY SSSGSEANDT NIRLVRTYWA EKGKPSKSII
TR2             ELSRLLSEV- TPKHMNHVFF TGSGSDSNDT ILRMVRYYWK LLGKPYKKVV
TRCV            ELSSLLAEV- TPAGFDRVFY TNSGSESVDT MIRMVRRYWD VQGKPEKKTL
TRAD            ELSHLLAEV- APEGFKQVFY TNSGSESVDT MIRMVRRYWD VKGKKDKKTL

                ....|....| ....|....| ....|....| ....|....| ....|....|
                       160        170        180        190        200
TR3             ISLKKGYHGT HFGGASVNGN NRFRINYEPL LPGCFHLPSP YPYRNPFNET
TRPD            LTRWNAYHGV TAVSASMTGK PYN-SVFGLP LPGFIHLTCP HYWRYGEEGE
TRSD            ISRKNAYHGS SVGSASLGGM TPMHEQGGLP IPGIHHIGQP DWWAEGGDQ-
TR6             ISRHNAYHGS TLGGASLGGM GGMHAQGGLP IPDIHHIDQP NWWAEGGDM-
TR2             ISRENAYHGS TVAGASLSGM KAMHAQGDLP IPGIEHIEQP YHFGRAPDM-
TRCV            IGRWNGYHGS TIGGASLGGM KYMHEQGDLP IPGMAHIEQP WWYKHGKDM-
TRAD            IGRWNGYHGS TIGGASLGGM TYMHEQGDLP IPGIVHVEQP WWYKHGKDM-

                ....|....| ....|....| ....|....| ....|....| ....|....|
                       210        220        230        240        250
TR3             DPAQLAQNIA AAFEDEIAFQ DANTIAAFIM EPIQGAGGVI VPDASFMGLM
TRPD            TEAQFVARLA RELEDTITRE GADTIAGFFA EPVMGAGGVI PPAKGYFQAI
TRSD            SPEEFGLARA RELEDKILEL GADNVAAFIG EPIQGAGGVV IPPSTYWPEI
TR6             DPAEFGLERA QQLEKAILKL GEDRVAAFIA EPVQGAGGVI VPPETYWPEI
TR2             DPAEFGRQAA QALERKIDEI GECNVAAFIA EPIQGAGGVI IPPDSYWPEI
TRCV            TPDEFGVVAA RWLEEKILEI GADKVAAFVG EPIQGAGGVI VPPATYWPEI
TRAD            TPEEFGLAAA KWVEDKILEV GADKVAAFVG EPIQGAGGVI VPPSTYWPEI
```

```
                 ....|....| ....|....| ....|....| ....|....| ....|....|
                         260        270        280        290        300
TR3              RDICDRHGIL LISDEVITGF GRTGDWSGAR HWGVKPDLMT TAKGITSGYF
TRPD             LPILRKYDIP MISDEVICGF GRTGNTWGCL TYDFMPDAII SSKNLTAGFF
TRSD             QRICDKHDVL LIADEVICGF GRTGNWFGSQ TMGIKPHIMT IAKGLSSGYA
TR6              QRICDKYEIL LIADEVICGF GRTGNWFGSE TVGWKPDIMT IAKGLSSGYQ
TR2              KRICAERDIL LIVDEVITGF GRLGTWFGSQ YYDLQPDLMP IAKGLSSGYM
TRCV             ERICRKYDVL LVADEVICGF GRTGEWFGHQ HFGFQPDLFT AAKGLSSGYL
TRAD             QRICQKYDIL LVADEVICGF GRTGEWFGQQ VFGFKPDIFT TAKGLSSGYQ

                 ....|....| ....|....| ....|....| ....|....| ....|....|
                         310        320        330        340        350
TR3              PVGACLLSEA VAEVFEKDTS GEAAIYHGYT YSAHPVGAAA VVATLAETQR
TRPD             PMGAVILGPD LAKRVEAAVE AIEEFPHGFT ASGHPVGCAI ALKAIDVVMN
TRSD             PIGGSIVCDE VAEVI----- NACEFNHGYT YSGHPVCAAV ALENLRIMQE
TR6              PIGGSIVSDE IATVI----- GNCEFNHGYT YHAHPVAAAV ALENLRILDE
TR2              PIGGVMVSDR VAKVV---IE EGGEFFHGYT YSGHPVAAAV AAENIRIMRD
TRCV             PIGAVFVGKR VAEGL----I AGGDFNHGFT YSGHPVCAAV AHANVAALRD
TRAD             PIGAVFVNEK VATTL----A EGGDFNHGFT YSGHPVAAAV AHANVKALRD

                 ....|....| ....|....| ....|....| ....|....| ....|....|
                         360        370        380        390        400
TR3              LDLKTNAAA- RGTQLFEGVK KLAEKHDIIG DVRGGHGLMT GIEIVSDKAA
TRPD             EGLAENVRRL -APRFEAGLK RI-ADRPNIG EYRG-IGFMW ALEAVKDKPT
TRSD             ENIIDHVQNV AAPALQEALN KL-GEHPLVG GVNV-SGLMA SLPLTPHKES
TR6              EGIVARVRDE TGPYLAQKWA AM-ADHPMVG EASI-VGMMG SIALTPNKST
TR2              EGIIERAGAE IAPYLQARWR EL-GEHPLVG EARG-VGMVA ALELVKSKQP
TRCV             EGIVQRVKDD IGPYMQKRWR ETFSRFEHVD DVRG-VGMVQ AFTLVKNKAK
TRAD             EGIVDRVKND TGPYMQKRWR EVFGQFEHVD DVRG-VGLIQ AFTLVKNKAT

                 ....|....| ....|....| ....|....| ....|....| ....|....|
                         410        420        430        440        450
TR3              KTPMDNET-- -MKRIHQTAY EAGAMVRLGA HNVLMSPPLT ISEAEVNTIL
TRPD             KTPFDANLSV S-ERIANTCT DLGLICRPLG QSIVLCPPFI LTEAQMDEMF
TRSD             RAKFASDAGT AGYLCREHCF ANNLVMRHVG DRMIISPPLI ITPEEIAIFA
TR6              RATFKAEAGT VGYICRERCF ANNLVMRHVG DRMIISPPLT LTRDEIDLLI
TR2              LERFE-EPGK VGSLCRDLSV KNGLVMRAVG GTMIISPPLV LSREQVDELI
TRCV             RELFP-DFGE IGTLCRDIFF RNNLIMRACG DHIVSAPPLV MTRAEVDEML
TRAD             RELFP-NFGE IGTMCRDIFF KNNLIMRACG DHIVSAPPLV ISKEEIDQML

                 ....|....| ....|....| ....
                         460        470
TR3              TALDAGFSAA ---------- ----
TRPD             EKLEKALDKV FAEVA----- ----
TRSD             DRATRALDAT YADLKDKDLL KAAS
TR6              ERAWKSLDEG MAEVKKQGLW QEG-
TR2              DKARRTLDET HKAIGGA--- ----
TRCV             AVAERCLEEF EQTLKARGLA ----
TRAD             ETAAKCMVEF EKQLKERGLV ----
```

Fig. A 32 Multiple sequence alignment of ω-TA sequences using ClustalΩ [178]. The catalytic lysine for PLP binding is highlighted in yellow, conserved amino acids of the L-pocket are colored in blue and amino acids of the S-pocket are colored in green. Figure modified and reproduced from [190] with permission from Springer Nature.

Publications

1. Coenen, A., Ferrer, M., Jaeger, K.-E. & Schörken, U. (2023). Synthesis of 12-aminododecenoic acid by coupling transaminase to oxylipin pathway enzymes. *Applied Microbiology and Biotechnology*, accepted manuscript.

   My part of the work: design of experiments (~ 80 %), methodology and experimental performance (~ 95 %), writing and revision of the manuscript and design of figures and tables (~ 80 %)

2. Coenen, A., Gala Marti, V., Müller, K., Sheremetiev, M., Finamore, L. & Schörken, U. (2022). Synthesis of polymer precursor 12-oxododecenoic acid utilizing recombinant papaya hydroperoxide lyase in an enzyme cascade. *Applied Biochemistry and Biotechnology*, *194*, 6194–6212. https://doi.org/10.1007/s12010-022-04095-0.

   My part of the work: design of experiments (80 %), methodology and experimental performance (70 %), writing and revision of the manuscript and design of figures and tables (80 %)

3. Gala Marti, V., Coenen, A. & Schörken, U. (2021). Synthesis of linoleic acid 13-hydroperoxides from safflower oil utilizing lipoxygenase in a coupled enzyme system with in-situ oxygen generation. *Catalysts*, *11*, 1119. https://doi.org/10.3390/catal11091119.

   My part of the work: design of experiments (~ 10 %), methodology and experimental performance (~ 10 %), writing and revision of the manuscript (~ 10 %)

Poster presentations on international conferences

1. Coenen, A., Gala Marti, V., Schörken, U. Poster: Enzymatic synthesis of 12-oxododecenoic acid, a lipid-based precursor for biopolymers. 18th Euro Fed Lipid Congress, Dresden, Germany, 18–21.10.2021

   My part of the poster: ~ 90 %

2. Gala Marti, V., Coenen, A., Schörken, U. Poster: Synthesis of hydroperoxides from safflower oil utilizing a coupled enzyme system with in situ oxygen generation.18th Euro Fed Lipid Congress, Dresden, Germany, 18–21.10.2021.

   My part of the poster: ~ 10 %

3. Gala Marti, V., Coenen, A., Schörken, U. Poster: Development of an enzymatic cascade for regioselective hydroperoxide synthesis with in situ oxygen generation. MECP 2020+1, Aachen, 13.-16.09.2021.

   My part of the poster: ~ 25 %

4. Coenen, A., Gala Marti, V., Schörken, U. Poster: Cloning, expression and characterization of hydroperoxide lysases for synthesis of 12-oxododecenoic acid. Biotrans 2021 Graz, Austria, 19.–22.07.2021.

   My part of the poster: ~ 90 %

5. Gala Marti, V., Coenen, A., Schörken, U. Poster: Regioselective synthesis of linoleic acid based hydroperoxides with in situ oxygen generation. European Biotechnology Congress, Prague, Czech Republic, 24.-26.09.2020.

   My part of the poster: ~ 25 %

Danksagung

Abschließend möchte ich mich bei allen bedanken, die mir bei dieser Arbeit geholfen und unterstützt haben.

Mein besonderer Dank gilt Prof. Dr. Karl-Erich Jaeger für die Betreuung dieser Promotion als Doktorvater. Vielen Dank für die nützlichen Tipps, die Vermittlung des Kontakts nach Spanien und die Arbeit am gemeinsamen Paper.

Ich möchte mich ganz herzlich bei Prof. Dr. Ulrich Schörken bedanken, der mich als Mentor stets unterstützt und motiviert hat. Vielen Dank für die Bereitstellung des interessanten Themas und Hilfe bei wissenschaftlichen Fragestellungen. Die gemeinsame Arbeit hat mir stets Spaß gemacht und mich fachlich weitergebracht.

Darüber hinaus danke ich Prof. Dr. Manuel Ferrer für die Überlassung der Enzyme und Vektoren und für die Zusammenarbeit beim Verfassen des Transaminase Papers.

Außerdem möchte ich mich bei unseren Projektpartnern Dr. Henrike Brundiek von Enzymicals und Dr. Oliver Thum von Evonik für die gemeinsamen Projekttreffen, hilfreichen Tipps und die Bereitstellung von Enzymen bedanken.

Ich möchte mich bei all meinen Kollegen und Kolleginnen für die schöne Zeit bedanken, die wir gemeinsam im Labor und bei der einen oder anderen Kaffee- und Kuchenpause verbracht haben. Mein besonderer Dank gilt den beiden anderen Doktoranden Valentin und Tristan, die mich bei vielen chemischen Fragestellungen unterstützt haben. Ich bedanke mich außerdem bei den Studierenden Lara, Lorenzo, Kira, Maria und Annika, die ich im Rahmen ihrer Bachelor-Arbeiten betreuen durfte und die einen wichtigen Beitrag zu dieser Arbeit geleistet haben.

Zu guter Letzt danke ich meiner Familie, meinen Freunden und meinem Freund Henrik dafür, mich während meines gesamten Studiums und der Doktorarbeit unterstützt zu haben.

Eidesstattliche Erklärung

Ich, Frau Anna Coenen, versichere an Eides Statt, dass die Dissertation von mir selbständig und ohne unzulässige fremde Hilfe unter Beachtung der „Grundsätze zur Sicherung guter wissenschaftlicher Praxis an der Heinrich-Heine-Universität Düsseldorf“ erstellt worden ist.

Ort, Datum Unterschrift